ANA MARTA MINEIRO GALVÃO DIAS NETO

REGULATION OF QUASI-STABLE CELL STATES BY THE BRAHMA COMPLEX SUBUNIT BAP60 DURING EYE DEVELOPMENT

Tese de Candidatura ao grau de Doutor em Ciências Biomédicas submetida ao Instituto de Ciências Biomédicas Abel Salazar da Universidade do Porto.

Orientador – Fernando Casares
Categoria – Investigador Principal
Afiliação – Centro Andaluz de Biología del Desarrollo, Sevilha, Espanha

Co-orientador – Paulo S. Pereira
Categoria – Investigador Principal
Afiliação – Instituto de Biologia Molecular e Celular, Instituto de Investigação e Inovação em Saúde, Universidade do Porto, Porto, Portugal

Co-orientador – Claudio Sunkel
Categoria – Professor Catedrático
Afiliação – Instituto de Ciências Biomédicas Abel Salazar da Universidade do Porto, Porto, Portugal

O trabalho apresentado nesta tese foi realizado no âmbito do Doutoramento em Ciências Biomédicas do Instituto de Ciências Biomédicas Abel Salazar (ICBAS) da Universidade do Porto, Portugal.

A investigação descrita nesta tese foi realizada no Centro Andaluz de Biología del Desarrollo (CABD), Universidad Pablo de Olavide, Sevilha, Espanha e no Instituto de Biologia Molecular e Celular, Universidade do Porto, Porto, Portugal.

Ana Marta Neto foi financiada pela Fundação Para a Ciência e Tecnologia, Portugal (bolsa SFRH/BD/69222/2010); co-financiada pelo Fundo Social Europeu (FSE) no âmbito do Programa Operacional Potencial Humano (POPH) do QREN.

FCT Fundação para a Ciência e a Tecnologia
MINISTÉRIO DA CIÊNCIA, TECNOLOGIA E ENSINO SUPERIOR

POPH QUALIFICAR É CRESCER.
QREN QUADRO DE REFERÊNCIA ESTRATÉGICO NACIONAL PORTUGAL 2007.2013
GOVERNO DA REPÚBLICA PORTUGUESA
UNIÃO EUROPEIA Fundo Social Europeu

De acordo com o regime jurídico dos graus e diplomas do ensino superior, nomeadamente com o disposto na alínea a) do n.º 2 do artigo 31.º do Decreto-Lei n.º 74/2006, de 24 de março, alterado e republicado pelos Decretos-Leis n.ºs 107/2008, de 25 de junho, 230/2009, de 14 de setembro, e 115/2013, de 7 de agosto, fazem parte integrante desta tese de doutoramento os seguintes trabalhos já publicados ou submetidos para publicação:

Neto, M., Aguilar-Hidalgo, D., Casares, F. (2016). Increased avidity for Dpp/BMP2 maintains the proliferation of progenitors-like cells in the *Drosophila* eye. Dev Biol **418**(1): 98-107.

Neto, M., Naval-Sánchez, M., Potier, D., Pereira, P.S., Geerts, D., Aerts, S., Casares, F. Nuclear receptors connect progenitor transcription factors to cell cycle control. (submetido)

De referir ainda que, o autor desta dissertação declara que interveio na conceção e na execução do trabalho experimental, na interpretação dos resultados e na redação dos manuscritos, sob o nome de Neto, M.

Durante a elaboração desta tese de doutoramento foi ainda publicado o seguinte trabalho, cujos resultados não fazem parte integrante da mesma:

Marinho, J., Martins, T., Neto, M., Casares, F., Pereira, P.S. (2013) The nucleolar protein Viriato/Nol12 is required for the growth and differentiation progression activities of the Dpp pathway during *Drosophila* eye development. Dev Biol **377**(1): 154-165.

CONTRIBUTIONS

During this PhD thesis we have collaborated with a group of people who have contributed importantly to this project. Here I will describe the contributions of each one of them and give them credits for their work presented in this thesis.

Marina Naval-Sánchez, Delphine Potier and Stein Aerts from the School of Medicine, University of Leuven, Belgium and Dirk Geerts from the Department of Pediatric Oncology, Erasmus University Medical Center, Rotterdam, The Netherlands contributed to the part I of results "Nuclear receptors connect progenitor transcription factors to cell cycle control". Marina Naval-Sánchez, Delphine Potier performed the bioinformatics analysis of RNA-seq and FAIRE-seq data, together with Stein Aerts. Dirk Geerts carried out statistical analysis of human tumour data.

Daniel Aguilar-Hidalgo from the Department of Biological Physics, Max Planck Institute for the Physics of Complex Systems, Dresden, Germany carried out mathematical analysis of quantitative data in the part II of results "Hh and Dpp signalling pathways contribute to the proliferation and undifferentiated state of hth+tsh-expressing eye progenitors".

Asunción Lago-Lestón performed the RNA-seq experiments as well as expression profiling and analysis of differential expression, gene ontology analysis and real-time qPCR of *tio>GFP* and *tio>GFP:hth* samples in the part III of results "*Bap60,* a component of the Brahma chromatin-remodeling complex, is necessary for the progenitor-to-precursor transition".

ACKNOWLEDGEMENTS

Durante a realização deste trabalho várias pessoas me ajudaram e apoiaram, directa ou indirectamente, para que esta tese fosse possível. Agora que está a chegar o seu final, não posso deixar de expressar o meu agradecimento a todos os que contribuíram para tal.

Ao Paulo e ao Fernando, por me terem dado a oportunidade de realizar este trabalho nos seus laboratórios.

Ao Paulo por me ter apresentado à Biologia do Desenvolvimento e por estar sempre presente e disponível, obrigado pela transmissão de tanto conhecimento e raciocínio científico. Os anos passados no laboratório foram sem dúvida cruciais para que hoje esteja aqui.

Ao Fernando, agradeço a disponibilidade constante e confiança depositada em mim. Agradeço-te todas as horas de discussões científicas, todo o conhecimento que me transmitiste e a maneira como sempre demonstras o teu incessante entusiasmo pela ciência.

À Joana Marinho, agradeço tudo o que me ensinou no laboratório e todas as importantes discussões científicas, mas principalmente agradeço todos os bons momentos que passámos no laboratório, com muita amizade e boa disposição.

Ao Torcato, agradeço a imensa amizade, inúmeras conversas sobre qualquer tema e todas as palavras de confiança durante todo este tempo.

Joana e Torcato, vocês mostraram-me o que é um bom ambiente de trabalho onde reina a amizade e confiança e todas as palavras são poucas para agradecer isso.

Agradeço ainda à Joana Santos e à Sofia Pinho pelos bons momentos passados no IBMC.

A M.A., muchas gracias por haberme ayudado e integrado en los primeros tiempos en Sevilla. A Antonella, gracias por el apoyo en el laboratorio y por todas las comidas de viernes. Un agradecimiento generalizado a Cristina, Carla, Jorge, Asun, Dani, Ana Sara, Max, Marta Magri, Amer, Gema, Carlos Luque, Isabel y a todos los estudiantes que pasaron por el laboratorio durante estos años, sin ustedes este trabajo no hubiera sido posible. Un agradecimiento especial a Diana, muchas gracias por todas las discusiones científicas, por tu gran amistad y por tu apoyo durante los últimos años de esta tesis, hiciste que este camino se hiciera un poco menos largo.

To Stein Aerts, for accepting me in his laboratory during three intense and fantastic weeks and for introducing me to the world of omics. To Marina Naval-Sánchez and Delphine Potier, for your help with the bioinformatics. To Valerie and

Lotte, for technical help and for teaching me the basics of RNAseq and FAIREseq. To all the members of the laboratory, for all the help and good moments during those weeks.

A toda la gente del coffee time, Ana, Calero, David, Elena, Helena, Kathy, Miriam y Sofí muchísimas gracias por los buenos momentos que hemos pasado juntos dentro y fuera del CABD. Para mí, Sevilla no seria la misma sin el Coffee Time. Ana y Elena, muchas gracias por vuestra amistad y vuestro apoyo siempre. Calero, gracias por la compañía en la sala de las moscas, espero que Lisboa te trate tan bien como Sevilla me ha tratado a mí. David, gracias por enseñarme tan bien tu andaluz y por la buena disposición siempre. Kathy, muchas gracias por tu apoyo siempre con confocales, ImageJ y Imaris y muchas gracias por tu amistad. Miriam, muchas gracias por los viajes al CABD y por todas las conversaciones sobre todos los temas. Helena y Sofí, gracias por todos los buenos momentos y por vuestra alegría y buena disposición.

Al vecino de laboratorio Carlos, por todas las muchas horas en la sala de las moscas y en el confocal y sin duda por todas las horas pasadas fuera del CABD.

Às minhas amigas de sempre Rita e Margarida e aos meus amigos mais recentes mas que também já são de sempre Filipa, Nuno e Catarina, pela vossa amizade e companhia, pelos sorrisos sinceros, pela paciência em momentos mais difíceis e por todo o apoio e motivação.

Un agradecimiento muy especial a Mario. Gracias por estar a mi lado siempre, gracias por las infinitas horas de skype todas las noches y por todos los momentos juntos. Gracias por ayudarme tanto durante esta tesis, sin ti hubiera sido muchísimo más difícil. Gracias por creer que la distancia nos haría más fuertes, así fue. No hay palabras para agradecerte suficiente. Gracias por todo, siempre.

Por fim, não posso deixar de agradecer à minha família. À minha irmã Rita por transformar todos os grandes dilemas em questões banais e de resolução simples, pelo seu sorriso sempre e pela amizade e protecção infindáveis. Ao meu irmão João, por conseguir arrancar sorrisos nos momentos de maior cansaço e pela companhia e amizade de sempre. Aos cunhados Ricardo e Ana Maria, obrigado pela vossa amizade e por todos os bons momentos que passamos juntos. Ao meu adorável sobrinho Joaquim, o teu sorriso faz milagres e transforma tudo em alegria. Aos meus pais, um agradecimento eterno pelo seu apoio e confiança incondicionais. À minha avó, obrigado por tudo o que me ensinas, pela tua perseverança e a tua força.

Muito obrigado a todos,

Marta

TABLE OF CONTENTS

i. List of Figures **1**

ii. List of Tables **5**

iii. List of Abbreviations **7**

iv. Abstract **9**

v. Resumo **11**

1 INTRODUCTION **13**
1. Systemic signals **15**
1.1 Insulin/Target of Rapamycin (Delgado and Torres) signalling pathway 16
1.2 Ecdysone pathway 18
1.3 Other systemic signals 21
2. Organ intrinsic signals **21**
2.1 Morphogens 22
2.1.1. Hh/SHH signalling pathway 23
2.1.2. Dpp/BMP signalling pathway 24
2.2 Hippo signalling pathway 26
2.3 Mechanosensory signals 28
3. How can generic signalling pathways control different responses? **29**
3.1 Transcription factors 30
4. How can cell state transitions happen? **31**
4.1 Polycomb group (PcG) complexes 33
4.2 Trithorax group (trxG) complexes 33
4.2.1. *Drosophila* Brahma / mammalian SWI/SNF complexes 34
5. *Drosophila* as a model organism **35**
6. *Drosophila* eye as a model system **35**
6.1 Proliferation control during second instar 38
6.2 Initiation and movement of the morphogenetic furrow 39
6.3 Delimitation of different domains in the eye disc during third instar 41
6.4 Proliferation control during third instar 42

2 OBJECTIVES **45**

3 MATERIALS AND METHODS **49**
1. Fly strains and genetic manipulations **51**
2. Clonal analysis **55**
3. Immunostaining **56**
4. Scanning electron microscopy (SEM) **58**
5. RNA-Seq **58**

6. FAIRE-Seq 58
7. RNA probe synthesis 59
8. In situ hybridization 59
9. Generation of UAS transgenic strains 60
10. Quantification of $PH3^+$ cells 61
11. pMad expression profiles 61
12. Adult eye phenotype scores 62

4 RESULTS 63

PART I Nuclear receptors connect progenitor transcription factors to cell cycle control. 65
I Perturbations of progenitor transcription factors result in tissue overgrowth..... 69
II Cell cycle genes and nuclear receptors are altered downstream of Hth+Tsh..... 71
III Open chromatin profiling confirms nuclear receptors as candidate regulators 77
IV Functional analysis indicates that regulation of Ecdysone Receptor or nuclear receptors ftz-f1 and Hr46/DHR3 controls Hth+Tsh-driven overproliferation..... 82
V Hr46/DHR3 is repressed by Hth+Tsh 88
VI Significant co-overexpression of *MEIS1* and *TSHZ* genes, the vertebrate *hth* and *tsh* homologues, is found in major human cancers 90
VII The homologues of yki, ftz-f1 and Hr46, YAP1, NR5A2 and RORA, show significant expression correlation with MEIS1 and TSHZ genes in some tumours ... 94

PART II Hh and Dpp signalling pathways contribute to the proliferation and undifferentiated state of hth+tsh-expressing eye progenitors 97
I The Hippo signalling pathway cannot fully explain the hth+tsh phenotype 101
II Proliferation induced by combined expression of hth+tsh requires Dpp signaling 104
III hth+tsh-expressing cells increase the levels of Dpp signalling in a position-dependent manner 107
IV hth+tsh cells accumulate Dpp 110
V Enhanced Dpp signalling and tissue growth is associated to increased levels of the proteoglycan components dally and Dlp and require normal proteoglycan biosynthesis..... 112
VI Hh signalling is required for the Hth+Tsh-induced proliferation 116
VII Hth+Tsh-expressing cells increase the levels of Hh signalling as seen by Ci and Ptc expression 117
VIII Hth+Tsh induce a de novo activation of hh transcription 118

PART III *Bap60,* a component of the Brahma chromatin-remodeling complex, is necessary for the progenitor-to-precursor transition 121
I A gene network model points to the chromatin remodeler *Bap60* as potentially involved in early eye development. 125
II *Bap60* is required specifically in undifferentiated cells for eye development 133
III *Bap60* is required downstream of *ey* 138
IV Loss of Bap60 function impairs the progenitor-to-precursor gene expression progression 139

5 DISCUSSION AND CONCLUSION 143

6 REFERENCES 163

7 ANNEXES 189
A. Additional Methods for Results Part I 191
B. Additional Methods for Results Part II 197
C. Additional Methods for Results Part III 203
D. Supplementary Figures 207
E. Publication 209

i. List of Figures

INTRODUCTION

Figure I.1. Diagram representing the Insulin/TOR signalling pathway in *Drosophila*. 17

Figure I.2. Diagram representing the ecdysone signalling pathway from late third instar larva to late prepupa. 20

Figure I.3. Diagram representing the core components of the Hedgehog signalling pathway in *Drosophila*. 23

Figure I.4. Diagram representing the Dpp signalling pathway. 25

Figure I.5. Diagram representing the Hippo signalling pathway in *Drosophila*. 27

Figure I.6. SWI/SNF chromatin remodelling complexes in yeast, *Drosophila* and humans. 34

Figure I.7. The eye antennal imaginal disc and its adult derivatives. 36

Figure I.8. Main epithelium (or disc proper) and peripodial epithelium representations in different cross sections. 37

Figure I.9. Mechanisms controlling proliferation during second instar. 38

Figure I.10. Movement of the morphogenetic furrow..... 40

Figure I.11. Schematic representation of the different domains in the eye disc during third instar. 42

Figure I.12. Representation of some of the mechanisms controlling cell proliferation in the eye disc during third instar. 43

RESULTS – PART I

Figure R1.1. The *optix2/3-GAL4* line (*"optix>"*) drives expression in undifferentiated cells anterior to the morphogenetic furrow (MF). 69

Figure R1.2. Forced maintenance of *hth and tsh* expression results in overgrowth and differentiation arrest. 70

Figure R1.3. hth+hsh do not affect epithelial polarity..... 71

Figure R1.4. RNA-seq profiling of hth+tsh cells. 72

Figure R1.5. Co-expression of hth+tsh regulates the expression of cell cycle-related genes. 73

Figure R1.6. Transcriptomic profile of hth+tsh cells. 74

Figure R1.7. i-cis-Target predicted transcription factor binding site motifs associated with the down-regulated genes. 75

Figure R1.8. Co-expression of hth+tsh downregulate EcR signaling. 76

Figure R1.9. FAIRE-seq open chromatin profiling of hth+tsh cells. 79

Figure R1.10. i-cis-Target predicted transcription factor binding site motifs located within FAIRE peaks with increased accessibility in optix>hth+tsh discs. 80

Figure R1.11. Transcriptomic profile of the genes co-expressed with EcR. . 81

Figure R1.12. Cell cycle-related genes functionally interact with hth+tsh in inducing tissue overgrowth. 83

Figure R1.13. EcR functionally interacts with hth+tsh in inducing tissue overgrowth. 84

Figure R1.14. The dominant negative form of EcRB1 partially rescues the hth+tsh-phenotype. 85

Figure R1.15. Nuclear receptors *Hr46* and *ftz-f1* functionally interact with hth+tsh in inducing tissue overgrowth. 86

Figure R1.16. Altering *Hr46* and *ftz-f1* expression regulates proliferation of eye progenitors. 87

Figure R1.17. Temporal expression of Hr46. 89

Figure R1.18. The expression domains of *hth* and *Hr46* are complementary and co-expression of hth+tsh repress *Hr46.* 89

Figure R1.19. Examples for MEIS1 and TSHZ2 in breast and colon cancer. . 93

RESULTS – PART II

Figure R2.1. Forced maintenance of Hth and Tsh results in overgrowths. . 101

Figure R2.2. Maintenance of Hth and Tsh results in higher mitotic activity in the anterior area of the eye disc. 102

Figure R2.3. Hth+Tsh and Yki expression result in different phenotypes. .. 103

Figure R2.4. Manipulations of the levels of several components of the Dpp pathway in a Hth+Tsh background show functional interactions. 105

Figure R2.5. Altered expression of Tkv levels, either through RNAi or overexpression, in an Hth+Tsh background results in clear functional genetic interactions. 106

Figure R2.6. Maintenance of Hth and Tsh results in an increase in the pMad signal. 108

Figure R2.7. Forced maintenance of Hth+Tsh in clones results in a cell-autonomous accumulation of pMad. 109

Figure R2.8. hth+tsh-expressing clones increase pMad levels without affecting *dpp* transcription. 110

Figure R2.9. Hth+Tsh cells located near an endogenous source of Dpp are able to accumulate the morphogen. 111

Figure R2.10. hth+tsh-expressing clones do not induce *tkv* transcription. 112

Figure R2.11. Hth+Tsh activate *dally* transcription and Dlp levels. 113

Figure R2.12. Reduction of *sulfateless (sfl)* levels through RNAi in an Hth+Tsh background results in a partial rescue of the Hth+Tsh-phenotype. 115

Figure R2.13. Reduction of *sfl* expression causes a reduction of stability and diffusion of Dpp. 116

Figure R2.14. Manipulations of the levels of components of the Hh pathway in a Hth+Tsh background show functional interactions. 117

Figure R2.15. Maintenance of Hth and Tsh results in an increase in the Ci signal. 118

Figure R2.16. Forced maintenance of Hth+Tsh in clones results in increased levels of Ci and Ptc. 119

Figure R2.17. Hth+Tsh activate *hedgehog* transcription. 120

RESULTS – PART III

Figure R3.1. Early eye gene regulatory model. 126

Figure R3.2. *tio>GFP* and *tio>GFP:hth* discs. 127

Figure R3.3. Examples of genes with or without changes in their expression levels between tio>GFP and tio>GFP:Hth. 128

Figure R3.4. Quantitative RT-PCR (qPCR) validation of a set of 19 genes identified as differentially expressed in the RNA-seq experiment. 129

Figure R3.5. *in situ* validation of the RNAseq results. 130

Figure R3.6. GO characterization of the *tio>GFP* (precursors/early differentiating cells) and *tio>GFP:hth* (progenitors) transcription profiles. 131

Figure R3.7. *Bap60 is a potential Homothorax and Eyeless target.* 132

Figure R3.8. *Bap60* RNAi-mediated knock-down results in aberrant eye development. 133

Figure R3.9. Overexpression of GFP-Bap60 rescues the lethal phenotype of *Bap60* RNAi-mediated knock-down. 134

Figure R3.10. *Bap60* influences *ELAV expression*. 135

Figure R3.11. Bap60 protein seems to be mainly required for survival of proliferating cells during the earlier phases of eye development. 136

Figure R3.12. Stage-specific requirement for Bap60. 137

Figure R3.13. Ectopic expression of *eyeless* in regions of the wing and antenna imaginal discs induces Bap60 expression and *Bap60* is required for eye development downstream of *ey*. 138

Figure R3.14. *Bap60* knock-down affects the spatial and temporal expression of retinal determination genes. 140

DISCUSSION AND CONCLUSION

Figure D.1. Intermediate levels of Hth and pMad overlap during normal eye development. 151

Figure D.2. Yki-expressing clones do not increase pMad levels near an endogenous Dpp source. 153

Figure D.3. Multi-tiered feedback loops might connect cell-specification transcription factors and chromatin remodeller complexes through *Bap60.* 158

Figure D.4. tsh+moiraRNAi induce huge overgrowths. 160

ANNEXES

Figure A.1. Comparison of Dpp profile shapes with moving and non-moving source. 198

Figure A.2. Functional interaction of hth+tsh with *Hr46* and *ftz-f1*. 207

Figure A.3. Adult phenotypes produce by the overexpression or RNAi-mediated attenuation of *Hr46/DHR3, ftz-f1* and *EcR.* 208

Figure A.4. Adult phenotypes produce by the overexpression or RNAi-mediated attenuation of *tkv, punt, dpp, sfl, ci* and *hh.* 208

CD

Figure C.1. FAIRE-seq open chromatin profiling of hth+tsh cells. ..... ---

ii. List of Tables

MATERIALS AND METHODS

Table M.1. GAL4 lines. 51

Table M.2. UAS lines. 52

Table M.3. UAS-RNAi lines. 53

Table M.4. lexA/lexO lines. 53

Table M.5. Reporter lines. 54

Table M.6. Primary antibodies. 56

Table M.6. Secondary antibodies. 57

RESULTS – PART I

Table R1.1. *MEIS1* and *TSHZ1-3* mRNA expression and correlation in human cancer datasets. 91

Table R1.2. *MEIS1* and *TSHZ1-3* mRNA over-expression and DNA copy gain in human cancer types. 92

Table R1.3. Overview of MEIS1 co-expression with TSHZ, YAP1, RORA, and NR5A2 genes from R2 data. 95

ANNEXES

Table A.1. Ratios of pMad signal intensity, length scale of the gradient, effective degradation and effective diffusion coefficient. 201

Table A.2. qPCR primers and amplicon sizes. 205

CD

Table C.1. RNA-seq data for results – Part I. .....---

Table C.2. FAIRE-seq data for results – Part I. .....---

Table C.3. Complete *MEIS1-TSHZ* mRNA co-expression data from the R2. ...---

Table C.4. Complete *MEIS1* and *TSHZ1-3* mRNA over-expression and DNA copy number gain data from Oncomine. .....---

Table C.5. RNA-seq data for Results – Part III. .....---

Table C.6. Gene ontology analysis for up- and downregulated genes in optix>hth and tio>hth. ..... ---

iii. List of Abbreviations

AP boundary – Anterior-Posterior boundary

ATP – Adenosine Triphosphate

ban – bantam

Bap60 – Brahma associated protein 60kd

Brm – Brahma

Cas3* – Activated Caspase 3

Ci – Cubitus interruptus

CNS – Central Nervous System

CREs – *cis*-regulatory elements

CycA – Cyclin A

CycB – Cyclin B

CycE – Cyclin E

Dac – Dachshund

Dad – Daughters against Dpp

DE – Differential gene expression

DHR3 – *Drosophila* hormone receptor 3

Dilps – *Drosophila* insulin-like peptides

Dlp – Dally-like

Dpp – Decapentaplegic

DroID – The Comprehensive Drosophila Interactions Database

DSHB – Developmental Studies Hybridoma Bank

ECM – Extracellular Matrix

EcR – Ecdysone Receptor

ELAV – Embryonic Lethal Abnormal Vision

Exd – Extradenticle

Ey – Eyeless

Eya – Eyes absent

Eyg - Eyegone

FAIRE-seq – Formaldehyde-Assisted Isolation of Regulatory Elements sequencing

GFP – Green Fluorescent Protein

GO – Gene Ontology

HA – Hemagglutinin

Hh – Hedgehog
Hr46 – Hormone receptor-like in 46
Hth – Homothorax
IGFs – Insulin-like growth factors
InR – Insulin Receptor
Iro-C – Iroquois complex
lexO – lexA Operator
Mad – Mothers Against Decapentaplegic
MF – Morphogenetic Furrow
Mor – Moira
PcG – Polycomb Group
PH3 – Phospho-Histone H3
Ptc – Patched
pMad – phosphorylated Mothers against decapentaplegic
Rbf – Retinoblastoma-family protein
RNAi – RNA interference
RNA-seq – RNA sequencing
Sfl – Sulfateless
So – Sine oculis
SWI/SNF - SWItch/Sucrose Non-Fermentable
TALE – Three-aminoacid Loop Extension
TF – Transcription Factor
Tio – Tiptop
Tkv – Thick veins
TOR – Target of Rapamycin
Toy – Twin of eyeless
trxG – Trithorax Group
Tsh – Teashirt
UAS – Upstream Activating Sequence
Upd - Unpaired
Usp – Ultraspiracle
VDRC – Vienna Drosophila Resource Center
Wg – Wingless
Yki – Yorkie

iv. Abstract

During development, the growth of organs depends largely on cell proliferation. Specific combinations of transcription factors and extracellular signals within the progenitor cell population are required to control this process. Often, maintenance of progenitor transcription factors leads to uncontrolled growth.

In this PhD project, we have used the *Drosophila* eye as a model to investigate the mechanisms acting downstream of the progenitor-specific transcription factors Homothorax (Hth) and Teashirt (Tsh) in driving the expansion of the progenitor cells.

The forced maintenance of Hth and Tsh results in a synergistic effect in stimulating proliferation of progenitor-like cells. We have shown that these transcription factors are able to control cell proliferation affecting systemic as well as organ-autonomous signals.

Using transcriptomics, open-chromatin profiling, transcription factor motif analysis and functional assays we have discovered that Hth and Tsh control the expression of a group of nuclear receptors of the ecdysone/estrogen signalling pathway, which are then responsible for the activation of the cell cycle genes that drive proliferation. This regulatory system seems to be relevant beyond *Drosophila*, since we have found significant co-expression of the human homologues of *hth*, *tsh* and nuclear receptor genes in specific cancer types.

Moreover, these progenitor-like cells upregulate the expression of extracellular matrix components, increasing the avidity of these cells for the locally produced signalling morphogen, Decapentaplegic (Dpp). This increased avidity leads to a cell autonomous hyperactivation of the Dpp pathway, which is required for the *hth+tsh*-induced tissue overgrowths. Additionally to the Dpp pathway, the Hedgehog (Hh) signalling pathway is also required to maintain the proliferation of the progenitor-like cells. In this situation the hyperactivation of the pathway depends, at least partially, on the transcriptional regulation of its ligand, Hedgehog.

Once cells stop proliferating, they need to undergo a series of transient states that would finally lead to their differentiation. In this PhD project, we have aimed to better understand the mechanisms controlling these cell transitions.

To do so, we generated a gene network comprising transcription factors and chromatin remodellers, as these proteins are key in regulating gene expression. We identify the Brahma complex subunit Bap60 as a component of this network likely under the control of the transcription factors Ey and Hth, both important regulators of the earliest stages of eye specification. We have found that when Bap60 function is attenuated, the dynamic patterns of retinal determination genes that characterize the progenitor to precursor transition are abnormal, pointing to a mutual regulation between fate determinants and chromatin remodelling complexes during normal eye development.

v. Resumo

Durante o desenvolvimento, o crescimento dos órgãos depende maioritariamente da proliferação celular. Combinações específicas de fatores de transcrição e de sinais extracelulares na população de células progenitoras são necessárias para controlar este processo. Frequentemente, a manutenção de fatores de transcrição específicos das células progenitoras leva a um crescimento descontrolado.

No projeto desenvolvido nesta tese de doutoramento, usámos o olho de *Drosophila* como modelo para investigar os mecanismos regulados pelos fatores de transcrição específicos das células progenitoras – Homothorax (Hth) e Teashirt (Tsh) – no control da expansão destas células.

A manutenção forçada de Hth e Tsh resulta num efeito sinérgico que estimula a proliferação destas células, células semelhantes às células progenitoras. Mostrámos que estes fatores de transcrição são capazes de controlar a proliferação celular afetando tanto sinais sistémicos como sinais autónomos do próprio órgão.

Usando transcritómica, caracterização do estado da cromatina no genoma completo, análise de motivos de união de fatores de transcrição e análises funcionais verificamos que Hth e Tsh controlam a expressão de um grupo de recetores nucleares da via de sinalização da ecdisona/estrogénios, que posteriormente são responsáveis pela ativação dos genes do ciclo celular que controlam a proliferação. Este sistema regulatório parece ser relevante não só em *Drosophila*, uma vez que verificamos que existe uma co-expressão significativa dos homólogos humanos de *hth*, *tsh* e dos genes de receptores nucleares em tipos específicos de cancro.

Além disso, estas células semelhantes às células progenitoras ativam a expressão de componentes da matriz extracelular, aumentando a avidez destas células pelo morfogéneo produzido localmente, Decapentaplegic (Dpp). Este aumento de avidez leva a uma ativação autónoma celular da via de Dpp, que é necessária para o sobrecrescimento de tecido induzido por *hth+tsh*. Juntamente com via de sinalização de Dpp, a via de sinalização de Hedgehog (Hh) é também necessária para manter a proliferação das células semelhantes às células

progenitoras. Neste caso a ativação da via depende, pelo menos parcialmente, da regulação da transcrição do seu ligando, Hedgehog.

No momento em que as células param de proliferar, passam por uma série de estados transitórios que finalmente conduzem à sua diferenciação. Neste trabalho focámo-nos em perceber de uma forma mais clara os mecanismos que controlam estas transições entre populações de células.

Para tal, criámos uma rede de regulação genética composta por fatores de transcrição e remodeladores de cromatina, uma vez que estas proteínas são essenciais para a regulação da expressão genética. Identificámos Bap60, uma sub-unidade do complexo Brahma, como um componente desta rede que muito provavelmente está sob o controlo dos fatores de transcrição Ey e Hth, ambos importantes reguladores dos estágios iniciais de especificação do olho. Verificámos que quando reduzimos a função de Bap60, os padrões dinâmicos dos genes que determinam a formação da retina e que caracterizam a transição de células progenitoras a células precursoras são afectados, apontando para uma regulação mútua entre genes que determinam a formação da retina e complexos remodeladores da cromatina durante o desenvolvimento normal do olho.

1

INTRODUCTION

In our daily life we are constantly exposed to a diversity of animal organisms that show incredible differences in their sizes and organ proportions. Multicellular animal life is extremely diverse in size, form and function. And yet, each animal begins its existence as a single cell. Therefore, organ and animal growth requires the increase in cell number. Then, the question is how is cell proliferation controlled so organs reach their “target” size?

Size and shape are species-specific traits and not in vain, most of the times we discriminate different species by their form and size. Additionally, bilateral organisms grow pairs of organs that grow to the same size, making the body symmetrical. For instance, human arms are shorter than legs, but the two arms or two legs grow to achieve the same final size. Nevertheless, a single extra round of cell division in each cell of the arm would be enough to totally change this proportion.

So what are the mechanisms that need to be controlled in order to achieve final and precise organ sizes? Over the years, several studies have shown that not only the growth rates need to be tightly controlled but also the timing of cessation of growth. This cessation of growth is usually coupled with a cell state transition, from proliferative and undifferentiated progenitors, to quiescent precursors and finally to differentiated cells. However, though much work and effort has been put into solving this question, there is not a final answer yet.

The size and number of cells that constitute an organ mainly define its final size. This final organ size is mainly controlled by two different types of signals – organ-extrinsic (systemic) or organ-intrinsic (organ-autonomous).

1. Systemic signals

One of the classic experiments that proved the existence of systemic signals that control growth was performed by Metcalf in 1964. In this study, when several fetal spleens where transplanted in newborn mice and allowed for some extra development it was observed that even though each transplanted spleen was smaller than a normal one, the total mass of all transplanted spleens was equivalent to the mass of a normal spleen. This experiment showed that spleen growth mainly relies on humoral factors, rather than intrinsic ones (Metcalf, 1964).

The organ-extrinsic signals act in a systemic fashion and are released as the organism reads environmental cues, nutrient availability or monitors its progression through developmental stages. This process acts simultaneously in the size control of several organs within an organism and its main players are hormones and growth factors.

1.1 Insulin/Target of Rapamycin (TOR) signalling pathway

From insects to humans, the Insulin/TOR signalling pathway is one of the major regulators of growth and the major link between nutrition and growth. When animals are under starvation or when there is a partial loss of insulin pathway function there is a similar result characterized by a reduction of the overall size of the animal caused by fewer and smaller cells (Chen et al., 1996; Bohni et al., 1999).

This nutrient-sensitive system is composed by two different branches– Insulin and TOR branches–, which share some of its key downstream regulators (Nijhout et al., 2014).

In vertebrates there are two types of insulin-like molecules – insulin and insulin-like growth factors (IGFs), whereas in *Drosophila* there is only one type of molecules – the *Drosophila* insulin-like peptides (Dilps). As a consequence, while in vertebrates metabolic and growth-promoting functions are controlled by different molecules (insulin and IGFs, respectively) (Nakae et al., 2001), in *Drosophila* both functions are controlled by Dilps (Garofalo, 2002).

Drosophila Dilps are mainly secreted by the central nervous system (Ikeya et al., 2002), but also by the gut, fat body, imaginal discs or salivary glands (Koyama et al., 2013). There are two described Dilp receptors in *Drosophila*: the Insulin-like Receptor (InR) that is able to bind several Dilps (Dilp1-7) (Chen et al., 1996; Brogiolo et al., 2001; Geminard et al., 2009) and the *Drosophila* Leucine-rich repeat-containing G protein-coupled receptor 3 (Lgr3) which binds Dilp8 in a subset of CNS neurons (Garelli et al., 2015).

Circulating Dilps act in several target tissues, through binding to their receptor on the surface of the cells and the activation of the downstream phosphorylation signalling cascade. Two of the downstream targets of this phosphorylation cascade are the RAS/MAP kinase and the protein kinase Akt

(Yenush et al., 1996). Akt is then responsible for the repression of several negative regulators of growth (Figure I.1; Gao and Pan, 2001; Gao et al., 2002; Junger et al., 2003).

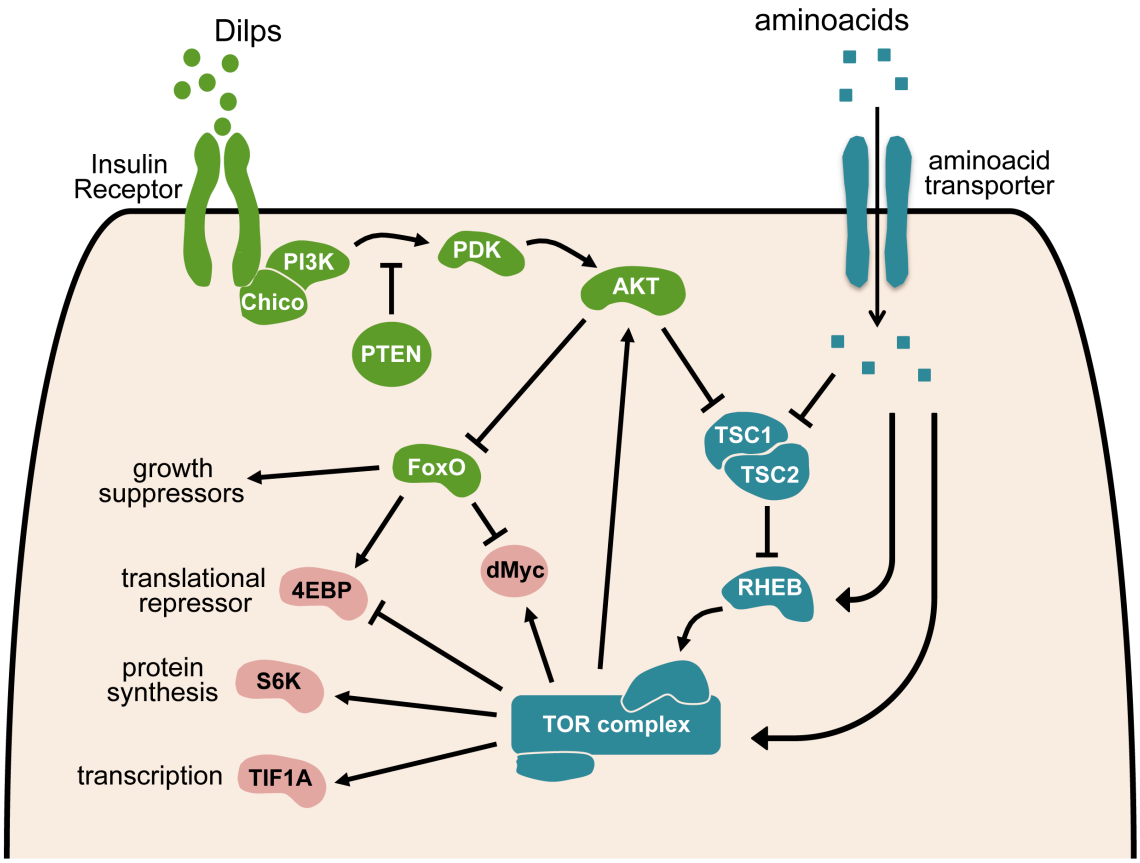

Figure I.1. Diagram representing the Insulin/TOR signalling pathway in *Drosophila*. The core elements of the insulin branch of the pathway are represented in green and the core elements of the TOR branch of the pathway are represented in blue. Some of the downstream efectors of this pathway are represented in pink. Arrows represent activation and bar-ended lines represent repression. For more details, see text. Adapted from Koyama et al., 2003.

While the insulin pathway responds to rich or low nutritional environment, the TOR pathway senses the intracellular aminoacid concentration (Gao et al., 2002), through TOR itself (Kim et al., 2002) or through its upstream regulator Ras Homolog Enhanced in Brain (RHEB) (Garami et al., 2003). TOR then promotes growth through activation of Akt (Sarbassov et al., 2005) and several other target genes (reviewed in Koyama et al., 2013).

The Insulin and TOR pathways are highly connected (Figure I.1). Interestingly, low aminoacids levels sensed by the TOR pathway are able to

induce the retention of Dilps in the brain and consequently to inhibit larval growth (Geminard et al., 2009).

One of the best studied downstream targets of the Insulin/TOR pathway in *Drosophila* is the steroid hormone ecdysone, which is similar to human sex steroids (Mangelsdorf et al., 1995). Several studies have shown that Dilps are able to activate the Insulin/TOR pathway in the prothoracic glands, the ecdysone-producing and -secreting organ. Indeed, inhibition of the pathway in this organ results in a reduction of ecdysone levels in third instar larvae resulting in an extended larval growth period and larger adults (Caldwell et al., 2005; Colombani et al., 2005; Mirth et al., 2005); while an activation of the pathway results in ecdysone biosynthesis and consequent reduced adult size (Walkiewicz and Stern, 2009).

1.2 Ecdysone pathway

Ecdysone is the major estrogen in insects. After secretion by the prothoracic glands, ecdysone is converted to its active form (ecdysteroid-20-hydroxyecdysone, 20E) in peripheral tissues. During development, there are several peaks of ecdysone expression, which are linked to larval molting and to the larva-to-pupa transition (Riddiford, 1993). These ecdysone peaks are controlled by the neuropeptide prothoracicotropic hormone (PTTH) (Rewitz et al., 2009) and are crucial to coordinate animal development.

The active form of ecdysone binds the ecdysone receptor heterodimer, formed by the Ecdysone Receptor (EcR) and Ultraspiracle (Usp) (Koelle et al., 1991; Yao et al., 1992; Thomas et al., 1993; Yao et al., 1993). The EcR is a member of the nuclear receptor family and has three different isoforms, which have conserved DNA- and ligand-binding domains but differ in their N-terminal regions (Talbot et al., 1993). While the EcR binds the active form of ecdysone, Usp optimizes the binding to DNA response elements of ecdysone-regulated genes. When the receptor is bound by ecdysone it activates the transcription of the target genes, while in its unbound state the transcription is repressed (Schubiger and Truman, 2000).

The Ashburner model explains the molecular events happening as a response to the binding of ecdysone to its functional receptor. Ashburner and colleagues proposed this model based on the study of puff induction in polytene chromosomes of the salivary glands during metamorphosis onset (Ashburner et al., 1974). Chromosomal puffs are uncoiled regions of the polytene chromosome, which represent regions where DNA is being actively transcribed. This *in vitro* experiment showed the induction of two types of puffs: the first ones were induced 10-15 minutes after ecdysone addition, while the second ones were induced 3 hours later and were sensible to the protein synthesis inhibitor, cycloheximide (Ashburner et al., 1974). This led them to propose that the first puffs correspond to direct target of ecdysone and that they encode transcription factors that would subsequently induce the activation of the later puffs.

Several years later, this model was validated through the sequential characterization of most (perhaps all) the genes involved in this cascade. The early puffs formed correspond to the induction of transcription of “early” ecdysone-induced genes E74 (Burtis et al., 1990; Thummel et al., 1990), E75 (Segraves and Hogness, 1990) and Broad-Complex (DiBello et al., 1991), which indeed encode transcription factors. These transcription factors are then responsible for the activation of a second set of secondary response genes and the repression of their own promoters. One of the first genes to be induced by the “early” genes is the “early-late” gene DHR3/Hr46, which is then required for the activation of the “late” gene ftz-f1 (Figure I.2; Lam et al., 1997).

Ecdysone has been shown to control animal growth rate through the transcriptional regulation of the growth regulator dMyc in the fat body. This work shows that an increase in ecdysone titer represses dMyc expression in the fat body, leading to the inhibition of ribosome biosynthesis and translation efficiency, that will ultimately lead to growth stop (Delanoue et al., 2010).

So far, we can picture a situation where the insulin/TOR pathway reads the nutritional status of the organism and acts in the prothoracic gland to control the ecdysone release. In the prothoracic gland, the insulin pathway represses the miRNA bantam, a cell-autonomous growth inducer that in this tissue is able to repress ecdysone production. This mechanism results in the release of the bantam-induced repression of ecdysone (Boulan et al., 2013). Once released,

ecdysone acts on the fat body to control the final body size. In this context, high levels of ecdysone are responsible for growth stop and final body size.

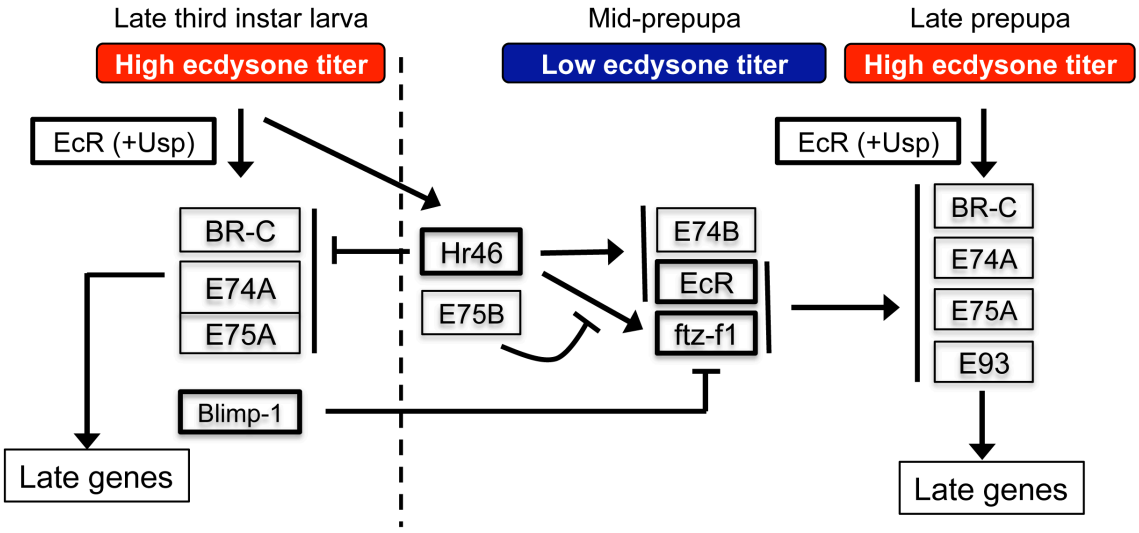

Figure I.2. Diagram representing the ecdysone signalling pathway from late third instar larva to late prepupa. Developmental stages characterized by high ecdysone titer are represented in red and the ones characterized by low ecdysone titer are represented in blue. Arrows represent activation and bar-ended lines represent repression. For more details, see text. Adapted from Lam *et al.*, 1999.

However, in order to coordinate the duration and rate of growth is easy to imagine a tighter connection between the insulin and ecdysone pathways. In fact, it has been recently described the role of Dilp8 in the control of organ size. Differently from what occurs with other Dilps, Dilp8 is activated by the imaginal discs as a response to atypical growth or damage. Dipl8 delays maturation through inhibition of ecdysone biosynthesis (Garelli et al., 2012).

Furthermore, an inverse relation between these two pathways has been described. For instance, high ecdysone levels reduce the insulin pathway via the fat body (Colombani et al., 2005). Yet, in the fat body both starvation and ecdysone levels activate Dilp6 during the larva-to-pupa transition and during the early stages of pupa development (Slaidina et al., 2009).

Altogether, these results show the intricate interactions happening between the insulin/TOR and the ecdysone pathways.

So far we described a role for ecdysone as a negative regulator of body growth, however there is also clear evidence that at the organ level it can promote growth.

While high levels of ecdysone clearly result in smaller discs due to inhibition of the insulin pathway systemically and consequent shortening of the growth period, it has been described that moderate levels of ecdysone are required to promote normal imaginal discs growth and differentiation (Mirth et al., 2009; Herboso et al., 2015).

1.3 Other systemic signals

Several other signals, like temperature fluctuations, juvenile hormone, oxygen or nitric oxide levels also play a role in the systemic control of growth. These signals will not be discussed in detail, but more information can be obtained in reviews about these topics (Nijhout et al., 2014; Day and Lawrence, 2000; Koyama et al., 2013).

2. Organ intrinsic signals

Although systemic signals play an essential role in the regulation of growth and size, there is clear evidence that organs have autonomous growth control mechanisms.

When Metcalf did the same kind of transplant experiments as explained before but this time transplanting several fetal thymuses to newborn mice, he observed that all thymuses grew to their normal adult size (Metcalf, 1963). This experiment showed that contrarily to what happen to the spleen that responds to systemic signals, the thymus has its own intrinsic growth control mechanism.

Long before, in the 30s, a similar intrinsic mechanism had been described in salamanders. When limbs where transplanted between two different species of salamander – the small *Amblystoma punctatum* and the large *Amblystoma tigrinum* – the transplanted organ grew to the normal size of the donor species (Twitty and Schwind, 1931).

Bryant and Simpson described this mechanism in *Drosophila* also using transplantation studies. They showed that wing imaginal discs from young larvae

transplanted to the abdomen of adult females grew until they reach their typical size at metamorphosis (Bryant and Simpson, 1984).

Organ-intrinsic mechanisms affect the organ locally by conveying information at a smaller scale – that of groups of cells or tissues. The main players in this case are morphogens, the hippo signalling pathway and mechanosensory signals.

2.1 Morphogens

Morphogens are secreted signalling molecules that provide positional information to the cells. These molecules are produced from a local source and secreted to the extracellular medium. Once released, morphogens disperse along the tissue and, upon binding to their receptors, form a signalling gradient, with highest signalling intensities closest to the source and lower farther away. In this way, morphogens convey spatial information to fields of cells exposed to them (Stathopoulos and Iber, 2013; Akiyama and Gibson, 2015). Therefore, the main function of morphogens has normally been associated with tissue patterning, through tight temporal and spatial regulation of the concentration sensed by different cell populations.

Although tissue patterning has been the traditional role described for morphogens, it is well know since their discovery that these molecules also regulate proliferation and growth (Kimelman and Kirschner, 1987). Nevertheless, how morphogens control this process is less clear.

Several evolutionarily conserved morphogens have been described, including Wingless/WNT, Dpp/BMP, Hh/SHH or Egf/EGF. The dual role they play in controlling patterning and growth has also been shown to be conserved. Next, two examples of morphogens that control growth will be given: first, Sonic hedgehog (SHH) in mammalian limb development and secondly, Decapentaplegic (Dpp) during *Drosophila* wing development.

2.1.1 Hh/SHH signalling pathway

The conserved Hh/SHH signalling pathway is one of the key pathways required for proper development and was first identified in *Drosophila* (Nusslein-Volhard and Wieschaus, 1980).

Once released, Hh (Shh, Idd and Dhh in mammals) interacts with its transmembrane protein receptor Patched (Ptc, PTCH in mammals), inhibiting it (Nakano et al., 1989; Alcedo and Noll, 1997). This interaction results in the accumulation and activation of Smoothened (Smo) through several phosphorylation events that results in a Smo conformation change to an active state (Fan et al., 2012, Zhao et al., 2007). In this activation, the cholesterol moiety harboured by Hh plays an essential role (Luchetti et al., 2016). This process results in the inhibition of the proteolytic cleavage of Cubitus interruptus (Ci, GLI in mammals), leading to the accumulation of its full-length and active form CiA. CiA enters the nucleus and acts as a transcription factor, activating Hh target genes (Hepker et al., 1997). When Hh is not present, the full-length form of Ci is cleaved into its repressor form (CiR), which acts as a co-repressor for Hh target genes (Aza-Blanc et al., 1997). Therefore, signal integration results from the ratio between CiA/GliA and CiR/GliR (Figure I.3; Junker et al., 2014).

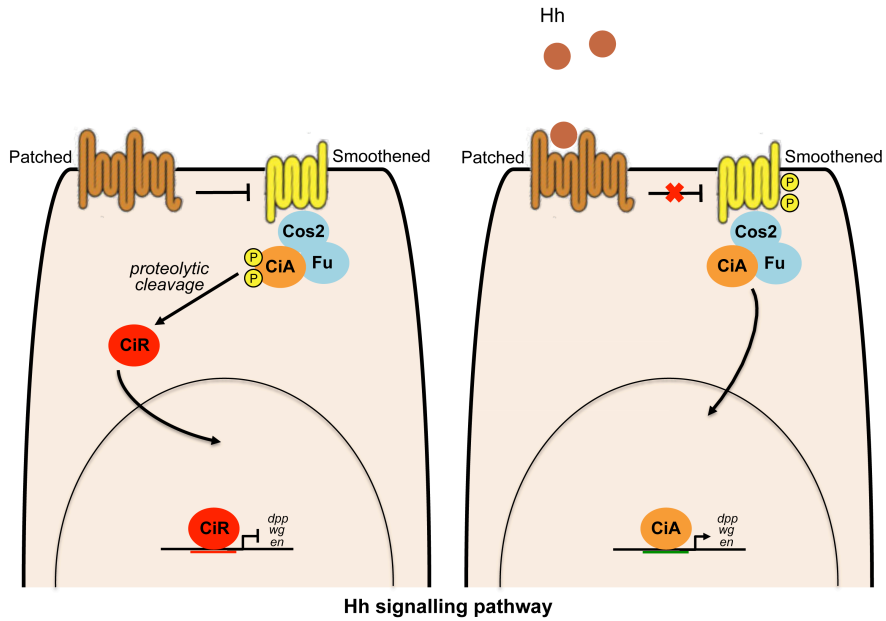

Figure I.3. Diagram representing the core components of the Hedgehog signalling pathway in *Drosophila*. Diagram on the left represents a situation in the absence of Hedgehog and the one on the right in the presence of maximum levels of Hedgehog. Intermediate Hedgehog signalling would result in a proporcion of CiA and CiR. Arrows represent activation and bar-ended lines represent repression. For more details, see text.

During mouse limb development, Shh activity seems to control digit identity and growth through a biphasic model. While its role in the control of digit identity is not clear yet, it is clear that it controls the size of the digit plate by stimulating limb anterior-posterior growth, ensuring the sufficient numbers of progenitor cells to form a normal limb (Delgado and Torres, 2016). During limb formation, digits are formed in an alternate fashion along the anterior-posterior axis: the first one to be formed is the digit 4, followed by digit 2, digit 5 and finally digit 3. In fact, timed removal of Shh results in limbs with a reduced numbers of digits, where digits reduction happens in the reverse sequence to the normal appearance order. This experiment clearly showed that Shh affects growth, but does not affect the digit identity along the anterior-posterior axis (Zhu et al., 2008). This growth induction seems to be achieved through the regulation of cell cycle genes (N-myc, cyclin D1 and cyclin D2) by Shh (Towers et al., 2008). This example shows how the morphogen Shh controls not only patterning, but also growth.

2.1.2 Dpp/BMP signalling pathway

decapentaplegic (dpp) was first described in *Drosophila* (Spencer et al., 1982) and later identified as a member of the TGFβ family of signalling molecules (Padgett et al., 1987).

In Drosophila, upon being released from the producing cells, Dpp (BMP2/4 in mammals) dimers bind to their receptor complexes. There are two types of receptors: type I receptors Thickveins (Tkv) and Saxophone (Sax) and type II receptors Punt (Put) and Wishful thinking (Wit). Dpp usually binds to Tkv that is activated through phosphorylation by the type II receptor after ligand binding. Once activated, Tkv phosphorylates the Smad Mothers against Dpp (Mad), which then binds to the co-Smad Medea (Med). The pMad-Med complex accumulates in the nucleus where it activates or represses the expression of target genes. The Dpp concentration-dependent transcriptional response in the *Drosophila* wing has been extensively studied and several target genes have been identified: *spalt* (*sal*), *optomotor blind* (*omb*) and *daughters against Dpp* (*dad*) are activated, while *brinker* (*brk*) and *pentagone* (*pent*) are repressed (Figure I.4; reviewed in Hamaratoglu et al., 2014).

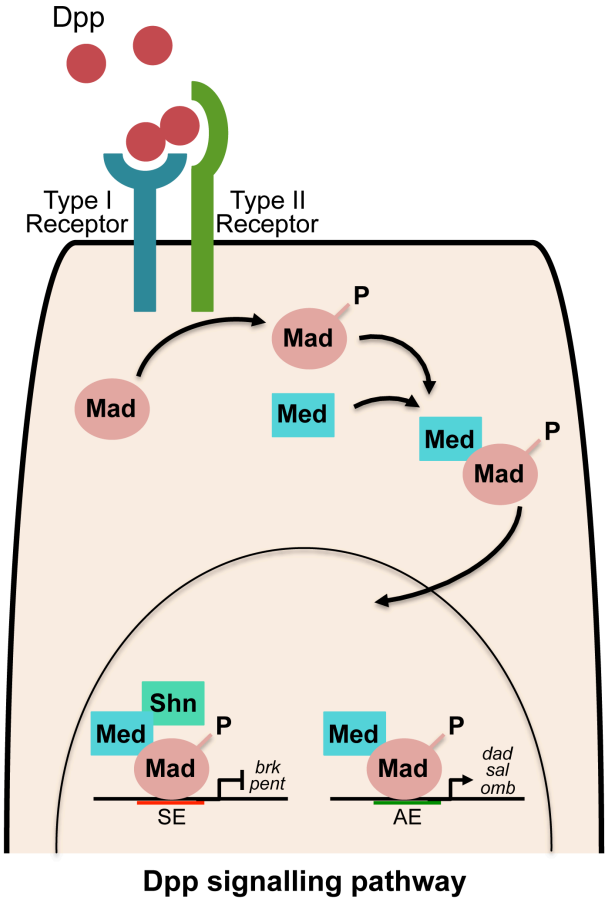

Figure I.4. Diagram representing the Dpp signalling pathway. The core components of the Dpp signalling pathway are represented. SE: Silencing element; AE: Activating element. For more details, see text. Adapted from Hamaratoglu et al., 2014.

In the wing, additionally to its patterning function Dpp is also involved in growth regulation. While a lower production of Dpp results in a severe reduction in the wing size (Spencer et al., 1982; Zecca et al., 1995); ectopic expression of Dpp or of the activated form of Tkv results in additional growth (Capdevila and Guerrero, 1994; Zecca et al., 1995; Burke and Basler, 1996; Lecuit et al., 1996; Nellen et al., 1996).

But how can the Dpp concentration gradient control the uniform proliferation seen during wing organ development? This is an extremely challenging problem and recently a lot of effort has been put into explaining this mechanism. While there is no final answer, there are several theoretical models that try to explain this (reviewed in Restrepo et al., 2014; Hariharan, 2015). These theoretical models can be either instructive, where Dpp as a direct role in driving cell proliferation; or permissive, where Dpp acts indirectly by giving cells the competence to respond to other regulators.

2.2 Hippo signalling pathway

Over the last ten years, the Hippo signalling pathway has emerged as one of the most important regulators of organ growth, acting in a cell-autonomous manner. Although initially discovered in *Drosophila*, this pathway is highly conserved in mammals and has been shown to act mainly through the regulation of both cell proliferation and cell death.

In both flies and mammals, mutations in several components of this pathway have been shown to induce huge overgrowths of epithelial tissues without affecting their epithelial integrity (Wu et al., 2003; Reddy et al., 2010; Reddy and Irvine, 2011; Halder and Johnson, 2011).

Moreover, it has been shown that mutations in components of the pathway are able to induce tumours in mouse models. Also, Hippo pathway-related mutations are present in a broad range of human carcinomas. These results have spotted Hippo pathway as a key player in tumorigenesis (Harvey et al., 2013).

At its core, the Hippo pathway comprises a kinase cassette composed of the kinases Hippo, Hpo (MST in vertebrates) and Warts, Wts (LATS in vertebrates) and their two cofactors Salvador, Sav (WW45 in vertebrates) and Mob as tumor suppressor, Mats (MOB in vertebrates). Hpo together with its adaptor protein Sav phosphorylate and activate Wts (Wu et al., 2003; Wei et al., 2007), which together with Mats (Lai et al., 2005) phosphorylate the transcriptional coactivator Yorkie, Yki (YAP and TAZ in vertebrates) at three Serine residues, being Serine residue 168 the most critical (Huang et al., 2005; Dong et al., 2007; Oh and Irvine, 2008; Zhang et al., 2008; Ren et al., 2010). Once phosphorylated by Wts, Yki binds to 14-3-3 proteins through strong protein-protein interactions, which results in the anchoring of Yki in the cytoplasm, preventing its transport to the nucleus (Figure I.5; Dong et al., 2007; Oh and Irvine, 2008; Zhang et al., 2008; Ren et al., 2010).

When the upstream kinases are inhibited, Yki enters the nucleus and drives the transcription of its targets genes. Yki itself does not possess a DNA-binding domain, so it must bind to transcription factors in order to activate transcription. In mammals, YAP/TAZ usually bind to TEAD transcription factors. In *Drosophila*, Yki has been shown to interact with the TEAD Scalloped (Sd) (Goulev et al., 2008; Wu et al., 2008; Zhang et al., 2008), Homothorax (Hth) and Teashirt (Tsh) (Peng et al., 2009) and Mad (Oh and Irvine, 2011), depending on the tissue or cell population.

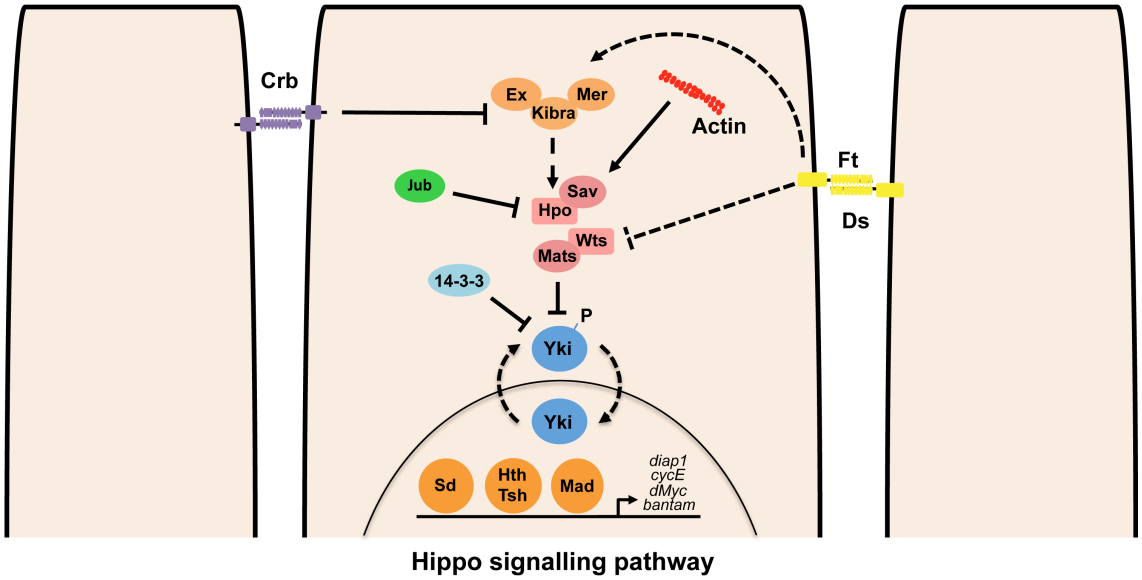

Figure I.5. Diagram representing the Hippo signalling pathway in *Drosophila*. This diagram represents the core components of the Hippo pathway. Arrows represent activation, bar-ended lines represent repression and dashed lines represent indirect or unknown mechanisms. For more details, see text. Adapted from Zhao et al., 2011.

In order to induce tissue growth and survival, it has been shown that Yki controls a number of targets involved in these processes. Some of its known targets include the *bantam* microRNA that promotes cell survival and proliferation (Nolo et al., 2006; Thompson and Cohen, 2006), *cycE* that regulates the G1 to S-phase transition during cell cycle (Tapon et al., 2002), the growth regulator *dMyc* (Neto-Silva et al., 2010) and the cell survival-promoting gene *Drosophila inhibitor of apoptosis*, *Diap-1* (Tapon et al., 2002; Wu et al., 2003).

Unlike other signalling pathways that normally respond to ligand- receptor interactions, the Hippo pathway is regulated by several upstream branches that either act directly on Yki or regulate the core kinase cassette. Although the process is not fully understood yet, in the past years a significant and increasing number of upstream regulators of the Hippo pathway had been described (Irvine and Harvey, 2015). Examples of these regulators include membrane-associated proteins, like FERM domain proteins Merlin and Expanded (Ex) and the WW and C2 domain-containing protein Kibra; cell polarity determinants, like Discs large (Dlg), Lethal giant larvae (Lgl), Scribble (Scrib) and Crumbs (Crb); cell-cell adhesion and junctional proteins, like Echinoid (Ed), E-cadherin (E-cad) or Ajuba (Jub); the planar cell polarity pathway and the actin cytoskeleton (Irvine and

Harvey, 2015). These regulators clearly link the Hippo pathway to the organization and integrity of the tissue, and finally to autonomous growth control. One important branch acting upstream of the Hippo pathway is the atypical cadherin Fat together with the related cadherin Dachsous, which additionally to control Wts and Ex abundance, also regulate the membrane localization of the atypical myosin Dachs through Vamana, a SH3-domain protein (Misra and Irvine, 2016).

2.3 Mechanosensory signals

Recently, one of the fastest-moving research topics in the growth control field is the role played by physical mechanisms.

A cell can sense physical modifications either through intracellular or surface tensions, generated by the actin-myosin cytoskeleton or the membrane, respectively.

In 2006, Engler and colleagues showed that simply changing the stiffness of the substrate where mesenchymal stem cells were growing was enough to make them develop into specific cell lineages (Engler et al., 2006). This experiment showed that cell specification and organ development are potentially controlled not only by biological signals, but also by mechanical ones.

Additionally to specification, mechanical stress also controls processes as diverse as gene expression (Farge, 2003), differentiation (McBeath et al., 2004), migration (Somogyi and Rorth, 2004) or proliferation (Huang et al., 1998).

In *Drosophila*, it has been shown that cells in the central region of the wing imaginal disc in early larval stages proliferate faster that cells on the outer region. This faster proliferation results in the compression of central cells and stretching of the outer ones, and in the consequent polarization of cell divisions in the wing discs (Aegerter-Wilmsen et al., 2012; Legoff et al., 2013; Mao et al., 2013). Several studies have shown that indeed the outer and stretched cells are at higher tension than the central ones (Nienhaus et al., 2009; Legoff et al., 2013; Mao et al., 2013).

The observation that the localization of Yki (and its orthologs YAP and TAZ) either in the nucleus or the cytoplasm is mainly controlled by the mechanical properties sensed by the cell points to a role of the Hippo pathway in controlling these processes (Pan et al., 2016).

In fact, stretching wing imaginal disc cells (especially from the outer region) by increased actin polymerization has been shown to increase Yorkie activity, resulting in overgrowth (Fernandez et al., 2011; Sansores-Garcia et al., 2011).

The requirement of YAP and TAZ to control proliferation through mechanosensory mechanisms has also been shown to happen in mammalian cells and 3D cultures.

In 2007, Zhao and colleagues showed that sparsely or densely populated cells behaviour differently. While sparsely cells that were not in contact proliferated more and showed YAP and TAZ localized in the nucleus, cells that were in contact showed YAP and TAZ localized in the cytoplasm (Zhao et al., 2007).

Some years later, it has been shown that the stiffness of the matrix substrate also affected YAP and TAZ localization: while a stiff matrix substrate allowed the nuclear localization of YAP and TAZ and consequently promoted growth, a soft matrix substrate limited growth by retaining YAP and TAZ in the cytosol (Dupont et al., 2011; Aragona et al., 2013).

Matrix stiffness also determines which kind of 3D structure mammary epithelial cells are able to form: while in soft matrix substrate YAP and TAZ were localized to the cytosol and were not able to give rise to organoid-like structures; cells that grew in a stiff matrix showed YAP and TAZ localized to the nucleus and gave rise to organoid-like structures (Aragona et al., 2013).

Finally, mechanosensors can explain why structures that show a gradient-like morphogen expression still show uniform patterns of cell proliferation and can also contribute to growth cessation at the end of development (Shraiman, 2005; Aegerter-Wilmsen et al., 2007; Hufnagel et al., 2007).

3. How can generic signalling pathways control different responses?

So far, we have described the role that organ-extrinsic and organ-intrinsic mechanisms play in order to control cell proliferation and organ growth. We have also described how these mechanisms crosstalk in an intricate and complex manner. Interestingly, several signalling pathways that control growth are also required for the control of specification and patterning. So, these generic mechanisms of growth should have additional layers of regulation in order to play specific roles depending on the cell population or tissue where they are acting.

A clear example of this is the role of *wingless (wg)* pathway in the *Drosophila* wing imaginal disc. While in the wing hinge, Wg (the Drosophila homologue of Wnt1) function is required to promote cell proliferation; in the wing pouch, it is required for cell fate specification (Neumann and Cohen, 1996). A similar effect for the WNT pathway has been described in the mouse central nervous system (Dickinson et al., 1994).

So how can a generic signalling pathway induce specific responses? So far, specific combinations of transcriptions factors have been identified as the main players in this process.

3.1 Transcription factors

Transcriptions factors are proteins that bind DNA, often through specific DNA sequences, of *cis*-regulatory elements (CREs) in order to regulate gene expression. They can bind to the DNA either alone or in complex with other proteins.

Transcription factors normally contain different functional domains: the DNA binding domain, which recognizes and binds to specific DNA sequences; the transcription domain that form an transcription complex through interaction with coactivators, corepressors or other general transcription factors like the RNA Polymerase; the dimerization domain that allows the formation of complexes with other transcription factors and the effector binding domain that permits the binding to effector molecules (Nestler and Hyman, 2002).

Specific DNA sequences to which transcription factors bind are normally inaccessible in the nucleus due to the high condensation of chromatin. In order for transcription factor binding to occur there might be factors able to bind chromatin in its condensed state. These factors have been identified as "pioneer" factors. Pioneer factors bind condensed chromatin independently of other factors for a stable period of time; preceding the binding of other transcription factors (reviewed in Zaret and Mango, 2016). Pioneer factors binding can facilitate transcription either by actively open up chromatin and exposing CREs or passively through reduction of the number of additional factors required to bind DNA (reviewed in Zaret and Mango, 2016).

In *Drosophila*, a good example of how transcription factors specifically modulate a signalling pathway is the one of the transcription factor and Hox gene *Ultrabithorax (Ubx)* in modulating the Dpp signalling pathway (de Navas et al., 2006; Crickmore and Mann, 2006). The wing and haltere discs present similar morphology but vary greatly in their size and give rise to obviously different adult appendages. These differences are determined by differential expression of Ubx – it is expressed in the haltere, but not in the wing (Beachy et al, 1985; Lewis, 1978). Works from the Sánchez-Herrero and Mann laboratories showed that Ubx modulates Dpp signalling by reducing Dpp diffusion through repression of *master of thick veins* (*mtv*) and *division abnormally delayed* (*dally*) expression and by increasing the levels of *tkv.* This results in a restricted distribution of Dpp in the haltere when compared with the wing and consequently in differences in their sizes (de Navas et al., 2006; Crickmore and Mann, 2006).

4. How can cell state transitions happen?

The unique combination of transcription factors and signalling pathways in a cell population is required to control cell behaviour. However, we know that during development cells need to follow a path of increasingly committed stages of specialization (i.e. a progressive loss of multipotency). In order for this to happen, a cell state needs to be stable enough in order to ensure coordinated action of signals on the cell population, but also transient so that they can be propelled to their next stage. Gene expression "stability" is a sort of cellular memory, and the best studied biological mechanism that confers this type of memory to the cells is the action of epigenetic factors. Currently, the most important epigenetic mechanisms are DNA methylation, histone modifications and chromatin remodelling.

The study of the hematopoietic system during development is an excellent example of how tight control of epigenetic mechanisms allow cells to undergo a series of sequential steps from hematopoietic stem and progenitor cells to all mature blood cell types. It has been long known that the niche factors, signalling pathways and transcription factors are fundamental during hematopoietic development and homeostasis. However, during the last years it has been shown

that controlling chromatin accessibility through epigenetic mechanisms is also key to this process (reviewed in Obier and Bonifer, 2016). In general in hematopoietic stem cells, multipotency genes are labelled with activating epigenetic marks, while genes required for lineage commitment and differentiation are labelled with pause epigenetic marks. After commitment, multipotency genes show silencing epigenetic marks. Finally, during differentiation genes that had paused signature are either activated or repressed depending on their lineage choice (reviewed in Kosan and Godmann, 2016).

Several studies have been made in order to characterize the types of chromatin that exist in a cell. In 2010, Ernst and Kellis identified 51 chromatin types divided into five large groups, depending on their combinations of chromatin marks. These chromatin states corresponded to promoter-associated states, transcription-associated states, active intergenic states, large-scale repressed states and repetitive states (Ernst and Kellis, 2010). The same type of analysis was done in *Drosophila* cells, but this time chromatin types were characterized based on the combinations of proteins that are bound to it. They identified five chromatin types corresponding to different activities and called them after colours: BLUE and GREEN chromatins corresponded to two types of heterochromatin, BLACK chromatin was repressive and RED and YELLOW chromatins were two types of transcriptionally active euchromatin (Filion et al., 2010).

Two of the most important groups of proteins that can bind chromatin in order to promote stable and heritable repression or activation of gene expression are the Polycomb (PcG) and Trithorax (trxG) groups. These proteins bind to DNA regulatory elements called PcG and trxG response elements (PREs and TREs), respectively.

These two groups of proteins are highly conserved in mammals and although initially associated with gene expression regulation, recently they have also been implicated in genomic imprinting, X inactivation, cell proliferation or oncogenic transformations (reviewed in Schuettengruber et al., 2007; Geisler and Paro, 2015).

These groups of genes were firstly identified in *Drosophila* as required for the maintenance of Hox genes expression. Hox genes are a family of transcription factors involved in the specification of cell populations along the anterior-posterior

body axis. Mutations in subunits of Polycomb complexes result in ectopic Hox gene expression and consequently in homeotic transformations, i.e. replacement of a body part for another one found elsewhere in the animal body (Slifer, 1942; Lewis, 1978). Mutations in mammalian homologues also result in homeotic transformations in the skeleton (Akasaka et al., 1996; van der Lugt et al., 1994).

4.1 Polycomb group (PcG) complexes

In *Drosophila*, Polycomb group proteins interact forming three different complexes: Polycomb repressive complex 1 (PRC1), Polycomb repressive complex 2 (PRC2) and Pho-repressive complex (PhoRC) (Geisler and Paro, 2015).

Alterations of the expression of genes encoding subunits of these complexes have been linked to cancer. However, this is a complex topic, because these genes can act both as oncogenes or tumour suppressors (reviewed in Geisler and Paro, 2015; Koppens and van Lohuizen, 2016). In fact, there is even evidence of activating and inactivating mutations on the same gene EZH2 present in different types of cancer (Hock, 2012).

4.2 Trithorax group (trxG) complexes

As described before, the Trithorax group of proteins is responsible for activation of gene expression. As the mechanism of gene activation is more complex than the one of repression, the Trithorax complexes need to perform more functions and consequently are composed by different types of proteins: DNA-binding proteins, chromatin remodelling proteins or proteins that promote histone modifications. These proteins associate to form different types of complexes, whose function depends on their composition: NURF, Brahma/SWI/SNF, ASH1 and ASH2, TAC1 and MLL1-3 complexes (Kingston and Tamkun, 2014).

The Trithorax complexes are required not only to activate general gene expression, but also to maintain Polycomb target genes in an “on” state (Kingston and Tamkun, 2014).

4.2.1 *Drosophila* Brahma / mammalian SWI/SNF complexes

The Brahma/SWI/SNF complexes are ATP-dependent chromatin remodelling complexes required for transcriptional regulation of specific target genes. These complexes use energy of ATP hydrolysis to perform alterations in the location or conformation of nucleosomes, resulting in the regulation of DNA accessibility (Bouazoune and Brehm, 2006).

The Brahma/SWI/SNF complexes are evolutionarily conserved from yeast to humans and can be divided at least in two subtypes: one includes yeast SWI/SNF, *Drosophila* BAP and mammalian BAF complexes; whereas the other includes yeast RSC, *Drosophila* PBAP and mammalian PBAF complexes (Figure I.6). The two subtypes share common subunits, but are characterized by different specific proteins (Mohrmann and Verrijzer, 2005).

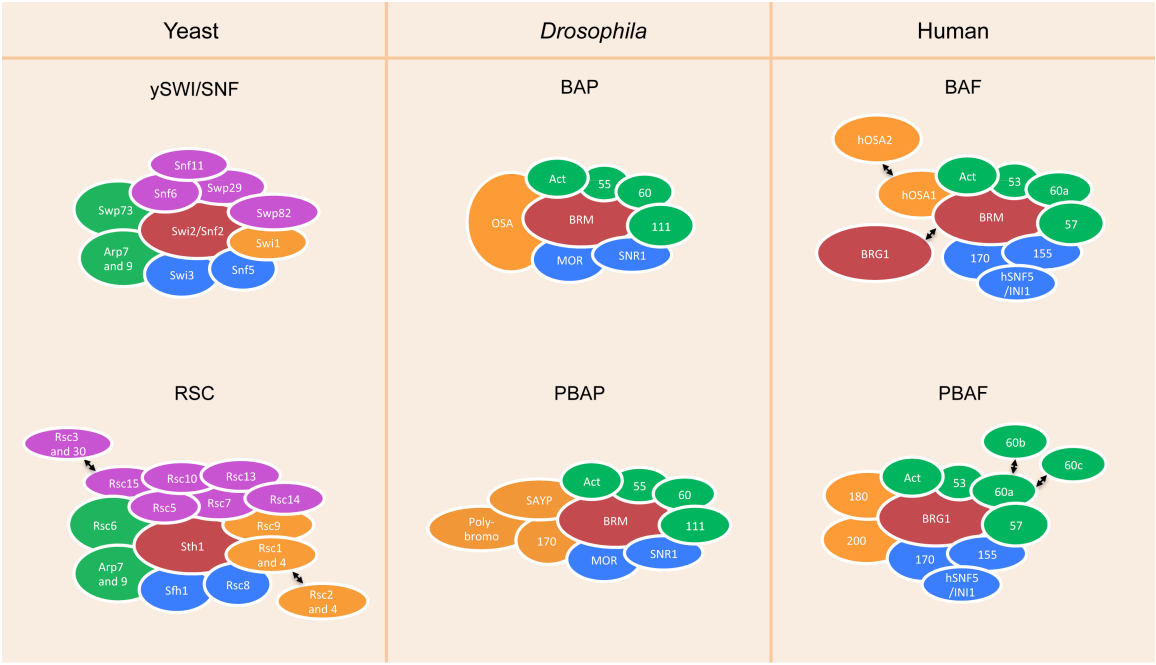

Figure I.6. SWI/SNF chromatin remodelling complexes in yeast, *Drosophila* and humans. The catalytic subunits are the SWI/SNF ATPases, here represented in red. This subunit together with the subunits represented in blue constitute the enzymatic core complex. The SWI/SNF complexes also contain a group of accessory components, represented in green. The unique subunits that allow the characterization of theses complexes into two groups are represented in orange. Purple represented subunits correspond to unique subunits only found in yeast. Double arrows indicate mutually exclusive subunits. Adapted from Kwon and Wagner, 2007.

These complexes show specific interactions with distinct transcription factors and regulate different subsets of genes and several signalling pathways

(reviewed in Reisman et al., 2009), playing multiple roles as regulators of development (Ho and Crabtree, 2010).

Mutations or deletions on genes encoding subunits of these complexes have been associated with sensitivity to UV light (Gaillard et al., 2003; Gong et al., 2008), genetic syndromes (Berdasco and Esteller, 2013) and cancer development in several cell types, suggesting that it may act as a tumour suppressor complex (Shain and Pollack, 2013).

5. *Drosophila* as a model organism

Drosophila melanogaster is a widely used model organism in several biological fields, from genetics to developmental biology or human diseases. One of the mainly reasons for this has to do with the high number of genetic and molecular tools available, which allow the accurate modulation of gene activity during development. This model acquires even more relevance taking into consideration the high level of homology between fly and human genes. In fact, it has been shown that 75% of the human genes that are associated with diseases are related to *Drosophila* genes (Reiter et al., 2001).

Another advantageous aspect of *Drosophila* is its short life generation time – 10 days at 25ºC. *Drosophila* life cycle is divided into four stages: embryonic, larval, pupal and adult stages. During the embryonic stage, body axes are established and all larval structures are specified. This period ends with hatching of the larva. The larval stage is divided into three instars that are separated by molts induced by ecdysone. This developmental stage corresponds to the feeding and growing period. At the end of the third instar larva enters the pupal stage, during which metamorphosis occurs. At the tenth day after egg laying, the adult fly emerges.

6. *Drosophila* eye as a model system

In this work, we mainly used the *Drosophila* eye as a model system to investigate the mechanisms that regulate cell proliferation and the state transitions leading to organ differentiation and growth outlined before.

The Drosophila compound eye consists of approximately 800 ommatidia arranged in a precise hexagonal array. Each ommatidium is composed of eight photoreceptors, four cone cells, six pigment cells and one mechanosensory bristle at alternate ommatidial vertices.

This structure originates from a group of about 20 cells that invaginate from the neuroectoderm as an epithelial sac, forming the eye-antennal imaginal disc (Garcia-Bellido and Merriam, 1969). From this moment and during the first larval instar, the cells that compose this imaginal disc express *twin of eyeless* (*toy*) and *eyeless* (*ey*) (Czerny et al., 1999; Quiring et al., 1994).

It is only during the second instar that two morphologically distinct fields are defined: an anterior region characterized by the expression of the transcription factor cut and the loss of *ey* expression and a posterior region that maintains the expression of *ey* and *toy* (Kenyon et al., 2003). The anterior part will give rise to the antenna, the maxillary palp and associated head capsule, whereas the posterior part gives rise to the compound eye, the ocelli and the surrounding head capsule (Figure I.7).

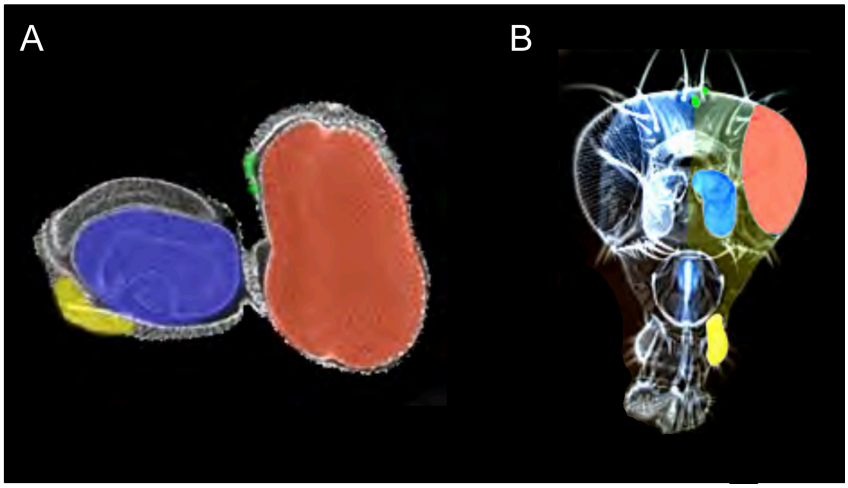

Figure I.7. The eye antennal imaginal disc and its adult derivatives. (A) Confocal image of an late third instar eye disc stained with phalloidin. Regions that will give rise to different adult structures are marked with colors. (B) Adult head with color-coded structures: yellow marks the maxillary palps, blue marks the antenna, red marks the compound eye and green marks the ocelli. Adapted from Almudi and Casares, 2016.

This developmental stage is also characterized by severe morphological alterations, that lead to the subdivision of the imaginal disc into two opposing epithelial layers: the main epithelium, which is formed by columnar cells that give

rise to the adult structures and the peripodial epithelium, which is formed by squamous cells that play an important role during eversion and fusion of the imaginal disc during the pupal stage. These two structures are separated by the cuboidal margin cells that give rise to part of the head capsule (Figure I.8).

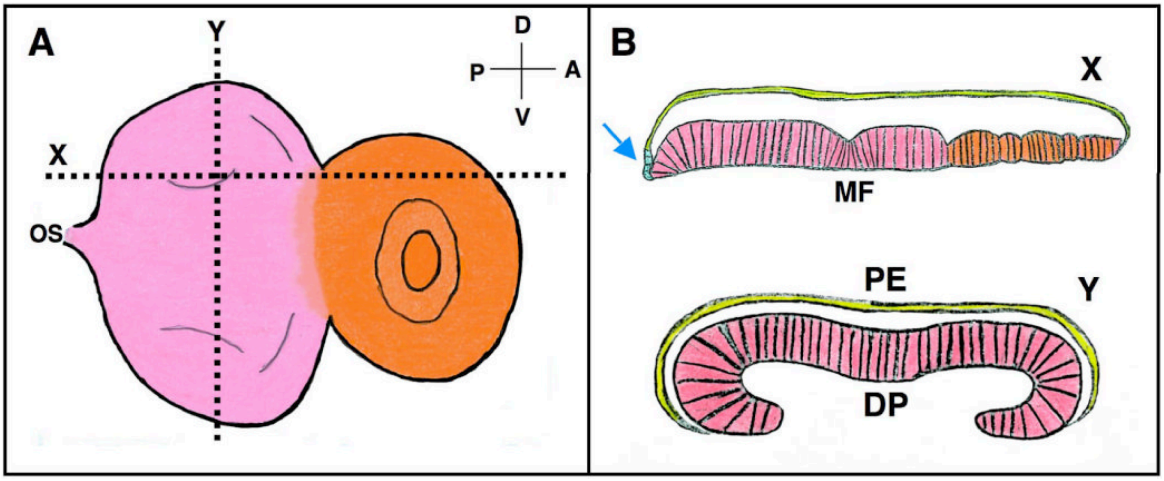

Figure I.8. Main epithelium (or disc proper) and peripodial epithelium representations in different cross sections. (A) Representation of the main epithelium section of a late third instar eye antennal imaginal disc. The region represented in pink corresponds to the eye disc and the region represented in orange is the antennal disc. The optic stalk (OS) is also indicated. (B) Vertical cross sections of the eye antennal imaginal disc that correspond to the dashed lines indicated by X and Y in (A). The peripodial epithelium (in green) is separated from the main epithelium (DP, in pink or orange) by a lumen. In the X cross section, morphogenetic furrow (MF) is represented in the eye disc as an apical constriction. The blue arrow points to the cuboidal margin cells. (Atkins M and Mardon G, 2009).

During the transition between second and third instar, there is a wave of differentiation that moves across the eye primordium in the anterior direction that marks the beginning of retinal differentiation. This wave is characterized by an indentation of the main epithelium, called morphogenetic furrow, which divides the disc in a region of undifferentiated cells localized ahead of the morphogenetic furrow and a posterior region where cells are differentiating giving rise to all the cell types required to assemble an ommatidium (Ready et al., 1976).

Here we will focus on the main epithelium of the eye region of the eye antennal imaginal disc.

6.1 Proliferation control during second instar

During the early larval stages of development, specifically from first instar until the end of the second instar, most cells of the eye disc are continuously proliferating. This proliferation is mainly controlled by the activation of the Notch signalling pathway along the dorsoventral boundary.

During the second instar, *wingless* transcriptional activation at the dorsal margin, together with *hedgehog*, activate the dorsal expression of the homeobox transcription factors of the Iroquois complex (iro-C) – *mirror*, *araucan* and *caupolican* (Figure I.9A; Heberlein et al., 1998; Cavodeassi et al., 1999; Yang et al., 1999).

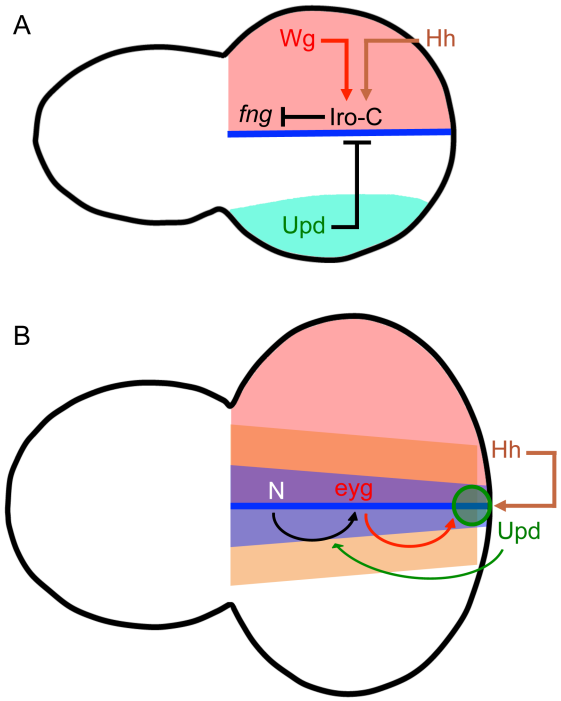

Figure I.9. Mechanisms controlling proliferation during second instar. (A) Schematic representation of a second instar eye disc. The dorsal-restricted expression of Wg (caused by the transient ventral expression of Upd) together with Hedgehog activate the iro-C genes resulting in a genetic dorsal-ventral division. (B) At this midline (blue), Notch pathway is activated and activates its downstream target gene *eyg*. Together, these two genes activate the expression of Upd at the firing point, inducing proliferation. Arrows represent activation, bar-ended lines represent repression. Adapted from Almudi and Casares, 2016.

These genes repress the expression of the glycosyltransferase *fringe* in the dorsal compartment, restricting their expression to the ventral compartment. *fringe* is then required to modify Notch affinity for its ligands, resulting in an increasing Notch affinity for its ligand Delta and reducing Notch sensitivity towards its ligand Serrate. The Notch signalling becomes activated along the dorsoventral boundary due to the compartmentalization of its ligands – Serrate expression is restricted to the ventral region, whereas Delta is mostly expressed in the dorsal region of the imaginal disc (Cho and Choi, 1998; Dominguez and de Celis, 1998; Papayannopoulos et al., 1998; Yang et al., 1999). Notch then activates the

transcription of its downstream target gene *eyegone* (*eyg*) (Figure I.9B; Dominguez et al., 2004).

The activation of Notch and *eyg* along the dorsoventral boundary results in eye disc growth. In fact, loss of Notch signalling or *eyg* loss-of-function mutations result in smaller or absent eyes; while constitutive activation of the Notch pathway results in tissue overgrowth (Cho and Choi, 1998; Dominguez and de Celis, 1998; Papayannopoulos et al., 1998; Jang et al., 2003; Chao et al., 2004; Dominguez et al., 2004; Reynolds-Kenneally and Mlodzik, 2005; Yao et al., 2008).

During this developmental stage, the JAK/STAT signalling pathway also plays an important role in growth control.

In early second instar, the JAK/STAT pathway is responsible for the restricted expression of iro-C genes to the dorsal region. This happens through the repression of those genes in the ventral region by the JAK/STAT pathway ligand, Unpaired (Upd), which is transiently expressed ventrally (Figure I.9A; Gutierrez-Aviño et al., 2009).

By the end of second instar, *upd* expression is transiently activated in the firing point, the point of intersection between the posterior margin of the eye disc and the *eyg* domain (Figure I.9B; Chao et al., 2004). *upd* mutants that lack the transient Upd pulse have smaller eyes, while *upd* overexpression results in overgrowths, showing that this activation is also important to control proliferation (Bach et al., 2003; Tsai and Sun, 2004).

6.2 Initiation and movement of the morphogenetic furrow

During early larval stages, *wg* is expressed in the dorsal/anterior region (Baker, 1988) and *hh* and *dpp* are expressed in the ventral/posterior region of the eye primordium (Heberlein et al., 1993; Ma et al., 1993). However, since *wg* and *dpp* are secreted molecules that act at long range and at this point the eye disc is too small, all cells are receiving both signals. In this situation, Wg is able to counteract one of Dpp functions as a retinal determination promoter signal (Lee and Treisman, 2001; Kenyon et al., 2003). Besides Wg role in repressing *dpp* transcription and Dpp signalling (Wiersdorff et al., 1996; Hazelett et al., 1998), it could also prevent an incorrect anterior retinal differentiation by blocking the odd-

skipped family genes (*drm*, *odd* and *sob*) in the dorsal/anterior disc margin (Bras-Pereira et al., 2006).

However during late second instar, the proliferation induced by Notch, Eyg and Upd is able to separate the anterior and posterior regions, restricting *dpp* expression to the most posterior region of eye disc, where it will be able to activate the early retinal determination genes. This separation is further invigorated through *wg* repression by the JAK/STAT signalling (Tsai and Sun, 2004; Ekas et al., 2006).

Once *dpp* activates the expression of retinal determination genes closer to the margin through *hth* repression, these cells are now able to differentiate (Bessa et al., 2002), giving rise to the first photoreceptors. These photoreceptors cells, with the exception of the R8 cell, activate *hh* expression (Rogers et al., 2005). *hh* in this cells activates *dpp* that will spread and repress *hth* expression in the next cells (Figure I.10). This mechanism allows the forward movement of the morphogenetic furrow. In fact, flies that cannot activate *hh* expression in the photoreceptors (*hh bar3* mutants) have small eyes due to furrow movement impairment (Rogers et al., 2005).

Dpp and Hh show a combined role during furrow progression. While loss of these pathways alone results in a delayed morphogenetic furrow; inhibition of both pathways results in a blockage of morphogenetic furrow movement and photoreceptor differentiation (Greenwood and Struhl, 1999; Curtiss and Mlodzik, 2000; Fu and Baker, 2003; Vrailas and Moses, 2006).

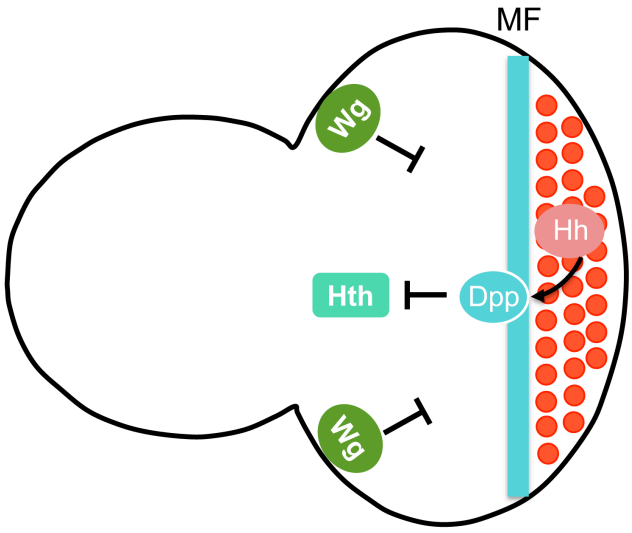

Figure I.10. Movement of the morphogenetic furrow. Photoreceptors (represented as red dots) activate the expression of hh. In these cells, Hh in then able to activate Dpp that will spread and repress Hth in the cells anterior to it. This process allows the movement of the morphogenetic furrow (blue line) in the anterior direction. Wingless expression in the ventral and dorsal anterior regions of the disc prevent differentiation in that region. Arrows represent activation, bar-ended lines represent repression.

Moreover, it has been shown that the Ecdysone signalling pathway is also required to control the morphogenetic furrow movement, although the precise mechanism is not clear (Brennan et al., 1998; Brennan et al., 2001).

6.3 Delimitation of different domains in the eye disc during third instar

During third instar and while the morphogenetic furrow moves anteriorly, the eye disc is divided in different cell population depending on their anterior-posterior position along the disc. While the cells closer to the posterior margin are the most differentiated, cells farther anterior are the least differentiated. Here, we will mainly focus on the most anterior cell populations.

As described before, one of the most important actions of the Dpp spreading from the furrow is the repression of the transcription factor Hth. This repression marks the transition between progenitors that proliferate asynchronously and are located in the most anterior part of the disc, and precursors that are G1-synchronized cells located closer to the morphogenetic furrow.

Simultaneously to *hth* repression, there is an activation of the retinal determination genes *eyes absent* (*eya*), *sine oculis* (*so*), *dachshund* (*dac*) and *optix*, as well as an activation of the cdc25 phosphatase *string* (*stg*, described below).

These two cell populations are genetically distinct, showing different transcription factor expression.

Progenitors are characterized by the expression of the Pax6 homologues Toy and Ey, the TALE-type homeoprotein Hth, the zinc finger-domain proteins Teashirt (Tsh) and Tiptop (Tio). Hth, Tsh and Ey have been shown to form a complex with a key role in controlling proliferation in this cell population (Bessa et al., 2002; Peng et al., 2009; described below) (Figure I.11).

Precursors maintain *toy*, *ey*, *tsh* and *tio* expression and start to express the retinal determination genes *dac*, the transcriptional co-activator *eya* and the SIX family genes *so* and *optix* (Figure I.11). Eya is a key player in this cell population and although it lacks a DNA-binding domain, it is able to interact with DNA binding proteins, like So (Pignoni et al., 1997) and Dac (Chen et al., 1997), in order to control gene expression.

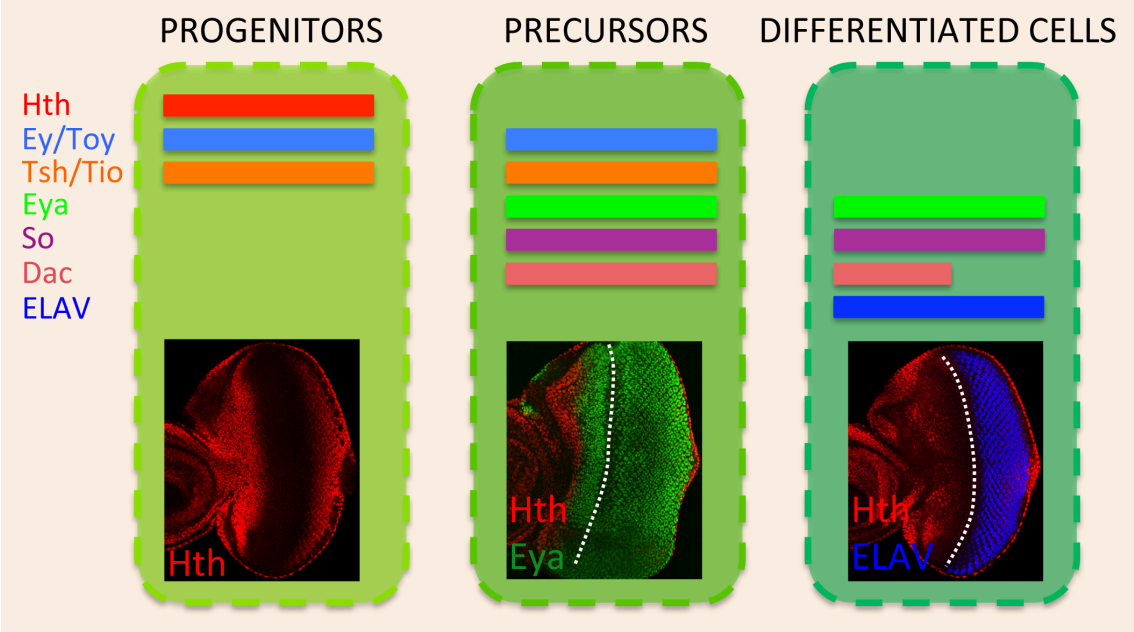

Figure I.11. Schematic representation of the different domains in the eye disc during third instar. Colored boxes represent the regions of expression of each gene. The eye disc represented in progenitors is stained with anti-Hth (red), showing the progenitor cell population in the most anterior part of the eye disc. The eye disc represented in precursors is stained with anti-Hth (red) and anti-Ella (green). The eya-expressing cells anterior to the morphogenetic furrow (dashed line) correspond to the precursors. The third disc is stained with anti-Hth (red) and anti-ELAV (blue). Cells marked in blue posterior to the morphogenetic furrow are differentiated cells.

6.4 Proliferation control during third instar

As described previously, the Dpp signal coming from the morphogenetic furrow as it moves anteriorly is able to repress the progenitor-specific gene *hth*, dividing the anterior region into two cell populations: progenitors and precursors. This process is tightly related to cell cycle-controlling mechanisms.

As cells loss *hth* expression and start to express the retinal determination genes, they also start to express *string* (*stg*). Progenitors cells are characterized by long G2 phase relative to G1 and S/mitosis, so *stg* expression in these cells force them to undergo mitosis and synchronize entry into G1 (Lopes and Casares, 2010, 2015). The G1 state is then maintained by the expression of the cyclin-dependent kinase inhibitor *dacapo* and *roughex* (Thomas et al., 1994; Thomas et al., 1997; de Nooij et al., 1996; Lane et al., 1996; Duman-Scheel et al., 2002).

The transcription factors Hth, Tsh and Ey, besides being required to provide eye identity to progenitor cells, have been shown to promote growth through stimulation of cell proliferation and prevention of apoptosis. While forced maintenance of *hth* and *tsh* causes overgrowths; knockdown of *hth* or *tsh* by RNAi result in smaller eyes. (Pichaud and Casares, 2000; Bessa et al., 2002; Singh et al., 2002; Peng et al., 2009, Lopes and Casares, 2010).

The control of cell proliferation by Hth and Tsh occurs, at least partially, via their physical interaction with the Hippo pathway transcriptional co-activator Yorkie (Figure I.12; Peng et al., 2009). This complex binds to an enhancer within the microRNA *bantam*, activating its expression in the progenitor cells and, consequently, mediating proliferative and anti-apoptotic functions (Peng et al., 2009). Recently, it has been shown that Dac is able to repress the cell proliferation induced by the Hth-Tsh-Yki complex. This interaction might be happening in the transition between progenitors and precursors, defining the separation between proliferating progenitors and quiescent precursors (Figure I.12; Bras-Pereira et al., 2015).

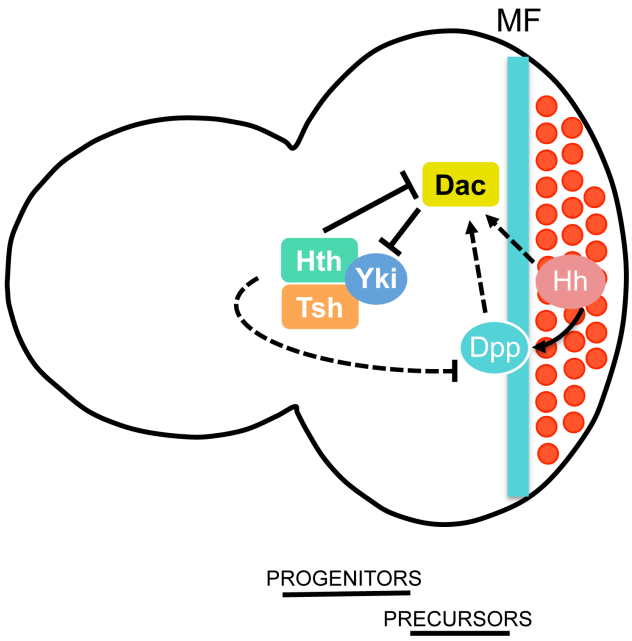

Figure I.12. Representation of some of the mechanisms controlling cell proliferation in the eye disc during third instar. In the most anterior part of the eye disc, the Hth-Tsh-Yki complex controls cell proliferation by activation of its downstream targets, like bantam. In the transition between progenitors and precursors, Dac is required to repress the cell proliferation induced by this complex, defining the separation between the two cell populations. Arrows represent activation, bar-ended lines represent repression. Morphogenetic furrow is represented as a blue line and photoreceptors as red dots.

As described before, growth control depends not only on organ-autonomous signals, but also on systemic ones. In fact, it has been recently

described that ecdysone levels regulate disc growth, through repression of the translational repressor 4E-BP, that consequently results in increased activity of the insulin/TOR signalling pathway (Herboso et al., 2015).

2

OBJECTIVES

During organogenesis, it is essential that cells know how and when to proliferate. Additionally, once they stop proliferating they need to follow certain cell transitions until they differentiate into specific cell types.

Throughout this thesis, in order to unravel some of the mechanisms that are acting in these two biological processes we used the *Drosophila* eye as a model system. During larval stages, as the morphogenetic furrow moves across the eye disc in the anterior direction it controls the transition from undifferentiated progenitors to precursors and finally differentiated cells. In this way, the eye disc is an excellent system because we can observe the entire range of differentiation states in a single developmental snapshot.

This thesis was divided into three main objectives:

1 – The first objective of this thesis was to identify the mechanisms lying downstream of the transcription factors Hth and Tsh in their synergistic growth-inducing ability. To do so, we have forcibly maintained their expression in order to generate progenitor-like cells. Our approach was based on genome-wide gene expression and open chromatin profiling together with computational models in order to analyse the global impact of these transcription factors on their target genes (results – part I).

2 – Secondly, we have aimed to find local signals contributing to the maintenance of progenitor-like features, such as vigorous proliferation. To do so, we have manipulated the Dpp/BMP and Hh signalling pathways (two pathways involved in growth control) in an Hth+Tsh background (results – part II).

3 – The third objective of this thesis was to identify components of chromatin remodelling complexes that play a specific role in the control of the progenitor-to-precursor transition during early stages of eye development. To do so, we built a gene regulatory network with transcription factors and chromatin remodellers that have a specific function in this process (results – part III).

3

MATERIALS AND METHODS

1. Fly strains and genetic manipulations

All crosses were set up and raised at 25ºC under standard conditions.

Two different binary transcriptional systems were used: the GAL4/UAS system (Brand and Perrimon, 1993) and the lexA/lexO system (Yagi et al., 2010).

The GAL4/UAS system was adapted from the yeast *Saccharomyces cerevisiae*. This is a very versatile system that consists in two main modules: the GAL4 driver, which is a regulatory region that induces the expression of the yeast transcription factor GAL4 and the UAS (Upstream Activating Sequence), the sequence where GAL4 binds in order to activate the expression of the downstream transgene (Brand and Perrimon, 1993).

This system is widely used in *Drosophila* since it allows obtaining GAL4/UAS flies with a single cross between one GAL4 and one UAS transgenic lines. The identification of several promoters and enhancers that have specific expression patterns during development allowed the establishment of a high number of GAL4 lines and consequently the spatial and temporal restricted expression of UAS transgenes (Elliott and Brand, 2008).

The GAL4 lines used during this study are listed in the table below.

Table M.1. GAL4 lines.

Gal4 lines	Origin
optix2.3-Gal4	gift from Rui Chen
yw, hs-FLP^{122};act<y^{+}<Gal4 *	Struhl and Basler, 1993
tioA4-Gal4	Tang and Sun, 2002
atoA2.3-Gal4	gift from Francesca Pignoni
ey-Gal4	Hazelett et al., 1998
GMR-Gal4	Song et al., 2000
dppblk-Gal4	Staehling-Hampton et al., 1994
***yw*, *hs*-FLP^{122}, *act*>*hs*CD2>Gal4**	Basler and Struhl, 1994

* with a recombined UAS-GFP transgene

Concerning the UAS lines, there can be different types of downstream transgenes, which can either drive the overexpression or the downregulation of a gene.

UAS lines used in this work to overexpress different genes (full-length, tagged versions, activated form or dominant negative) are listed here:

Table M.2. UAS lines.

UAS lines	Origin
UAS-GFP	Bessa and Casares, 2005
UAS-lacZ	Phelps and Brand, 1998
UAS-myr-RFP	
UAS-131-GFPhth	Casares and Mann, 2000
UAS-ey	Halder et al., 1995
UAS-yki	Staley and Irvine, 2010
UAS-Flag-HA-tsh	Synthesized by C.M. Luque *
UAS-Flag-HA-hth	Synthesized by C.M. Luque *
UAS-GFP-Bap60	This work
UAS-TkvQD [§]	Nellen et al., 1996
UAS-Punt	Nellen et al., 1996
UAS-Dad.T	Tsuneizumi et al., 1997
UAS-Dpp.S	Staehling-Hampton et al., 1994
UAS-S-Hr46 [#]	Gift from Jacques Montagne
UAS-Hr46-RB	Gift from Jacques Montagne
UAS-αftzF1	Gift from Rosa Barrio
UAS-βftzF1	Gift from Rosa Barrio
UAS-EcRB1^{W650A} [‡]	Gift from Lilach Gilboa
UAS-EcRB1	Gift from Alberto Ferrús
UAS-Rbf^{280} [¥]	Xin et al., 2002
UAS-Ci	Alexandre et al., 1996
UAS-Hh	

* formerly at the Casares laboratory, currently at Universidad Autónoma, Madrid, Spain

§ activated form

Zn-finger truncated

‡ dominant negative

¥ constitutively active form

Another technique that can be used in combination with the GAL4/UAS system is the RNA interference (RNAi) technique. This technique allows gene-specific silencing using an endogenous cellular mechanism and double-stranded

RNAs that target the degradation of specific messenger RNAs (Fire et al., 1998; Kennerdell and Carthew, 1998).

In the table below we listed the UAS-RNAi lines used during this work.

Table M.3. UAS-RNAi lines.

UAS-RNAi lines	Origin
UAS-Bap60RNAi	VDRC #12675
UAS-Bap60RNAiKK	VDRC #103634
UAS-sflRNAi	Trip #34601
UAS-TkvRNAi	VDRC #3059
UAS-puntRNAi	VDRC #37279
UAS-Hr46RNAi	VDRC #12044
UAS-Hr46RNAi	VDRC #20157
UAS-Hr46RNAi	VDRC #106837
UAS-Hr46RNAi	Gift from Jacques Montagne
UAS-ftzf1RNAi	VDRC #2959
UAS-ftzf1RNAi	VDRC #104463
UAS-ftzf1RNAi	Trip #33625
UAS-moiraRNAi	VDRC #110712
UAS-ykiRNAi	Gift from Florence Janody
UAS-poloRNAi	VDRC #20177
UAS-RbfRNAi	VDRC #102159
UAS-hhRNAi	Trip #31042

As previously mentioned, the other binary transcriptional system used was the lexA/lexO system (Yagi et al., 2010). As the GAL4/UAS system, this system also functions through two components: the lexA transactivator, which is a transcriptional activation domain that induces the expression of a bacterial transcription factor and the lexA operator (lexO), where lexA binds to drive expression of the downstream transgene (Yagi et al., 2010). In this study, two lines were used:

Table M.4. lexA/lexO lines.

lexA/lexO lines	Origin
dpp-LHG86Fb	Yagi et al., 2010
lexO-eGFP::Dpp	Yagi et al., 2010

The use of two independent binary transcriptional systems is particularly essential and relevant when multiple genetic manipulations are required simultaneously.

Finally, two types of reporter lines were used: transcriptional reporters and protein traps.

Transcriptional reporters allow the description of the transcriptional status of a gene. Reporters consist of a reporter gene (for instance, the *lacZ* gene from *E.coli*) fused to a weak promoter. This promoter is not able to induce the expression of the reporter gene unless there is a nearby enhancer (O'Kane and Gehring, 1987). This fusion is randomly inserted in the genome or directly fused to a known enhancer, allowing the detection of an enhancer's activity.

Protein traps allow the characterization of protein expression patterns during development and are usually obtained through the insertion in the correct orientation (and correct reading frame) of a transposable element containing a fluorescent marker into an intron between protein-coding exons (Lowe et al., 2014).

Table M.5. Reporter lines.

Reporter lines	Origin
eya-lacZ *	Katsuyama et al., 2005
dpp-lacZ	Masucci et al., 1990
tkv-lacZ	Tanimoto et al., 2000
EcRE-lacZ	Bloomington #4517
hth-lacZ l(3)06762	Rieckhof et al., 1997
dally-lacZ	Nakato et al., 1995
hh-lacZ	Bloomington #5530
hth-YFP	CPTI-001356; Flannotator

* enhancer trap on *eya* gene, reflects endogenous expression of eya

In order to obtain *optix>hth+tsh* flies we used two strategies: either we crossed the optix2.3-GAL4 driver to *UAS-Flag-HA-tsh;UAS-131-GFPhth* flies or used a stable *optix2.3-GAL4,UAS-Flag-HA-tsh;UAS-131-GFPhth/SM6^TM6B* stock. We observed that the phenotypes in eye discs, adult eyes and pMad profiles were stronger in individuals from the cross.

For RNA-seq and FAIRE-seq experiments, *optix>hth* and *optix>tsh* larvae were collected from *optix2.3-GAL4* to *UAS-GFP:hth* or *UAS-HA:tsh* crosses. *optix>GFP:hth+tsh* larvae were obtained directly from a *optix2.3-GAL4,UAS-Flag-HA-tsh;UAS-131-GFPhth/SM6^TM6B* stock ("hth+tsh_stock"; biological replicate #1) or derived from the cross of *optix2.3-GAL4 to UAS-Flag-HA-tsh; UAS-GFP:hth* ("hth+tsh_cross"; biological replicate #2). As FAIRE-seq control we used the data sets previously obtained in Stein Aerts' laboratory using two reference strains, Oregon-R (wild type) and *FRT82B*.

Adult flies were observed under a LEICA MZ 9.5 stereomicroscope and pictures of adult heads from each genotype were taken with a LEICA DFC320 digital camera.

2. Clonal analysis

Random ectopic expression clones were generated using the Flip-out method (Struhl and Basler, 1993) combined with the GAL4/UAS system. This method was created using the basis of the FLP/FRT (Flipase/FLP recognition target) system. This system consists in the excision by flipase-mediated recombination of a FLP-out cassette – a DNA segment flanked by FRT sequences. This cassette prevents transgene expression before recombination through the presence of a transcriptional termination site. After flipase induction, in our study using a heat-shock promoter, the FLP-out cassette is removed allowing the fusion of the promoter to the coding sequence of the transgene (Struhl and Basler, 1993).

yw, hs-FLP122, act>y+>Gal4;; UAS-GFP/TM6B females were crossed to *UAS-yki*, *UAS-Flag-HA-tsh*, *UAS-131-GFPhth* or *UAS-Flag-HA-tsh;UAS-131-GFPhth* males. Clones were induced by heat shock (20 minutes at 37°C) between 48 hours and 72 hours AEL (after egg laying) and then maintained at 25°C. Clones were positively marked with GFP.

Bap60 knockdown clones were induced by heat shock (1 hour at 37°C) at 48 hours AEL in larvae of the genotype: *y w hsflp*^{122}/+; *act*>y+>Gal4, UAS-GFP/+; UAS-*Bap60*RNAi/+.

For the combination of Gal4/UAS and lexA/lexO systems, yw, hs-FLP122, act>hsCD2>Gal4;UAS-FLAG-HA-hth;lexO-eGFP:Dpp females were crossed to UAS-FLAG-HA-tsh;dpp-LHG86Fb males. Flip-out clones were induced by heat shock (10 minutes at 35,5ºC) between 72 hours and 96 hours AEL and then maintained at 25ºC. Clones were stained with anti-HA and Dpp with anti-GFP.

3. Immunostaining

Larvae were dissected in cold Phosphate Buffer Saline (PBS) and kept on ice. Afterwards, imaginal discs were fixed in 3,7% formaldehyde (in PBS) during 20 minutes at room temperature.

After fixation, discs were washed in PBT 0,1% (PBS with 0,1% of Triton-X100) during 30 minutes (3 washes of 10 minutes each) and immunostained with the primary antibodies in PBT 0,1%. The immunostaining step was maintained for 2 hours at room temperature or overnight at 4ºC. The primary antibodies and the final concentration used are listed below.

Table M.6. Primary antibodies.

Antibody	Host Species	Concentration	Origin
Arm	mouse	1:100	DSHB (N27A1)
aPKC	rabbit	1:500	Sta Cruz Biotechnology
ßGal	mouse	1:1000	Sigma
ßGal	rabbit	1:1000	Cappel
Cas3*	rabbit	1:200	Cell Signaling
Ci	rat	1:5	DSHB (2A1)
CycA	mouse	1:10	DSHB (A12)
CycB	mouse	1:100	DSHB (F2F4)
CycE	mouse	1:20	Helena Richardson
Dacapo	mouse	1:4	DSHB (NP1)

Antibody	Host Species	Concentration	Origin
Dlp	mouse	1:5	DSHB (13G8)
ELAV	rat	1:1000	DSHB (7EBA10)
Ey	mouse	1:400	P. Callaerts
Eya	mouse	1:100	DSHB (10H6)
GFP	mouse	1:1000	Molecular Probes
HA	rabbit	1:1000	Abcam (9110)
HA	rat	1:500	Roche
Hr46	rabbit	1:50	Carl S. Thummel
Hth	guinea pig	1:3000	Casares and Mann, 1998
Hth	rabbit	1:5000	N. Azpiazu
PH3	rabbit	1:1000	Sigma
pSmad3 ‡	rabbit	1:100	Epitomics
Ptc	mouse	1:100	DSHB (Apa1)

‡ used to detect *Drosophila* phosphorylated-Mad (pMad) because of its crossreactivity

Discs were then washed in PBT 0,1% during 30 minutes (3 washes of 10 minutes each) and incubated with the secondary antibodies in PBT 0,1% for one and a half hours at room temperature. A list of secondary antibodies and the final concentration used is shown below.

Table M.7. Secondary antibodies.

Antibody	Concentration	Origin
Alexa-Fluor conjugated	1:1000	Molecular Probes
Rhodamine phalloidin	1:400	Molecular Probes (R415)

Finally, discs were washed in PBT 0,1% during 30 minutes (3 washes of 10 minutes each) at room temperature and stored in 50% glycerol (in PBS) at 4ºC.

Images were acquired with Laser Scanning Confocal Microscope Leica SP2 AOBS and processed with ImageJ and Adobe Photoshop.

4. Scanning electron microscopy (SEM)

Adult female flies were collected and transferred to 75% ethanol for 24 hours at room temperature. Flies were then dehydrated through an ethanol series – 80%, 90%, 95% and twice 100% – for 12-24 hours each step.

After dehydration, flies were air-dried and mounted onto SEM stubs covered with carbon tape and sputter coated with gold, using an Edwards Six Sputter. Samples were imaged using a JEOL 6460LV scanning electron microscope.

5. RNA-Seq

Late third instar larvae were dissected in cold PBS on ice. For each experiment, 25 larvae were dissected to finally extract 50 eye-antennal imaginal discs.

RNA was extracted using the RNAqueous-Micro Kit from Ambion following the standard protocol. RNA quantity was measured with Qubit and RNA quality was checked using Agilent RNA 6000 Nano Kit.

RNA libraries were prepared for sequencing using a standard Illumina TruSeq protocol.

Libraries were validated quantitatively (Qubit) and qualitatively using an Agilent DNA 1000 Kit (Agilent Technologies 2100 Bioanalyzer).

6. FAIRE-Seq

For each experiment, 100 eye-antennal imaginal discs from late third instar larvae were dissected in cold PBS.

First, imaginal discs were fixed with formaldehyde and lysed. The eye-antennal discs were then uncrosslinked and immediately sonicated using a Bioruptor UCD-200 (Diagenode).

DNA purification was performed by phenol chloroform extraction using MaXtract High Density Kit from QIAGEN following the standard protocol and after that DNA was precipitated. DNA concentration was measured with Qubit.

DNA libraries were prepared for sequencing using a standard protocol – end repair, adenylation, ligation of adapters and DNA fragments enrichment.

Libraries were validated quantitatively using Qubit and qualitatively using an Agilent High Sensitivity DNA Kit (Agilent Technologies 2100 Bioanalyzer).

7. RNA probe synthesis

A Bap60 digoxigenin (DIG)-labelled RNA probe was synthesised using the Bap60 GOLD clone LD09078 from DGRC (Drosophila Genomics Resource Center, Bloomington, IN).

DH5alpha competent cells were used to transform the Bap60 clone, applying the protocol described in Processing clones for Whatman FTA discs (McKillip E and Klueg K, 2006).

After transformation, plasmid DNA was purified with the QIAprep Spin Miniprep Kit from Qiagen and a microcentrifuge using the standard protocol (QIAprep Miniprep Handbook Protocols).

The restriction enzyme NotI was used to linearize the DNA, which was then purified by precipitation with ethanol, EDTA and sodium acetate.

Using the DIG RNA Labelling Kit (SP6/T7) from Roche, the RNA probe was synthesised with T7 RNA polymerase.

After synthesis, precipitation of the probe was done using LiCl and ethanol. The probe was then ressuspended in DEPC treated water.

8. *in situ* hybridization

Larvae were dissected in cold PBS, fixed in 3,7% paraformaldehyde (in PBS) during 20 minutes and refixed in 3,7% paraformaldehyde (in PBT) during 20 minutes, always at room temperature.

After fixation, discs were washed at room temperature in PBTween (PBS with 0,1% Tween) during 25 minutes (5 washes of 5 minutes each), in PBTween:Hybridization solution (1:1) during 5 minutes and in hybridization

solution during 5 minutes. Hybridization solution (HS) contains formamide, 20x SSC, salmon sperm DNA 10mg/mL, Tween20 (10%) and DEPC treated water.

Then, discs were prehybridized for 2 hours at 60°C in HS. The hybridization reaction was carried out overnight at 60°C with a hybridization mix (HS, single stranded DNA (4,6mg/mL) and labelled probe).

After incubation, discs were washed in HS during 20 minutes at 60ºC, in HS:PBT (1:1) during 20 minutes at 60ºC and finally, were washed in PBT during 1 hour (3 washes of 20 minutes each) at room temperature.

Afterwards, discs were incubated for 2 hours at room temperature with anti-digoxigenin antibody coupled to alkaline phosphatase (Roche Diagnostics) diluted 1:1000 in PBT. Excess antibody was removed by washing with PBT (a quick wash and then three washes of 20 minutes each) at room temperature.

Discs were then equilibrated for 10 minutes (two washes of five minutes each) at room temperature in AP Buffer (fresh solution containing 1M Tris pH 9,5, 1M $MgCl_2$, 4M NaCl, Tween20 (10%) and DEPC treated water).

Color development was performed at 37ºC (3 to 5 minutes) in AP Buffer containing NBT and BCIP.

Staining was stopped with PBT (two washes of 5 minutes each) at room temperature and then stored at 4ºC in 50% glycerol/PBS.

Discs were mounted in 50% glycerol/PBS and images were obtained with the Olympus BX50 microscope with a coupled digital camera (Olympus DP71).

9. Generation of UAS transgenic strains

The LD09078 cDNA was used to PCR amplified the *Bap60* ORF using the FideliTaq DNA polymerase (Affymetrix) and the primers 5'-CACCATGTCGCAACGCTTTG-3' and 5'-GCCGTTGCGTATGCCCAG-3'.

According to supplier's instructions, the amplified fragment was then cloned into pENTR/D-TOPO (Invitrogen).

Using the Gateway LR Clonase II enzyme mix from Invitrogen, the ORF was cloned by in vitro recombination into the pUASt-GFP vector (pTGW; a gift of T. Murphy, The Carnegie Institution of Washington, Baltimore, MD, USA).

Using standard germline transformation methods, several transgenic UAS-GFP:*Bap60* lines were generated and five independent lines were analyzed.

10. Quantification of $PH3^+$ cells

Third instar eye imaginal discs were stained with phospho-histone H3 (PH3), a mitosis-specific marker.

The area of interest of the eye disc was defined by creating a surface and the identification of $PH3^+$ cells followed two steps: first they were automatically identified and the manually curated.

Finally, the number of $PH3^+$ cells that fall within the created surface was detected. This analysis was made using the IMARIS x64 7.7.2 software.

The ratios between $PH3^+$ cells and the area of interest were calculated using Microsoft Excel and represented as dots, squares, triangles, plus or cross; the means were represented as horizontal bars.

The graphical output was generated using GraphPad Prism 6.0 or R. An ANOVA test was used to determine the statistical significance.

11. pMad expression profiles

optix>GFP, optix>131-GFPhth, optix>Flag-HA-tsh and *optix>131-GFPhth+Flag-HA-tsh* late third instar eye discs were stained simultaneously with anti-Arm and anti-pSmad3. *optix>GFP, optix,131-GFPhth+Flag-HA-tsh/TM6B and optix>131-GFPhth+Flag-HA-tsh+UASsflRNAi* third instar eye discs were stained with anti-pSmad3.

Confocal images were acquired on the same day after the laser intensity stabilization. The expression profiles were obtained using ImageJ. Signal intensity for anti-pSmad3 was measured in at least five independent discs. Measurements were taken ahead of the morphogenetic furrow, when present, or starting at the posterior margin of the disc when absent.

The mean profile of each set of profiles and the standard error of the mean were represented in arbitrary units using Microsoft Excel.

12. Adult eye phenotype scores

Adult flies from *optix>GFP*, *optix>131-GFPhth+Flag-HA-tsh+UAS-GFP*, *optix>131-GFPhth+Flag-HA-tsh+UAS-tkvRNAi*, *optix>131-GFPhth+Flag-HA-tsh+UAS-tkvQD* and *optix>131-GFPhth+Flag-HA-tsh+UASsflRNAi* were collected and several representative pictures of adult eyes (n=36-68) were obtained. Each phenotype was scored in a semi-quantitative manner by grouping the phenotype scores in phenotypic classes. These classes were defined as: flies with normal eyes (represented in green), flies with an mild reduction (represented in blue), flies with a severe eye reduction, comprising a small number of organized ommatidia (represented in orange), and flies with a total loss of retina (represented in red). Proportion of flies belonging to each class were represented.

4

RESULTS

PART I

Nuclear Receptors Connect Progenitor Transcription Factors To Cell Cycle Control

The programs for organ development are encoded in organ specification networks. In these networks, transcription factors tightly control the specification and proliferation of progenitor cells to ensure that the right types and amounts of cells are produced. Several organ specification networks have been described in detail in vertebrates and invertebrates (Amore and Casares, 2010; Peter and Davidson, 2011; Arda et al., 2013; Buckingham and Rigby, 2014; Cvekl and Ashery-Padan, 2014; Gottgens, 2015). However, how transcription factors act upon the cell cycle machinery to regulate progenitors proliferation is still poorly understood. To investigate this issue we have resorted to the developing *Drosophila* eye*,* for which a detailed transcriptional network is available (Amore and Casares, 2010; Kumar, 2010; Potier et al., 2014).

In the fly eye primordium, eye progenitors are specified by the co-expression of a set of transcription factors: the two *Drosophila* Pax6 genes *eyeless (ey)* and *twin of eyeless (toy),* the TALE-class homeodomain *homothorax (hth)* and the Zn-finger encoding gene *teashirt (tsh)* (Quiring et al., 1994; Bessa et al., 2002; Amore and Casares, 2010). This gene expression combination is transient: the undifferentiated, proliferative state of progenitors is maintained as long as they express *hth.* Accordingly, the forced maintenance of *hth* blocks retina differentiation. In its progenitor role, *hth* is known to interact with *tsh* (Bessa et al., 2002). One important aspect of this interaction is that it is synergistic. Maintenance of *hth* stalls differentiation, while maintaining *tsh* only causes a mild retinal differentiation impairment. However, maintaining the expression of both TFs ("hth+tsh") results in large tumour-like overgrowths formed by progenitor-like cells (Bessa et al., 2002; Peng et al., 2009). This suggests that hth+tsh together control the cell cycle machinery, directly or indirectly.

The synergistic growth-inducing ability of Hth and Tsh has been attributed, at least in part, to their direct protein interaction with Yki (Peng et al., 2009), the nuclear effector and transcriptional co-activator of the Salvador-Warts-Hippo tumour suppressor pathway (Pan, 2007). Only one direct transcriptional target of the Hth:Tsh:Yki complex has been functionally validated to date, though, the miRNA-encoding gene *bantam (ban)* (Peng et al., 2009). Even though *ban* is expected to have a rather pleiotropic effect (Nolo et al., 2006; Thompson and Cohen, 2006), on its own it does not account for the large overgrowths induced by Hth:Tsh:Yki. Therefore, we still lack a global picture of the transcriptional changes specifically induced by *hth* and *tsh* and how these are connected to tissue growth.

Here we have analysed the global impact that hth+tsh have on the developing eye to establish links between these transcription factors and target genes, using genome-wide gene expression and open chromatin profiling, together with computational methods.

Perturbations of progenitor transcription factors result in tissue overgrowth

During development, the expression of eye progenitor transcription factors is transient to allow cell cycle stop and differentiation. However, the forced maintenance in the eye disc of two of these transcription factors simultaneously, *hth* and *tsh*, cause the overgrowth of progenitor-like cells (Bessa et al., 2002; Peng et al., 2009).

To analyse how the forced maintenance of Hth+Tsh affects tissue growth we expressed hth and tsh, either alone or in combination, using the eye-specific GAL4 driver *optix2.3-GAL4*, which is active in the undifferentiated cells of the eye primordium (Figure R1.1 and Figure R1.2, Ostrin et al., 2006). Using this driver we made sure that the observed effects reflect effects on the undifferentiated population of cells.

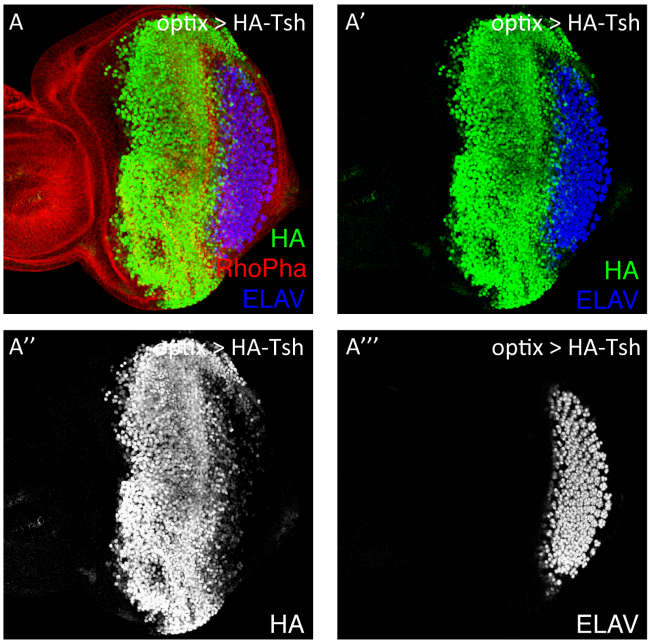

Figure R1.1. The *optix2/3-GAL4* line (*"optix>"*) drives expression in undifferentiated cells anterior to the morphogenetic furrow (MF). *optix2/3-GAL4; UAS-HA:tsh ("optix>HA:tsh")* L3 eye disc, stained for actin (Rhodamine-phalloidin, to outline tissue shape, red), HA, which tags *tsh* (green) and the photoreceptor marker Elav (blue). Anterior is left, dorsal is up (this orientation will be maintained throughout). Most of the HA:tsh driven by *optix2/3-GAL4* is detected anterior to the MF (line in A).

The forced maintenance of *hth* or *tsh* alone (*optix> hth* or *optix>tsh*) did not produce overproliferation. In optix>GFP:hth individuals, eye differentiation was impaired, resulting in smaller eye discs and adult retinas (Figure R1.2A,B). In optix>tsh, discs and eyes were slightly reduced in size, but retinal morphology was normal (Figure R1.2A,C).

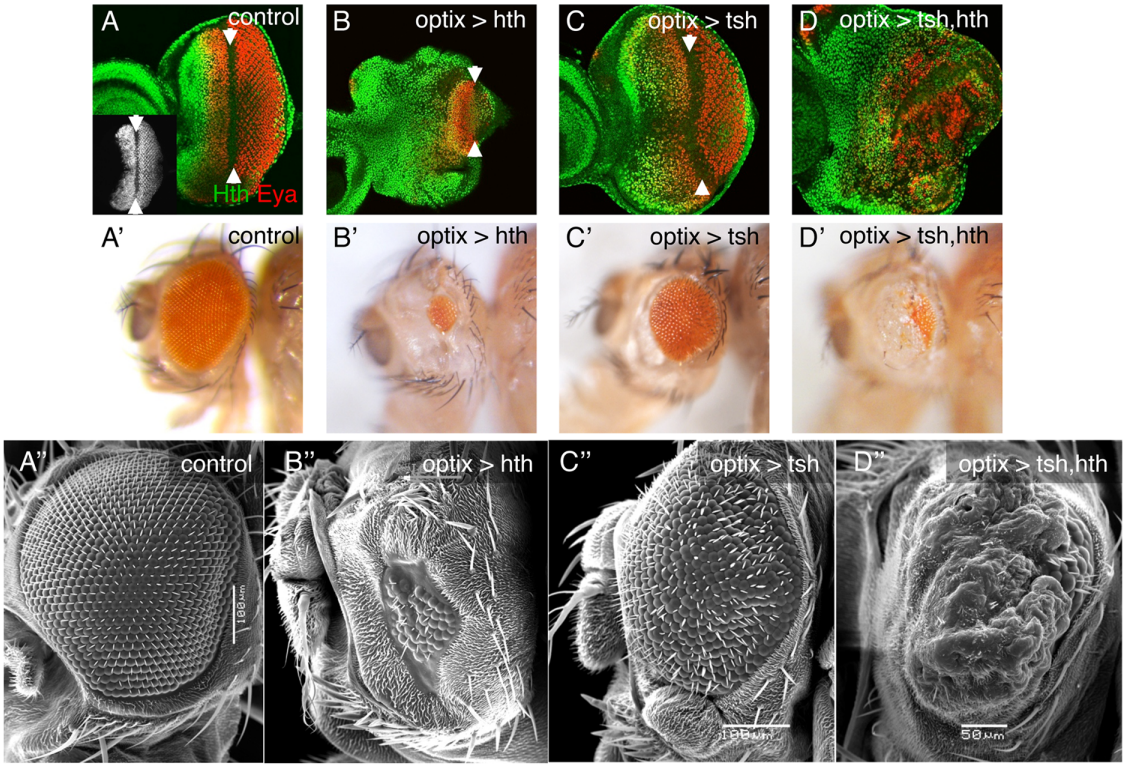

Figure R1.2. Forced maintenance of *hth and tsh* expression results in overgrowth and differentiation arrest. Late third instar (L3) eye discs (A-D) and adult heads (A'-D' and A''-D'') from control (*optix>GFP*) and hth- (*optix>hth*), tsh- (*optix>tsh*) or hth+tsh- (*optix>hth+tsh*) expressing animals. The GFP expression driven by *optix>* (*optix2/3-GAL4; UAS-GFP*) is shown in the inset in (A). Discs are stained with anti-Eya and anti-Hth. (A'–D') Lateral views of adult heads of the same genotypes as above. (A''–D'') SEM images of lateral views of adult heads of the corresponding genotypes. Overexpression of *hth* (*optix*>hth) results in a reduced eye disc area and smaller adult eye (B-B''). *tsh*-overexpressing flies (*optix*>tsh) show almost normal discs and retinal morphology (C-C''). However, forced maintenance of hth and tsh (*optix>hth+tsh*), results in overgrown eye discs showing abnormal folds. Adult heads develop a small retinal patch and an overgrowth of indistinct cuticle (D-D'').

In contrast, forced maintenance of both transcription factors (*optix> hth+tsh*) gave rise to disc overgrowths and to adult heads with a small patch of retinal tissue surrounded by overgrown indistinct cuticle (Figure R1.2A,D).

To be considered as a malignant transformation, this phenotype should be accompanied by modifications in epithelial polarity that ultimately would lead to a metastatic behaviour of these cells. To check if this was indeed the case, larvae of this genotype were checked for GFP under the scope and no GFP was found outside of the eye discs.

Furthermore, staining for aPKC (an epithelial polarity marker) shows no differences between control and *hth+tsh*-expressing discs (Figure R1.3).

All these results point to a premalignant situation where cells are able to proliferate more, but are not able to metastasize and invade other tissues.

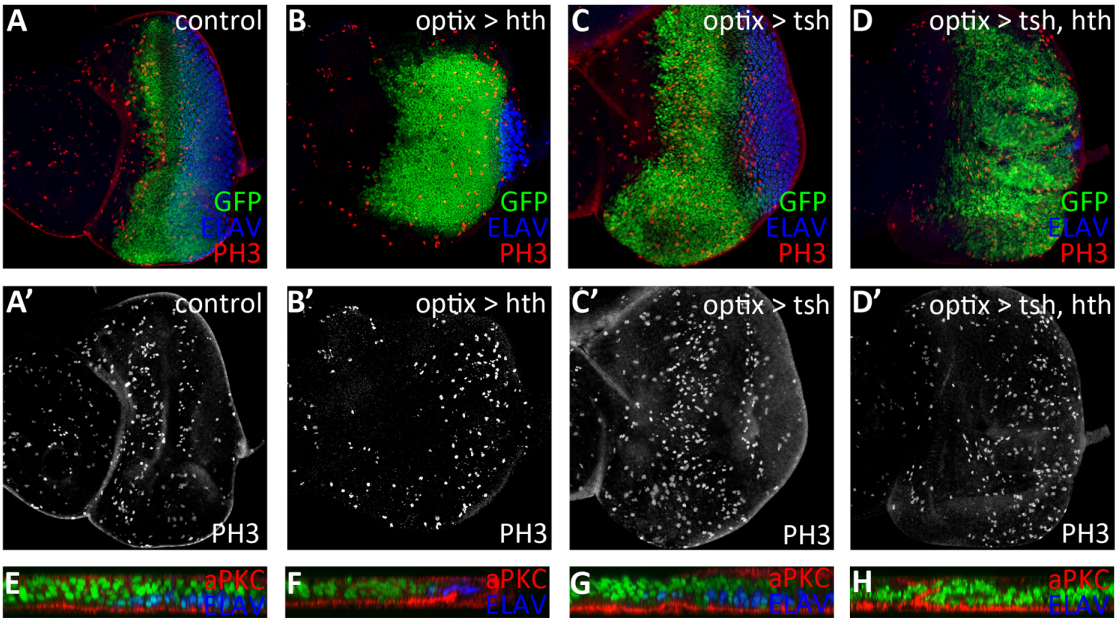

Figure R1.3. hth+hsh do not affect epithelial polarity. Late third instar (L3) eye discs from (A,A') control (*optix>GFP*), (B,B') hth- (*optix>hth*), (C,C') tsh- (*optix>tsh*) or (D,D') hth+tsh- (*optix>hth+tsh*) expressing flies stained with anti-ELAV (blue) and anti-PH3 (red). Optical cross-sections of (E) control (*optix>GFP*), (F) hth- (*optix>hth*), (G) tsh- (*optix>tsh*) or (H) hth+tsh- (*optix>hth+tsh*) eye discs stained with anti-ELAV (blue) and anti-aPKC (red). Forced maintenance of hth+tsh results in increased proliferation, but does not affect epithelial polarity.

Cell cycle genes and nuclear receptors are altered downstream of Hth+Tsh

To obtain a global view of the impact of the co-expression of Hth and Tsh on gene expression, we obtained the transcriptional profiles of late third larval stage eye discs from control (optix>GFP), hth-expressing (optix>hth), tsh-expressing (optix>tsh), and hth+tsh-expressing (optix> hth+tsh) larvae using RNA-seq (Table C.1).

Principal component analysis of the RNA-seq data (Figure R1.4A) showed that *optix>tsh* clustered closest to the control, in agreement with its weak phenotype. o*ptix>hth* and the two *optix>hth+tsh* replicates were clearly distinguished.

When the differential gene expression (DE) between the *optix>hth+tsh* and control samples was analysed, the majority of DE-genes were down-regulated (Figure R1.4B). GO-enrichment analysis of the 503 significantly down-regulated genes (p.adj<0.05 and log fold change(FC)<-1) identified "generation of neurons" and "compound eye photoreceptor cell differentiation" as enriched terms (Figure

R1.4C), in agreement with the vestigial retina that develops in *optix>hth+tsh* adults.

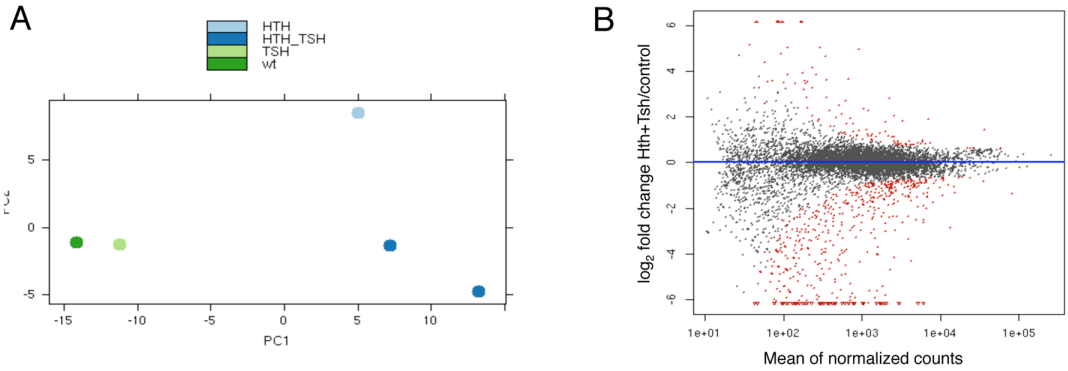

C ***Hth+Tsh down-regulated genes***

Gene Ontology Term	P-adjusted
Generation of neurons	*2.23E-28*
Nervous system development	*2.96E-21*
Signaling	*6.31E-21*
Cell communication	*1.78E-20*
System development	*3.87E-19*
Axon development	*8.49E-19*
Anatomical structure morphogenesis	*6.06E-18*
Compound eye photoreceptor cell differentiation	*3.40E-17*
Cell projection organization	*9.85E-17*

D ***Hth+Tsh up-regulated genes***

Gene Ontology Term	P-adjusted
DNA-dependent DNA replication	*5.82E-14*
DNA metabolic process	*1.13E-07*
Nuclear cell cycle DNA replication	*2.93E-07*
Cell cycle	*3.05E-05*
Single organism organelle organization	*8.82E-05*
Mitotic cell cycle process	*0.00048*
Pyrimidine deoxyribonucleotide metabolic process	*0.00137*
Cytoskeleton organization	*0.00191*
Meiotic cell cycle process	*0.00241*

Figure R1.4. RNA-seq profiling of hth+tsh cells. (A) Principal Component analysis of the RNA-seq data from the five samples used. The analysis highlights the similarity of optix>tsh ("TSH") to the control, optix>GFP ("WT"), and between the two optix>hth+tsh biological replicates. optix>hth stands out as a different set. (B) MA-plot representing the log2 fold gene expression change of optix>hth+tsh over optix>GFP ("control") (y-axis), versus the abundance (x-axis). Red dots are differentially expressed genes. (C,D) Selected GO terms associated to genes that are down-regulated (C) or up-regulated (D) in optix>hth+tsh compared to the control optix>GFP.

On the other hand, among the functions associated to the 103 upregulated genes (p.adj<0.05 and logFC>1) were those related to "cell cycle" and "DNA replication" (Figure R1.4D), which agree with the overgrowths observed in optix>hth+tsh eye discs.

In order to test how hth+tsh cells affect the cell cycle regulation, we generated hth+tsh-expressing clones and examined the expression of different cell cycle markers: G2/mitotic cyclin-A, cyclin-dependent kinase inhibitor Dacapo and G1/S-phase cyclin E. As expected from our overgrown phenotype, hth+tsh cells are able to induce cyclin A and cyclin E expression and also to repress Dacapo expression (Figure R1.5).

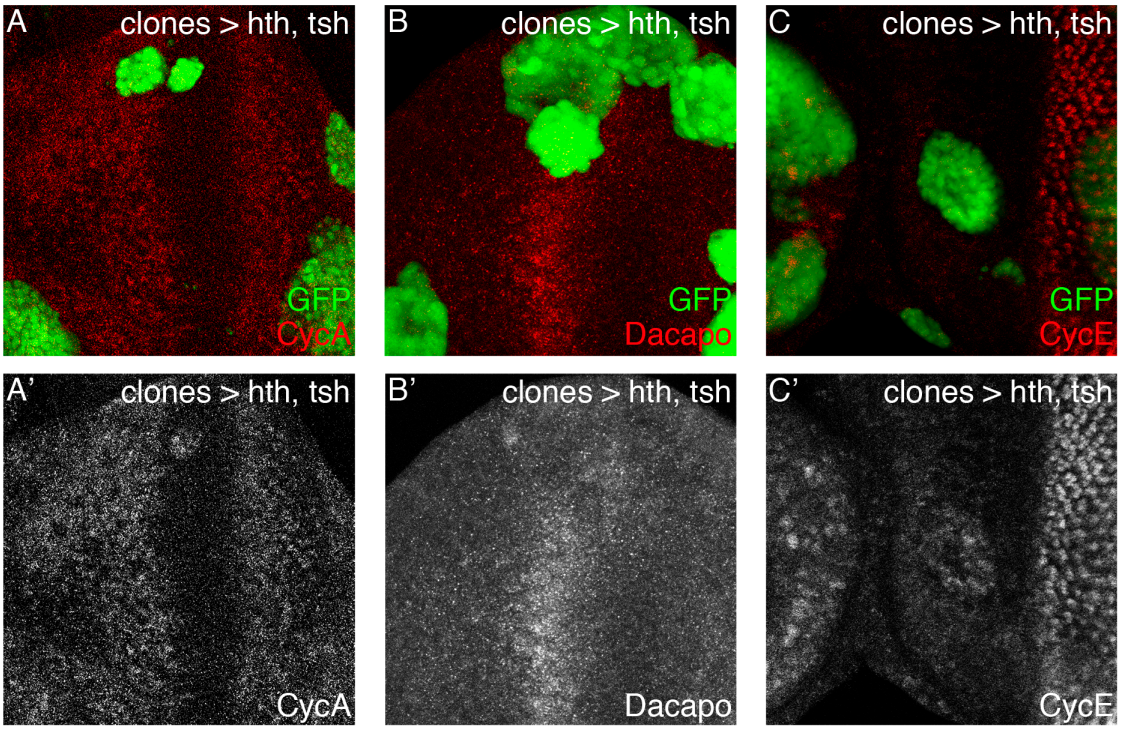

Figure R1.5. Co-expression of hth+tsh regulates the expression of cell cycle-related genes. GFP-marked clones overexpressing *hth+tsh* were induced in the eye imaginal disc at 48-72 hours after egg laying. Discs are stained with (A,A') anti-CycA, (B,B') anti-Dacapo and (C-C') anti-CycE (red). *hth+tsh*-expressing clones activate CycA and CycE expression and repress the expression of Dacapo.

If instead of analysing the set of 103 upregulated genes we consider the entire gene rank, the effect is even stronger. In this case, 74 cell cycle genes were recovered in the top 770 genes (p.adj 10^-32) (Figure R1.6A). When taking the 74 cell cycle genes and organizing them in a heatmap, we observed that their upregulation is a consequence of the hth+tsh synergistic effect rather than the action of hth or tsh alone (Figure R1.6B). Among these genes we found key cell cycle regulators, such as *polo* kinase, *dp53*, *Rbf* and *Rbf2* (Figure R1.6B).

Next, we looked for transcription factor binding site motif enrichment in the vicinity of differentially expressed genes using i-*cis*Target (Herrmann et al., 2012; Potier et al., 2012) (See Annex A) as a way to identify the transcription factors that may control directly these differentially expressed genes and to define potential regulatory relationships among them. Down-regulated and up-regulated genes showed different motif enrichment (Figure R1.6C and Figure R1.7).

A

GO Term	Description	FDR q-value	Enrichment
GO:0022402	cell cycle process	1.93E-32	2.85
GO:1903047	mitotic cell cycle process	1.46E-31	2.66
GO:0007052	mitotic spindle organization	1.18E-31	3.67
GO:0007051	spindle organization	6.94E-29	3.39
GO:0034645	cellular macromolecule biosynthetic process	1.84E-27	2.61
GO:0006259	DNA metabolic process	3.81E-24	4.05
GO:0000226	microtubule cytoskeleton organization	9.73E-24	3.47
GO:0009059	macromolecule biosynthetic process	8.94E-24	2.41
GO:0006260	DNA replication	6.82E-21	15.82
GO:0022008	neurogenesis	3.93E-20	2.28
GO:0006412	translation	1.12E-19	3.16
GO:1902589	single-organism organelle organization	1.42E-19	2.29
GO:0043933	macromolecular complex subunit organization	4.97E-19	2.33
GO:0007017	microtubule-based process	5.62E-18	2.87
GO:0006996	organelle organization	5.25E-17	2.01
GO:0007010	cytoskeleton organization	5.44E-17	2.7
GO:0051297	centrosome organization	7.27E-17	4.43
GO:0051298	centrosome duplication	1.05E-16	5.63
GO:0031023	microtubule organizing center organization	4.23E-16	4.28
GO:0090304	nucleic acid metabolic process	6.20E-16	1.84

B

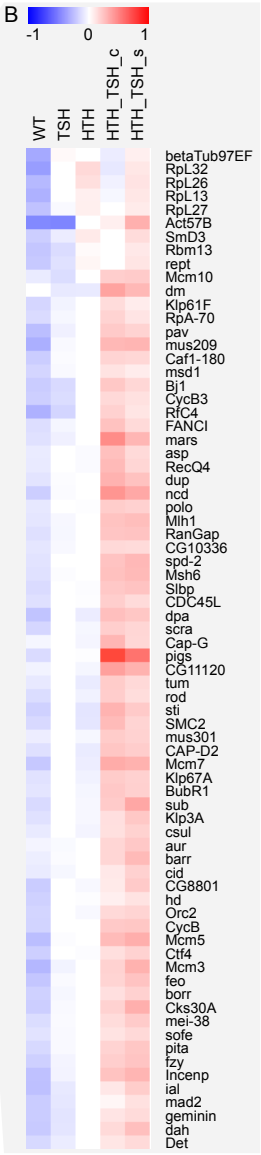

C

Cluster Rank	NES	Best motif logo	Best motif name	Candidate TFs
1	6.3		yetfasco-2051	bHLHs: Met, Max, tai, tgo ...
2	5.3	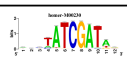	homer-M00230	Dref
4	4.6	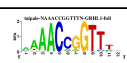	taipale-NAAACCGGTTTN-GRHL1-full	grh
5	4.4	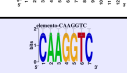	elemento-CAAGGTC	NRs: Ftz-f1, ERR , Hr39 ...
6 & 7	4.2	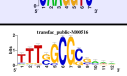	transfac_public-M00516	E2f, E2f2, Dp
9	3.9	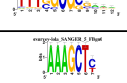	flyfactorsurvey-lola_SANGER_5	lola
10	3.7	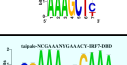	taipale-NCGAAANYGAAACY-IRF7-DBD	Blimp-1
Not found	<2.5	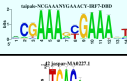	jaspar-MA0227.1	hth

D

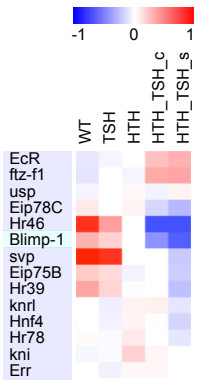

Figure R1.6. Transcriptomic profile of hth+tsh cells. (A) Gene Ontology enrichment of genes up-regulated in hth+tsh compared to control eye discs (EA). Analysis performed by GOrilla (Eden et al., 2009) on a ranked list of genes sorted by (signed) –log10(p-value). The sign indicates that up-regulated genes are on top (logFC>0) and down-regulated genes (logFC<0) are on the bottom of the list. (B) Heatmap with row-normalized expression values of the most significantly up-regulated cell-cycle related genes. (C) Motif enrichment on the up-regulated genes (770 genes, selected as the "leading edge" of the GOrilla analysis for cell cycle enrichment). Enrichment analysis is performed by i-cisTarget (Herrmann et al., 2012) and enriched motifs are clustered within i-cisTarget using STAMP. NES = Normalized Enrichment Score (>2.5 is significant). The Hth motif was not found enriched. (D) Heat map of expression profiles of motif related Nuclear Receptor genes and Blimp-1, showing strongest up-regulation of EcR and ftz-f1, and strongest down-regulation of Hr46 and Blimp-1.

Potential binding sites for E-box (top-enriched motif with a NES score of 4.73) and Glass (Gl) (motif also enriched with a NES score of 3.16) were found associated to down-regulated genes (Figure R1.7). E-box-binding bHLH proteins

Hairy, Daughterless, Emc and E(spl)-family members are known to participate in the specification of retinal precursors, regulating, among other genes, *atonal,* another bHLH transcription factor required for the specification of the R8 founder photoreceptor precursor (Brown et al., 1995; Jarman et al., 1995; Ligoxygakis et al., 1998; Tanaka-Matakatsu and Du, 2008; Bhattacharya and Baker, 2011); *gl* encodes a five Zn-finger transcription factor required for the development of all photoreceptors (Moses et al., 1989). These results were expected, since hth+tsh cause a shutting off of the retinal developmental program.

Motif Rank	NES	LOGO	Motif	Candidate TF
1	4.73316		transfac-pro-M00712	nau, da, ato, amos, cato
8	3.16512		flyfactorsurvey-gl_SANGER_5_FBgn0004618	gl
18	2.90881		jaspar-PB0046.1	myb

Figure R1.7. i-cis-Target predicted transcription factor binding site motifs associated with the down-regulated genes. Enrichment analysis is performed by i-cisTarget (Herrmann et al., 2012) and enriched motifs are clustered within i-cisTarget using STAMP. NES = Normalized Enrichment Score (>2.5 is significant).

Up-regulated genes showed enrichment in potential binding sites for a bHLH TF (possibly Taiman), and for the general transcriptional co-factors Dref (Hirose et al., 1996) and Grainyhead (Venkatesan et al., 2003). Additionally, motifs for E2F and nuclear hormone receptors are also strongly enriched, including EcR (Ecdysone receptor), ERR (estrogen-related receptor), ftz-f1, Hr46/DHR3 or Hr39 (Figure R1.6C). E2F is necessary for normal proliferation and DNA synthesis (Frolov and Dyson, 2004; Baonza and Freeman, 2005; Firth and Baker, 2005) and the enrichment in E2F potential target gene might reflect the vigorous proliferation of hth+tsh cells.

At this point, the enrichment of binding sites for nuclear hormone receptors of the EcR pathway in up-regulated genes was unexpected and suggested that a

critical subset of the up-regulated genes could be under the direct control of nuclear hormone receptors.

The finding of EcR/nuclear receptor-related motifs led to the investigation of the expression profile of the members of the EcR signalling cascade differentially expressed specifically in *hth+tsh* cells (Figure R1.6D). These included the nuclear receptors EcR and ftz-f1 (up-regulated) and the nuclear receptor Hr46/DHR3 and the transcriptional repressor Blimp-1 (down-regulated), this latter is also a regulator of the ecdysone pathway (Thummel, 2001). We noted that this pattern of nuclear receptor gene expression, characterized by high *EcR/ftz-f1* and low *Hr46/Blimp-1,* is typical of a low activity of the pathway (Woodard et al., 1994; Thummel, 2001; Agawa et al., 2007; Herboso et al., 2015). Indeed, activity of the ecdysone pathway in late third instar eye discs, monitored using an Ecdysone Response Element-lacZ (EcRE-Z (Koelle et al., 1991), can be observed straddling the morphogenetic furrow, but not in more anterior regions, where the hth+tsh-expressing progenitor cells reside (Figure R1.8; Brennan et al., 1998).

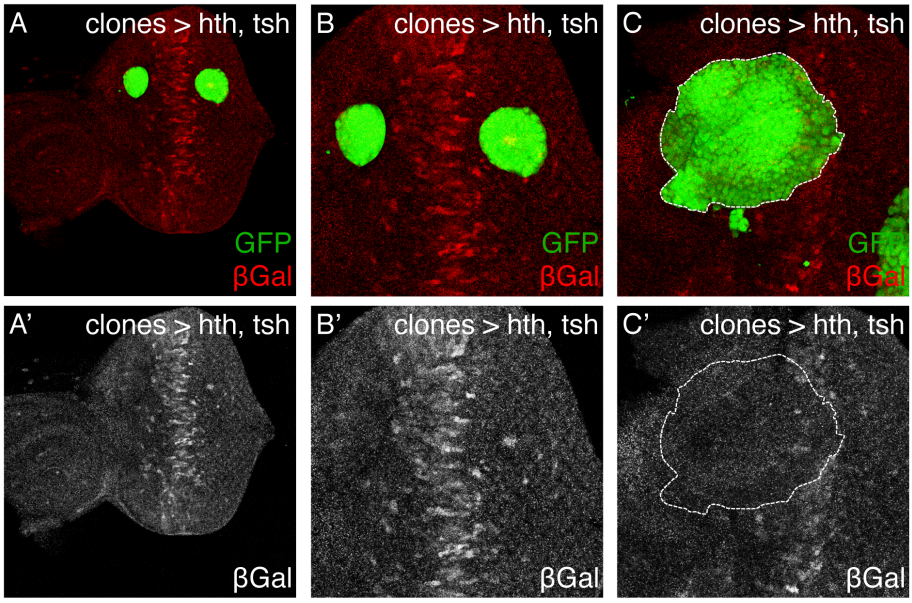

Figure R1.8. Co-expression of hth+tsh downregulate EcR signaling. hth+tsh-expressing clones (marked with GFP) induced in an Ecdysone Response Element-*lacZ* (EcRE-Z) background analyzed in L3 eye discs. *lacZ* expression is monitored with an anti-β galactosidase antibody (β gal). EcRE-Z is expressed straddling the morphogenetic furrow (dashed line) exclusively (A,A'). hth+tsh-clones overlapping the EcRE-Z domain repress its expression (B), while clones elsewhere do not (A,A'). (A) is a lower magnification view of the disc shown in (A') where the whole pattern of EcRE-Z can be seen. The EcRE-Z signal is shown separately in the lower panels.

To test whether hth+tsh could reduce ecdysone signalling, we generated hth+tsh-expressing clones in an EcRE-Z background. Clones that span the MF showed reduced EcRE-Z activity, while clones located elsewhere did not modify this reporter's activity (Figure R1.8A-C). Therefore, co-expression of hth+tsh is able to downregulate in a cell autonomous manner the response of cells to ecdysone signalling.

Interestingly, we did not find an enrichment of Hth binding site (BS) motifs among the collection of hth+tsh DE genes (Figure R1.6C; TGACA; http://pgfe.umassmed.edu/ffs/TFdetails.php?FlybaseID=FBgn0001235; note that a Tsh binding motif has not yet been described). This fact could be explained by either one of two possibilities. First, Hth might bind to regulatory regions of many DE genes, but using a non-canonical BS. We find this unlikely, because all available experimental evidence (bacterial-1-hybrid in *Drosophila*, ChIP-seq in mouse, SELEX, protein binding microarrays, and manual curation) has retrieved the same binding motif for Hth/MEIS in invertebrates and vertebrates: the monomeric motif TGTCA or the palindromic dimer motif TGACA_NN_TGTCA (Weirauch *et al.*, 2014). Neither of these two motifs was found enriched in the up- or down-regulated DE gene set. We further noted that the DE genes regulated by hth+tsh were not enriched in Hth binding sites previously identified using ChIP-seq (White *et al.*, 2008; Slattery *et al.*, 2013). Alternatively, Hth might bind using its canonical BSs, but only to a relatively small subset of DE genes (primary targets), which then would amplify Hth regulation through secondary (indirect) targets. In such a situation, motif enrichment procedures would not detect the Hth motif as significantly enriched. With this idea in mind, we looked for candidate direct targets by analysing activity changes in associated regulatory regions.

Open chromatin profiling confirms Nuclear Receptors as candidate regulators

Accessible chromatin regions are associated to active promoters and *cis*-regulatory elements (CREs). Therefore, we reasoned that changes in the activity of distal CREs overlapping Hth binding sites (from Hth-ChIP data), and located

near differentially expressed genes would point to Hth+Tsh direct targets. To this end, we carried out open chromatin profiling using FAIRE-seq (Giresi et al., 2007; Gaulton et al., 2010; Davie et al., 2015). Particularly, we compared the FAIRE-seq eye disc profiles of two control strains and *optix>hth*, *optix>tsh* and *optix>hth+tsh* (Table C.2 and Figure C.1). We identified relatively few CREs with significantly altered chromatin accessibility. This finding was rather unexpected because (1) the severe overgrowth phenotype and the large amount of differentially expressed genes suggested otherwise and (2) in another *Drosophila* model of eye overgrowth/cancer (induced by simultaneous expression of oncogenic *ras* and loss of *scribble)* dramatic chromatin changes have been described (Davie et al., 2015). Particularly, using stringent parameters, we identified only 86 FAIRE regions showing significantly increased accessibility when Hth+Tsh were co-expressed (log2(FC)>1 and (p-adj<0.05)), and 87 with significantly decreased accessibility (log2(FC)<1 (p-adj<0.05)). These regions were associated to differentially expressed genes (Table C.2). The regions with decreased accessibility are significantly associated with down-regulated genes (Figure R1.9A), mostly related to the loss of the differentiation program in the eye disc. On the other hand, only a handful of regions with increased accessibility are associated with down-regulated genes, of which *Hr46* and *Blimp-1* are the most prominent examples (Figure R1.9C,D). We did not find a significant association between peaks with increased accessibility and up-regulated genes (Figure R1.9B). We next used i-*cis*Target to identify transcription factor motifs within the FAIRE peaks showing increased accessibility, and again found Nuclear Receptor motifs (in this case the EcR motif is the strongest, see Figure R1.10), but did not identify the Hth motif as enriched in the set. However, the few CREs with increased accessibility located near the down-regulated genes *Hr46* and *Blimp-1*, showed overlapping or nearby ChIP-peaks for Hth (data from embryos (White et al., 2008) and eye discs (Slattery et al., 2013)), suggesting that Hth+Tsh may be directly repressing these nuclear receptor genes (Figure R1.9C,D). Interestingly, these peaks also overlap EcR binding sites (Figure R1.9C,D).

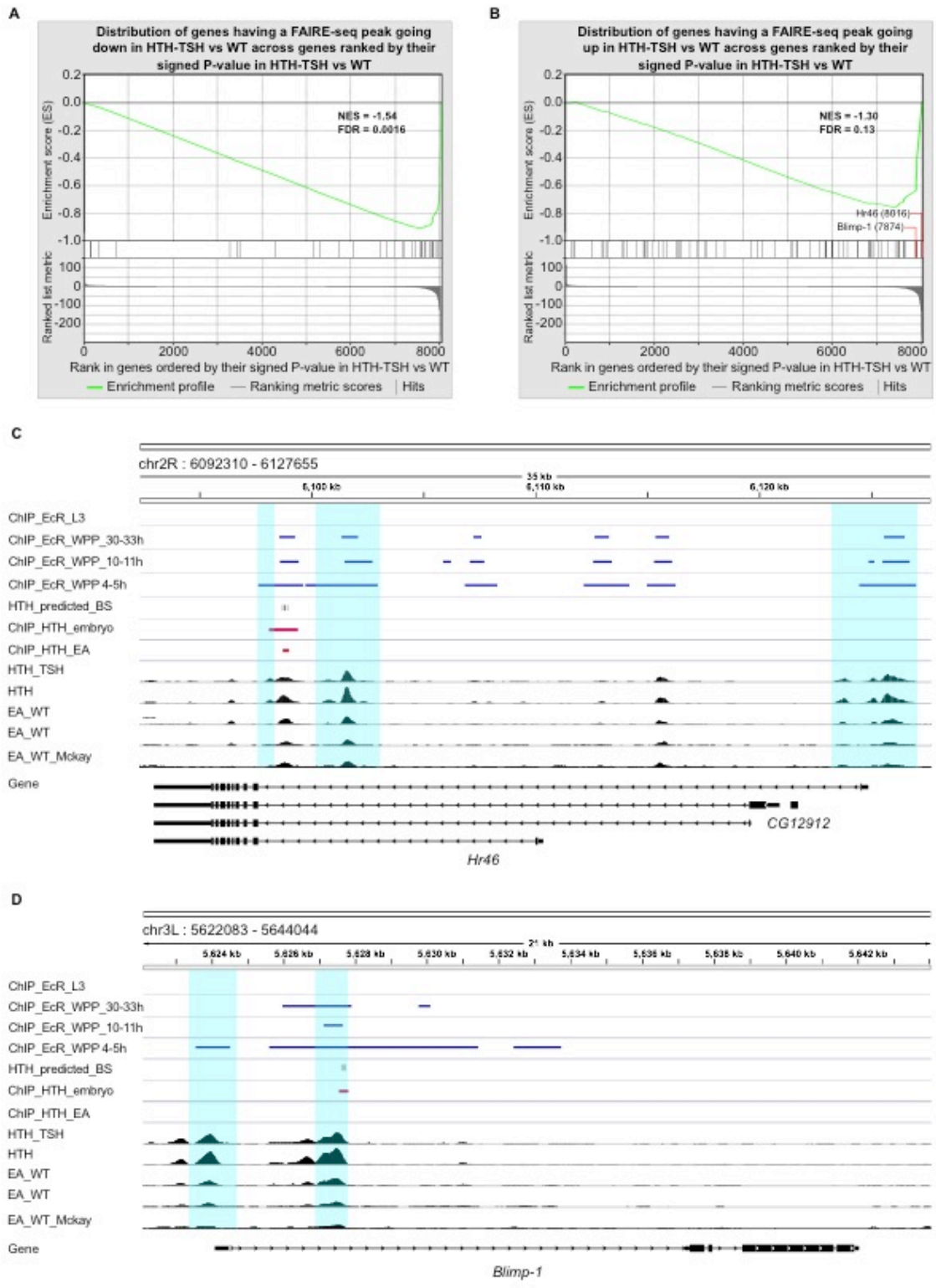

Figure R1.9. FAIRE-seq open chromatin profiling of hth+tsh cells. (A) Gene Set Enrichment Analysis (GSEA, (Subramanian et al., 2005)) compares gene expression changes with open chromatin changes. In the x-axis are all genes, ranked by the significance p-value of differential expression of control versus hth+tsh samples, with genes down-regulated in hth+tsh on the left, and genes up-regulated on the right. The tested gene sets (shown as black vertical lines) are genes with nearby (in 5kb upstream and intronic space) FAIRE-seq peaks showing significant *decreased accessibility*. The correlation between both is highly significant (FDR<0.001). (B) Similar plot, comparing changes in gene expression with genes showing nearby FAIRE-peaks with *increased accessibility*. In this case, the correlation is not significant, but the most down-regulated

nuclear receptors Hr46 and Blimp-1 (indicated) are among the few genes showing peaks with increased accessibility. (C-D) Genomic view of Hr46 (C) and Blimp-1 (D) showing FAIRE-seq open chromatin profilling data for *optix>hth+tsh* ("HTH_TSH"), *optix>hth* ("HTH") and control eye-antennal discs (EA) (EA_WT: black wiggle plot tracks); Hth ChIP-seq target regions in embryo and EA disc are shown with a red line; HTH-TSH versus WT differentially open chromatin peaks are highlighted with a cyan background; and prediction of binding sites within Hth ChIP peaks are shown as black ticks marked as "HTH_predicted_BS" (Cluster-Buster (Frith et al., 2003)) motif score >6 using FlyFactorSurvey PWMs). In addition, ModENCODE EcR ChIP data are shown with a blue line, for L3 (modEncode_2640), WPP 4-5h (modEncode_3398), WPP 10-11h (modEncode_2641), WPP 30-33h (modEncode_2642).

Cluster Rank	NES	Best motif logo	Best motif name	Candidate TFs
1	7.4		jaspar-PF0001.1	ewg
4	4.9	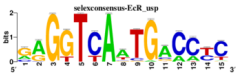	selexconsensus-EcR_usp	EcR
6	4.8		transfac_public-M00027	sd
9	4.4		homer-M00191	Stat92E
18	3.9	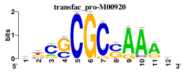	transfac_pro-M00920	E2f, E2f2, Dp
21	3.8		transfac_pro-M01345	so, Optix

+bcd + ATF3 +Adf1 +slbo +oc +MAd +DNApoliota +gem + pnr

Figure R1.10. i-cis-Target predicted transcription factor binding site motifs located within FAIRE peaks with increased accessibility in optix>hth+tsh discs. Enrichment analysis is performed by i-cisTarget (Herrmann et al., 2012) and enriched motifs are clustered within i-cisTarget using STAMP. NES = Normalized Enrichment Score (>2.5 is significant).

The reiterated finding of an EcR signal in our results made us look for those genes in the EcR "gene neighbourhood" – i.e. those genes whose expression profiles are similar to that of the EcR gene expression profile – using Pavlidis Template Matching (Pavlidis and Noble, 2001) (Figure R1.11A). The EcR neighbourhood showed a strong enrichment in genes functionally annotated as "cell cycle" (adj. p-value=1.21E-25) (using FlyMine) (Figure R1.11B). Among these

genes we again found cell cycle regulators, such as *polo* kinase, *dp53*, *Rbf* and *Rbf2* (Figure R1.11C and Figure R1.6B).

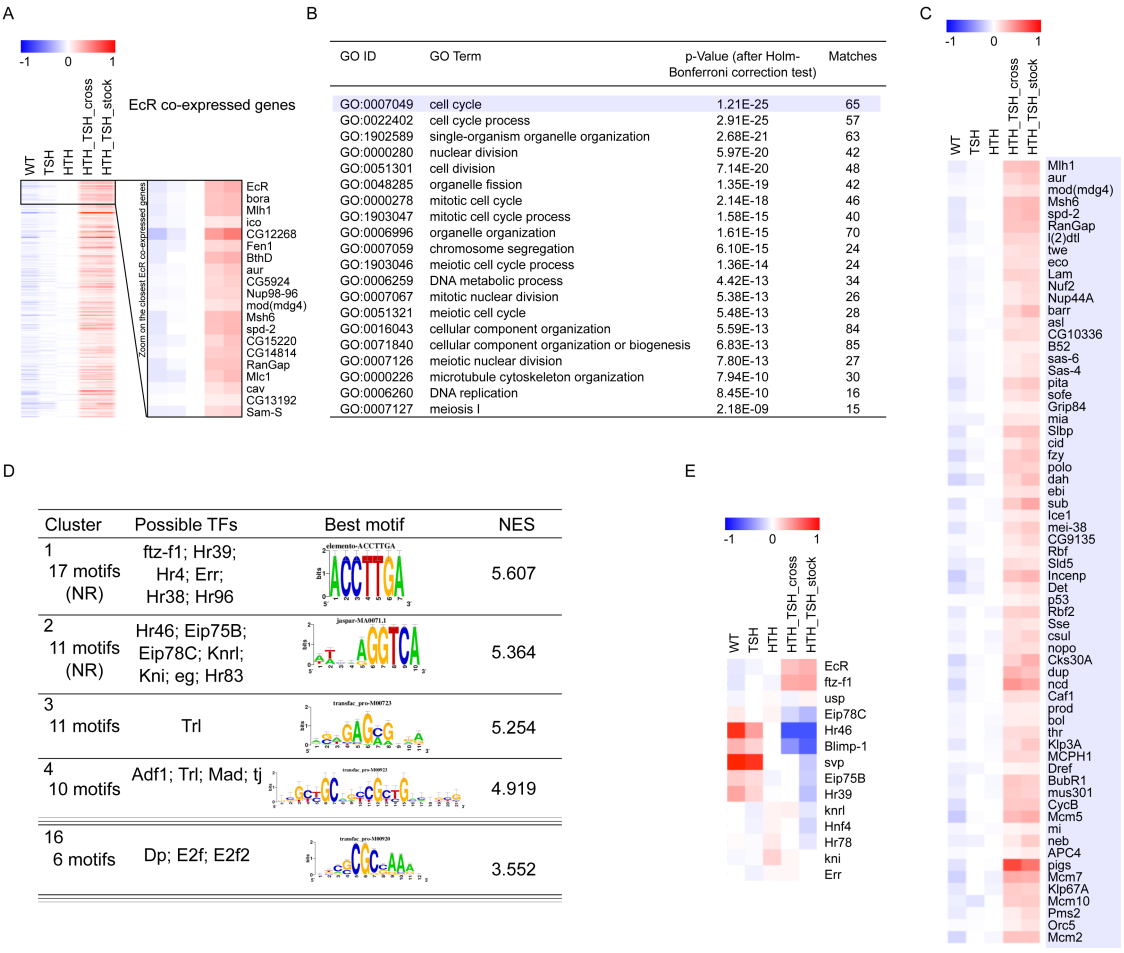

Figure R1.11. Transcriptomic profile of the genes co-expressed with EcR. (A) Heatmap of the 202 genes co-expressed with EcR (derived by correlation, PTM p-value<0.01). A zoom of the most correlated genes is also shown. (B) Most enriched GO terms of the EcR co-expressed genes (Flymine Gene Ontology enrichment analysis). (C) Heatmap of the subset of 65 genes annotated with “cell cycle”. (D) Selected iRegulon motif enrichment results on the EcR co-expressed gene set. (E) Heatmap showing expressed NR and Blimp-1 expression profiles.

Also, and as previously identified, this list included additional components of the EcR pathway: *ftz-f1, Hr46/DHR3* and *Blimp-1* (Thummel, 2001) (Figure R1.11E and Figure R1.6D). In order to infer the transcriptional network that was operating these coordinated gene expression changes, we used iRegulon to identify TF binding motifs enriched in the *cis*-regulatory elements (CREs) of the EcR neighbourhood. This analysis identified a number of potential binding sites for transcription factors such as the nuclear receptors Hr46/ftz-f1, the proliferation

controllers E2f and E2f2 or Mad, the nuclear transducer of the Dpp/BMP2 signalling pathway (Figure R1.11D).

So far these data indicate that Hth+Tsh progenitor-like cells drive a specific pattern of nuclear receptor expression, characteristic of low ecdysone signalling, and that this expression pattern could be playing a direct role in the hth+tsh-induced overgrowths by in turn controlling a large set of cell cycle genes. Likely, this control occurs in conjunction with other factors, including E2F and the Dpp/BMP2 pathway.

If this hypothesis was true, some of these nuclear receptors should be required for the hth+tsh-driven tissue overgrowth. In addition, their expression should be regulated by Hth+Tsh *in vivo*. We next tested these two assumptions in turn.

Functional analysis indicates that regulation of Ecdysone Receptor or nuclear receptors ftz-f1 and Hr46/DHR3 controls hth+tsh-driven overproliferation

To test whether differentially expressed genes in the EcR pathway genes participated in controlling the hth+tsh induced overgrowth, we altered the expression levels of EcR, Hr46/DHR3, ftz-f1 and Blimp-1 in the *optix>hth+tsh* background, either through double-stranded RNAi-specific knockdowns, dominant negative forms (in the case of EcR) or by overexpression. When available, we used several different RNAis per gene.

To evaluate whether varying the expression levels of a gene enhanced or suppressed the hth+tsh-driven phenotype, we took into consideration changes in size and extent of differentiation in eye discs and, in adults, we assessed retina size and amount of undifferentiated cuticle.

As positive controls, we tested first a number of interactions for which we could predict the outcome. Thus, hth+tsh+yki-RNAi caused a reduction in eye disc size and adult cuticle (Figure R1.12B) while hth+tsh+yki exacerbated growth of both eye discs and adult cuticle (Figure R1.12C). Both results agreed with the known requirement of Yki for hth+tsh-driven tissue growth (Peng et al., 2009). Also as expected, knocking down the proliferation gene *polo* (Figure R1.12D) or

overexpressing the E2F repressor *Rb* in hth+tsh-expressing discs caused a reduction in eye disc and adult cuticle growth (Figure R1.12F). These results confirmed that we could use the enhancement or suppression of disc and adult eye *optix>hth+tsh* phenotypes to test functional interactions between hth+tsh and EcR pathway genes.

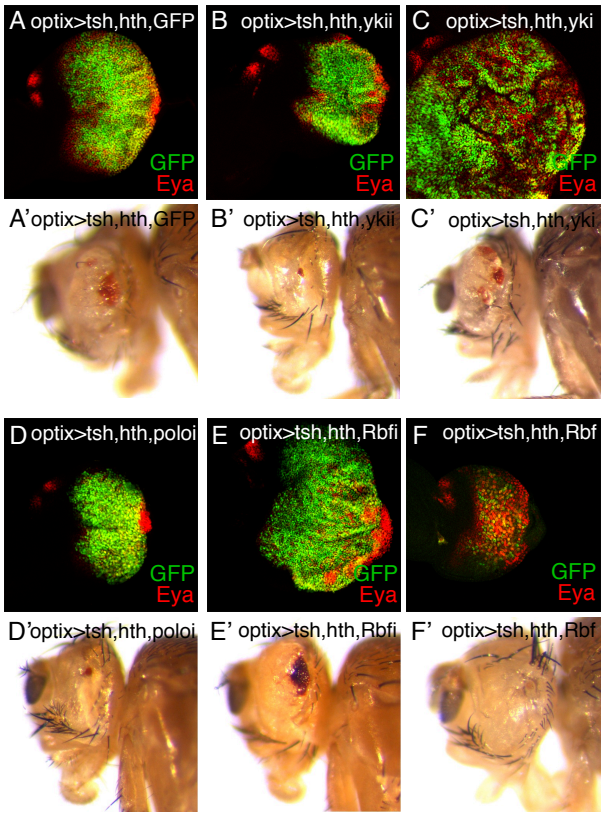

Figure R1.12. Cell cycle-related genes functionally interact with hth+tsh in inducing tissue overgrowth. Functional interactions between hth+tsh and *yki*, *polo* and *rbf*. Eye discs (upper panels) and adult heads (lateral views; lower panels) of *optix>hth+tsh* co-expressing (A,A') UAS-GFP (used to equalize the number of UAS sequences), (B,B') UAS-ykiRNAi, (C,C') UAS-yki, (D,D') UAS-polo-RNAi (20177), (E,E') UAS-Rbf-RNAi (102159) or (F,F') UAS-Rbf280.

Of the EcR pathway nuclear receptors showing differential expression in *optix>hth+tsh* discs (EcR, Hr46/DHR3, ftz-f1 and Blimp-1), we found strong interactions with EcR, Hr46/DHR3 and ftz-f1 (Figure R1.13-15 and Figure A.2).

On its own, overexpression of *EcR* (*optix*>EcRB1) did not result in any abnormality (Figure A.3). However, when EcR was co-overexpressed with hth+tsh (*optix>hth+tsh+EcRB1*) the overgrowth of adult cuticle was exacerbated dramatically (Figure R1.13A,C). This was also observed in the eye discs, with co-

overexpression of *EcR* further increasing the overgrowth of the tissue (Figure R1.13B,D).

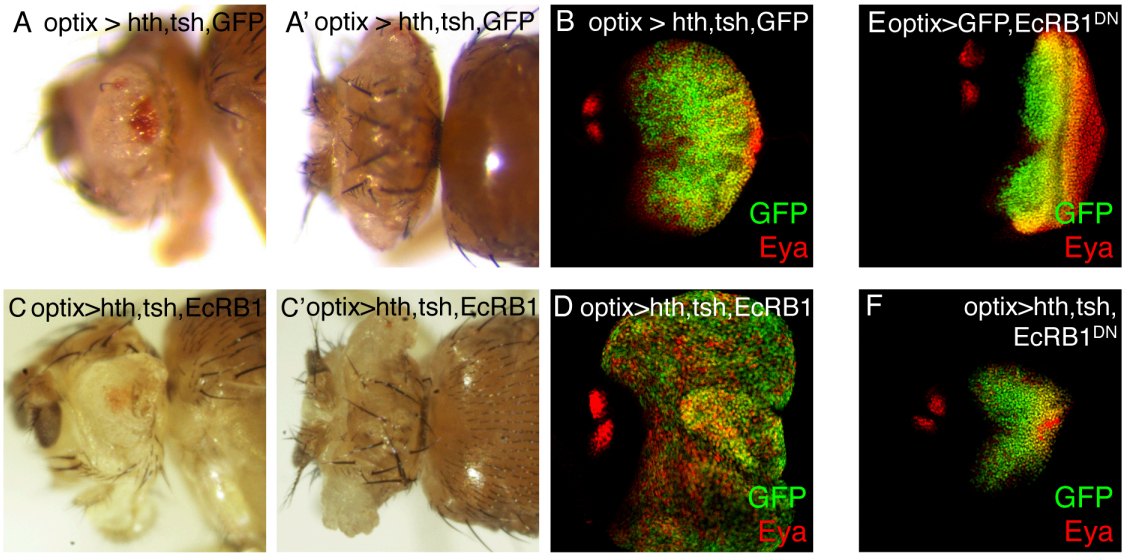

Figure R1.13. EcR functionally interacts with hth+tsh in inducing tissue overgrowth. Adult heads (A,C lateral and A',C' dorsal views) and eye discs (B,D) of *optix>GFP:hth+tsh+GFP* (A-B) and *optix>GFP:hth+tsh+EcRB1* (C-D) (note that both genotypes harbor equal number of UAS-transgenes). Co-overexpression of EcRB1 enhances the overgrowth of lateral head cuticle and eye disc tissue. Comparison between eye discs overexpressing a dominant-negative form of the EcRB1 (E: *optix>GFP+EcRB1-DN*) and the co-overexpression of EcRB1-DN with hth+tsh (F: *optix>GFP:hth+tsh+EcRB1-DN*). Expression of EcRB1 causes a mild reduction in eye disc size (E). Coexpression of EcRB1-DN suppresses the overgrowth produced by hth+tsh (compare F with B). Discs are stained with anti-GFP (green) and anti-Eya (red) antibodies.

Co-overexpression of a dominant-negative form of the same receptor *(optix>hth+tsh+EcRB1W650A)* caused adult lethality, so we analysed the effects only on eye discs. *optix>EcRB1W560A* discs exhibited moderately reduced retinal differentiation and eye disc size (46% smaller that optix>GFP control discs). The overgrowth in *optix>hth+tsh+EcRW650A* discs was suppressed in comparison with *optix>hth+tsh* discs (*optix>hth+tsh+EcRW650A* discs were 42% smaller than *optix>hth+tsh discs*) (Figure R1.13E,F and Figure R1.14). This set of results indicates that EcR, the expression of which is increased in hth+tsh cells, contributes positively to the hth+tsh-driven tissue overgrowth.

When Hr64 (Figure R1.15A,B) or ftz-f1 (Figure R1.15A,D) were attenuated using RNAi, the *optix>hth+tsh* disc overgrowths were exacerbated, most notably in the case of ftz-f1-mediated knockdown. In the case of Hr46/DHR3 and ftz-f1, it is

important to note that neither of the RNAis assayed against either of the two genes produced any significant phenotypic alteration on their own (Figure A.3).

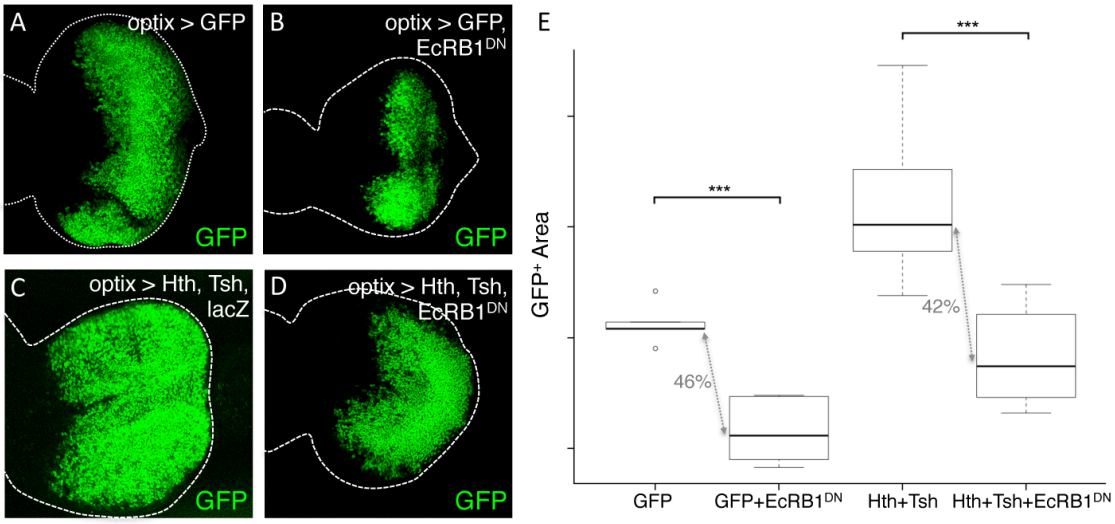

Figure R1.14. The dominant negative form of EcRB1 partially rescues the hth+tsh-phenotype. Late third instar eye discs from (A) *optix>GFP*, (B) *optix>GFP+EcRB1^{DN}*, (C) *optix>hth+tsh+lacZ* or (D) *optix>hth+tsh+EcRB1^{DN}* expressing flies. GFP in (A,B) comes from the UAS-GFP line and in (C,D) from the UAS-131-GFPhth line. The dashed lines outline the discs. (E) Statistical analysis of the GFP-positive area in the different genotypes.

However, the disc phenotypes were not identical: while in *optix>hth+tsh+Hr46RNAi* the portion of differentiating retina (marked by Eya-only cells) was almost totally obliterated as in hth+tsh eye discs (Figure R1.15A',B'), in *optix>hth+tsh+ftz-f1RNAi* there was a moderate, but consistent rescue of the Eya-expressing retina (Figure R1.15A',D').

The co-overexpression of Hr46 or ftz-f1 produced the opposite effects: a clear reduction of the disc size (Figure R1.15A,C,E) and a total obliteration of the retina. This obliteration could derive, in part, from the fact that the expression of Hr46 (UAS-DHR3 RB) or ftz-f1 (UAS-βftz-f1) on their own resulted in approximately 40% and 60% reduction in adult eye size, respectively (Figure A.3).

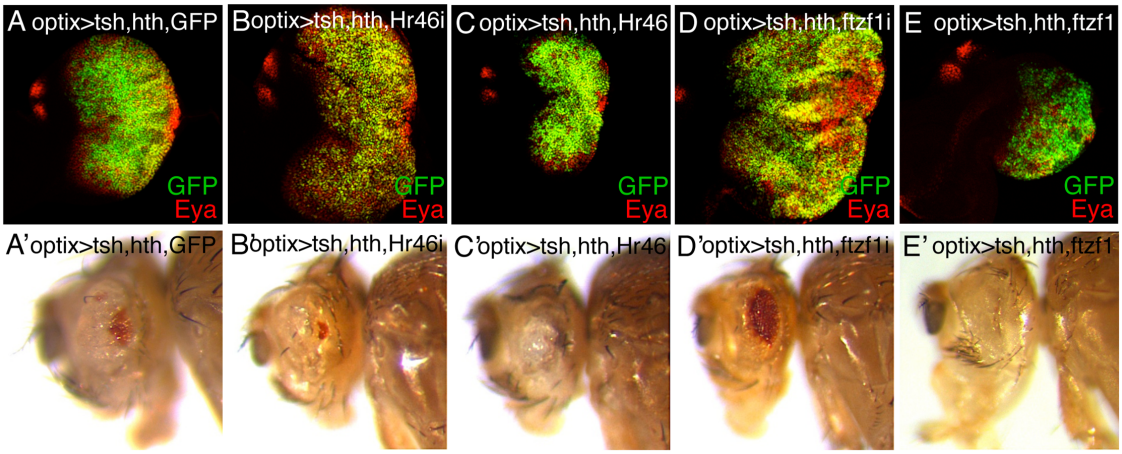

Figure R1.15. Nuclear receptors *Hr46* and *ftz-f1* functionally interact with hth+tsh in inducing tissue overgrowth. L3 eye discs, stained for GFP and Eya (upper panel) and lateral views of adult heads (lower panels) of the indicated genotypes (note that all genotypes harbor equal number of UAS-transgenes). RNAi-mediated attenuation (B) or overexpression (C) of *Hr46* enhances or suppresses, respectively, the hth+tsh-induced eye disc overgrowth. In adults, however, while Hr46 attenuation enhances the tissue overgrowth/loss of eye (B'), its overexpression reduces the tissue overgrowth, but without rescuing retina differentiation (C'). RNAi-mediated attenuation of *ftz-f1* (D) or overexpression (E) enhances or suppresses, respectively, the hth+tsh-induced eye disc overgrowth. In this case, *ftz-f1* attenuation partly rescues the eye reduction of hth+tsh individuals (D'). Co-overexpression of *ftz-f1* suppresses the lateral cuticle overgrowth, without rescuing retina differentiation (E').

In all, these experiments proved that EcR, Hr46 and ftz-f1, which are transcriptionally regulated by Hth+Tsh, were functionally required to their synergistic effect on growth.

In addition, our transcriptomic/bioinformatics analysis suggested that some, or all of these nuclear receptors might be exerting their function through the regulation of cell cycle genes. This implied that *EcR, Hr46* and/or *ftz-f1* should have the potential to regulate the proliferation rates of cells anterior to the MF, where *hth* and *tsh* are normally coexpressed. Recent work indicates that indeed ecdysone is required for the proliferation of imaginal discs (Herboso et al., 2015), supporting this notion. To test specifically if either *Hr46* or *ftz-f1* affect proliferation, we monitored the expression of the G2/mitotic cyclin cyclin-B and the mitotic rate (using the mitotic marker phospho-Histone H3, PH3) of undifferentiated cells in *optix>Hr46, optix>ftz-f1* and *optix>ftz-f1-RNAi* (Figure R1.16).

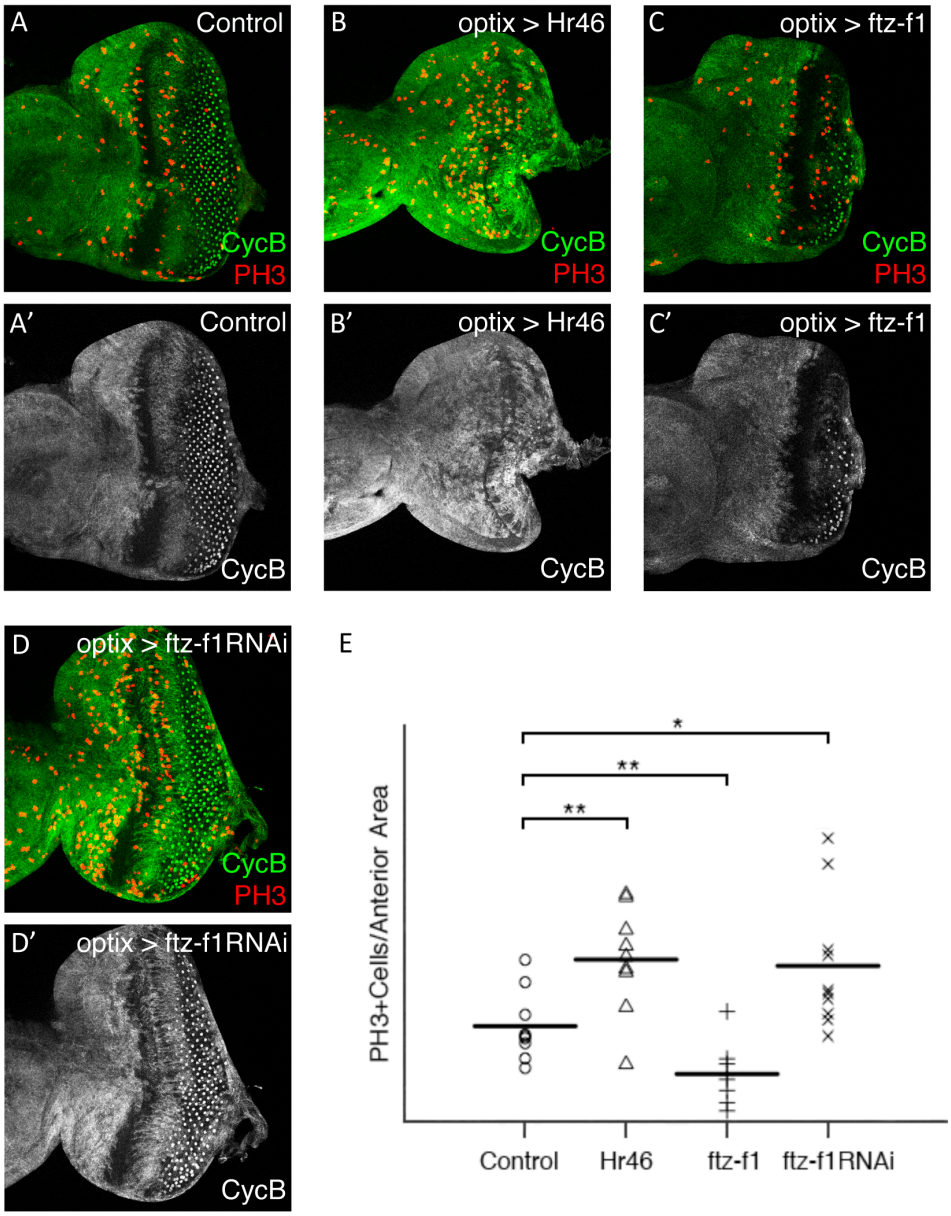

Figure R1.16. Altering *Hr46* and *ftz-f1* expression regulates proliferation of eye progenitors. L3 eye discs of the indicated genotypes (A-D) stained for cyclinB (cycB, green) and the mitotic marker PH3 (red). Merged and cycB signals are shown. Control discs are *optix*>+. PH3-positive cells were counted in the anterior region of the eye disc, where undifferentiated progenitors reside (outlined in white in A). In (A') the double-headed arrow marks the width of the G1-arrested domain (see text for details). (E) Statistical analysis of the mitotic density (PH3+ cells/anterior area) indicates that overexpression of Hr46 and RNAi-mediated attenuation of *ftz-f1* result in increased proliferation. Note that in both genotypes the G1 arrested domain is narrower than in the control (especially for *optix>Hr46*; B). On the contrary, overexpression of *ftz-f1* results in reduced proliferation.

In control discs (*optix>GFP*), proliferation is patterned: proliferation is restricted to progenitors, located at the far anterior of the disc, which express cycB and are mitotically active. Closer to the MF, cells stall their cell cycle transiently in

G1, so they lose cycB (Figure R1.16A). In *optix>Hr46* discs, though, the density of mitotic (PH3-positive) cells increased dramatically and the cycB gap anterior to the MF narrowed or disappeared, indicating an increased and continuous proliferation (Figure R1.16B,E). Next, we tested *ftz-f1.* Overexpression of *ftz-f1* (*optix>ftz-f1*) resulted in a strong decrease in the density of PH3 cells in the anterior disc and a widening of the cycB gap anterior to the MF (Figure R1.16C,E). While in the contrary experiment, *ftz-f1* attenuation (*optix>ftz-f1-RNAi*) increased anterior proliferation, and the cycB gap narrowed (Figure R1.16D,E). These results indicate that both *Hr46* and *ftz-f1* have the potential to act as cell cycle regulators during eye disc development, and that they have opposing effects on proliferation.

Hr46/DHR3 is repressed by Hth+Tsh

So far, four sets of results indicated that Hr46 could be a key player in the response of cells to the combined expression of hth and tsh: (1) its transcription was specifically downregulated in hth+tsh discs; (2) potential binding sites for Hr46 were found enriched in CREs linked to differentially expressed genes characterized as cell cycle regulators; (3) Hr46 functionally interacted with hth+tsh, so that further attenuation of Hr46 by RNAi exacerbated the overgrowth/differentiation blockade phenotype induced by hth+tsh and (4) Hth-binding plus FAIRE-seq data suggested that *Hr46* was a Hth direct target.

If Hr46 regulation were direct, and taking into account that globally Hr46 was downregulated by hth+tsh, we expected Hr46 to be repressed by Hth+Tsh in a cell-autonomous manner. First, we characterized Hr46 expression during third larval stage to, then, check the effect of hth+tsh expressing clones on its expression. During the third (and last) larval period, the expression of Hr46, monitored with an anti-Hr46 antiserum, builds up (Figure R1.17). During early third instar, Hr46 is expressed weakly and ubiquitously in the eye disc. As differentiation moves across the disc, Hr46 levels increase straddling the morphogenetic furrow, peaking anterior to it.

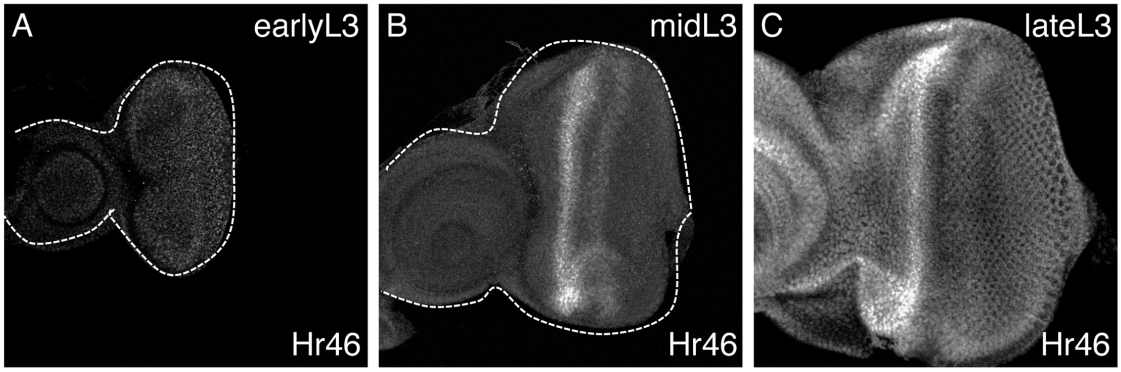

Figure R1.17. Temporal expression of Hr46. Hr46 expression during L3 development in the eye-antennal imaginal disc. Control disc at different developmental stages (early L3 (A), mid L3 (B) and late L3 (C)) stained with anti-Hr46. In (A) and (B) the dashed line outlines the disc.

This expression is in agreement with ecdysone signalling being active in this region of the disc during L3 (Figure R1.8 and Brennan et al., 1998). Notably, its expression is exclusive to that of Hth. Only at the third instar-pupal transition, Hr46 levels raise uniformly throughout the disc, coinciding with the ecdysone pulse that triggers this molting (Figure R1.17). Therefore, during most of the retinal differentiation period, the expressions of Hth and Hr46 are complementary (Figure R1.18A).

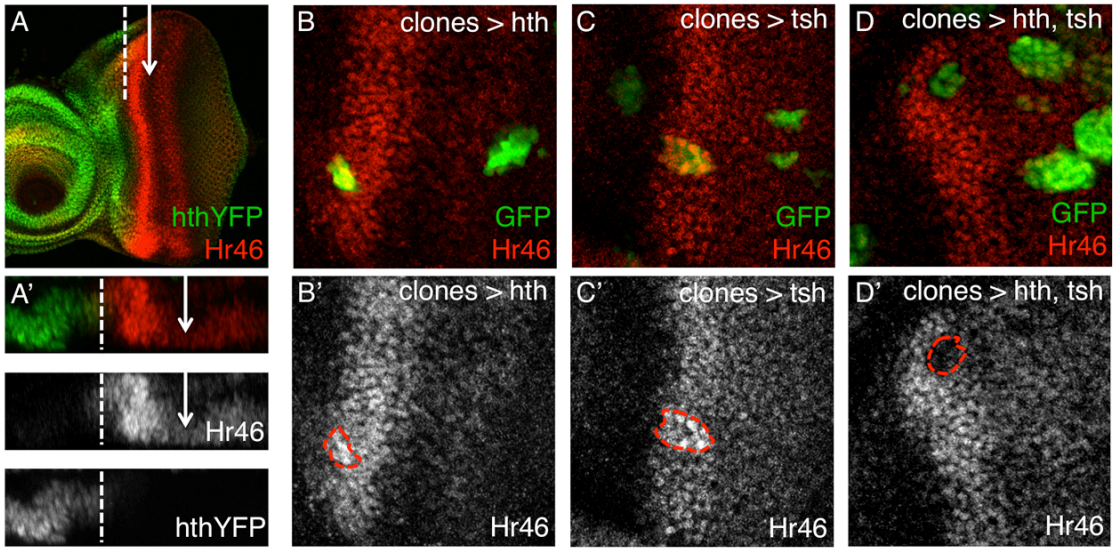

Figure R1.18. The expression domains of *hth* and *Hr46* are complementary and co-expression of hth+tsh repress *Hr46*. hth:YFP late L3 disc stained with anti-Hr46 (A) and the corresponding optical cross-section (A'). The arrow marks the morphogenetic furrow (MF) and the dashed line marks the boundary between Hth and Hr46 expression. Clones overexpressing *hth* (B,B'), *tsh* (C,C') or both (D,D'), marked by GFP (and outlined with the red dashed line), were induced in the eye imaginal disc at 48-72 hours after egg laying. Discs are stained with anti-Hr46.

Since *tsh* expression overlaps *hth* in this anterior region of the eye primordium (Bessa et al., 2002), the complementarity between *hth* and *Hr46* was consistent with *Hr46* being repressed by hth+tsh. To test this point specifically, we induced cell clones, marked with GFP, expressing either *hth* or *tsh* alone or hth+tsh. Only hth+tsh clones reduced the levels of Hr46 and did so in a cell-autonomous manner (Figure R1.18D), which agrees with a direct regulation of *Hr46* by hth+tsh.

Significant co-overexpression of *MEIS1* and *TSHZ* genes, the vertebrate *hth* and *tsh* homologues, is found in major human cancers

The over-proliferative phenotype caused by co-expression of *hth* and *tsh* in the *Drosophila* eye prompted us to ask whether co-ocurrence of the *hth* and *tsh* homologues, members of the *MEIS* and *TSHZ* gene families, could also be detected in human tumours. A causal relation between MEIS1 and cancer, both in mice and humans, including several hematopoietic and solid tumour types (Knoepfler et al., 1997; Geerts et al., 2003; Zeisig et al., 2004; Geerts et al., 2005; Wang et al., 2006; Crijns et al., 2007; Orlovsky et al., 2011; Tomoeda et al., 2011; Dardaei et al., 2014; Koller et al., 2014; Okumura et al., 2014) is well established. However, a potential relationship with TSHZ genes had not been previously explored. To this end, we analysed publicly available gene expression profiling data for different cancers (Table C.3). A total of 116 datasets representing most major human tumour types (WCRF; Jemal et al., 2011) downloaded from the NCBI GEO repository were analysed using the R2 expression analysis and visualization web platform (http://r2.amc.nl). We distinguished between hematopoietic (n=25) and solid tumour types (n=91). Significant *MEIS1* and *TSHZ1* mRNA expression was found in almost all solid tumour samples (96% and 97%, respectively). Average *TSHZ2* and *TSHZ3* expression was lower and was found in fewer tumour samples (54% and 85%, respectively). mRNA expression levels were lower for *MEIS1* and *TSHZ1-3* in hematopoietic tumours, and their expression was less widespread (Table R1.1A). We found that *MEIS1* mRNA expression was significantly correlated with the expression of *TSHZ1*, *TSHZ2*, and *TSHZ3* in the

majority of the solid tumour datasets (52, 58, and 67 of the 91 datasets, respectively; Table R1.1B and Table C.3).

Table R1.1. *MEIS1* and *TSHZ1-3* mRNA expression and correlation in human cancer datasets. (A) *MEIS1* and *TSHZ1-3* mRNA expression in human cancer datasets. Average MAS5.0-normalized data for mRNA expression, with their S.E.M., for the 116 different cancer datasets representing all major cancer types present in the R2 suite, 91 datasets for solid, and 25 for hematopoietic tumors. Only significant expression ("present call" for the probeset in that sample) is counted. Between brackets is the percentage of samples with such a present call. *MEIS1* and *TSHZ1* are almost invariantly well-expressed in solid tumor types, and also *TSHZ2-3* are significantly expressed in the majority of tumor samples. In hematopoietic tumors, *MEIS1* and *TSHZ1-3* are more rarely expressed, and their expression levels are lower, especially *TSHZ2-3*. For comparison: MAS5.0-normalized *GAPDH* and *ACTB* household gene mRNA expression in these datasets ranges between 5,000 and 10,000. (B) *MEIS1* and *TSHZ1-3* mRNA expression correlations in human cancer datasets. Cancer datasets in R2 with a significant correlation between *MEIS1* and *TSHZ1-3* mRNA expression levels. The number of sets with significant positive and negative expression correlations are listed in the top and bottom rows, respectively. In solid tumor types, MEIS1 is predominantly positively correlated with TSHZ1-3, most notably with TSHZ2-3, in hematopoietic tumors these correlations are also present, but much more infrequent. Complete data are in Table C.3. Correlations were calculated using a 2log Pearson test, as described in the Annex A.

A

116 cancer sets				
	MEIS1	TSHZ1	TSHZ2	TSHZ3
Solid tumors (n=91)	313 ± 35 (96%)	268 ± 17 (97%)	114 ± 7 (54%)	112 ± 6 (85%)
Hematopoietic tumors (n=25)	294 ± 74 (52%)	168 ± 14 (74%)	75 ± 11 (8%)	76 ± 6 (25%)

B

91 solid cancer sets			
	MEIS1-TSHZ1	MEIS1-TSHZ2	MEIS1-TSHZ3
Significant positive	46	56	60
Significant negative	6	2	7

25 hematopoietic cancer sets			
	MEIS1-TSHZ1	MEIS1-TSHZ2	MEIS1-TSHZ3
Significant positive	3	8	10
Significant negative	3	1	4

Interestingly, almost all correlations were positive, i.e. high *MEIS1* expression coincided with high *TSHZ* expression. Often, simultaneous co-expression of *MEIS1* with more than one *TSHZ* gene was found, especially with *TSHZ2* and *TSHZ3*. The *MEIS1-TSHZ* co-expression appears specific for certain cancer types (Table C.3). Significant *MEIS1-TSHZ* co-expression was not nearly as pervasive in hematopoietic tumours (Table R1.1B). This coincides well with the higher and more widespread *MEIS1-TSHZ* mRNA expression in solid versus hematopoietic cancer types (Table R1.1A). *MEIS1-TSHZ* co-expression was found most often in epithelial tumours (i.e. carcinomas). It is interesting to note that several of the most common carcinomas, responsible for the large majority of the

worldwide cancer deaths, like bladder, breast, colon, kidney, lung, and ovary cancer (Jemal et al., 2011) show frequent *MEIS1-TSHZ* co-expression. The correlations found were usually consistent for a given tumour type. In breast and colon cancer for instance, significant *MEIS1-TSHZ2/3* co-expression was almost invariantly present in all datasets tested (≥11 of 12 breast, and ≥ 20 of 22 colon cancer sets), suggesting that the correlation patterns obtained are very robust.

Table R1.2. *MEIS1* and *TSHZ1-3* mRNA over-expression and DNA copy gain in human cancer types. Tumor types are indicated in the first column. Examples of tumor subtypes with multiple datasets and consistent *MEIS1* and/or *TSHZ1-3* mRNA overexpression and/or DNA copy number gain in the Oncomine website are listed. The number of sets is indicated in the second column, the specific tumor subtypes in the third column. The last four columns list the number of datasets per tumor subtype that show significant mRNA over-expression and/or DNA gain. When in bold type and on a green background, *MEIS1* is also significantly positively correlated with *TSHZ1, -2,* or *- 3* as analyzed in R2 (Table C.3). Various * enfolds 4 anaplastic large cell, 2 Burkitt's, 2 follicular, 3 Hodgkin's, 5 large B-cell, and 2 T-cell lymphoma datasets. Complete data are in Table C.4.

Solid tumor						
Tumor type	**Sets**	**Subtype**	**MEIS1**	**TSHZ1**	**TSHZ2**	**TSHZ3**
Bladder	4	Bladder urothelial carcinoma	**3**		**3**	**4**
Brain	16	Astrocytoma, glioblastoma, oligodendroglioma	**10**	**7**	7	**4**
Breast	8	Breast carcinoma, invasive	**5**	1	**4**	**3**
Cervix	3	Cervical squamous cell carcinoma	**3**		3	1
Colon	18	Colorectal adenocarcinoma	**9**		**13**	**4**
Endometrium	2	Endometrial adenocarcinoma	**2**		**2**	
Esophagus	2	Esophageal adenocarcinoma				2
Germ cell	2	Teratoma, testicular	**1**	**2**	**1**	**1**
Head & Neck	3	Head & neck squamous cell carcinoma	**2**		**2**	1
Kidney	5	Renal cell carcinoma	**1**		**5**	**1**
Liver	6	Hepatocellular carcinoma	**4**	**1**	3	**3**
Lung	13	Lung adenocarcinoma, squamous cell carcinoma	**8**		**12**	**6**
Ovary	7	Ovarian adenocarcinoma, carcinoma	**7**		**1**	**1**
Pancreas	5	Pancreatic adenocarcinoma	**1**	1	**4**	4
Prostate	2	Prostate adenocarcinoma	**2**		2	**2**
Thyroid	1	Thyroid gland papillary carcinoma	**1**		**1**	1

Hematopoietic tumor						
Tumor type	**Sets**	**Subtype**	**MEIS1**	**TSHZ1**	**TSHZ2**	**TSHZ3**
Leukemia	8	Acute lymphoblastic leukemia	**6**	6	1	
Leukemia	7	Acute myeloid leukemia	7	2		1
Lymphoma	18	Various *	**17**	5	5	**13**
Myeloma	2	Multiple myeloma, smoldering myeloma		1		**1**

We next analysed *MEIS1/TSHZ* mRNA expression and copy number aberrations between cancerous and normal tissue in Oncomine (www.oncomine.org). We found widespread *MEIS1* and *TSHZ* mRNA over-expression and DNA copy number gain in cancerous versus normal tissue in many of the major cancer types. The overexpression and DNA copy gains were usually consistent for the same tumour subtype. The most consistent patterns occurred in

solid tumours, mostly in carcinomas, more than in hematopoietic tumours. The data often coincided with the MEIS1-TSHZ co-expression findings described above (Table R1.2 and Table C.4). Figure R1.19 shows examples for MEIS1 and TSHZ2 in breast and colon cancer with R2 (A, B), and Oncomine (C-F).

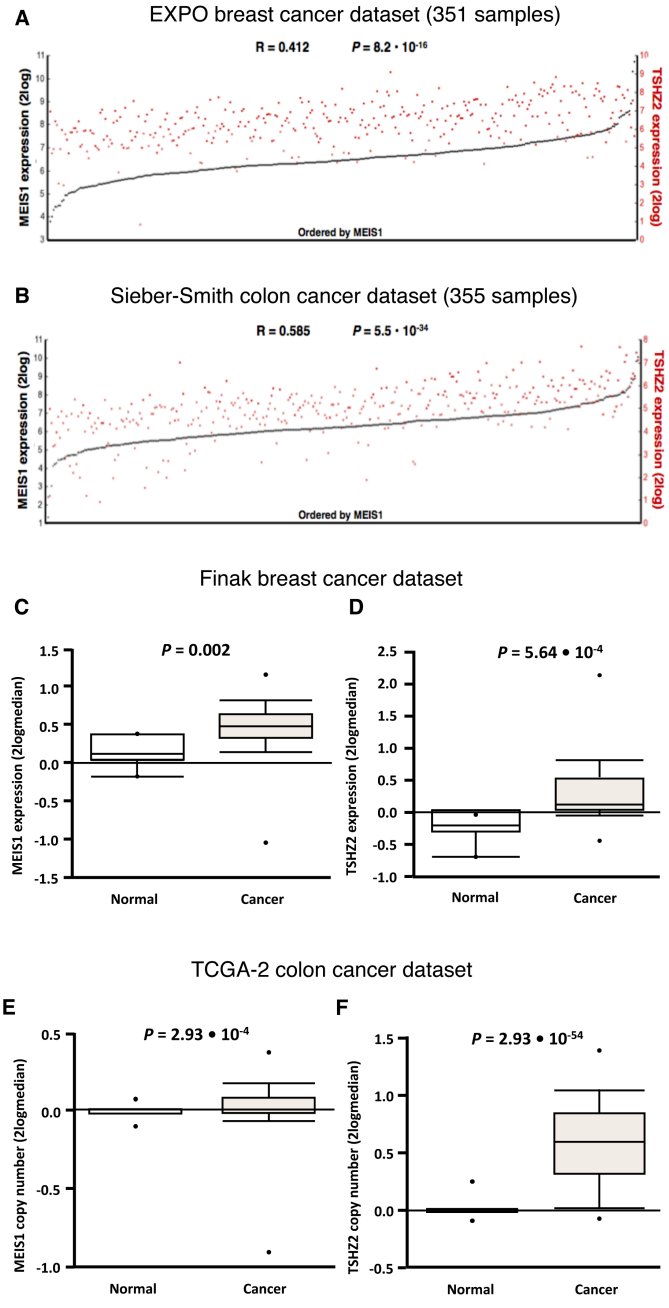

Figure R1.19. Examples for MEIS1 and TSHZ2 in breast and colon cancer. Visual representation of MEIS1 and TSHZ2 mRNA expression in (A) all 351 samples of the EXPO breast cancer dataset and (B) all 355 samples of the Sieber-Smith colon cancer dataset as analyzed using the R2 website. The tumors are ranked horizontally from left to right according to their MEIS1 expression as determined by Affymetrix array analyses (2log values). MEIS1 and TSHZ2 expression values for each tumor are visualized with black circles and red rectangles, respectively. Dark and light colors denote samples with significant ("present call"), and absent expression, respectively. mRNA expression correlations were calculated with a 2log Pearson test. Full details are in Table C.3. Visual representation of MEIS1 (C) and TSHZ2 (D) mRNA expression in the Finak breast cancer dataset, and MEIS1 (E) and TSHZ2 (F) DNA copy number levels in the TCGA-2 colon cancer dataset, as analyzed using the Oncomine website. Values are represented as 2log-median centered. *P* values are calculated with a Student's t-test. Full details are in Table C.4.

Together, all these data strongly suggested oncogenic roles for MEIS1 and the TSHZ genes in many major cancers, with coordinated over-expression in cancer cells. Therefore, the synergistic growth-inducing capacity of Hth and Tsh in

Drosophila could have a parallel in oncogenic coordinated over-expression of MEIS1 and TSHZ genes in human cancer.

The homologues of yki, ftz-f1 and Hr46, YAP1, NR5A2 and RORA, show significant expression correlation with MEIS1 and TSHZ genes in some tumours

Our global characterization of the hth+tsh-induced overgrowths in *Drosophila* involved alterations in nuclear receptor expression and pointed to two of these receptors, Hr46 and ftz-f1, as being required for the overgrowths. This adds to previous work showing that Hth and Tsh directly interact with Yki, the co-activator of the Salvador-Warts-Hippo pathway, and that this interaction is necessary for the pro-proliferative action of this transcription factor combination (Peng et al., 2009; Slattery et al., 2013). This led us to look for a similar expression signature in human tumours with MEIS1 and TSHZ co-overexpression on the R2 Platform. We found significant and consistent correlations between MEIS1 and YAP1 (the human yki homologue) in several of the major solid tumour types, including breast and lung cancer (Table R1.3, see also Table C.3). The mRNA expression of NR5A2 (also known as Liver Receptor Homologue-1, LRH-1), the human ftz-f1 homologue, was also significantly correlated with MEIS1 in for example breast, colon, and lung cancer. Similar positive correlations were found for the Retinoid-related Orphan Receptor alpha (RORA), one of the human homologues of Hr46, again also in breast, colon, and lung cancer. In this case, though, we had expected a *negative* correlation for RORA, as Hr46 showed a clear repression in hth+tsh cells. However, this difference may be explained either by differences in the “tumour stage” between the *Drosophila* overgrowths and human tumours – for instance the *Drosophila* overgrowths are not metastatic – or by species-specific differences in the mechanisms driving overproliferation. However, and when considered together, the functional genomics analysis in *Drosophila* and the correlations presented strongly suggest a causal link between MEIS1 and TSHZ co-overexpression with changes in nuclear hormone receptor expression in several major human cancer types. These results identify a

parallelism between the progenitor proliferation program controlled by hth+tsh and the MEIS1/TSHZ-associated oncogenic program.

Table R1.3. Overview of MEIS1 co-expression with TSHZ, YAP1, RORA, and NR5A2 genes from R2 data. The first two columns list tumor type and amount of datasets. Columns 3-8 show whether at least half of the datasets showed consistent significant positive (POS; green field) or negative (NEG; orange field) mRNA expression correlations with MEIS1. Statistics and other details are as in Table C.3.

Solid tumor types	Sets	TSHZ1	TSHZ2	TSHZ3	YAP1	RORA	NR5A2
Brain ependymoma	4	POS					
Brain glioma	12			NEG		POS	
Breast	20		POS	POS	POS	POS	POS
Cervix	3	POS				POS	
Colon	25	POS	POS	POS		POS	POS
Esophagus	5	POS				POS	NEG
Germ cell	4	POS	POS	POS	POS	POS	POS
Head & Neck	3	POS	POS			POS	
Kidney	3	POS	POS	POS	POS		POS
Liver	5	POS		POS		NEG	NEG
Lung	6	POS	POS	POS	POS	POS	POS
Ovary	5	POS	POS	POS	POS		
Pancreas	3		POS			POS	POS
PNS neuroblastoma	6		POS	POS	NEG	POS	NEG
Prostate	3	POS		POS	POS		
Sarcoma, Ewing	3			POS			

Hematopoietic tumor types	Sets	TSHZ1	TSHZ2	TSHZ3	YAP1	RORA	NR5A2
Leukemia ALL	7			POS			
Leukemia AML	12						
Leukemia CLL	7						
Lymphoma	8			POS	POS	POS	POS
Myeloma	5		POS	POS	POS		POS

PART II

Hh and Dpp signalling pathways contribute to the proliferation and undifferentiated state of hth+tsh- expressing eye progenitors

We have shown that the hth+tsh-driven proliferation of progenitors is partially sustained by a systemic system that links the growth of the organ to that of the whole organism – an organ extrinsic system. Still, as described previously, growth is controlled more locally, by the same signals that generate cell diversity and patterning – an organ intrinsic set of cues. In overproliferative diseases, specific aberrant combinations of intrinsic factors and signals result in deregulated growth and organ failure. Therefore it is essential to define these specific combinations of intrinsic and extrinsic factors to understand both normal development and overproliferative diseases.

As mentioned before, one of the intrinsic signals that act together with Hth+Tsh in driving proliferation is the Hippo signalling pathway (Peng et al., 2009). But once again, this pathway only explains partially the proliferation induced by Hth+Tsh.

In the eye primordium, there are several signaling molecules including wingless-Int (Wnt), Decapentaplegic (Dpp)/BMP2, Hedgehog (Hh) and JAK/STAT (reviewed in Amore and Casares, 2010). However, neither the Wnt, JAK/STAT nor the Notch pathway (another non-autonomous but locally acting signaling pathway) seemed to contribute to Hth+Tsh function (Peng et al., 2009). A potential role for Dpp or Hh had not been tested.

Here we have tested specifically the effects that manipulating the Dpp/BMP2 and Hh pathways has on the maintenance of Hth+Tsh-driven progenitor state, as a model of progenitor-induced tissue overgrowth.

The Hippo signalling pathway cannot fully explain the hth+tsh phenotype

The TALE-homeodomain protein Hth and the Zn finger transcription factor Tsh are co-expressed in the progenitor cells of the Drosophila eye primordium (Bessa et al., 2002). Previous work has shown that these transcription factors work together to repress the retinal determination genes in the retina and to promote proliferation in the progenitors (Bessa et al., 2002; Peng et al., 2009). The forced maintenance of Hth and Tsh results in the overgrowth of the progenitor population and the blockade of differentiation (Bessa et al., 2002; Peng et al., 2009).

In order to better understand the mechanisms that drive the Hth+Tsh-mediated overgrowth, forced maintenance of these two transcription factors was driven to the undifferentiated population of the eye disc using the optix2.3-Gal4 driver (Ostrin et al., 2006, Figure R1.2 and Figure R2.1).

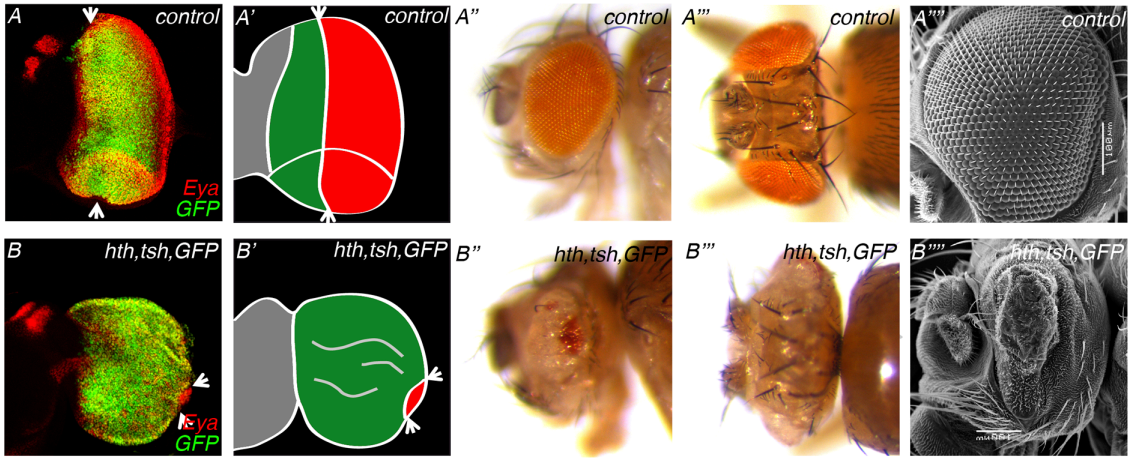

Figure R2.1. Forced maintenance of Hth and Tsh results in overgrowths. Control late third instar (L3) eye disc (A) or eye discs expressing *Hth+Tsh+GFP* (B) in undifferentiated cells using the optix2.3-GAL4 line. Discs are stained with anti-Eya (red); GFP in (A) comes from an UAS-GFP line and in (B) from UAS-GFP + UAS-131-GFPhth lines. Morphogenetic furrow is marked with arrows. (A',B') Schematic representation of the discs –antenna in grey, progenitor cells in green and differentiated cells in red. Lateral (A",B") and dorsal views (A"',B"') of adult heads of the same genotypes. Vertical bars represent the percentages of flies with different phenotypes: flies with normal eyes (represented in green), flies with a medium eye (represented in blue), flies with a small number of organized ommatidias (represented in orange) and flies with a total loss of retina (represented in red). (A"",B"") SEM images of lateral views of adult heads of the same genotypes. In imaginal discs, Hth+Tsh overexpression resulted in the maintenance of progenitors and in the almost complete disappearance of the morphogenetic furrow, which marks the wavefront of retinal differentiation. Adult flies showed small patches of differentiated retina surrounded by an indistinct cuticle.

In a normal situation during late third instar, the morphogenetic furrow has spanned part of the disc leaving a posterior region of differentiated cells (red in Figure R2.1A and R2.1A') and an anterior region of progenitor and precursor cells (green in Figure R2.1A and R2.1A'). In *optix>hth+tsh* discs, the morphogenetic furrow is almost absent with only a small number of posterior differentiated cells and an anterior region where *hth+tsh* cells accumulate, giving rise to several folds in the epithelium (Figure R2.1B and R2.1B'). *optix>hth+tsh* adult ommatidia were absent or severely reduced due to differentiation blockade and were replaced by undifferentiated cuticle (Figure R2.1).

An augmented cell proliferation is an usual mechanism to achieve overgrowths, to test this possibility the mitotic index was measured by counting the number of PH3-positive cells for anterior area in control and *optix>hth+tsh* eye discs. Indeed, we observed a significant 25% mitotic index increase in *optix>hth+tsh* discs compared to control ones (Figure R2.2).

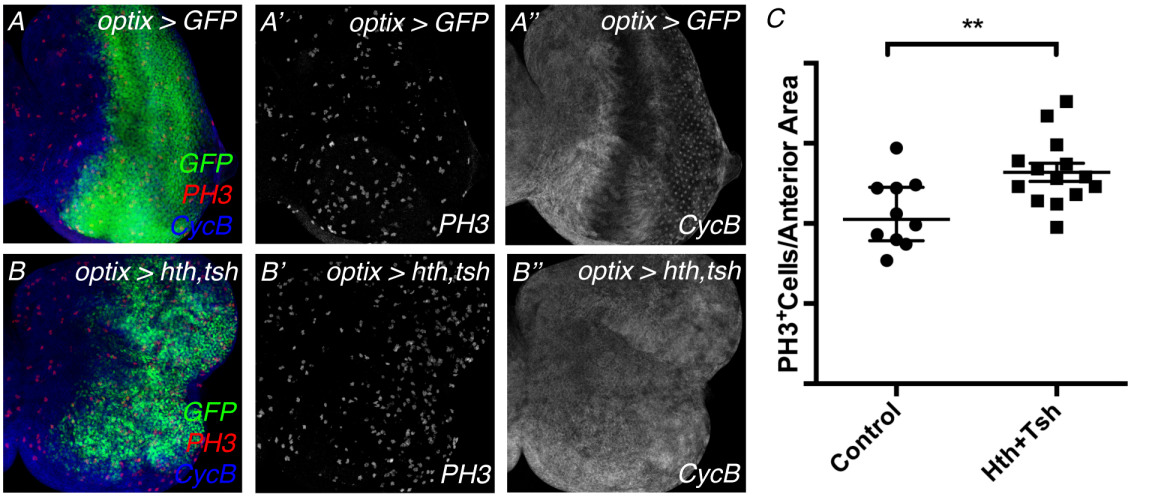

Figure R2.2. Maintenance of Hth and Tsh results in higher mitotic activity in the anterior area of the eye disc. Late third stage eye discs from control (A; *optix>GFP*) or hth+tsh-expressing larvae (B; *optix>hth,tsh*). Discs are stained with anti-CycB (blue); anti-PH3 (red) and GFP. In (B) GFP marks the expression of GFP::Hth. (C) Distribution of PH3+ cells/anterior area for control and hth+tsh-expressing discs. Horizontal bars show mean values and individual measurements are represented as dots and squares (n=10-14). **p < 0.01 using ANOVA. hth+tsh discs show a statistically significant increase in the mitotic activity in the eye anterior area when compared to control discs.

During normal eye development, Hth+Tsh control progenitors proliferation partially by acting together with Yki, the Hippo pathway nuclear transducer. In progenitors, Hth and Tsh act as transcription cofactors of Yki, forming a complex that acts in a cell-autonomous manner (Peng et al., 2009). In fact, it has been

shown that Yki overexpression in eye discs results in overgrown primordia (Huang et al., 2005).

The expression of Hth+Tsh or Yki in undifferentiated cells by the optix2.3-Gal4 driver resulted in overgrowths, however the type of cuticle formed in adult flies was different (Figure R2.3). While Yki expression resulted in small eyes usually excluded from the normal eye field and an overgrown cuticle that maintains the fate of the most anterior part of the head, Hth+Tsh expression resulted in small patches of differentiated retinal tissue surrounded by an overgrowth undifferentiated cuticle, a type of cuticle found nowhere else in the adult fly (Figure R2.3). The differences between these phenotypes indicated that, although the Hippo pathway contributed to the Hth+Tsh phenotype, it could not fully explain it. As expected the Hth+Tsh phenotype is a result of interactions between different signalling pathways.

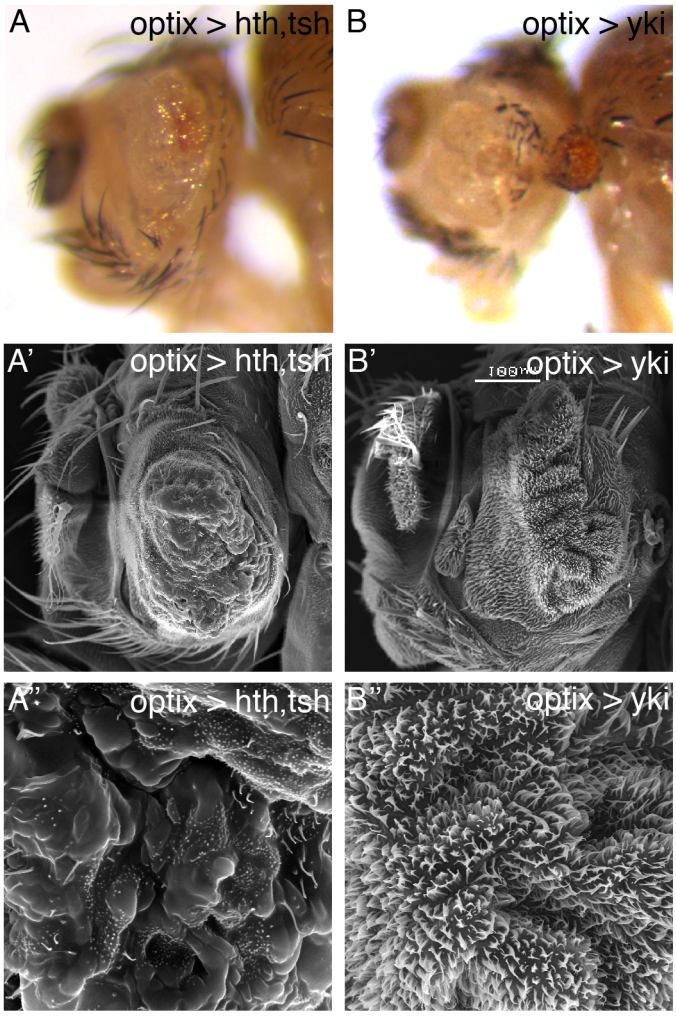

Figure R2.3. Hth+Tsh and Yki expression result in different phenotypes. Lateral views of *optix>hth+tsh* (A) and *optix>yki* (B) adult heads. (A', B') Lateral SEM views of adult heads of the above genotypes. A'' and B'' show high magnification details of the cuticle formed. While Yki expression resulted in cuticle reminiscent of the cuticle around the eye anteriorly, Hth+Tsh coexpression led to an indistinct cuticle surrounding residual patches of differentiated cells.

As described previously, besides the Hippo pathway several other signalling pathways had been linked to organ growth and patterning in the *Drosophila* eye, including Wingless (Wg), Decapentaplegic (Dpp), Hedgehog (Hh), JAK/STAT and Notch (N) (Amore and Casares, 2010). Peng and collegues had negatively tested the role for Wingless, Notch and JAK/STAT pathways during the Hth+Tsh-mediated overgrowths (Peng et al., 2009). We decided to test whether the Dpp and Hh pathways might synergize with Hth+Tsh in driving the observed overgrowths.

Proliferation induced by combined expression of hth+tsh requires Dpp signalling

During eye development the Dpp pathway has been traditionally involved in the transition between the progenitor and the precursor states: by repressing *hth* at long range and contributing to *tsh* repression at short range (Bessa et al., 2002; Firth and Baker, 2009; Lopes and Casares, 2010). This repression role contributes to the initiation of the retinal differentiation process.

While the role of the Dpp pathway during eye patterning has been widely studied, there are fewer studies on its proliferative role in this tissue. Work by Firth and Baker showed that the activation of this pathway in eye progenitors resulted in increased proliferation (Firth and Baker, 2009; Wartlick et al., 2014). However, the proliferative role of this pathway has been extensively studied in other tissues, like the wing imaginal disc (Restrepo *et al.*, 2014; Hamaratoglu et al., 2014).

Taking all this information into account we decided to examine the possible role of Dpp together with Hth+Tsh in driving overgrowths in the eye imaginal disc. To do so, we altered the expression levels of components of this pathway in the Hth+Tsh background, either through RNAi-induced knockdowns or by overexpression (Figure R2.4 and Figure R2.5).

The observed interactions were evaluated considering changes in size and amount of differentiated cells in late third instar eye discs, as well as the retina size and amount and type of undifferentiated cuticle in the adults. We expect that an enhancement of the phenotype result in an increase in eye disc size and adult indistinct cuticle and/or a reduction of the number of differentiated cells; while a

suppression would result in a decrease in eye disc size and adult cuticle and/or in an increase in the number of differentiated cells in the eye disc that would result in a rescue of the adult retina. In order to maintain the GAL4/UAS ratio that allows a comparison between phenotypes, the number of UAS-transgenes was the same in each genotype.

During the functional interaction analysis several components of the Dpp signalling pathway were tested: the morphogen *Decapentaplegic* (*Dpp*), the type I Dpp receptor *thick veins* (*tkv*), the type II Dpp receptor *punt* and the pathway specific inhibitor *daughters against Dpp* (*dad*).

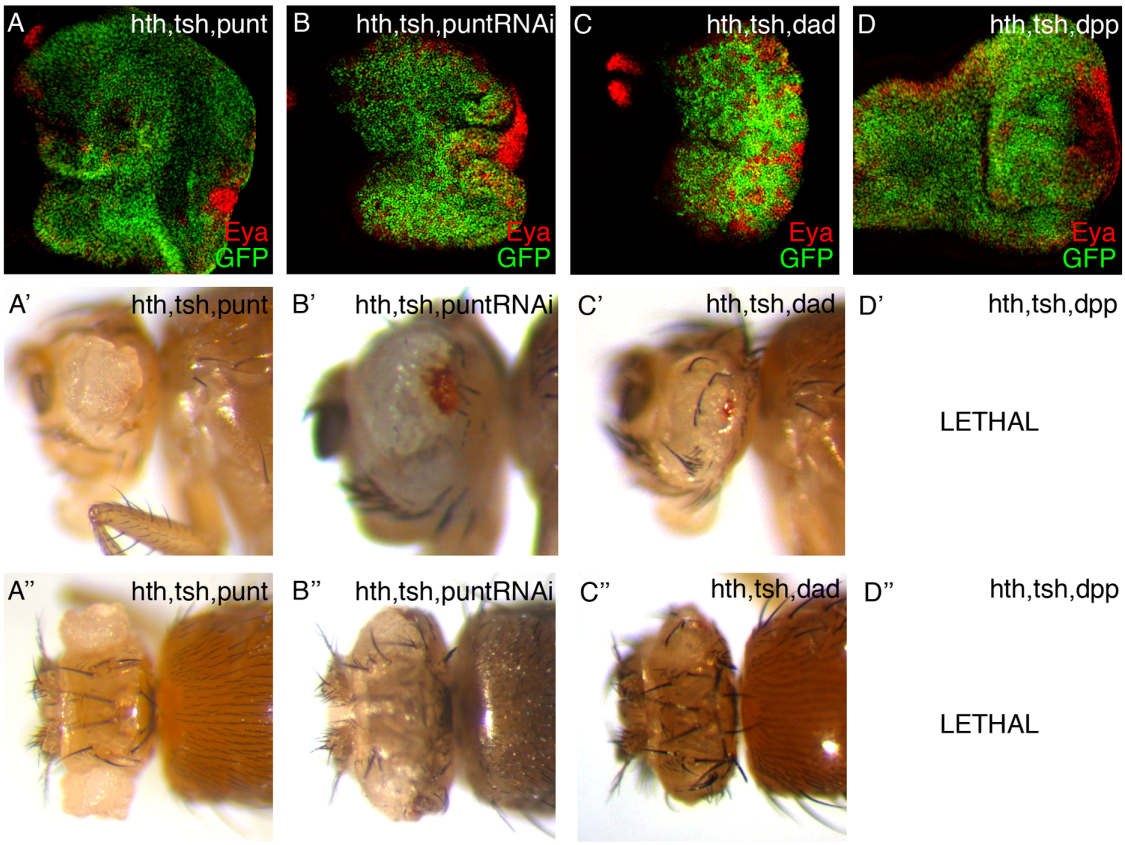

Figure R2.4. Manipulations of the levels of several components of the Dpp pathway in a Hth+Tsh background show functional interactions. Late third larval stage eye discs expressing *hth+tsh+punt* (A), *hth+tsh+puntRNAi* (B), *hth+tsh+Dad* (C) or *hth+tsh+Dpp* (D) driven in undifferentiated cells by the *optix2.3-GAL4* line. All discs are stained with anti-Eya (red); GFP signal comes from the UAS- 131-GFP::hth line. Lateral (A'–D') and dorsal views (A''–D'') of adult heads of the same genotypes as above are shown. Silencing expression of *punt* by RNAi and overexpression of the pMad repressor *Dad* in an *optix*>hth+tsh background resulted in a partial rescue of the overgrowth phenotype, while the overexpression of *punt* or *dpp* resulted in a severely enhanced phenotype. The overexpression of *dpp* in an *optix*>hth+tsh background was lethal –flies died within the puparium before full metamorphosis.

The overexpression of the morphogen Dpp in the hth+tsh background resulted in extremely overgrown and folded eye discs without differentiated cells and to letality in the adults (Figure R2.4D-D''); while the overexpression of the pathway inhibitor Dad resulted in a rescue of the eye disc size with small patches of eyes absent-expressing cells that give rise to small number of ommatidia surrounded by reduced sacs of undifferentiated cells (Figure R2.4C-C'').

However, the Dpp receptors Punt and Tkv are the ones that showed the clearest interactions. Silencing expression of Punt or Tkv by RNAi caused a partial rescue of the differentiated area in the eye disc that consequently resulted in a partially rescue of the adult eye size (Figure R2.5A and Figure R2.4B-B''). Whereas the overexpression of Punt or an constitutively active form of Tkv (TkvQD) dramatically enhanced the phenotype – the eye disc size was severely overgrown and folded with no differentiated cells, giving rise to adult flies with huge amounts of undifferentiated cuticle without ommatidia, in the form of large sacs (Figure R2.5B and Figure R2.4A-A'').

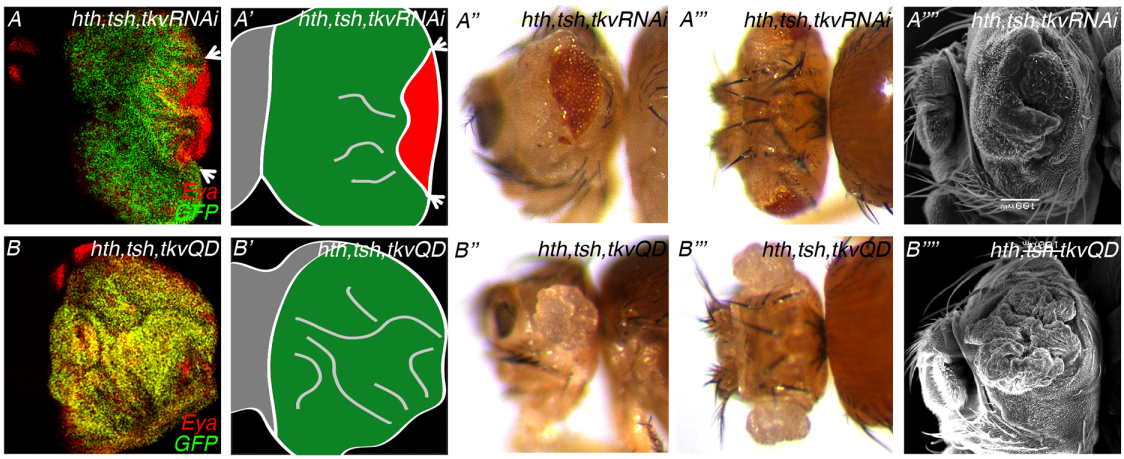

Figure R2.5. Altered expression of Tkv levels, either through RNAi or overexpression, in an Hth+Tsh background results in clear functional genetic interactions. Eye discs expressing *Hth+Tsh+tkvRNAi* (C) or *Hth+Tsh+tkvQD* (D) in undifferentiated cells using the optix2.3-GAL4 line. Discs are stained with anti-Eya (red); GFP comes from the UAS-131-GFPhth line. Morphogenetic furrow is marked with arrows. (A',B') Schematic representation of the discs –antenna in grey, progenitor cells in green and differentiated cells in red. Lateral (A",B") and dorsal views (A"',B"') of adult heads of the same genotypes. Vertical bars represent the percentages of flies with different phenotypes: flies with normal eyes (represented in green), flies with a medium eye (represented in blue), flies with a small number of organized ommatidias (represented in orange) and flies with a total loss of retina (represented in red). (A"",B"") SEM images of lateral views of adult heads of the genotypes. Reducing the levels of Tkv by RNAi in an Hth+Tsh background resulted in a partial rescue of the morphogenetic furrow movement that led to a partly rescued eye. The expression of an activated version of Tkv (TkvQD) together with Hth+Tsh gave rise to highly folded discs with no morphogenetic furrow and overgrowths of indistinct cuticle in the adult.

In all, these results indicated that the Dpp pathway components play a role together with Hth+Tsh in driving overgrowths.

Hth+Tsh-expressing cells increase the levels of Dpp signalling in a position-dependent manner

We next sought if the Hth+Tsh phenotype could be explained by an activation of the pathway, by analysing the expression of the readout of the pathway – phosphorylated Mad (pMad) – in the eye and wing imaginal discs. Dpp binding to its receptors (Punt and Tkv) leads to Mad phosphorylation (pMad). pMad then forms a complex with Medea and enters the nucleus, acting as the active form of the signal transducer of the Dpp pathway (Affolter and Basler, 2007). Whereas Mad is ubiquitously expressed, pMad expression depends on the Dpp gradient, showing higher levels of expression close to the Dpp source (Affolter and Basler, 2007).

Initially, pMad signal was measured in eye discs where Hth, Tsh or Hth+Tsh were forced maintained in the undifferentiated cells using the optix2.3-Gal4 driver. While Hth or Tsh alone only slightly affected pMad signal, the forced maintenance of Hth+Tsh affected both the amplitude and range of pMad signal, resulting in a clear increase of the activity status of the Dpp pathway (Figure R2.6).

Interestingly, while in optix>Hth and optix>Tsh eye discs the pMad signal maintained the pattern of expression observed during normal development (a peak of high signal just before the morphogenetic furrow, followed by a gap in the furrow and the expression derived from the Dpp gradient ahead of the furrow), the optix>Hth+Tsh discs (without morphogenetic furrow movement) showed an accumulation of pMad signal close to the margin (Figure R2.6). In earlier stages of development, when the morphogenetic furrow has not started to sweep the eye disc, *dpp* is produced at the margin – the same location where Hth+Tsh-dependent pMad signal accumulates (Figure R2.6D-D').

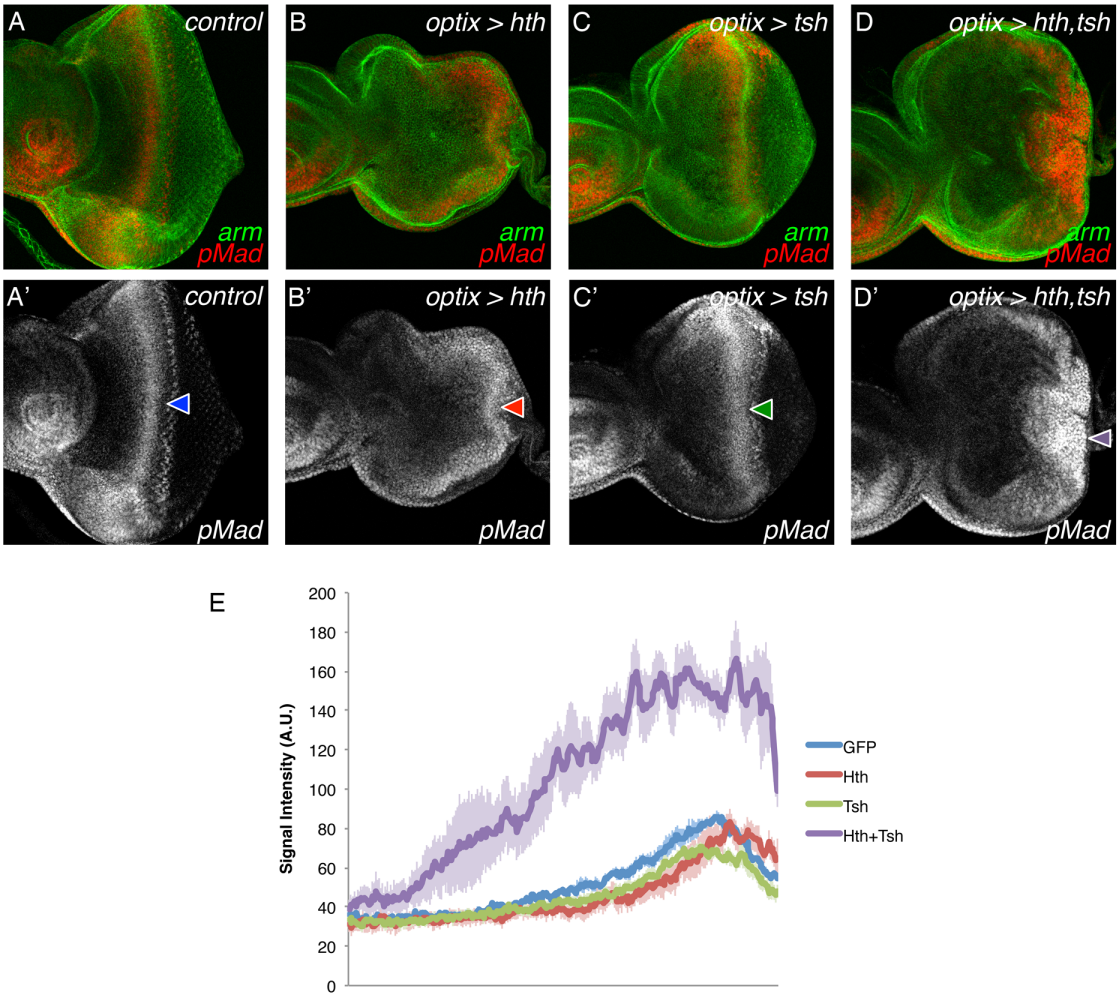

Figure R2.6. Maintenance of Hth and Tsh results in an increase in the pMad signal. (A-D) Late third stage eye discs from control larvae (A) or larvae expressing *hth* (B), *tsh* (C) or *hth+tsh* (D) under the control of the *optix2.3-GAL4* driver. Discs are stained with anti-Arm (green), to outline the tissue, and anti-pSmad3 (red), which crossreacts with endogenous pMad. (E) pMad signal intensity histograms of control (*optix*>+, blue), *hth*-expressing (red), *tsh*-expressing (green) and *hth+tsh*-expressing (purple) discs. Signal intensity, expressed in arbitrary units, is measured ahead of the MF in control, *hth*- and *tsh*-expressing discs (arrowheads in A-C) and from the posterior margin in *hth+tsh*-expressing discs (arrowhead in D), as the MF does not initiate in these discs (n≥5 for each genotype). The standard error to the mean is represented with a lighter shaded area. Hth+Tsh discs show an increase in the range and amplitude of pMad signal.

This position-specific accumulation of pMad led us to consider the possibility that pMad signal accumulation might be spatially controlled. To analyse this possibility we induced cell clones, marked with GFP, expressing either Hth or Tsh alone or in combination, Hth+Tsh. At this point, we decided to randomly induce clones in the eye and wing imaginal discs in order to check if this is a tissue-dependent or -independent mechanism.

Hth or Tsh-expressing clones, either in eye or wing imaginal discs, were not

able to induce pMad signal accumulation (Figure R2.7A,B). However, some Hth+Tsh-expressing clones showed a clear cell autonomous activation of pMad (Figure R2.7C,D). This activation though was not consistent in every clone – only clones located near a Dpp source were able to activate pMad at high levels. As the distance from the clone to the Dpp source increased, the accumulation of pMad signal decreased (Figure R2.7C,D).

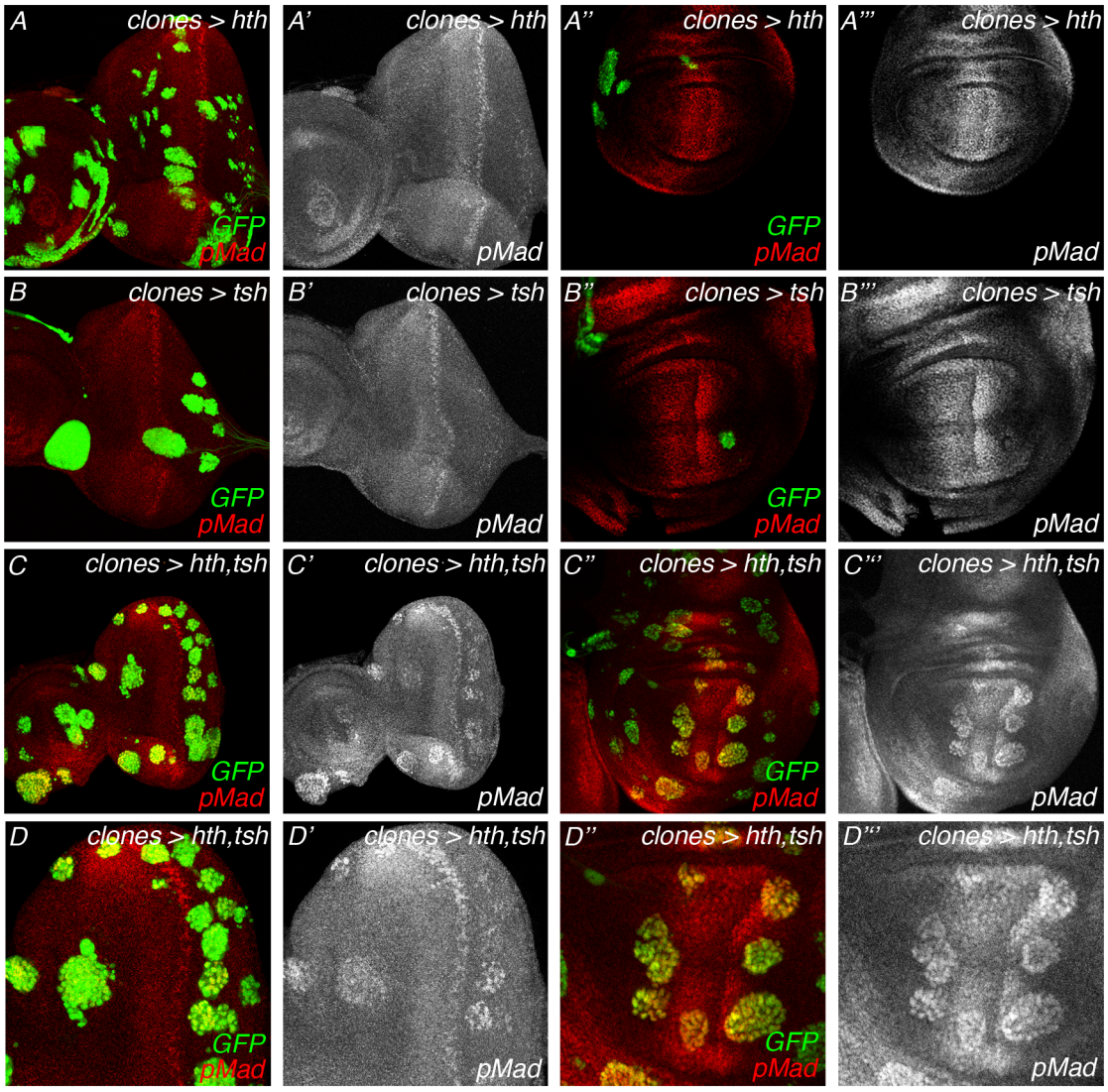

Figure R2.7. Forced maintenance of Hth+Tsh in clones results in a cell-autonomous accumulation of pMad. Hth- (A-A'''), Tsh- (B-B''') or Hth+Tsh-expressing (C-D''') clones, marked by GFP, were induced in the eye and wing imaginal discs at 48–72 h after egg laying. Anti-pSmad3 was used to detect endogenous pMad. Clones expressing Hth or Tsh alone did not show changes in the levels of pMad when compared to the wild-type neighboring cells. Hth+Tsh clones showed a spatial dependent accumulation of pMad in a cell-autonomous manner. pMad levels ranged from high in clones nearby sources of Dpp (AP boundary in the wing disc and posterior margin, and morphogenetic furrow in the eye disc) to background in clones located far away from these sources.

This result points to an activation of the Dpp pathway that does not depend on the upregulation of *dpp* by Hth+Tsh. Rather, the endogenous Dpp produced at its normal sites activates the pathway in the Hth+Tsh cells.

To test this hypothesis, Hth+Tsh clones were induced in a background with a *dpp* transcriptional reporter. This transcriptional reporter contains the *dpp*-disc enhancer that drives expression in the endogenous *dpp*-expression domains (Masucci and Hoffmann, 1993). We observed that Hth+Tsh clones showing high levels of pMad did not activate dpp transcription (Figure R2.8).

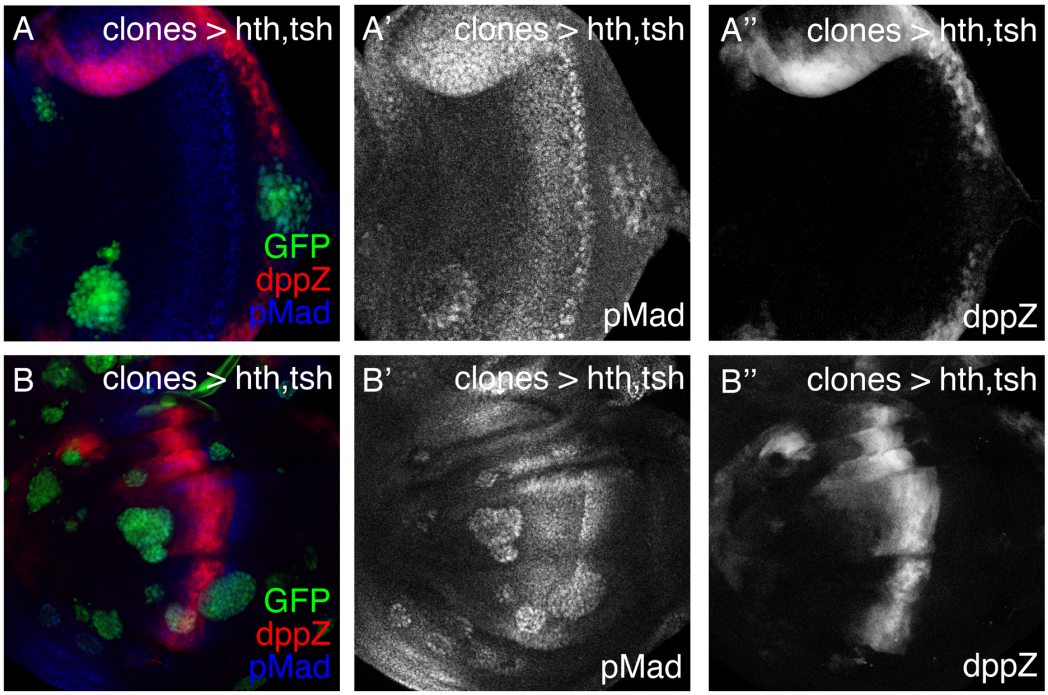

Figure R2.8. hth+tsh-expressing clones increase pMad levels without affecting *dpp* transcription. (A–B'') hth+tsh-expressing clones, marked by GFP, were induced in a *dpp*-lacZ background at 48-72 hours after egg laying. (A-A''', eye disc; B-B''', wing disc). Discs are stained with anti-β-galactosidase and anti-pSmad3. Clones located near an endogenous Dpp source increased pMad levels, while *dpp* transcription was not affected.

Taking into consideration this results, we can rule out the Dpp production from Hth+Tsh cells as responsible for the observed Dpp pathway activation.

Hth+Tsh cells accumulate Dpp

Since Hth+Tsh clones did not activate *dpp* but even so they show an activation of the pathway in a spatial dependent manner, together with the fact that Hth+Tsh growth depends on the presence of the *tkv and punt* receptors (Figure

R2.4 and Figure R2.5), one possibility is that Hth+Tsh cells were able to uptake Dpp from the endogenous source. To explore this hypothesis, we used a combination of two dual binary transcriptional systems: Gal4/UAS (Brand and Perrimon, 1993) and lexA/lexO systems (Yagi et al., 2010).

While HA-tagged Hth+Tsh clones were randomly induced in the eye and wing imaginal discs using the Gal4/UAS system; a GFP-tagged version of Dpp (lexO-eGFP::Dpp) was expressed in the cells where Dpp is endogenously expressed – AP boundary in the wing disc and posterior margin and morphogenetic furrow in the eye disc – using a *dpp-lexA* transgene (Figure R2.9A).

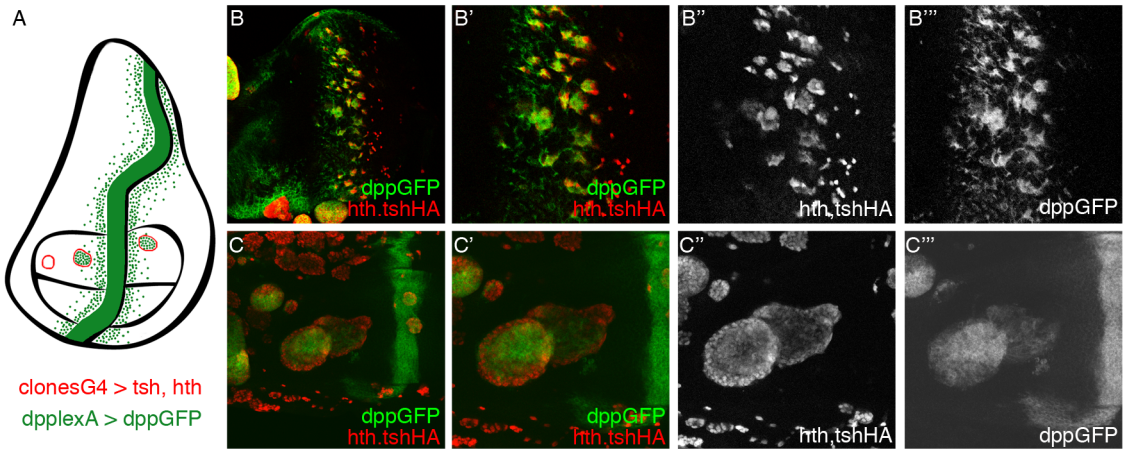

Figure R2.9. Hth+Tsh cells located near an endogenous source of Dpp are able to accumulate the morphogen. (A) Schematic representation of a Hth+Tsh wing imaginal disc using a combination of two binary gene expression systems. Green represents eGFP::Dpp produced at the endogenous *dpp*-expressing stripe along the AP boundary under the control of the lexA/lexO system. Hth+Tsh clones are represented in red, induced by the Gal4/UAS system. (B–C''') Hth+Tsh-expressing clones, marked by anti-HA, were induced in the eye and wing imaginal discs at 72–96 h after egg laying using the Gal4/UAS system; simultaneously in the same discs eGFP::Dpp was expressed using the *dpp-lexA* driver through the lexA/lexO system. Hth+Tsh-expressing clones located near the Dpp source accumulated GFP-tagged Dpp.

In this experiment, our biggest concern was to make sure that Dpp production is independent of Hth+Tsh. To do so, we decided to use the dpp-disc enhancer previously mentioned. Using this enhancer, we knew that since Hth+Tsh did not activate it (Figure R2.8) we were making sure that Dpp-eGFP production was Hth+Tsh-independent. Moreover, this driver allowed the expression of Dpp in the endogenous expression domains.

We observed that Hth+Tsh clones were able to retain high levels of eGFP::Dpp expressed in the endogenous sites of production (Figure R2.9).

Our results confirmed that though Hth+Tsh overgrowths are not able to cell-

autonomously activate *dpp* transcription, they are able to cell-autonomously activate the pathway by retaining the Dpp produced at endogenous sites.

So far, this type of mechanism has been described in clones that express a membrane-tethered nanobody that traps eGFP (Harmansa et al., 2015). To our knowledge this is the first time that this mechanism is described in cells in the absence of non-physiological particles.

Enhanced Dpp signalling and tissue growth is associated to increased levels of the proteoglycan components dally and Dlp and require normal proteoglycan biosynthesis

There are different ways that can explain how Hth+Tsh improved capacity to catch Dpp from endogenous cells might be achieved. One possibility is that Hth+Tsh cells increase the transcription of the Dpp pathway receptor *tkv*, since it is well known that this receptor is able to sequester the Dpp morphogen enhancing the signalling pathway (Haerry et al., 1998; Lecuit and Cohen, 1998; Tanimoto et al., 2000).

To test this hypothesis, Hth+Tsh-expressing clones were induced in eye discs with a *tkv* transcriptional reporter (*tkv-lacZ*) in the background. Rather than showing an activation of *tkv* transcription, Hth+Tsh clones often repressed the transcription of the receptor (Figure R2.10).

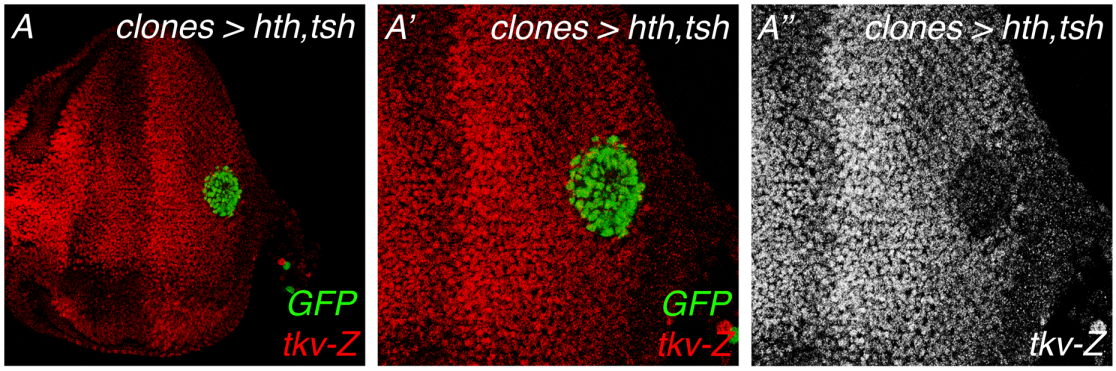

Figure R2.10. hth+tsh-expressing clones do not induce *tkv* transcription. hth+tsh-expressing clones in the eye disc, marked by GFP, were induced in a *tkv*-lacZ background at 48-72 hours after egg laying. Discs are stained with anti-β-galactosidase. hth+tsh-expressing clones reduce *tkv* transcription.

On the one hand, and since *tkv* is a negative target of the Dpp pathway (Lecuit and Cohen, 1998; Tanimoto et al., 2000), this result corroborated the activation of the pathway. On the other hand, this result excluded the transcriptional upregulation of *tkv* as the mechanism that increases the avidity for Dpp of Hth+Tsh-cells.

Another process through which Hth+Tsh cells could concentrate Dpp would be increasing the expression of two glypican members of the heparin-sulphate proteoglycans, Dally and Dally-like (Dlp). These are extracellular matrix components that had been shown to act as key regulators of morphogen distribution, playing an important role in the activity of different signalling pathways, such as Hh, Dpp or Wg pathways (reviewed in Yan and Lin, 2009). We decided to test if their expression was affected by hth+tsh through the analysis of *dally* transcription (transcriptional reporter *dally-lacZ*) and Dlp levels (anti-Dlp antibody) in hth+tsh-expressing clones (Figure R2.11).

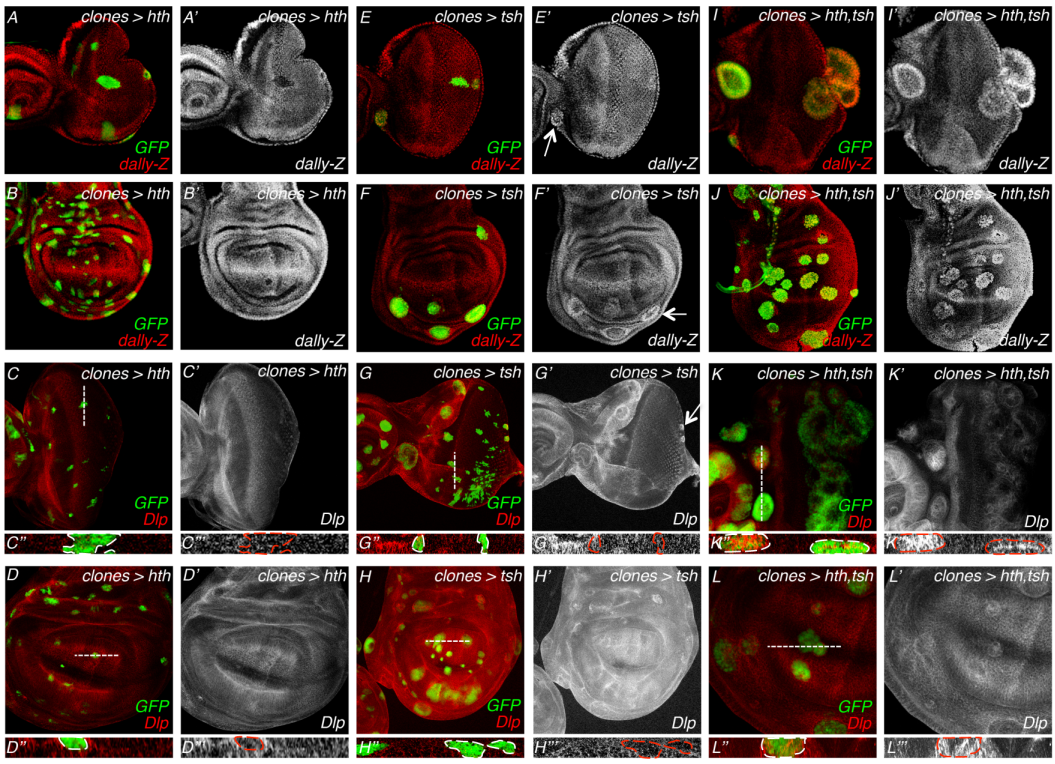

Figure R2.11. Hth+Tsh activate *dally* transcription and Dlp levels. Hth- (A-D"'), Tsh- (E-H"') or Hth+Tsh-expressing (I-L"') clones, marked by GFP, induced in the eye and wing imaginal discs at 48–72 h after egg laying. Clones induced in a *dally*-lacZ background were stained with anti-β-galactosidase to monitor *dally* transcription (A-B', E-F', I-J'). The other discs (C-D"', G-H"', K-L"') were stained with anti-Dlp. The dashed lines approximately mark the optical cross-sections shown in (D", D"', H", H"', L", L"'). Hth-expressing clones showed a decrease *dally-Z* levels and no significant changes in Dlp levels. Clones expressing Tsh did not show detectable differences in *dally* or Dlp, unless they were in a domain that expresses *hth* endogenously, in which case they showed higher levels of both glypicans (arrow). Hth+Tsh-expressing clones showed increased levels of *dally* transcription and Dlp protein.

The expression of Hth alone resulted in a cell autonomous downregulation of *dally* transcription, while the Dlp levels did not seem to be affected (Figure R2.11A-D). Tsh-expressing clones that fell within an endogenous Hth-expressing domain showed upregulation of *dally* transcription and Dlp levels, but the other clones did not (Figure R2.11E-H). However, hth+tsh-clones showed high levels of *dally* and accumulation of Dlp in the membrane (Figure R2.11I-L).

We then decided to functionally assess if the hth+tsh-induced upregulation of glypican levels was responsible for the hth+tsh phenotype. To reduce the levels of Dally and Dlp, we decided to decrease the levels of one of the enzymes involved in the biosynthesis of proteoglycans, *sulfateless* (*sfl*) (Ferreira and Milan, 2015; Lin et al., 1999). The RNAi-mediated silencing of *sfl* in the hth+tsh-expressing background (*optix>hth+tsh*) resulted in a partial rescue of the adult eye size (Figure R2.12A-C), even though reducing the levels of *slf* alone (*optix>sfl*) caused a small eye reduction (Figure A.4G).

Additionally to the adult eye morphology, we decided to analyse the effects that reducing *sfl* levels had on the Dpp signalling gradient. The pMad profiles were quantified and fitted to an exponentially decaying gradient, gaining information regarding two key Dpp properties: the Dpp effective degradation rate, *k* (which is an inverse measure of its stability) and the Dpp effective diffusion coefficient, *D* (Wartlick et al., 2011 and Annex B; Figure R2.12D). When we compared the pMad profile in *optix>hth+tsh* to controls (*optix>GFP*), we observed a relative increase in Dpp stability (k_{HT}/k_{GFP}=0.74) and diffusion (D_{HT}/D_{GFP}=1.30). The additional RNAi-mediated attenuation of *sfl* (*optix>hth+tsh+slfRNAi*) partly rescued the normal pMad profile, indicating an almost normal Dpp stability (k_{HTS}/k_{GFP}=1.17) and a further decrease in Dpp diffusion (D_{HTS}/D_{GFP}=0.65) (Figure R2.12D). Indeed, the sole attenuation of *slf* function in *ey>slf* resulted in a clear reduction of both stability and diffusion of Dpp (Figure R2.13).

Altogether, these experiments indicate that hth+tsh induce the expression of two glypicans, Dally and Dlp, thus facilitating the retention of endogenous Dpp and consequently leading to an increase in the intracellular signalling. This would contribute to the Hth+Tsh-mediated tissue overgrowth and differentiation blockade.

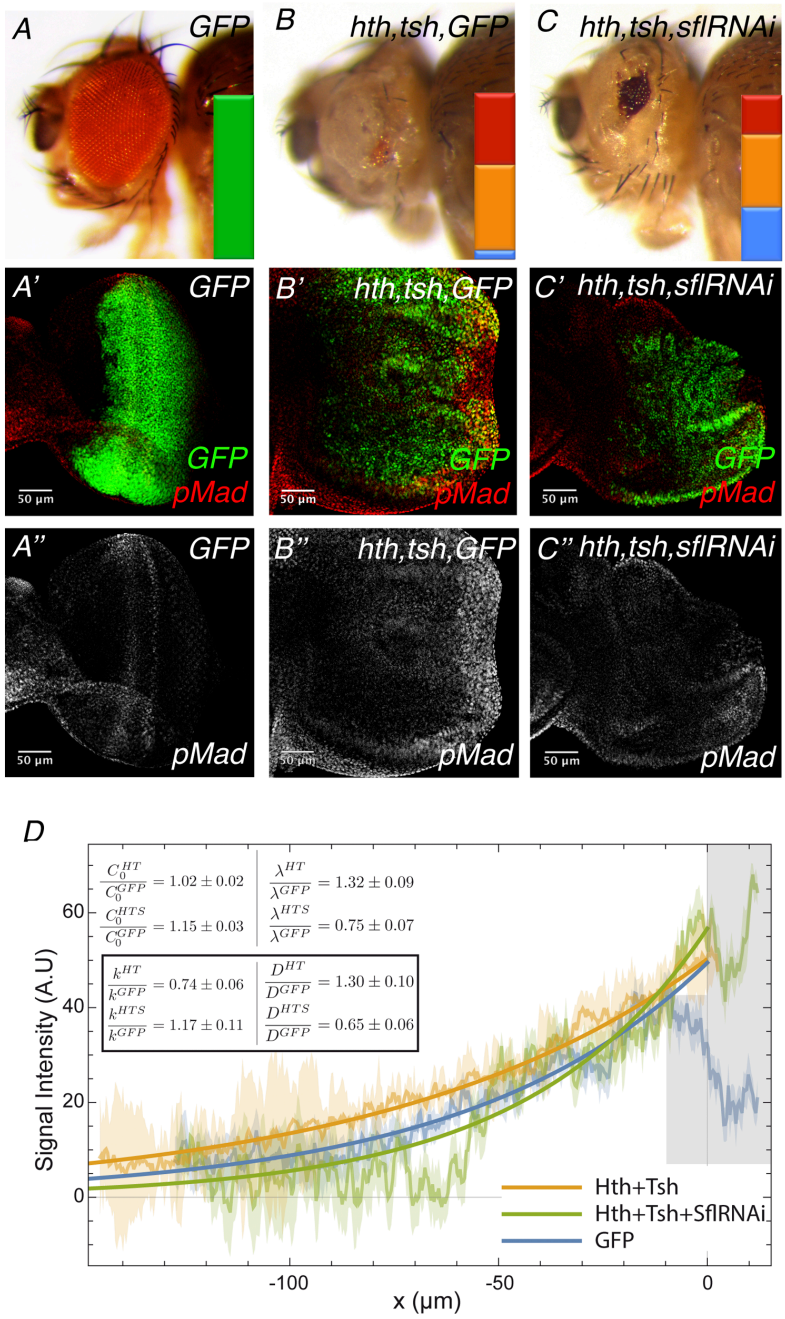

Figure R2.12. Reduction of *sulfateless (sfl)* levels through RNAi in an Hth+Tsh background results in a partial rescue of the Hth+Tsh-phenotype. Lateral view of adult heads from control (A), Hth+Tsh+GFP (B), Hth+Tsh+sflRNAi (C) expressed in undifferentiated cells using the optix2.3-GAL4 line. Horizontal bars represent the percentages of flies with different phenotypes: flies with normal eyes (represented in green), flies with a medium eye (represented in blue), flies with a small number of organized ommatidias (represented in orange) and flies with a total loss of retina (represented in red). (A'-C') Late third instar eye discs of the above genotypes stained with anti-pSmad3. (D) Signal intensity histograms of pMad of control (blue), hth+tsh-expressing (green) and hth+tsh+sflRNAi-expressing (red) discs. Signal intensity, expressed in arbitrary units, is measured ahead of the MF in control, and from the posterior margin in hth+tsh- and hth+tsh+sflRNAi-expressing discs (n≥5 for each genotype). The standard error to the mean is represented with a lighter shaded area. Fit to mean in solid lines. Data in a shaded grey area was excluded from fits. Ratios of signal intensity at position x=0 (C0), characteristic length scale of the gradient (λ), effective degradation (k) and effective diffusion coefficient (D) are shown inlay. Reducing the levels of *sfl* by RNAi in an hth+tsh background resulted in a partial rescue of the phenotype and in slightly reduced pMad signal.

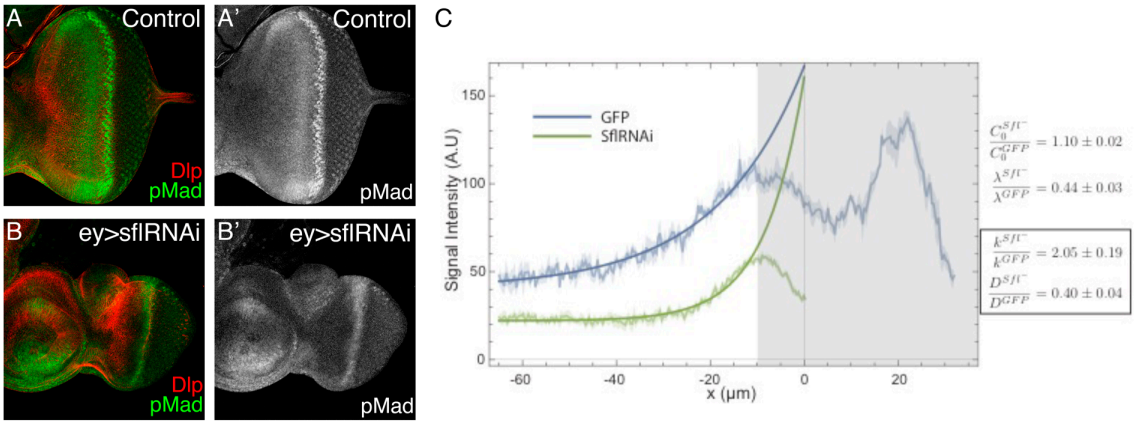

Figure R2.13. Reduction of *sfl* expression causes a reduction of stability and diffusion of Dpp. Late third instar eye discs from control larvae (A,A') or larvae expressing *sflRNAi* (B), under the control of the *ey-GAL4* driver. Discs are stained with anti-pSmad3 (green) and anti-Dlp (red). (C) Signal intensity, expressed in arbitrary units, is measured ahead of the MF in control and SflRNAi-expressing discs (n=8 for each genotype). The standard error to the mean is represented with a lighter shaded area. Fit to mean in solid lines. Data in a shaded gray area was excluded from fits. Ratios of signal intensity at position x=0 (C0), characteristic length scale of the gradient (l), effective degradation (k) and effective diffusion coefficient (D) are shown aside. Silencing the expression of *sfl* by RNAi results in a reduction of Dpp's stability and diffusion.

Hh signalling is required for the Hth+Tsh-induced proliferation

Besides the known role of the Hippo pathway in controlling the Hth+Tsh-mediated overgrowths (Peng et al., 2009), in this chapter we have established a new player in this process – the Dpp signalling pathway.

The signaling microenvironment of the eye disc also includes Hedgehog (Hh). The Hh pathway has been shown to activate the Dpp pathway during *Drosophila* eye development (Heberlein et al., 1993) and has been implicated in cancer through proliferation induction/maintenance (reviewed in Jia et al., 2015). In what follows, we focus on testing the requirement of the Hh signalling pathway to the hth+tsh-phenotype.

To test this hypothesis we manipulated the expression levels of components of the Hh pathway in the hth+tsh-background, by Hh RNAi-induced knockdown and by Hh or Ci overexpression (Figure R2.14).

While Hh knockdown resulted in a rescue of the eye disc size and a smaller quantity of undifferentiated cuticle in the adult (Figure R2.14C); the overexpression of either Ci or Hh resulted in an enhanced phenotype (Figure R2.14 B,D).

In the case of Hh overexpression the interaction was dramatic, resulting in

huge overgrowths of the eye primordium size (at least three times larger than hth+tsh discs) and to lethality in the adults (Figure R2.14D,D'). Although, the overgrowth observed in hth+tsh+Hh eye discs was massive, the apico-basal polarity of the tissue was not affected as seen by the apical marker, aPKC (Figure R2.14D''), indicating that the integrity of the epithelium was preserved.

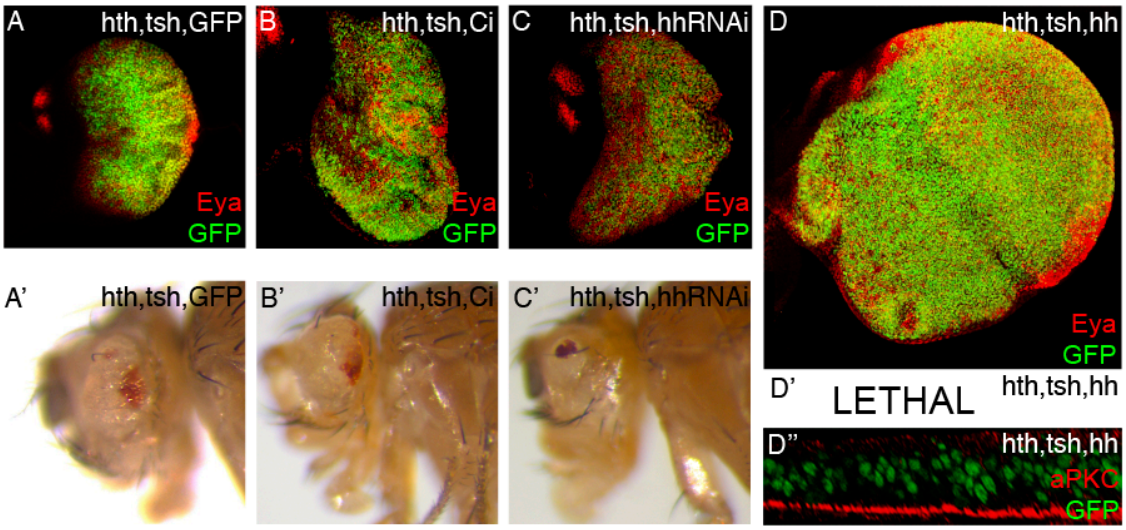

Figure R2.14. Manipulations of the levels of components of the Hh pathway in a Hth+Tsh background show functional interactions. Late third larval stage eye discs expressing *hth+tsh+GFP* (A), *hth+tsh+Ci* (B), *hth+tsh+hhRNAi* (C) or *hth+tsh+Hh* (D) driven in undifferentiated cells by the *optix2.3-GAL4* line. All discs are stained with anti-Eya (red); GFP signal comes from (A) the UAS-GFP + UAS-131-GFPhth lines and (B-D) the UAS- 131-GFP::hth line. Lateral views (A'–D') of adult heads of the same genotypes as above are shown. Overexpression of Ci in an optix>hth+tsh background resulted in a slightly enhanced phenotype; while silencing expression of *hh* by RNAi in the same background resulted in a partial rescue of the overgrowth phenotype. The overexpression of *hh* in an *optix*>hth+tsh background was lethal – flies died within the puparium before full metamorphosis; the imaginal discs showed a severe enhancement of the phenotype, but cell polarity was not affected.

hth+tsh-expressing cells increase the levels of Hh signalling as seen by Ci and Ptc expression

We next tested if the synergism observed between Hth+Tsh and the Hh pathway could be explained by an activation of the pathway. To do so, we analysed the expression of Cubitus interruptus (Ci) in the eye disc. Ci is a direct target of the Hh signalling pathway and can be used as readout of the pathway.

We analysed the Ci expression in eye discs where Hth, Tsh or Hth+Tsh were forcibly maintained using the optix2.3-Gal4 driver. While Hth or Tsh alone only slightly affected Ci signal, the forced maintenance of Hth+Tsh resulted in a

clear increase of the Hh pathway activity (Figure R2.15).

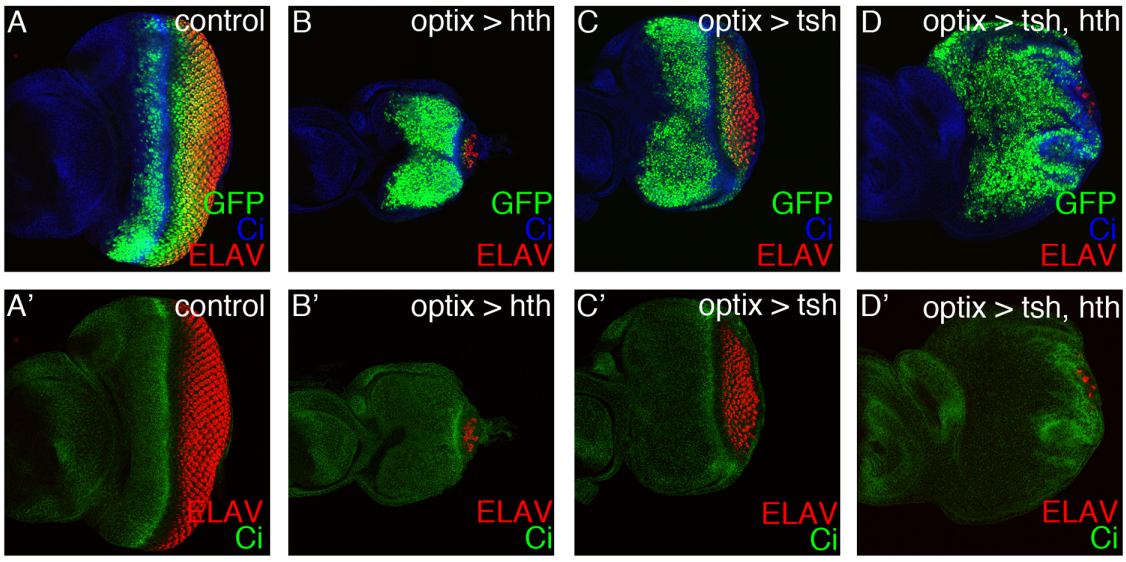

Figure R2.15. Maintenance of Hth and Tsh results in an increase in the Ci signal. (A-D) Late third stage eye discs from control larvae (A) or larvae expressing *hth* (B), *tsh* (C) or *hth+tsh* (D) under the control of the *optix2.3-GAL4* driver. Discs are stained with anti-ELAV (red), and anti-Ci (blue in A-D and green in A'-D'). Hth+Tsh discs show increased Ci levels closer to the posterior margin.

To test this in more detail, we analysed the expression of Ci and Ptc, another direct target of the Hh pathway (Alexandre et al., 1996) in randomly induced clones expressing Hth, Tsh or Hth+Tsh in the eye disc. Clones showed that both proteins are expressed at higher levels in Hth+Tsh-expressing clones, but not in clones where these genes are expressed alone (Figure R2.16). Interestingly, in some Hth+Tsh-clones we could observe a non-autonomous activation of Ci and Ptc in cells surrounding the clones.

Hth+Tsh induce a de novo activation of *hh* transcription

We next decided to test if the observed activation of the Hh pathway resulted from a direct induction of *hh* transcription, what would explain the non-autonomous activation of the readouts of the pathway.

We induced Hth-, Tsh- or Hth+Tsh-expressing clones in an *hh-lacZ* background (a reporter of *hh* transcription).

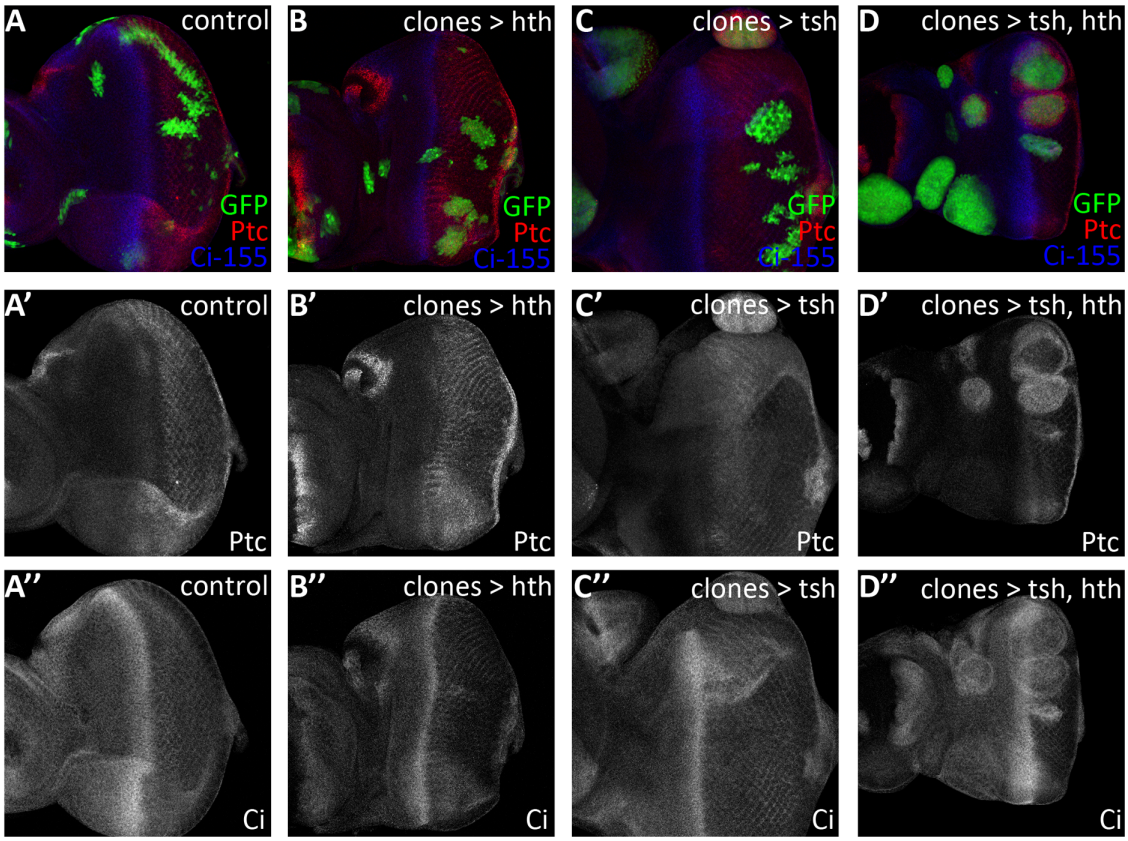

Figure R2.16. Forced maintenance of Hth+Tsh in clones results in increased levels of Ci and Ptc. Control (A-A''), Hth- (B-B''), Tsh- (C-C'') or Hth+Tsh-expressing (D-D'') clones, marked by GFP, were induced in the eye imaginal discs at 48–72 h after egg laying. Discs are stained with Ptc in red and Ci-155 in blue. Clones expressing Hth alone did not show changes in the levels of Ci or Ptc when compared to the wild-type neighboring cells. Clones expressing Tsh did not show detectable differences Ci or Ptc, unless they were in a domain that expresses *hth* endogenously, in which case they showed higher Ci and Ptc levels. Hth+Tsh clones show increased levels of both Ci and Ptc.

Hth-expressing clones did not show an increase in *hh* transcription (Figure R2.17A). Interestingly, Tsh-expressing clones that fall in a region where Hth is normally expressed showed a slightly increase in *hh* transcription levels. When Tsh-expressing clones are induced in regions of the disc where *hth* is normally not expressed, *hh* transcription levels are not affected (Figure R2.17B). Forced maintenance of Hth+Tsh resulted in higher levels of *hh* transcription when compared with the neighbouring cells (Figure R2.17C,D). These results point to a *de-novo* activation of *hh* transcription driven by hth+tsh expression.

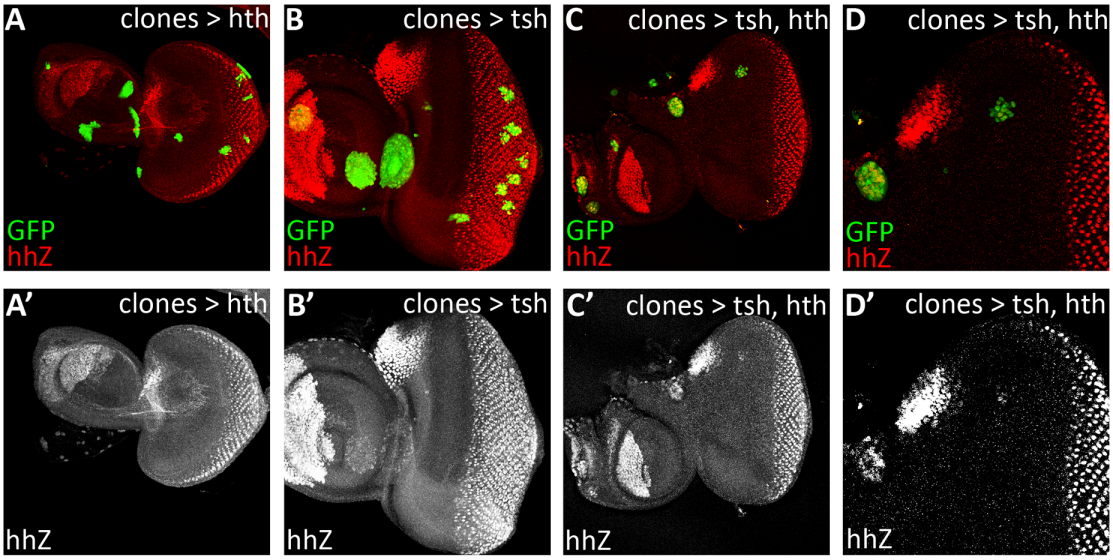

Figure R2.17. Hth+Tsh activate *hedgehog* transcription. Hth- (A,A'), Tsh- (B,B') or Hth+Tsh-expressing (C-D') clones, marked by GFP, induced in the eye imaginal discs at 48–72 h after egg laying. Clones were induced in a *hh*-lacZ background and stained with anti-β-galactosidase to monitor *hh* transcription (A-D'). Hth+Tsh-expressing clones showed increased levels of *hedgehog* transcription.

In all, besides the previously described role for the Hippo pathway in hth+tsh-mediated overgrowths (Huang et al., 2005; Peng et al., 2009) we here show that these two transcription factors are able to induce several other signalling pathways in order to control cell proliferation.

In the Part I of results, we show that hth+tsh are able to modulate the expression of components of the Ecdysone signalling pathway in order to control cell proliferation. This pathway was originally involved in the systemically control of developmental stages and growth, but here we show that modulation of this pathway affects proliferation in a specific cell population: progenitor (or progenitor-like) cells.

In this chapter, we tested the role of two organ-autonomous signalling pathways –Hh and Dpp– and showed that both are capable of modulating the hth+tsh-induced overgrowths.

Together, these results show how the transcription factors Hth and Tsh exert a global impact on the proliferation machinery by modulating the action of several signalling pathways that act systemically as well as locally. We find similar gene expression signatures in eye progenitor-like cells than in specific tumour types, highlighting a potential mechanistic parallel between progenitor proliferation growth and human cancer.

PART III

Bap60, A Component Of The Brahma Chromatin-Remodelling Complex, Is Necessary For The Progenitor-to-Precursor Transition

Organogenesis requires of a tight coordination between the specification of organ-progenitor cells, their expansion through proliferation and their subsequent recruitment out of the cell cycle as precursors. These precursors ultimately differentiate into the organ's specific cell types. The layout of these processes is particularly clear during *Drosophila* eye development.

Under normal conditions, *Drosophila* eye development is very robust, despite the fact that it is a very fast process: most of the patterning of the retina is completed in two days. Speed and robustness require that cells exhibit two apparently contradictory properties. On the one hand, gene expression patterns in progenitors, precursors or differentiating cells must be stable enough as to guarantee an orderly progress through these cells states. On the other, these states must be sufficiently labile as to allow fast transitions. This property of "transient stability" can in principle derive from gene regulation by *cis*-acting elements and chromatin modifications (Schuettengruber et al., 2007). The *Drosophila* Brahma (Brm) complexes, homologous to mammalian SWI/SNF complexes, promote chromatin remodelling and act as both transcriptional activators and repressors. These complexes use ATP to regulate the location and conformation of nucleosomes on DNA, regulating DNA accessibility, which is required for gene-selective transcription regulatory functions (Clapier and Cairns, 2009; Ho and Crabtree, 2010). Earlier work in *Drosophila* has implicated Osa, a subunit of the BAP-class of Brm complexes, as a regulator of the proliferation and survival of eye progenitor cells and of photoreceptor differentiation (Treisman et al., 1997; Baig et al., 2010). Still, the precise mechanisms of action of Brm complexes during eye development and, in particular, how these complexes integrate in the eye-specific gene regulatory network, remain unclear. Chromatin modifiers have no DNA-sequence specificity so they need to be recruited to the chromatin at specific sites by sequence-specific transcription factors. Therefore, in principle, chromatin complexes are guided to the DNA by transcription factors, and in turn transcription factor binding can be affected by remodelled chromatin.

In this work we set to identify chromatin-remodelling components with specific roles during the early stages of eye development.

A gene network model points to the chromatin remodeller Bap60 as potentially involved in early eye development

In order to get a better picture of the genes controlling the transition from progenitors to precursors, we decided to build a gene network that included transcription factors and chromatin remodellers, as these are major controllers of gene expression. First, we selected transcription factors expressed in the eye and chromatin remodelling genes that had been described as potential targets of *eyeless* (*ey*) (Ostrin et al., 2006), *eyes absent* (*eya*) and *sine oculis* (*so*) (Jemc and Rebay, 2007; Jusiak et al., 2014), or the proneural gene *atonal* (*ato*) (Aerts et al., 2010), which imposes a retinal fate. Recently, genome-wide binding data for Hth in the eye disc have been published (Slattery et al., 2013). Since Hth expression in progenitors is required to maintain the progenitor proliferative and undifferentiated state (Bessa et al., 2002; Lopes and Casares, 2015; Neto et al., 2016), we used these binding data to directly link Hth to transcription factors expressed in the eye and chromatin remodellers, representing the potential direct regulation by Hth. To further enrich the network, DroID (The Comprehensive Drosophila Interactions Database; www.droidb.org) was used to add genetic and protein interaction data, comprising reported genetic interactions, protein-protein interactions and predicted interactions based on interactions between orthologous proteins in other species (yeast, *C.elegans* and human). As the resulting network is very complex, two filters were applied: only interactions that were direct with retinal determination genes and with a correlation value higher than 0.4 were considered (Figure R3.1, orange box). The resulting network comprises most retinal determination and early eye differentiation transcription factors, as well as transcription factors acting as transducers of major signalling pathways involved in eye development, most notably those in the Dpp, Notch and EGF-receptor pathways (circular nodes in Figure R3.1). The network also includes a number of chromatin remodellers (hexagonal nodes in Figure R3.1). One of these chromatin related genes is Bap60 whose product is predicted to interact physically with Eya (protein-protein interaction predicted by yeast two-hybrid screen by Curagen). Additionally, one of the other chromatin related genes is Moira (Mor), which is a known Bap60 interactor and part of the Brm complex (reviewed by Kwon and Wagner, 2007;

Reisman et al., 2009). Mor is also predicted to interact with Eya (based on interactions between the orthologous proteins in *C.elegans*).

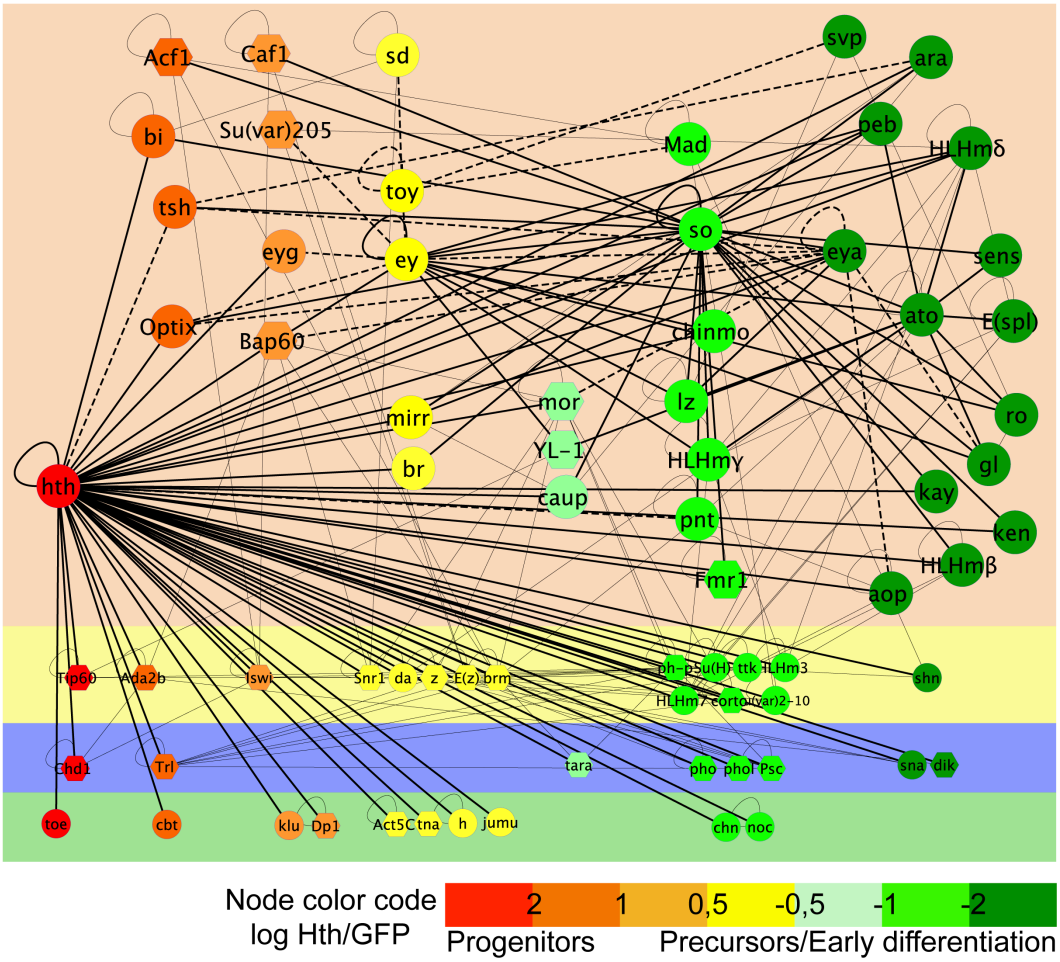

Figure R3.1. Early eye gene regulatory model. Transcription factors are represented as circular nodes; chromatin remodellers as hexagonal ones. The color code indicates the range of fold enrichment in *tio>GFP:hth* cells ("progenitors") versus *tio>GFP* cells ("precursors/early differentiation"). Thicker black lines represent interactions between retinal genes and their potential targets (*ey* (Ostrin EJ et al., 2006), *eya* and *so* (Jemc J and Rebay I, 2007), *ato* (Aerts S et al., 2010), *so* (Jusiak B et al., 2014) and *hth* (Slattery et al., 2013)); dashed lines represent genetic and protein-protein interactions between retinal determination genes and eye transcription factors and chromatin remodellers taken from DroID and thinner black lines represent genetic and protein-protein interactions taken from DroID between non-retinal determination genes. Orange panel contains genes with direct interactions with retinal determination genes (besides genes that only interact with *hth*) and *ato*, yellow panel contains genes that interact with *hth* and with genes from the orange panel, blue panel contains genes interacting with *hth* and genes from the yellow panel and green panel contains genes that only interact with *hth*. For details, see text.

Although the resulting network comprises genes and links that are supported by several sources of experimental evidence, none of the published experiments considered were able to discriminate between interactions happening in progenitors or in more committed cell states. To obtain this information, we designed an experiment that allowed us to get the transcriptional profile of

progenitors and precursors/early differentiating retinal cells separately. The insertion *tioA4-GAL4* (Tang and Sun, 2002) is a GAL4 reporter of the *tiptop* (*tio*) gene (Bessa et al., 2009). In *tioA4-GAL4; UAS-GFP* (*tio>GFP*) discs, GFP marks cells anterior to the morphogenetic furrow (progenitors and precursors) and also cells at and immediately posterior to the morphogenetic furrow (these latter marked with the photoreceptor marker ELAV) (Figure R3.2). Therefore, the *tio>GFP* cell population comprises progenitors (which, at late L3 stage are already a minor subpopulation within the disc), precursors and early differentiating retinal cells.

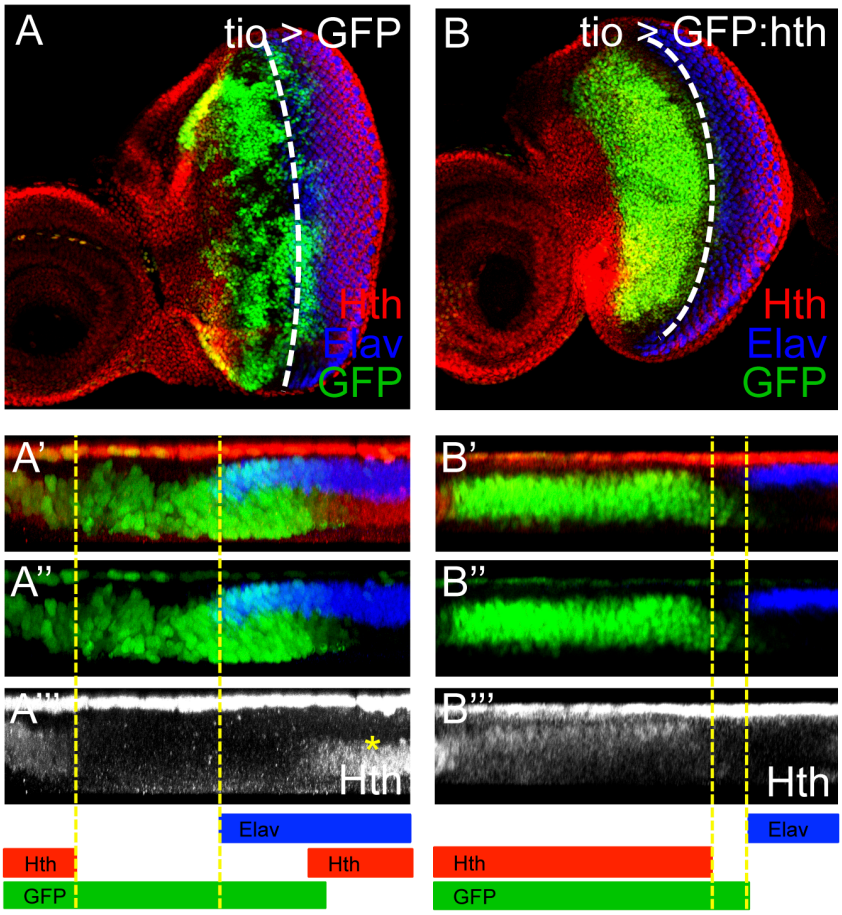

Figure R3.2. *tio>GFP* and *tio>GFP:hth* discs. (A,B) Late third instar (L3) eye discs from *tioA4-GAL4; UAS-GFP* (*tio>GFP;* A) and *tioA4-GAL4; UAS-GFP:hth* (*tio>GFP:hth,* B) stained for Hth (red) and Elav (Blue). Anterior is left. GFP marks the *tio-GAL4* expression domain. A vertical cross-section through a *tio>GFP* disc (A'). GFP cells comprise from anterior Hth-expressing progenitors to the first rows of differentiating ommatidia, marked with Elav (A'', A'''). In *tio>GFP:hth* discs all GFP-positive cells express Hth (B', B'', B'''). White dashed line marks the morphogenetic furrow position, yellow dashed lines mark the different domains of the eye disc.

To enrich specifically for progenitors, we drove the expression of a GFP-tagged-Hth in the *tio* domain (*tioA4-GAL4; UAS-GFP:hth* or *tio> GFP:hth*) (Figure R3.2). As noted previously, *hth* is a progenitor-specific gene and its forced expression results in progenitor cell maintenance and blockade of differentiation (Pai et al., 1998; Pichaud and Casares, 2000; Bessa et al., 2002). The Hth protein levels in *tio>GFP:hth* discs are likely within the physiological range: Hth protein is degraded if not bound to its partner Exd (Rieckhof et al., 1997), so all Hth excess driven in *tio>GFP:hth* discs is expected to be degraded. Indeed, we find that the levels of Hth protein in *tio>GFP:hth* discs are comparable to the maximal levels found in progenitors in control discs (Figure R3.2). Late L3 discs from both genotypes (*tio>GFP* and *tio>GFP:hth*) were dissected, their cells dissociated and the GFP-positive cell populations FAC-sorted and pooled. RNA extracted from the *tio>GFP* and *tio>GFP:hth* cells was used for RNA-sequencing (see Annex C) and the two transcriptional profiles compared. Fold change was calculated as the log2 (tio>GFP:hth/tio>GFP) ratio (Table C.5; Figure R3.3 for some examples).

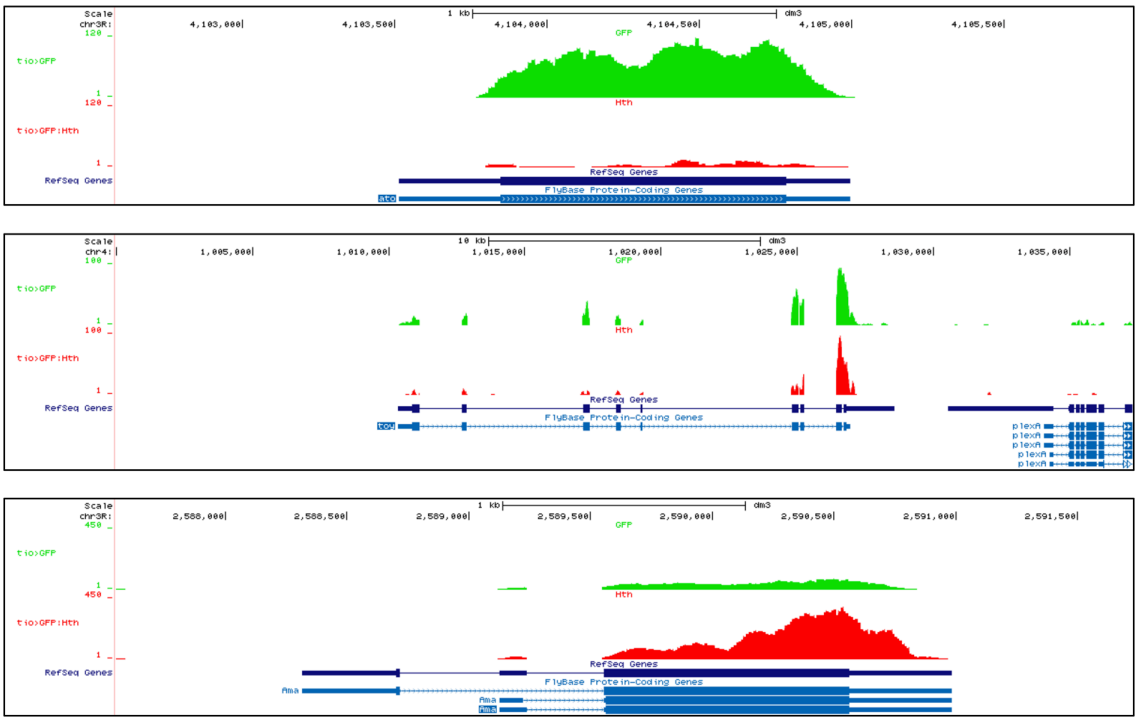

Figure R3.3. Examples of genes with or without changes in their expression levels between tio>GFP and tio>GFP:Hth. Gene expression levels as a genome browser track of the mapped reads for ato (precursors/early differentiating gene), toy (expression does not change between tio>GFP and tio>GFP:Hth) and ama (progenitor gene). Green tracks represent the expression levels in tio>GFP and red tracks represent the expression levels in tio>GFP:Hth.

Finally, as a technical validation of the RNA-seq results, the expression of a set of nineteen differentially expressed genes was measured using real-time PCR. Of these 19 genes, 18 showed qualitatively and quantitatively similar results in both tests (Figure R3.4).

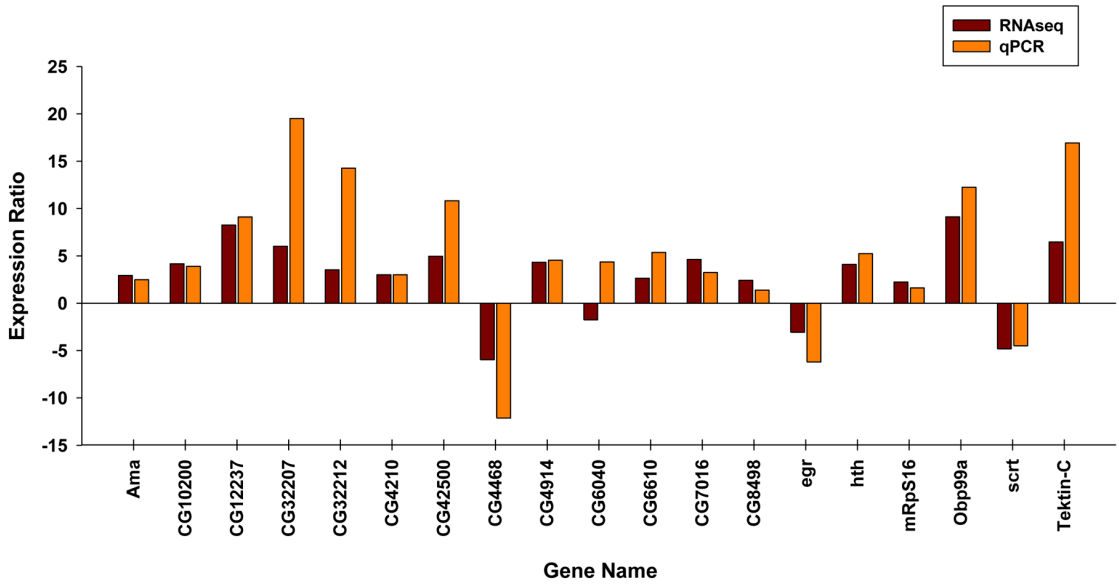

Figure R3.4. Quantitative RT-PCR (qPCR) validation of a set of 19 genes identified as differentially expressed in the RNA-seq experiment. Gene expression ratios in *tio>GFP:hth* versus *tio>GFP* cells estimated by RNA-seq and qPCR. With the exception of *egr,* all other genes show congruent expression changes using both methods of gene transcription quantification.

To validate these results we decided to check which proportion of genes show expression patterns in the eye disc that are consistent with being differentially expressed in progenitors or precursors. We selected genes which are expressed in control cells (RPKM higher than 5) and expressed in *tio>GFP:hth* cells (RPKM higher than 0), and which show a 3-fold expression difference in the RNA-seq experiment (log2(fold change) higher than 1.5 or lower than -1.5) and compared their expression with results from an *in situ* hybridization expression database (Pavel Tomancak, MPI-CMB, Dresden, unpublished). 98% and 66% of the genes predicted to be enriched in progenitors or precursors, respectively, show a pattern of expression that is consistent with this prediction (Figure R3.5).

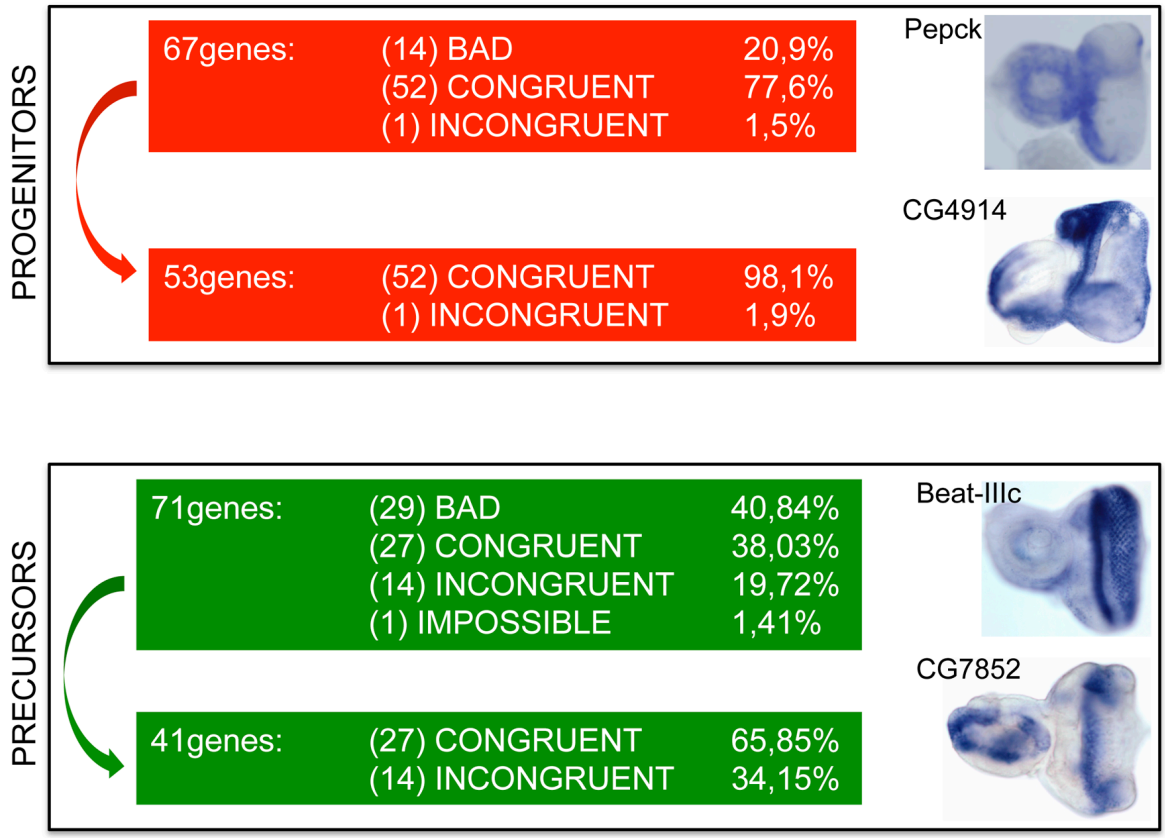

Figure R3.5. *in situ* validation of the RNAseq results. Percentage of genes predicted to be more expressed in progenitors (upper panel) or precursors (lower panel) that show a congruent or incongruent *in situ* pattern of expression (Pavel Tomancak database, unpublished). Eye-antennal imaginal discs showing examples of *in situ* for progenitor genes (upper panel) and precursor genes (lower panel).

Next, genes that were differentially expressed in progenitors and precursor/early differentiating cells in RNA-seq experiments were globally characterized using gene ontology (GO) annotations, using GeneCoDis (http://genecodis.dacya.ucm.es) (Figure R3.6). The biological functions associated to each population differed significantly. Precursor/early differentiating cell genes, as expected, were enriched in functions related to the development of the eye, such as "Compound eye development", "Sensory organ precursor cell fate determination", "R7 cell fate commitment" or "R3/R4 cell fate commitment". Progenitor cells, a more poorly characterized population, showed significant enrichment in terms associated with energy production, protein synthesis and metabolism (Figure R3.6), which are in agreement with progenitors being a heavily proliferative cell population. In the discussion, we will compare this analysis with a

similar analysis of the GO terms in optix>hth discs, a genotype that resembles the one described here.

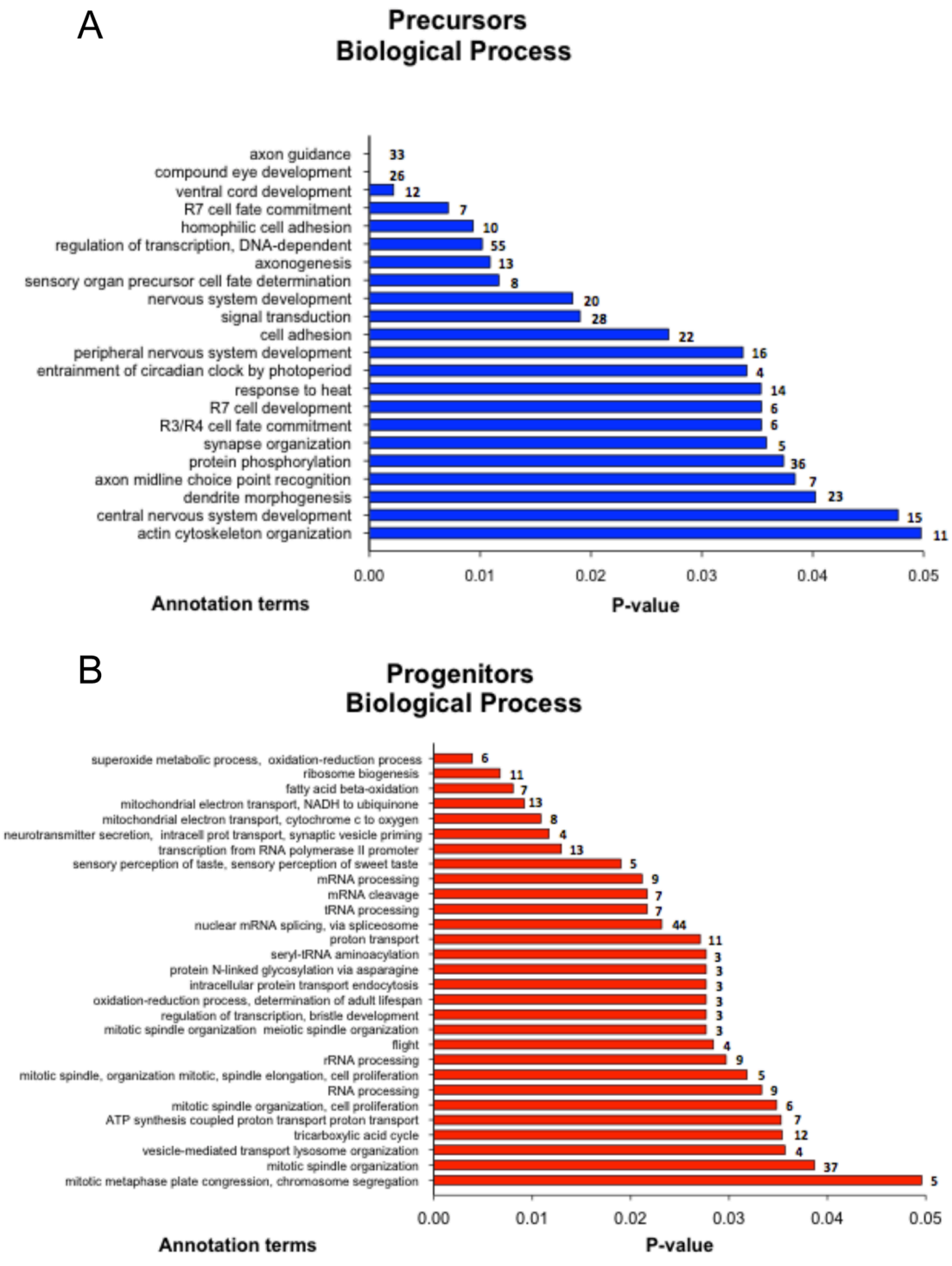

Figure R3.6. GO characterization of the *tio>GFP* (precursors/early differentiating cells) and *tio>GFP:hth* (progenitors) transcription profiles. GO categories for biological process of precursor/early differentiating cells population (graphic includes all genes with a expression level of at least 3-fold change) (A) and of progenitor population (graphic includes all genes with a minimum expression level of 2-fold change) (B). Column numbers represent the number of genes in each GO category.

Using this information, we added a dynamical component to the network – i.e the network interactions were ordered to represent the progenitor → precursor → early differentiation direction as the transcription factors/chromatin remodellers show decreasing, increasing or constant expression along this transition (Figure R3.1 and Table C.5). In this network, on a constant background of Pax6 genes *ey* and *toy* expression (yellow nodes in Figure R3.1), high levels of *hth*, *tsh* or *optix* characterize progenitors (red and orange nodes in Figure R3.1), while retinal determination genes, such as *eya* and *so*, and more markedly *ato* and other genes directly involved in the differentiation of the retina, such as *glass*, characterize precursors/early differentiating cells (green nodes in Figure R3.1).

Within this network, the Brm complex component *Bap60* (*Brahma associated protein of 60kd*) is highly connected within the network: it is linked to Hth and Ey (Ostrin et al., 2006; Figure R3.7) as their potential target.

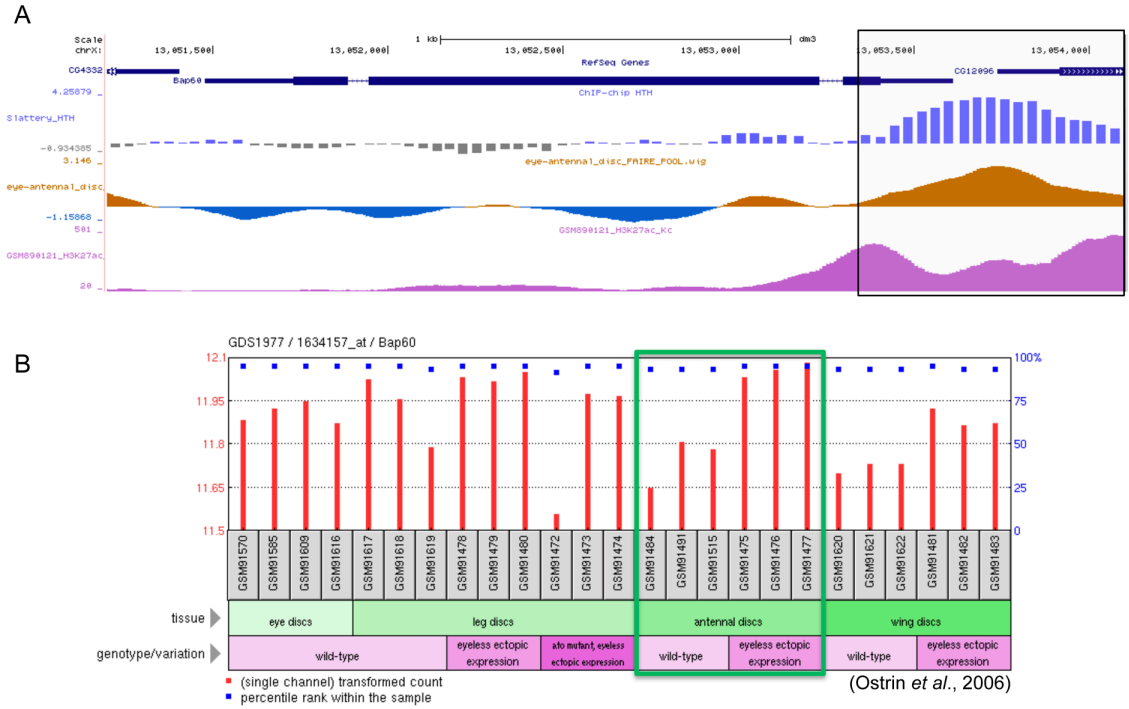

Figure R3.7. *Bap60* is a potential Homothorax and Eyeless target. (A) Hth peak in Bap60 promoter. Peaks of Hth binding (Slattery et al., 2013), FAIRE results in wild type eye-antennal imaginal discs (McKay and Lieb, 2013), histone mark H3K27ac (marks active enhancers) in the vicinity of Bap60 in chromosome X. Black box marks the region in the vicinity of the Bap60 promoter that show a peak for Hth binding in an open chromatin region enriched for H3K27ac signal. (B) Microarray analysis of *Bap60* expression profile of leg, wing, and antenna imaginal discs ectopically expressing the retinal determination protein Eyeless in the atonal wild-type or mutant background (this information can be found at GEO profiles – NCBI: http://www.ncbi.nlm.nih.gov/geoprofiles?term=GDS1977[ACCN]+bap60) (data from Ostrin *et al.*, 2006).

Bap60 physically interacts with Eya, in addition to other described interaction with Brm complex members, Brm itself and Moira (Mor) (Figure R3.1). Moreover, *Bap60* is enriched in progenitors (1.8 times, as measured by RNA-seq and real-time PCR; Figure R3.8A).

Hereafter, we focus our study on Bap60 since its connectivity within the network points to its playing an important role in the transition from progenitor to precursor cells.

Bap60 is required specifically in undifferentiated cells for eye development

To analyse if *Bap60* function was required during eye development, we attenuated its expression in developing eyes by driving UAS-Bap60-RNAi with *ey-GAL4* (*ey>Bap60RNAi*).

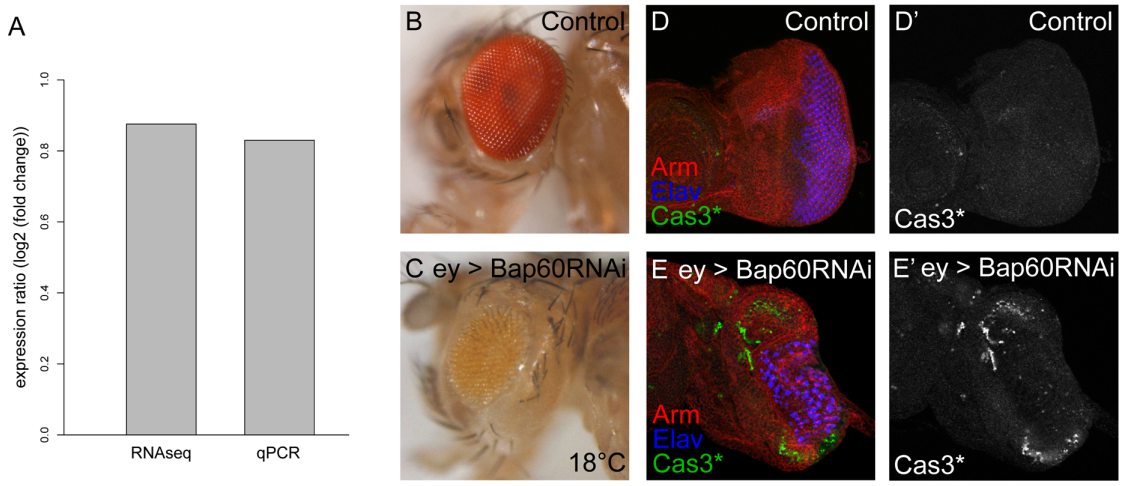

Figure R3.8. *Bap60* RNAi-mediated knock-down results in aberrant eye development. (A) Expression ratio (log2 (fold change)) between Bap60 transcript levels in tio>GFP:hth and tio>GFP larvae, measured by RNAseq and quantitative RT-PCR using RNA isolated from eye imaginal discs. Adult heads (lateral views) of wild-type (B) and *ey>Bap60-RNAi* (C) flies. Late L3 eye discs from control (D), and *ey>Bap60-RNAi* (E) larvae, stained for cleaved Caspase 3 (green), Elav (blue) and Armadillo (red). Depleting *Bap60* levels specifically in the eye causes significant adult retina loss, induces high levels of apoptosis mainly in the most anterior region of the eye imaginal disc and also results in incorrect pattern of differentiation.

The eyes of *ey>Bap60RNAi* adults were severely reduced in size (Figure R3.8B,C) (Marinho et al., 2013). When eye discs were examined, fewer and abnormally patterned ELAV-positive photoreceptors were observed (Figure R3.8D,E). This was accompanied by increased apoptosis, as detected by

augmented activated-caspase 3 signal, although this was only noticeable in the undifferentiated region of the disc (Figure R3.8D,E). Two RNAi lines were used with similar effects (see Materials and Methods). In addition, co-expression of a UAS-GFP:Bap60 construct (see Materials and Methods) together with UAS-Bap60-RNAi rescued the small eye phenotype in adults, suggesting that the phenotypes observed are due to a specific *Bap60* knockdown (Figure R3.9).

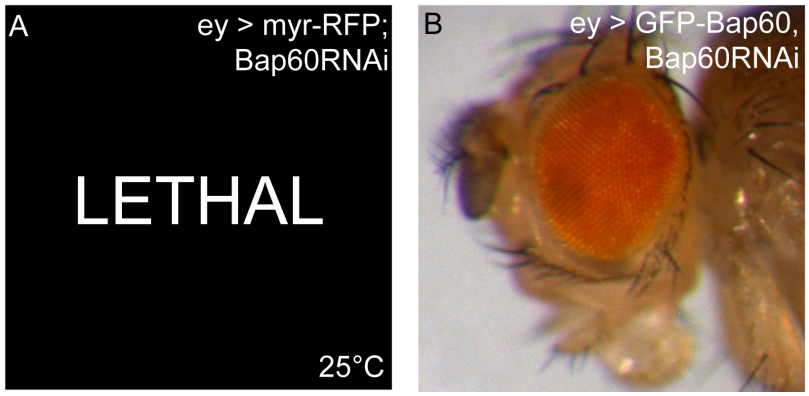

Figure R3.9. Overexpression of GFP-Bap60 rescues the lethal phenotype of *Bap60* RNAi-mediated knock-down. Adult heads (lateral views) of *ey>myr-RFP;Bap60-RNAi* (A) and *ey>GFP-Bap60,Bap60-RNAi* (B) flies.

To analyse in detail the results obtained in ey>Bap60RNAi eye discs, clones where we knocked down *Bap60* function by RNAi were induced. These clones were generated by the flip-out technique at different developmental time points (Struhl and Basler, 1993) and were marked positively by the expression of GFP.

As observed in ey>Bap60RNAi discs, *Bap60* knockdown clones showed strongly reduced ELAV signal cell-autonomously, indicating that loss of Bap60 finally affects photoreceptor formation (Figure R3.10). This result however might be due the accumulated effect of the Bap60 knockdown, because the clones were induced earlier during development.

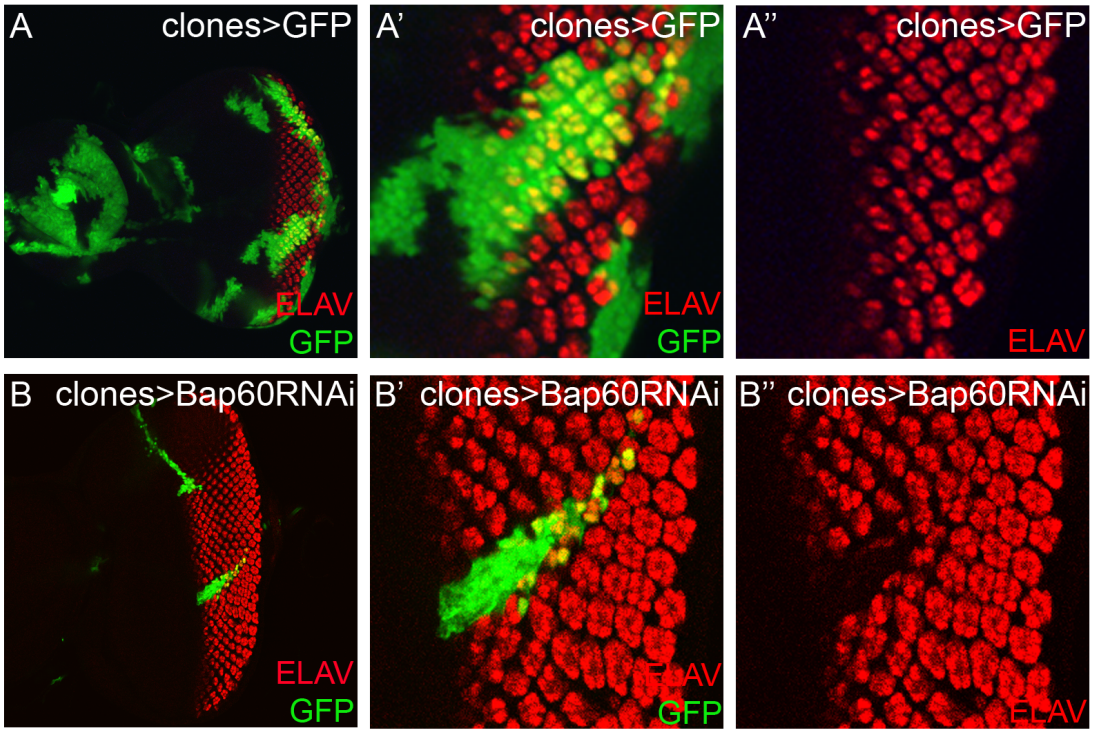

Figure R3.10. *Bap60* influences *ELAV expression*. *Bap60* loss-of-function mitotic clones were induced in the eye antennal imaginal discs at 24-48 hours after egg laying and the imaginal discs were analysed in late third instar **(B, B', B'')**. Neutral clones were also induced at 24-48 hours after egg laying and analysed in late third instar **(A, A', A'')**. Clones were marked positively by the presence of GFP. **(A, A')** and **(B, B')** images show higher magnifications of clones and **(A'', B'')** show the ELAV channel. *Bap60* knockdown clones result in a considerably reduction of *ELAV* expression.

To test if *Bap60* is specifically required for the survival of proliferating cells and if *Bap60* is essential during the entire eye developmental process or if, in contrast, it is required at specific developmental stages, neutral and Bap60 knockdown clones were induced between 24h-48h and 48h-72h after egg laying, corresponding to the first and the second instars (L1 and L2), respectively, and the imaginal discs were analyzed in the third instar (late L3 larvae).

The first important feature observed after this experiment was the number and size of neutral and *Bap60* knockdown clones obtained. As would be expected for neutral clones, we observed that the clones generated earlier in eye development were larger and fewer than the ones generated later (Figure R3.11). Clones induced during L1 where *Bap60* expression was attenuated by RNAi were much smaller than the neutral ones. This result indicated that the *Bap60* knockdown cells proliferated less or died more or both. In addition, we could also observe cleaved caspase-3 staining in *Bap60* knockdown clones localized in the

anterior region of the eye imaginal disc, but not in clones localized in the differentiated photoreceptor clusters. These results are in agreement with the previously prediction by which *Bap60* should be mainly required in proliferating cells.

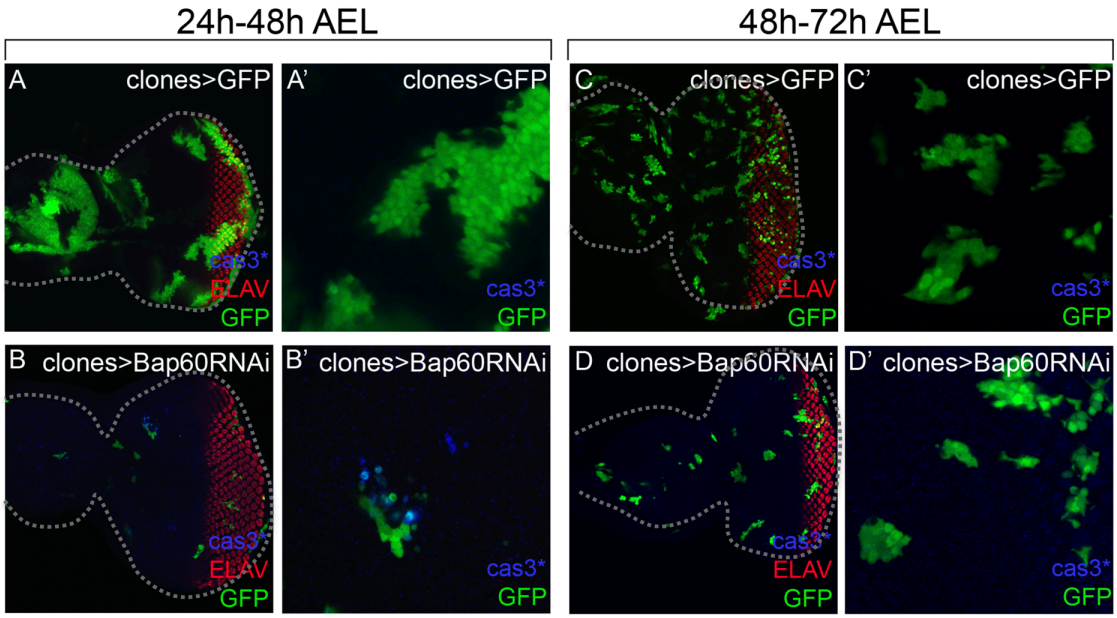

Figure R3.11. Bap60 protein seems to be mainly required for survival of proliferating cells during the earlier phases of eye development. *Bap60* loss-of-function mitotic clones were induced in the eye antennal imaginal discs at 24-48 **(B, B')** or 48-72 **(D, D')** hours after egg laying and the imaginal discs were analysed in late third instar. Neutral clones were also induced at 24-48 **(A, A')** or 48-72 **(C, C')** hours after egg laying. Clones were marked positively by the presence of GFP. **(B)** *Bap60* RNAi clones generated during the first instar are smaller than the corresponding neutral ones, meaning that they proliferate less. **(B')** Additionally these clones show cleaved caspase-3 positive cells whereas neutral clones show no caspase-3 activation. **(D)** and **(D')** *Bap60* RNAi clones generated during the second instar result in lesser clones than in the wildl-type, although the clones size is similar. These clones show no caspase-3 activation.

Regarding the *Bap60* knockdown clones generated during L2, the number of clones in the eye disc was significantly reduced when compared with the control (neutral) clones, although the clone size was approximately the same. It is also important to note the lack of cleaved caspase-3 staining, i.e. the lack of apoptosis associated with these clones, in the most anterior proliferating but also in the posterior clones (Figure R3.11).

To further prove that *Bap60* function was required in specific regions of the primordium rather than having a generalized function, we expressed UAS-Bap60RNAi with region-specific GAL4 drivers (Figure R3.12). Three GAL4 drivers were used: *optix2.3-GAL4* drives expression in precursor cells anterior to the

morphogenetic furrow (Figure R3.12A); *ato-GAL4* is expressed only at the morphogenetic furrow and in cells immediately posterior to it (that is, in early differentiating retina) (Figure R3.12B); *GMR-GAL4* is expressed exclusively posterior to the morphogenetic furrow in all differentiating cells (Figure R3.12C) (Song et al., 2000). While ato>Bap60RNAi and GMR>Bap60RNAi flies showed normal adult eyes, *optix>Bap60RNAi* flies showed reduced and rough eyes (Figure R3.12D-F). Since the only domain that is exclusively affected by *optix2.3-GAL4* is the region anterior to the morphogenetic furrow, these results indicate that *Bap60* function is primarily required in the undifferentiated cells of the eye primordium.

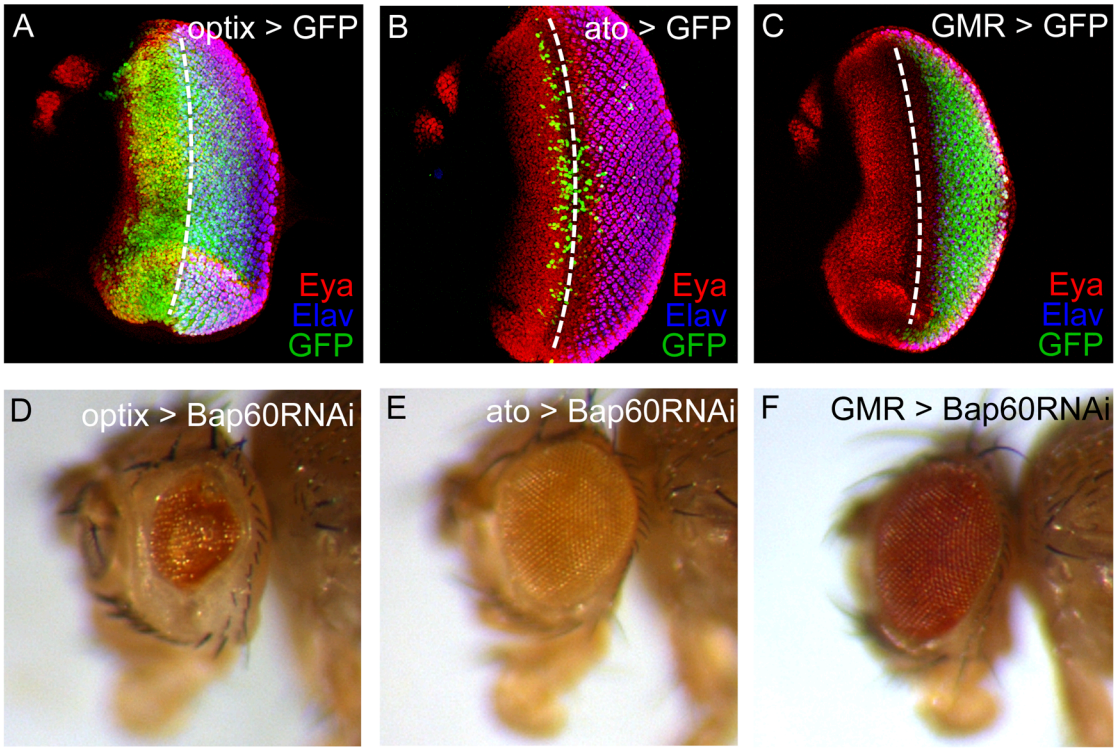

Figure R3.12. Stage-specific requirement for Bap60. (A-C) late L3 eye discs from *optix>GFP* (A), *ato>GFP* (B) and *GMR>GFP* (C) larvae, stained for Eya (red) and Elav (blue). Approximate span of the progenitor, precursor and retinal differentiation domains are marked. (D-F) Adult heads (lateral views) of *optix>Bap60-RNAi* (D), *ato>Bap60-RNAi* (E) and *GMR>Bap60-RNAi* (F) flies. Only *optix>Bap60-RNAi* flies exhibit an abnormal eye development. Dashed line marks the morphogenetic furrow position.

Bap60 is required downstream of *ey*

Bap60 has been proposed to be controlled transcriptionally by Ey (Ostrin et al., 2006). To test this hypothesis functionally, we took advantage of the ability of Ey to drive eye development when ectopically expressed (Halder et al., 1995).

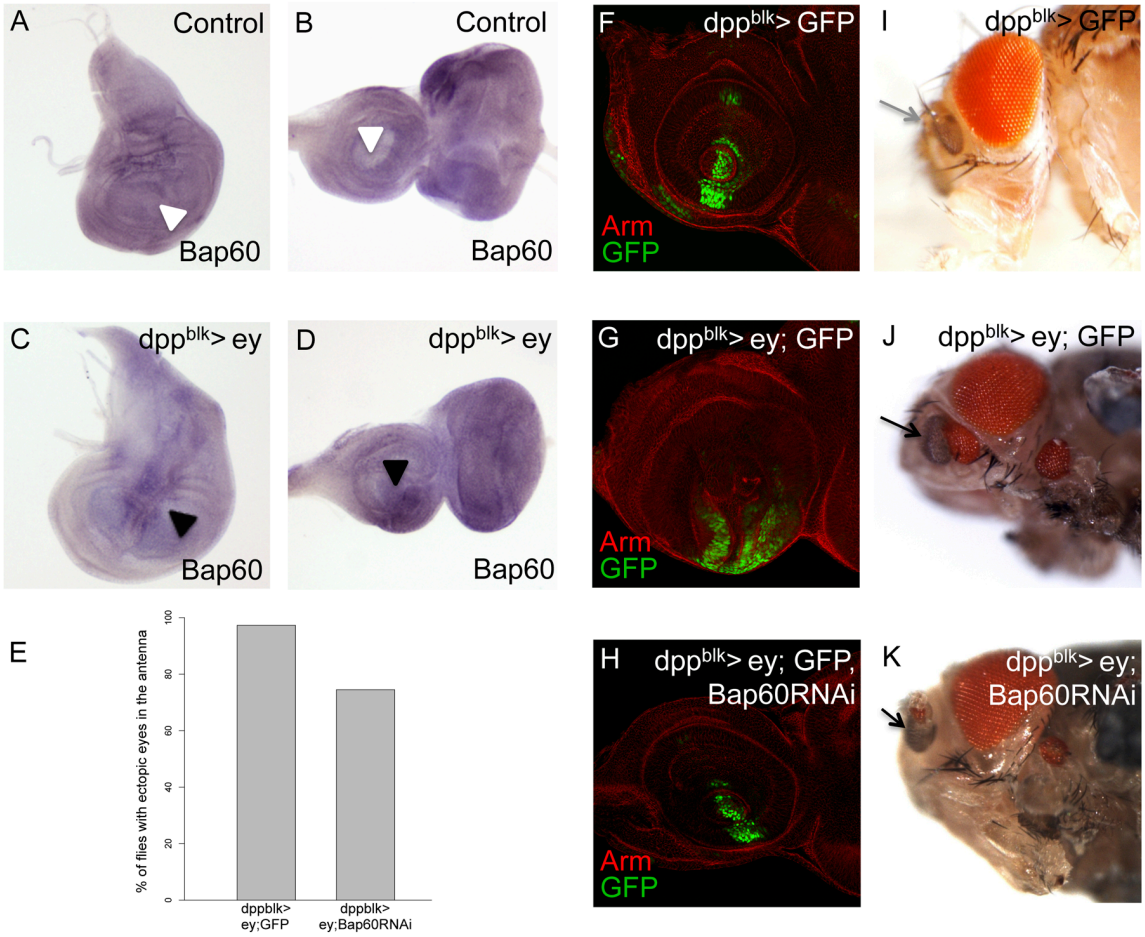

Figure R3.13. Ectopic expression of *eyeless* in regions of the wing and antenna imaginal discs induces Bap60 expression and *Bap60* is required for eye development downstream of *ey*. RNA *in situ* hybridization of the whole-mount third-instar wing (A, C) and eye imaginal discs (B, D), from wild-type (A, B) and dppblk-Gal4/UAS eyeless (C, D) larvae. *Bap60* is transcribed in wild-type wing (A) and eye antennal (B) imaginal discs; Bap60 is expressed in a dynamic pattern in the eye imaginal disc, with high expression in the anterior region and low levels in the region posterior to the morphogenetic furrow where differentiation occurs. *eyeless* misexpression driven by dppblk-Gal4 results in higher Bap60 levels in the dppblk domain (black arrowheads). (E) Graphic representing the percentage of flies with ectopic eyes in the antenna. Inhibition of Bap60 function by RNAi downstream of Eyeless results in a decrease of approximately 20% of the flies with ectopic eyes in the antenna. (I-K) Adult and pharate heads (lateral views) showing the absence or presence of ectopic eyes and (F-H) the corresponding antennal imaginal discs expressing GFP in the dppblk domain. Grey arrow points to the wild type antenna, black arrows point to antennas with ectopic eyes. Inhibition of Bap60 function downstream of Eyeless results in smaller ectopic eyes.

When *ey* is expressed under the control of the *dppblk-GAL4* driver, the expression of *Bap60* mRNA, monitored by *in situ* hybridization with a Bap60 anti-sense RNA probe, increases in both the eye-antennal and wing discs (Figure R3.13C,D). This supports the idea that *Bap60* expression is regulated by Ey. In *dppblk>ey* flies, large antennal eyes are formed with high penetrance (Salzer and Kumar, 2010 and Figure R3.13G,J). When *Bap60*RNAi is driven together with *ey*, both the size and the frequency of these ectopic eyes are reduced (Figure R3.13E,H,K), indicating that *Bap60* is required downstream of *ey* for eye development.

Loss of Bap60 function impairs the progenitor-to-precursor gene expression progression

Progenitors and precursors are maintained as distinct cell states by the mutual repression of *eya* by *hth* (in progenitors) and of *hth* by *eya* (in precursors). The transition from progenitors to precursors is driven by Dpp which, produced at the morphogenetic furrow tips the equilibrium towards *hth* repression, thus allowing the increase in expression of *eya*, *so* and *dachshund* (*dac*) (Bessa et al., 2002). These genes then lock-in the retinal differentiation process (Almudi and Casares, 2016). If *Bap60* was required for a normal progenitor-to-precursor transition, its loss should affect the expression of *hth* and *eya*. We found it to be the case, as in *Bap60*RNAi clones the expression of Eya is lost or severely reduced (100%, N=29), while that of Hth is maintained in regions where it should be already repressed (72% of the clones, N=7). Interestingly, within these clones, Hth expression is heterogeneous (Figure R3.14A). The expression of a *hth* transcriptional reporter (*hth-lacZ*) in *Bap60*RNAi clones showed a similar behaviour (expression heterogeneity and abnormal posterior maintenance in the same percentage of clones) (Figure R3.14B) suggesting that Bap60 acts on *hth* at a transcriptional level. However, when we carried out a similar experiment for *eya*, using a lacZ-reporter insertion that reproduces *eya* expression faithfully (*eya-lacZ*), *eya-lacZ* signal was not lost (in 60% of the clones, N=18), despite the fact that in the same *Bap60*RNAi clones the signal of Eya protein was absent or severely reduced (Figure R3.14C).

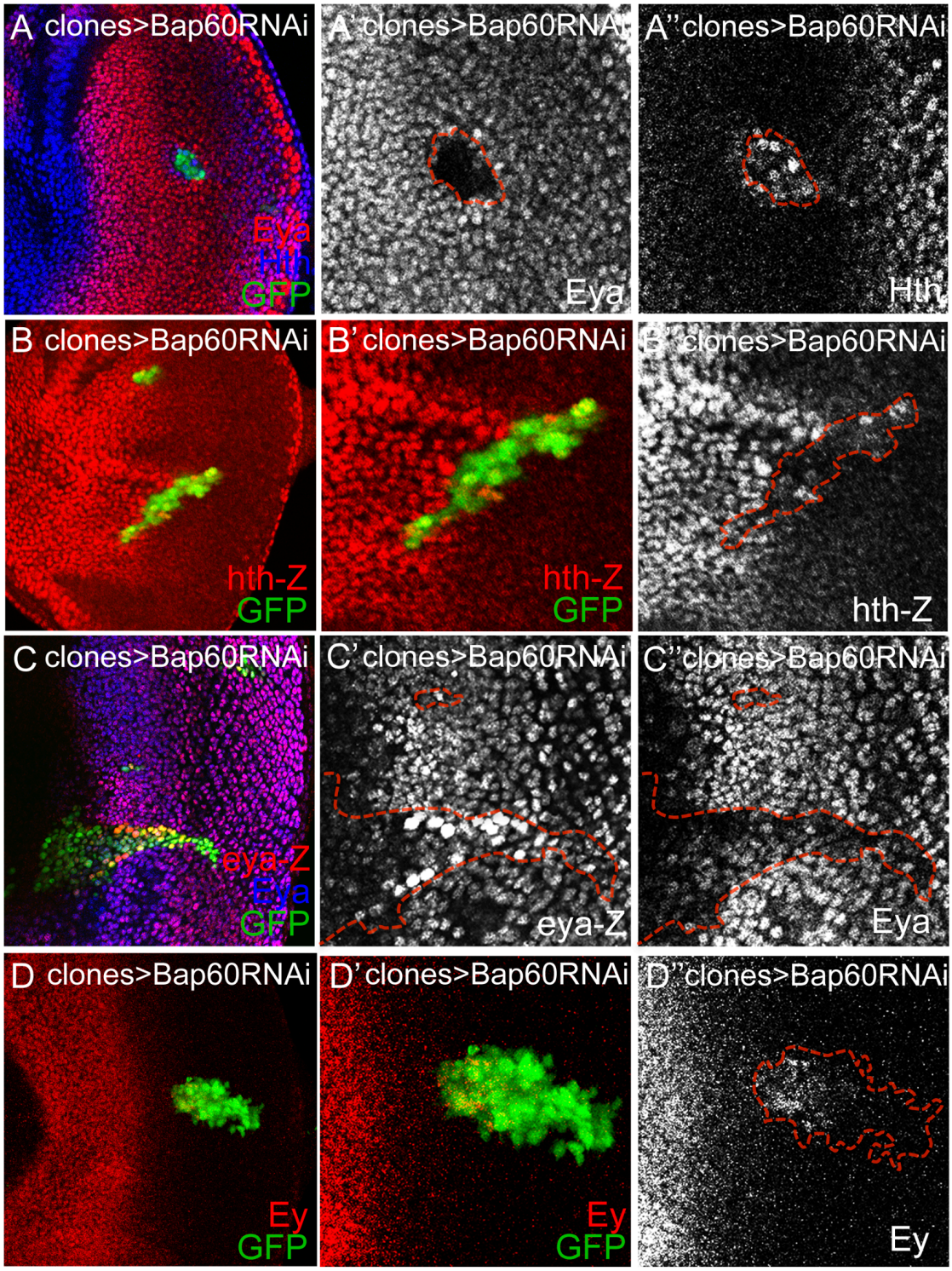

Figure R3.14. *Bap60* knock-down affects the spatial and temporal expression of retinal determination genes. (A-D) *Bap60-RNAi* clones, induced around 48 hours after egg laying and visualized in late L3 discs by the expression of GFP. Clones were induced in a *hth*-Z background (B) and in an *eya*-Z background (C). Late L3 eye discs were stained for (A) Eya (red) and Hth (blue); (B) β-Gal (red); (C) β-Gal (red) and Eya (blue) and (D) Ey (red). Depleting *Bap60* levels results in an uneven expression and abnormal posterior maintenance of Hth and Ey and in a reduction of Eya expression within the clones. Analysis of the hth transcriptional reporter shows that Bap60 acts on *hth* at a transcriptional level, while for *eya* the regulation seems to be at post-transcriptional level.

This result indicates that, unlike *hth*, the regulation of *eya* by *Bap60* might be mainly posttranscriptional.

The expression defects caused by *Bap60* depletion extended to other genes. Thus, the expression of *ey*, monitored by an anti-Ey antibody, was affected very much like that of *hth* (Figure R3.14D, 60% of the clones, N=10). These results indicate that reduction of *Bap60* function likely has a global effect on the dynamics of retinal determination gene expression.

Considered together, these results position Bap60 both downstream as well as upstream of Ey and Hth, and indicate it affects the expression of Eya, a gene that is positively and negatively regulated by Ey and Hth, respectively. In the absence of *Bap60,* the expression of key retinal determination genes becomes highly variable. This variability is accompanied of cell death and unpaired retinal differentiation.

5

DISCUSSION AND CONCLUSION

During normal organ development and tissue homeostasis, cell numbers must be tightly controlled so that organs reach their precise final size and shape. Exact cell numbers are mainly achieved through a regulated balance between rates of progenitor cell proliferation and the speed at which these progenitors are recruited out of the cell cycle as committed precursors.

Here we used the *Drosophila* eye development as a model to study these two processes. This is an excellent system since all processes take place simultaneously in the same tissue – the eye imaginal disc.

In the first part of this work we focused on the control of proliferation and maintenance of undifferentiated state of eye progenitors mediated by two conserved transcription factors normally expressed in this population of cells – *hth*/MEIS1 and *tsh*/TSHZ. To do so, we performed analysis of transcriptomes, chromatin accessibility and transcription factor binding motif enrichment data from *hth+tsh*-induced overgrowths and the appropriate controls.

Our results pointed to the activation of a transcriptional network related to the Ecdysone Receptor (EcR) pathway in *hth+tsh* cells.

The Ecdysone Receptor pathway has been classically associated to the molting periods and metamorphosis. At these stages during development, pulses of the active form of the ecdysone hormone (20-hydroxiecdysone) trigger the response of this pathway through changes in nuclear receptors expression (Thummel, 2001).

More recently, this pathway has been also shown to be involved in growth control mechanisms in *Drosophila* imaginal discs (Colombani et al., 2005; Herboso et al., 2015). Interestingly, the gene expression pattern that is typical of a low/moderate ecdysone signalling (high EcR/ftz-f1 and low Hr46/Blimp-1 levels) was the one that we found in *hth+tsh* cells and that we propose to be key to trigger the *hth+tsh*-mediated overgrowths. This hypothesis is supported by the following facts: (1) the modulation of EcR, Hr46 or ftz-f1 expression affects the hth+tsh-induced overgrowths; (2) changes in nuclear receptors are paralleled by increased expression of cell cycle genes; (3) CREs linked to these cell cycle genes show an enrichment of Hr46/ftz-f1-type DNA binding motifs, pointing to a direct regulatory

linkage; and (4) Hr46 and ftz-f1 have the potential to regulate progenitor proliferation.

During eye development in *Manduca sexta*, moderate levels of ecdysone are required for stimulation of eye proliferation during larval stages. However, low levels of ecdysone arrest cells in the G2 phase, while the high pulse of ecdysone released later during development is responsible for cell cycle exit (Champlin and Truman, 1998a,b). A similar situation might be happening during *Drosophila* eye development. In this case, forced maintenance of hth+tsh might induce cell proliferation through the maintenance of a moderate activity of the Ecdysone pathway.

Our results suggest that the potential direct regulation by Hth and Tsh of genes like Hr46 or Blimp-1 would lead to a specific pattern of nuclear receptor transcription. Then, these nuclear receptors would affect (probably directly) the expression of several cell cycle related genes that show nuclear receptors DNA-binding motifs to their CREs. This cascade effects would ultimately lead to the sustained growth and observed overgrowths.

We have noted a discrepancy between the direction of the functional interactions of *Hr46* and *ftz-f1* with hth+tsh, and the capacity to enhance (Hr46) or decrease (ftz-f1) cell proliferation when assayed individually. For example, co-overexpression of *Hr46* partially rescued the hth+tsh-mediated overgrowth, suggesting an anti-proliferative role, while overexpression of *Hr46* alone *increases* proliferation rates.

We do not have an explanation for this discrepancy, however similar situations had been described in other model systems. While it has been shown that RORβ, one of the Hr46 homologues, is expressed in rat retinal progenitor cells and that increased expression of this gene in progenitors results in an increase in the number of large cell clones (Chow et al., 1998); RORα is normally downregulated or hypoactivated in breast cancer cells (reviewed in Du and Xu, 2012).

Additionally, the EcR pathway is very complex, with temporally delayed feedbacks. With this complexity, it is difficult *a priori* to predict the direction of the interactions. Still, we believe the we present solid evidence indicating that hth+tsh promote a specific pattern of nuclear receptor expression; that these nuclear receptors functionally interact with hth+tsh in modulating the overgrowth these TFs induce in progenitor-like cells and that Hr46 and ftz-f1 are capable of modulating the proliferative pace of undifferentiated progenitors.

Besides its role in modulating developmental transitions, our work and that of others (Colombani et al., 2005; Herboso et al., 2015) has shown that the ecdysone pathway is able to control growth rates. These results point to a key role for the ecdysone pathway in controlling the crosstalk between two major processes, the global and organ-specific growth control systems, to allow matching organ size and organismal size.

We have found within transcriptional profiling data of Yki overexpressing wing primordia, reported in Supplementary table 4 by Oh and co-workers (Oh et al., 2013), a similar signature of differential expression of nuclear receptors as the one we find in hth+tsh overexpressing eye discs. Specifically, overexpressed EcR and ftz-f1 and reduced levels of Blimp-1 and Hr46. This similarity may stem from the fact that, in the eye, Hth and Tsh have been shown to be direct partners of Yki (Peng et al., 2009), the transcriptional coactivator of the Hippo tumour suppressor pathway (Huang et al., 2005).

In an epithelia cancer model in the *Drosophila* eye disc characterized by loss of function of *scribbled* (an apico-basal cell polarity regulator) and overexpression of *abrupt* (a BTB-zinc finger transcription factor), a similar pattern of expression was observed, with reduced levels of *Hr46* and *Blimp-1* and high levels of *ftz-f1* (in this case *EcR* levels were not affected) (Turkel et al., 2013). Interestingly, ChIP-seq data analysis showed that Abrupt is able to directly regulate *Hr46*, *Blimp-1*, *ftz-f1* and *EcR* (Turkel et al., 2013). A similar repression of ecdysone response genes has been also described in the *Drosophila* ovary, where Abrupt interacts with Taiman, a steroid hormone receptor coactivator (Jang et al., 2009). In our work, *abrupt* expression levels were upregulated in eye discs where there was forced maintenance of hth or hth+tsh (with a fold change of

approximately 2 in both situations), suggesting also a pathway for the control of the expression of nuclear receptors in progenitors.

More recently, overexpression of *taiman* and *ftz-f1* was also shown to be present in a model of invasive cancer driven by RAS in the eye disc (Atkins et al., 2016).

In the cancer models mentioned above, a role for the Hippo pathway has been described (Turkel et al., 2013; Atkins et al., 2016). Therefore, a similar nuclear receptor (and probably *abrupt*) expression pattern might be a general feature of Hippo-related tissue overgrowth. Whether this is also the case in human tumours where components of the Hippo-YAP pathway are mutant needs to be investigated.

One interesting aspect of the global regulatory response elicited jointly by *hth* and *tsh* is that this response is quantitative, not qualitative. That is, expression of hth+tsh drives the transcriptional upregulation of many genes but with minor changes in the profile of their CRE activity, as measured by open chromatin profiling. This suggests that hth+tsh operate through CREs that are already active (i.e., open chromatin), rather than by inducing the *de novo* opening of new ones. This behaviour contrasts with results analysing the transcriptional response and CRE activity profiles in eye tumours in the *rasV12/scrib* model. Here, the transcriptional changes were paralleled by qualitative changes in CRE activity, with the *de novo* opening of hundreds of promoters and enhancers (Davie et al., 2015). This fact might be related to the different nature of the tissues overgrowths in each of the two genotypes. While hth+tsh expression drives continuous proliferation of progenitors (i.e. hyperplastic growth), *rasV12/scrib* tissues are metastatic.

The dual control of cell fate and proliferation makes organ specification transcription factors a “vulnerable link”. Particularly, it is often the case that mutations affecting the expression of an organ- or cell-type selector transcription factor result in cancer developing from this same organ. Examples of this are the eye and pancreas transcription factor Pax6 in retinoblastoma and pancreatic cancer (Mascarenhas et al., 2009; Bai et al., 2011); myogenic MyoD1 in rhabdomyosarcoma (Agaram et al., 2014); hematopoietic progenitor transcription

factors MEIS1 and TAL1 in leukemia (Chen et al., 1990; Wong et al., 2007); neural crest SOX10 and MITF in melanoma (Tani et al., 1997; King et al., 1999) or GATA3 in breast cancer (Usary et al., 2004). And more generally, many cancer driver mutations affect transcription factors (Aerts and Cools, 2013). In particular, the oncogenic role of MEIS1 has been documented. Here, we have established for the first time that MEIS1 and TSHZ occur in coordinated overexpression in several major solid tumour types, an association that may recapitulate the functional synergism of *hth* and *tsh* in the fly eye primordium.

In this study, the epithelial overgrowth triggered by co-overexpression of hth+tsh results in transcriptional changes and functional interactions that bear similarity with those observed in tumours where Estrogen Receptor alpha (ERα), RORα (one of the *Hr46* homologues) and NR5A2/LHR-1 (*ftz-f1* homologue) play important roles, such as breast cancer (Annicotte et al., 2005; Chand et al., 2010; Thiruchelvam et al., 2011; Xiong and Xu, 2014).

Interestingly, it has been reported that NR5A2/LHR-1 expression is also increased in pancreatic cancer where it promotes cell growth through stimulation of major cell cycle regulators cyclin D1, cyclin E1 and c-Myc (Benod et al., 2011). In colon cancer it has been shown that NR5A2/LHR-1 represses the expression of the cell cycle inhibitor p21 (Kramer et al., 2016) and that it has major effects in cell cycle regulation, showing a clear pro-proliferative function (Bayrer et al., 2015). Indeed, through ChIP-seq and gene expression experiments, the estrogen receptor (and other nuclear receptors, such as the androgen receptor) has been shown to directly regulate genes involved in cell cycle progression (Carroll et al., 2006; Kwon et al., 2007; Welboren et al., 2009; Cicatiello et al., 2010).

NR5A2/LHR-1 has also been involved in cell proliferation control during intestinal cell renewal. NR5A2/LHR-1 directly induces cyclin E1 expression and, through a crosstalk with the β-catenin signalling pathway, indirectly induces cyclin D1 expression (Botrugno et al., 2004; Schoonjans et al., 2005).

On the contrary, the Hr46 homologue RORα has been shown to bind to E2F1, inhibiting cell cycle progression (Xiong and Xu, 2014). RORα expression is reduced in a high number of breast cancers and its ectopic expression is able to inhibit tumour growth, pointing to a potent tumour suppressor gene (reviewed in

Du and Xu, 2012). This result is in agreement with our finding that Hr46 expression reduces hth+tsh-driven overgrowth.

These similarities suggest a scenario where MEIS1 and TSHZ genes, if co-overexpressed, might be driving transformation through the regulation of nuclear receptors which, then, would be translated into a general regulatory effect on many cell cycle-related genes.

The bioinformatics predictions of our data also suggested the involvement of additional players. For example, enrichment of Mad motifs in CREs of differentially expressed genes in hth+tsh cells points to a role of the Decapentaplegic (Dpp) signalling pathway. Dpp is a BMP2/4 molecule, and BMPs and TGFβ molecules have been involved in tumourigenesis (Massague, 2008). Indeed, BMP2 has been shown to suppress proliferation of breast (Jung et al., 2014) and colorectal (Zhang et al., 2014) cancer cells.

Therefore, we decided to identify additional pathways modulating, either positively or negatively, the *hth+tsh*-induced tissue overgrowth that is mediated by an altered expression of specific nuclear receptors.

Previous studies had shown that hth+tsh-induced overgrowths are mediated by Yki, the transcriptional coactivator downstream of the Hippo pathway (Huang et al., 2005; Peng et al., 2009). Moreover, Peng and colleagues showed that these overgrowths do not depend on the Wingless, Notch and JAK/STAT pathways (Peng et al., 2009).

During eye development, two other signalling pathways are normally involved in the linkage between organ patterning and growth: the Dpp pathway and the Hh pathway (reviewed in Amore and Casares, 2010).

In the second part of this work, we showed that hth+tsh-cells trap Dpp produced at local sources, which then causes an increase in intracellular signalling, that is ultimately needed to maintain the proliferative/undifferentiated phenotype.

During normal eye development, Dpp produced at the furrow first represses *hth* and then, closer to the furrow, also represses *tsh*. This way, cells approaching the furrow are receiving the highest Dpp levels while no longer co-expressing *hth* and *tsh* (Bessa et al., 2002; Firth and Baker, 2009; Lopes and Casares, 2010). The forced maintenance of Hth and Tsh in eye precursors exposes these cells to Dpp signalling levels higher than they would normally encounter.

During normal development, the loss of *hth* marks the transition between proliferation/undifferentiation and cell quiescence/commitment, which coincides with a transient proliferative wave that precedes entry into G1 – the first mitotic wave (Escudero and Freeman, 2007; Lopes and Casares, 2010; Bras-Pereira et al., 2015). This transition zone corresponds to a region where low, but not null, levels of Hth and pMad signals overlap (Figure D.1).

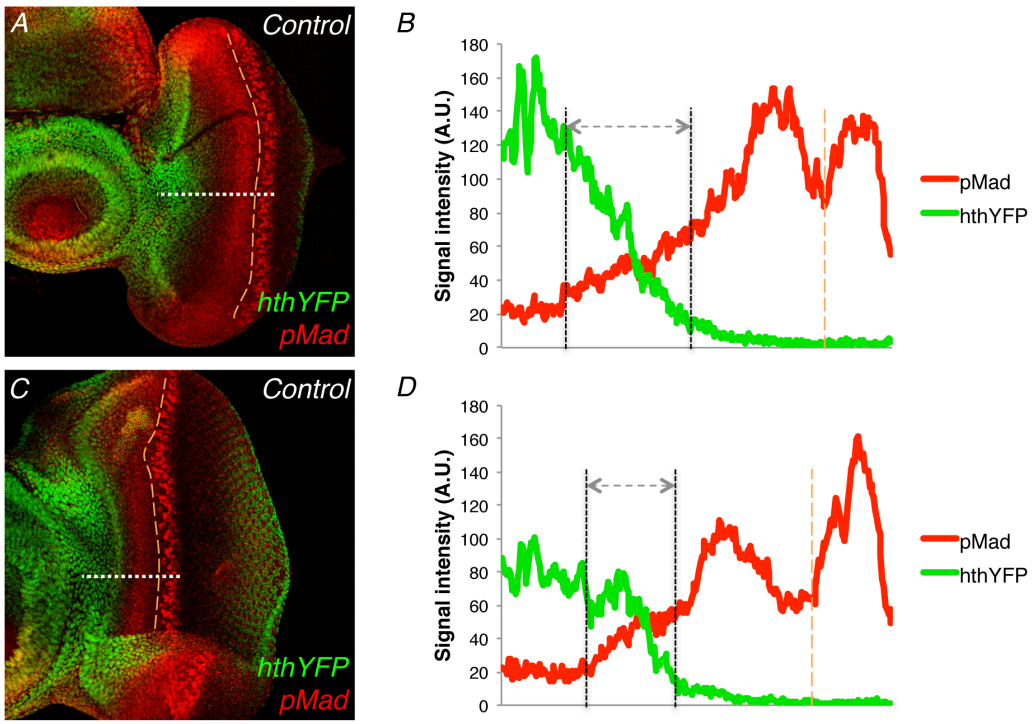

Figure D.1. Intermediate levels of Hth and pMad overlap during normal eye development. *hth::YFP* discs at early (A) and late (C) third instar stages stained with anti-pSmad3. Signal intensity histograms of pSmad3 (red) and hth::YFP (green) of the same discs (B and D, respectively). Signal intensity, expressed in arbitrary units, is measured from the MF. Vertical dashed lines (B and D) highlight the region where intermediate levels of Hth:YFP and pMad overlap. In (A,C) orange dashed lines mark the morphogenetic furrow and white dashed lines highlight the region where signal intensity was measured and represented in the histograms.

If the interaction between *hth+tsh* and the Dpp pathway we have described here were to hold also in the zone of Hth/pMad signal overlap during normal eye

development (*hth*-cells normally co-express *tsh*), one prediction would be that the mitotic wave would be lost if either *hth* or *dpp* signalling were removed. Indeed, this has been shown to be the case: RNAi-mediated attenuation of *hth* (Lopes and Casares, 2010) or abrogation of Dpp signalling (Wartlick et al., 2014) result in the loss of the first mitotic wave.

The mechanism responsible for the trapping of Dpp in *hth+tsh*-cells seems to be the increase of extracellular matrix components. There are several facts that support this hypothesis: (1) *hth+tsh*-cells show a cell-autonomous increase in the two major heparane sulphate proteoglycans (specifically, *dally* transcription and Dlp membrane levels increase); (2) *sulfateless (sfl)*, a gene encoding an enzyme required for the biosynthesis of these proteoglycans, is required for the *hth+tsh*-induced phenotype and (3) the Dpp signalling (i.e. pMad) profiles are modified in *hth+tsh* or *hth+tsh+sflRNAi* eye discs.

Considering that the Dpp production remains unaltered, *hth+tsh* eye discs show an increase in both pMad signal amplitude and range, which is consistent with the increase in proteoglycans simultaneously augmenting Dpp diffusion and stability (Fujise et al., 2003; Belenkaya et al., 2004; Akiyama et al., 2008; Ferreira and Milan, 2015). On the contrary, reducing proteoglycan biosynthesis in *hth+tsh+sflRNAi*-cells results in the retraction of the pMad signalling range back towards control values, which again is expected if Dpp's diffusion depends on proteoglycans.

The upregulation of *dally* and *dlp* by *hth+tsh* is likely the consequence of the transcriptional activity of hth+tsh in partnership with Yki, the YAP/TAZ homologue, as previous work showed that loss of the protocadherin genes *fat* (*ft*) and *dachsous* (*ds),* which causes the activation of Yki, results in an upregulation of *dally* and *dlp* in the wing primordium (Baena-Lopez et al., 2008). In fact, Slattery and co-workers found, in imaginal tissues, binding of Yki and Hth to nearby sites on the *dlp* locus (Slattery et al., 2013), suggesting that some of this regulation might be direct.

All these data make Yki a necessary component of the molecular machinery responsible for the increased avidity of *hth+tsh*-cells for Dpp. However, in this work we showed that in the eye primordium, the overexpression of Yki induces a

different phenotype than *hth+tsh*. More importantly, in the eye primordium, *yki*-expressing clones do not cause the autonomous upregulation of pMad signal that hth+tsh clones do (Figure D.2).

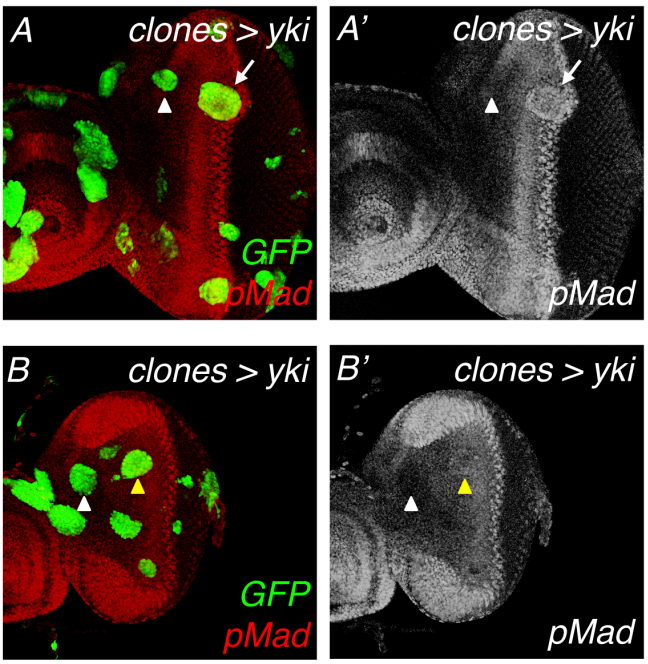

Figure D.2. Yki-expressing clones do not increase pMad levels near an endogenous Dpp source. (A–B') Yki-expressing clones in the eye imaginal disc, marked by GFP, were induced at 48-72 hours after egg laying. Discs are stained with anti-pSmad3. Clones located near an endogenous Dpp source are not able to induce pMad (white arrowheads), while clones located within the endogenous pMad-expressing region show similar (yellow arrowheads) or slightly higher (white arrow) levels of pMad.

Therefore, a specific stoichiometry among Hth, Tsh and Yki is likely necessary to induce the Dpp signaling-dependent properties of *hth+tsh*-cells, at least in the developing eye. Alternatively, Hth and Tsh may activate Yki-independent targets that would be required for the full expression of the phenotype.

Recently, Oh and Irvine described that Yki and the Dpp pathway synergize in stimulating tissue overgrowth, both in eye and wing primordia, through the physical association between Yki and Mad (Oh et al., 2013). Our results suggest that hth+tsh progenitor-like cells establish a positive feedback, in which the growth promoting activity of the Hth:Tsh:Yki complex would be enhanced by increasing levels of pMad activated by Dpp. This feedback would be region-specific, as it depends on sources of Dpp that are localized within the eye primordium. Further work is needed to investigate the molecular mechanisms behind this feedback.

Finally, it has been recently shown that tissue growth promoted by the PI3K/PTEN and TSC/TOR nutrient-sensing pathways also requires Dally, which in turn increases the avidity of the growing tissue for Dpp (Ferreira and Milan, 2015). Therefore, increasing the avidity for Dpp by augmenting proteoglycan levels may be a common strategy of tissues to sustain their growth.

In mouse mammary glands and breast cancer cells, it has been described a crosstalk between nuclear receptors and the TGF-β pathway – cancer cells and mammary glands overexpressing NR5A2/LHR-1 show a clear activation of the TGF-β signalling pathway (Lazarus et al., 2014). More experiments would be necessary in order to sort out if the activation of the Dpp pathway that we observe in the hth+tsh cells might be, at least, partially nuclear receptor-dependent, but this is a tantalizing possibility.

A crosstalk between Dpp/Activin and Ecdysone signalling pathways was also defined during *Drosophila* brain development. In this case, an activated form of *tkv* and an activated form of the activin pathway receptor *baboon* induce the expression of the Ecdysone receptor isoform B1, *EcR-B1* (Yang et al., 2004).

Moreover, we showed that the Hedgehog signalling pathway is able to modulate the *hth+tsh*-induced phenotype.

While Dpp pathway mediates the *hth+tsh*-induced overgrowths by an enhanced trapping of Dpp by the *hth+tsh*-cells, in the case of the Hh pathway we observed a transcriptional activation of the *hh* ligand itself in *hth+tsh*-cells.

This autocrine, ligand-dependent activation of the Hh pathway in *hth+tsh*-cells explains the activation of the direct targets of the pathway not only in these cells but also in the neighbouring cells, supporting the tissue growth. This type of ligand-dependent activation of the pathway has been shown in several types of tumours (reviewed in Gupta et al., 2010).

During normal *Drosophila* eye development, Hh signalling pathway has been shown to have an inhibitory role in cell cycle control anterior to the morphogenetic furrow, however in the second mitotic wave (posterior to the furrow) it upregulates cyclin D and cyclin E promoting cell growth and proliferation (Duman-Scheel et al., 2002). Moreover, during vertebrate retina development, the

Hh pathway activates cyclin A2, cyclin B1, Cyclin D and cdc25c, promoting the transient proliferation of retinal precursor cells (Wang et al., 2005; Locker et al., 2006)

In fact, our hth+tsh clones show an upregulation of cyclin E and cyclin A. We have suggested that this effect might be mediated by the nuclear receptors downstream of hth+tsh. However, we cannot rule out a contribution of the Hh signalling pathway.

Although during normal eye development, *hh* activates the transcription of *dpp* (Heberlein et al., 1993; Ma et al., 1993; Borod and Heberlein, 1998); hth+tsh-cells show an activation of the Hh pathway and yet *ddp* transcription is not altered. Our experiments also show slightly different outcomes when *hh* or *dpp* morphogens are overexpressed in an hth+tsh-background. Further experiments would be needed in order to define if these pathways are independently activated downstream of hth+tsh or if instead there is a crosstalk between them.

Finally, in the third and last part of this work, we aimed to better understand the transition from undifferentiated and proliferative progenitors through cell cycle quiescent, committed precursors to newly differentiated cells during *Drosophila* eye development. To do so, we have outlined a gene regulatory network model that takes into consideration transcription factors and chromatin remodellers with a specific role in this process.

In general, the network shows an increase in the number of differentially transcribed transcription factors as differentiation progresses, which correlates with an increased diversification of cell types being specified.

A gene ontology comparison between the terms obtained for the progenitor and precursor/early differentiation populations (results – part III) and the ones obtained for the optix>hth upregulated and downregulated genes (results – part I) respectively, showed enrichments for similar terms. The precursor/early differentiation genes and the downregulated genes in optix>hth discs when compared with control ones showed an enrichment in functions related to eye development, while the progenitor genes and the upregulated genes in optix>hth

discs compared with control ones showed an enrichment in terms associated with metabolism and protein synthesis (Table C.6). This analysis confirms that these two manipulations (tio>hth and optix>hth) give rise to similar cell populations.

Hth's connectivity is especially rich, but this probably only reflects the fact that the network includes the recently published ChIP-on-chip data for Hth binding in the eye disc (Slattery et al., 2013). Therefore, many of the genes linked to Hth are potential direct targets, although this has not yet been experimentally validated. These include a number of chromatin remodelling genes more highly transcribed in progenitors (Tip60, Chd1, Ada2b, Iswi, Trl, Acf1, Caf1 and Bap60).

In particular, *Bap60* is predicted to interact directly not only with chromatin remodelling genes (like *Brm, Snr1* and *Ada2b*) but also it has been shown to be regulated downstream of *ey* (Ostrin et al., 2006). Additionally, in this work we showed that its expression is enriched in progenitors. Bap60 also presents an Hth binding peak in its vicinity (Slattery et al., 2013) and yeast two-hybrid data suggests that Bap60 physically interacts with Eya and Exd (Giot et al., 2003).

All these interactions with major components of the retinal determination gene network point to a role of Bap60 in the regulation of the early transitions during eye differentiation.

Our results indicate that indeed Bap60 is required for the dynamics of retinal determination genes expression, including *hth, ey* and *eya.* When *Bap60* is attenuated in progenitors, the expression of Hth and Ey within the clones becomes uneven. Interestingly, these same clones keep showing expression of Hth and Ey, albeit patchy, in region where these two genes should be already off (i.e. posterior to the morphogenetic furrow), indicating that Bap60 is required for the timely and even activation and repression of both genes. Importantly, the loss or abnormal maintenance of either of the two genes is deleterious for eye development (Pai et al., 1998; Pichaud and Casares, 2000). At least for Hth expression, the requirement seems to be transcriptional. Thus, the expression of an *hth-lacZ* transcriptional reporter shows a similar uneven expression in *Bap60*-RNAi clones.

Also *Bap60-RNAi* clones lose expression of *eya.* This loss could be the result of the maintenance of Hth expression, which in turn, would repress *eya* transcriptionally. However, this does not seem to be the case: in Bap60-RNAi clones, while Eya protein levels are decreased, we detect transcription of an *eya-*

lacZ transcriptional reporter, arguing for a transcription-independent requirement of Bap60 for Eya expression.

Brahma complexes are chromatin regulators with broad effects on gene expression (Bouazoune and Brehm, 2006; Clapier and Cairns, 2009; Ho and Crabtree, 2010). However, we have shown by depleting its function in specific cell populations along the eye differentiation pathway, that Bap60 is required in progenitors and precursors to allow proper establishment of gene expression patterns. This stage-specific requirement suggests that Bap60 does not act as a general transcriptional regulator. Other Brm complex members, such as *osa, Polybromo* or *Brm* itself have been proposed to regulate a limited number of target genes (Collins et al., 1999; Armstrong et al., 2002; Mohrmann et al., 2004).

Functional studies have shown previously that *osa,* like *Bap60*, is required for eye development. However, Osa is required for photoreceptor differentiation (Treisman et al., 1997) but its loss does not affect expression of anterior eye genes (Janody et al., 2004). This contrasts with *Bap60* requirement in the anterior region of the eye primordium, but not during differentiation. This difference may stem from the fact that while Bap60 may be part of the two types of Brm complexes (BAP and PBAP, reviewed in Bouazoune and Brehm, 2006), Osa is an exclusive subunit of the BAP subtype. This suggests that, during the early steps of eye development, either Osa plays a non-essential function within BAP complexes or PBAP-type Brm complexes have a predominant role during the early steps of eye development.

Molecularly, Bap60 has been shown to be able to bind DNA non-specifically but to interact physically with two sequence-specific transcription factors, Sisterless A (SisA) and Scute (Sc) in the context of sex determination (Moller et al., 2005). Direct interactions between the mammalian Bap60 homologues BAF60a and BAP60c with tissue-specific transcription factors have also been described (Ito et al., 2001; Hsiao et al., 2003; Debril et al., 2004; Lickert et al., 2004). Therefore Bap60/BAF60 could tether Brm remodelling complexes to specific target genes through their interaction with sequence-specific transcription factors.

The proposed physical interactions between Bap60 and Eya might serve a similar purpose, as Eya, in complex with its partner transcription factor So, binds specific targets sites in the genome (Jemc and Rebay, 2007). Similarly, the proposed Bap60:Exd interaction could be instrumental in tether Bap60-containing chromatin remodelling complexes to Hth-target sites, as the Pbx protein Exd is an obligatory Hth partner (Rieckhof et al., 1997).

Our results indicate that Bap60 is required for the dynamics of retinal determination genes expression, namely *hth, ey* and *eya* and at the same time *Bap60* lies transcriptionally (Ostrin et al., 2006) and functionally (this work) downstream of *ey*. Moreover, *Bap60* is transcriptionally enriched in *hth*-expressing progenitors, which together with the fact that Hth has been shown to bind in the vicinity of Bap60 (peak partially overlapping the *Bap60* promoter) further suggests a direct regulation of *Bap60* by *hth.*

Considered together, these results indicate the existence of a positive feedback loop between retinal determination genes and *Bap60,* a core component of the Brm chromatin remodelling complexes. In turn, the organ selector transcription factors that regulate *Bap60* require Bap60 themselves to ensure the maintenance and the timely regulation of their expression (Figure D.3).

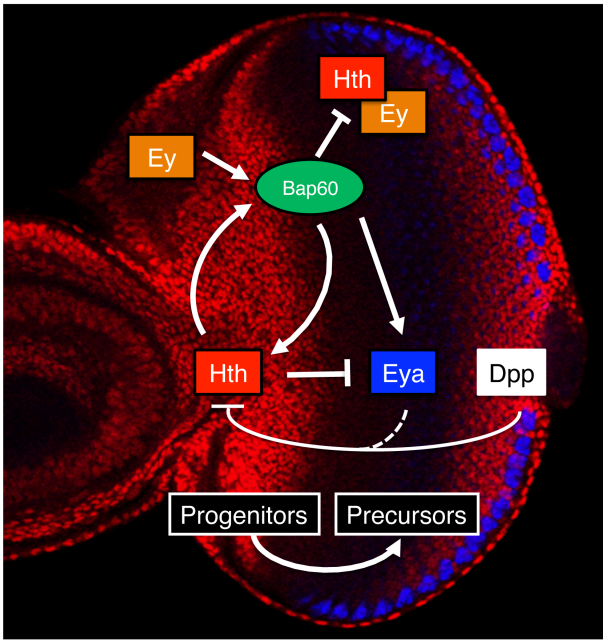

Figure D.3. Multi-tiered feedback loops might connect cell-specification transcription factors and chromatin remodeller complexes through *Bap60.*

The fact that Eya expression seems to be post-transcriptionally regulated adds an additional layer of regulatory complexity to this feedback loop. One possibility might be that Eya protein stability would depend on the reported Bap60:Eya protein-protein interaction detected in yeast-two hybrid assays, an interaction not yet confirmed in *Drosophila* tissues. However, in the mice inner ear it has been described that EYA1 is able to interact with the SWI/SNF chromatin-remodelling complex (Ahmed et al., 2012). Alternatively, Eya's stability could be regulated by Bap60 indirectly, through the transcriptional regulation of some other unknown factor(s).

Interestingly, a similar role for SWI/SNF chromatin remodelling complexes in propelling sequential cell state transitions as the one described here has been proposed previously for the progression through the differentiation pathway of T cells (Chi et al., 2003).

More recently, two studies in *Drosophila* show that Osa-containing Brahma complexes are required for the control of other early cell-state transition. In one of these studies, the transition from intestinal stem cells into enteric cell types through the regulation of the *asense* transcription factor (Zeng et al., 2013). In the other, Osa complexes are necessary to limit the proliferation of neuronal progenitors and to guarantee their irreversible differentiation, a function mediated by the Osa target *Hamlet*, a Prdm family protein (Eroglu et al., 2014).

It is therefore possible that feedbacks from SWI/SNF chromatin remodellers, such as Bap60, and organ-selector transcription factors may be a general way of ensuring swift, coordinated and stable gene expression changes.

Recently, it has been shown that Yki forms nuclear protein complexes with the Brahma complex; specifically Yki is able to interact directly with Moira, a Brahma complex subunit (Oh et al., 2013). This type of interaction is essential to control the Yki-mediated transcriptional activation and consequently to regulate tissue growth (Oh et al., 2013; Zhu et al., 2015). As mentioned before, Yki forms a complex with Hth and Tsh, driving tissue growth. Moreover the *tsh* homologue TSHZ3 interacts with the SWI/SNF complex subunit BAF57 to maintain the undifferentiated state of muscle stem cells (Faralli et al., 2011).

We have tested the interaction between Tsh and subunits of the Brahma chromatin remodelling complexes. We have observed that while the RNAi-mediated knockdown of Moira in undifferentiated cells with the optix2.3-Gal4 driver resulted in smaller adult eyes and as mentioned before the overexpression of Tsh affected slightly eye development; reducing Moira levels and simultaneously increasing Tsh ones resulted in adult lethality (Figure D.4).

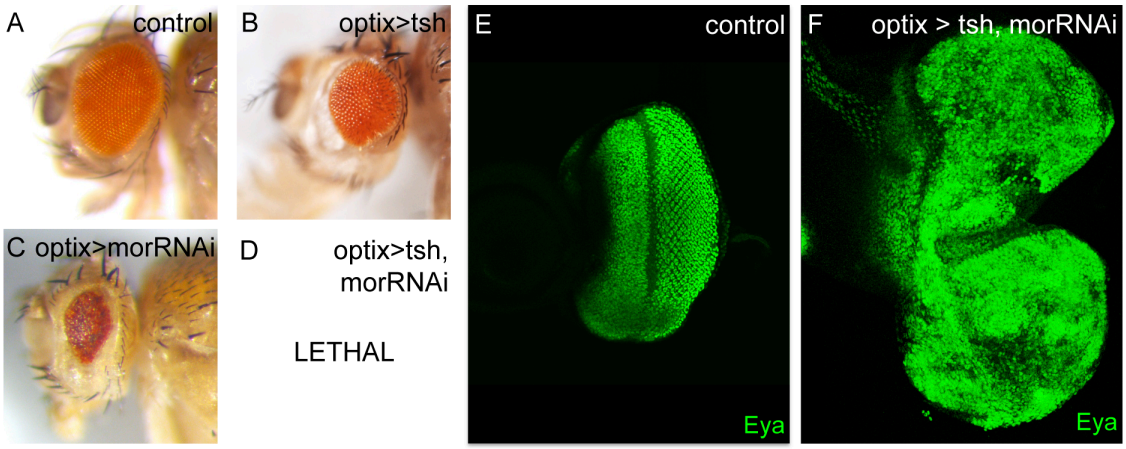

Figure D.4. tsh+moiraRNAi induce huge overgrowths. Lateral views of *control* (A), *optix>tsh* (B), *optix>moiraRNAi* (C) and *optix>tsh+moiraRNAi* (D) adult heads. Control late third instar (L3) eye disc (E) and optix>*Tsh+moiraRNAi* (F) eye disc stained with anti-Eya (green). Simultaneous *tsh* overexpression and RNAi-mediated knockdown of moira results in huge overgrowths in the eye discs and in lethality – flies die within the puparium.

If the same interaction as the one described above was operating in this situation, we would expect this lethality to result from smaller eye discs, however eye discs in this genotype are massive when compared with wild type eye discs (Figure D.4E,F). The Brahma complexes seem to be necessary to maintain the chromatin structure in order to control the expression of Tsh target genes. This points to an extremely complex situation, where interactions between the same chromatin remodellers and transcription factors affect transcription differently depending on the tissue or organism. This complexity can be reduced if you understand better the interactions between chromatin remodellers and transcription factors.

Globally considered, the results obtained during this PhD thesis unravelled some of the mechanisms acting downstream of Hth+Tsh in regulating the proliferation of progenitor-like cells. These two transcription factors are able to

regulate systemic (ecdysone pathway) as well as organ-autonomous (Dpp and Hh pathways) signals that modulate the proliferation status of these cells.

Additionally, we showed the co-occurrence of MEIS1, TSHZ and nuclear receptors of the estrogen pathway in specific tumour types. In the future, it will be of great importance to test if the mechanisms controlled by Hth+Tsh in *Drosophila* are conserved in driving proliferation of cancer cells in humans. If this were the case, it would be interesting to test the response of cancer cells that show high levels of MEIS1 and TSHZ genes to drugs that affect the estrogen response.

Finally, we propose that not only the transcriptional feedbacks between chromatin remodellers and organ-specific transcription factors, but also their physical interactions are key in the control of normal development as well as abnormal situations that might drive overgrowths and ultimately cancer.

6

REFERENCES

Aegerter-Wilmsen, T., Aegerter, C.M., Hafen, E., and Basler, K. (2007). Model for the regulation of size in the wing imaginal disc of Drosophila. Mechanisms of development 124, 318-326.
Aegerter-Wilmsen, T., Heimlicher, M.B., Smith, A.C., de Reuille, P.B., Smith, R.S., Aegerter, C.M., and Basler, K. (2012). Integrating force-sensing and signaling pathways in a model for the regulation of wing imaginal disc size. Development 139, 3221-3231.
Aerts, S., and Cools, J. (2013). Cancer: Mutations close in on gene regulation. Nature 499, 35-36.
Aerts, S., Quan, X.J., Claeys, A., Naval Sanchez, M., Tate, P., Yan, J., and Hassan, B.A. (2010). Robust target gene discovery through transcriptome perturbations and genome-wide enhancer predictions in Drosophila uncovers a regulatory basis for sensory specification. PLoS biology 8, e1000435.
Affolter, M., and Basler, K. (2007). The Decapentaplegic morphogen gradient: from pattern formation to growth regulation. Nat Rev Genet 8, 663-674.
Agaram, N.P., Chen, C.L., Zhang, L., LaQuaglia, M.P., Wexler, L., and Antonescu, C.R. (2014). Recurrent MYOD1 mutations in pediatric and adult sclerosing and spindle cell rhabdomyosarcomas: evidence for a common pathogenesis. Genes, chromosomes & cancer 53, 779-787.
Agawa, Y., Sarhan, M., Kageyama, Y., Akagi, K., Takai, M., Hashiyama, K., Wada, T., Handa, H., Iwamatsu, A., Hirose, S., et al. (2007). Drosophila Blimp-1 is a transient transcriptional repressor that controls timing of the ecdysone-induced developmental pathway. Molecular and cellular biology 27, 8739-8747.
Ahmed, M., Xu, J., and Xu, P.X. (2012). EYA1 and SIX1 drive the neuronal developmental program in cooperation with the SWI/SNF chromatin-remodeling complex and SOX2 in the mammalian inner ear. Development 139, 1965-1977.
Akasaka, T., Kanno, M., Balling, R., Mieza, M.A., Taniguchi, M., and Koseki, H. (1996). A role for mel-18, a Polycomb group-related vertebrate gene, during theanteroposterior specification of the axial skeleton. Development 122, 1513-1522.
Akiyama, T., and Gibson, M.C. (2015). Morphogen transport: theoretical and experimental controversies. Wiley Interdiscip Rev Dev Biol 4, 99-112.
Akiyama, T., Kamimura, K., Firkus, C., Takeo, S., Shimmi, O., and Nakato, H. (2008). Dally regulates Dpp morphogen gradient formation by stabilizing Dpp on the cell surface. Developmental biology 313, 408-419.
Alcedo, J., and Noll, M. (1997). Hedgehog and its patched-smoothened receptor complex: a novel signalling mechanism at the cell surface. Biol Chem 378, 583-590.
Alexandre, C., Jacinto, A., and Ingham, P.W. (1996). Transcriptional activation of hedgehog target genes in Drosophila is mediated directly by the cubitus interruptus protein, a member of the GLI family of zinc finger DNA-binding proteins. Genes & development 10, 2003-2013.
Almudi, I., and Casares, F. (2016) Organogenetic Gene Networks: Genetic Control of Organ Formation, Chapter 4: Fast and Furious 800. Springer.
Amore, G., and Casares, F. (2010). Size matters: the contribution of cell proliferation to the progression of the specification Drosophila eye gene regulatory network. Developmental biology 344, 569-577.
Anders, S., and Huber, W. (2010). Differential expression analysis for sequence count data. Genome biology 11, R106.

Annicotte, J.S., Chavey, C., Servant, N., Teyssier, J., Bardin, A., Licznar, A., Badia, E., Pujol, P., Vignon, F., Maudelonde, T., et al. (2005). The nuclear receptor liver receptor homolog-1 is an estrogen receptor target gene. Oncogene 24, 8167-8175.
Aragona, M., Panciera, T., Manfrin, A., Giulitti, S., Michielin, F., Elvassore, N., Dupont, S., and Piccolo, S. (2013). A mechanical checkpoint controls multicellular growth through YAP/TAZ regulation by actin-processing factors. Cell 154, 1047-1059.
Arda, H.E., Benitez, C.M., and Kim, S.K. (2013). Gene regulatory networks governing pancreas development. Developmental cell 25, 5-13.
Armstrong, J.A., Papoulas, O., Daubresse, G., Sperling, A.S., Lis, J.T., Scott, M.P., and Tamkun, J.W. (2002). The Drosophila BRM complex facilitates global transcription by RNA polymerase II. The EMBO journal 21, 5245-5254.
Ashburner, M., Chihara, C., Meltzer, P., and Richards, G. (1974). Temporal control of puffing activity in polytene chromosomes. Cold Spring Harb Symp Quant Biol 38, 655-662.
Atkins, M., and Mardon, G. (2009). Signaling in the third dimension: the peripodial epithelium in eye disc development. Developmental dynamics : an official publication of the American Association of Anatomists 238, 2139-2148.
Atkins, M., Potier, D., Romanelli, L., Jacobs, J., Mach, J., Hamaratoglu, F., Aerts, S., and Halder, G. (2016). An Ectopic Network of Transcription Factors Regulated by Hippo Signaling Drives Growth and Invasion of a Malignant Tumor Model. Current biology : CB 26, 2101-2113.
Aza-Blanc, P., Ramirez-Weber, F.A., Laget, M.P., Schwartz, C., and Kornberg, T.B. (1997). Proteolysis that is inhibited by hedgehog targets Cubitus interruptus protein to the nucleus and converts it to a repressor. Cell 89, 1043-1053.
Bach, E.A., Vincent, S., Zeidler, M.P., and Perrimon, N. (2003). A sensitized genetic screen to identify novel regulators and components of the Drosophila janus kinase/signal transducer and activator of transcription pathway. Genetics 165, 1149-1166.
Baena-Lopez, L.A., Rodriguez, I., and Baonza, A. (2008). The tumor suppressor genes dachsous and fat modulate different signalling pathways by regulating dally and dally-like. Proceedings of the National Academy of Sciences of the United States of America 105, 9645-9650.
Bai, S.W., Li, B., Zhang, H., Jonas, J.B., Zhao, B.W., Shen, L., and Wang, Y.C. (2011). Pax6 regulates proliferation and apoptosis of human retinoblastoma cells. Investigative ophthalmology & visual science 52, 4560-4570.
Baig, J., Chanut, F., Kornberg, T.B., and Klebes, A. (2010). The chromatin-remodeling protein Osa interacts with CyclinE in Drosophila eye imaginal discs. Genetics 184, 731-744.
Baker, N.E. (1988). Transcription of the segment-polarity gene wingless in the imaginal discs of Drosophila, and the phenotype of a pupal-lethal wg mutation. Development 102, 489-497.
Baonza, A., and Freeman, M. (2005). Control of cell proliferation in the Drosophila eye by Notch signaling. Developmental cell 8, 529-539.
Barrett, T., Troup, D.B., Wilhite, S.E., Ledoux, P., Rudnev, D., Evangelista, C., Kim, I.F., Soboleva, A., Tomashevsky, M., Marshall, K.A., et al. (2009). NCBI GEO: archive for high-throughput functional genomic data. Nucleic acids research 37, D885-890.
Basler, K., and Struhl, G. (1994). Compartment boundaries and the control of Drosophila limb pattern by hedgehog protein. Nature 368, 208-214.

Bayrer, J.R., Mukkamala, S., Sablin, E.P., Webb, P., and Fletterick, R.J. (2015). Silencing LRH-1 in colon cancer cell lines impairs proliferation and alters gene expression programs. Proceedings of the National Academy of Sciences of the United States of America 112, 2467-2472.
Beachy, P.A., Helfand, S.L., and Hogness, D.S. (1985). Segmental distribution of bithorax complex proteins during Drosophila development. Nature 313, 545-551.
Belenkaya, T.Y., Han, C., Yan, D., Opoka, R.J., Khodoun, M., Liu, H., and Lin, X. (2004). Drosophila Dpp morphogen movement is independent of dynamin-mediated endocytosis but regulated by the glypican members of heparan sulfate proteoglycans. Cell 119, 231-244.
Benod, C., Vinogradova, M.V., Jouravel, N., Kim, G.E., Fletterick, R.J., and Sablin, E.P. (2011). Nuclear receptor liver receptor homologue 1 (LRH-1) regulates pancreatic cancer cell growth and proliferation. Proceedings of the National Academy of Sciences of the United States of America 108, 16927-16931.
Berdasco, M., and Esteller, M. (2013). Genetic syndromes caused by mutations in epigenetic genes. Hum Genet 132, 359-383.
Bessa, J., Carmona, L., and Casares, F. (2009). Zinc-finger paralogues tsh and tio are functionally equivalent during imaginal development in Drosophila and maintain their expression levels through auto- and cross-negative feedback loops. Developmental dynamics : an official publication of the American Association of Anatomists 238, 19-28.
Bessa, J., and Casares, F. (2005). Restricted teashirt expression confers eye-specific responsiveness to Dpp and Wg signals during eye specification in Drosophila. Development 132, 5011-5020.
Bessa, J., Gebelein, B., Pichaud, F., Casares, F., and Mann, R.S. (2002). Combinatorial control of Drosophila eye development by eyeless, homothorax, and teashirt. Genes & development 16, 2415-2427.
Bhattacharya, A., and Baker, N.E. (2011). A network of broadly expressed HLH genes regulates tissue-specific cell fates. Cell 147, 881-892.
Bohni, R., Riesgo-Escovar, J., Oldham, S., Brogiolo, W., Stocker, H., Andruss, B.F., Beckingham, K., and Hafen, E. (1999). Autonomous control of cell and organ size by CHICO, a Drosophila homolog of vertebrate IRS1-4. Cell 97, 865-875.
Borod, E.R., and Heberlein, U. (1998). Mutual regulation of decapentaplegic and hedgehog during the initiation of differentiation in the Drosophila retina. Developmental biology 197, 187-197.
Botrugno, O.A., Fayard, E., Annicotte, J.S., Haby, C., Brennan, T., Wendling, O., Tanaka, T., Kodama, T., Thomas, W., Auwerx, J., et al. (2004). Synergy between LRH-1 and beta-catenin induces G1 cyclin-mediated cell proliferation. Molecular cell 15, 499-509.
Bouazoune, K., and Brehm, A. (2006). ATP-dependent chromatin remodeling complexes in Drosophila. Chromosome research : an international journal on the molecular, supramolecular and evolutionary aspects of chromosome biology 14, 433-449.
Boulan, L., Martin, D., and Milan, M. (2013). bantam miRNA promotes systemic growth by connecting insulin signaling and ecdysone production. Current biology : CB 23, 473-478.
Brand, A.H., and Perrimon, N. (1993). Targeted gene expression as a means of altering cell fates and generating dominant phenotypes. Development 118, 401-415.
Bras-Pereira, C., Bessa, J., and Casares, F. (2006). Odd-skipped genes specify the signaling center that triggers retinogenesis in Drosophila. Development 133, 4145-4149.

Bras-Pereira, C., Casares, F., and Janody, F. (2015). The retinal determination gene Dachshund restricts cell proliferation by limiting the activity of the Homothorax-Yorkie complex. Development 142, 1470-1479.
Brennan, C.A., Ashburner, M., and Moses, K. (1998). Ecdysone pathway is required for furrow progression in the developing Drosophila eye. Development 125, 2653-2664.
Brennan, C.A., Li, T.R., Bender, M., Hsiung, F., and Moses, K. (2001). Broad-complex, but not ecdysone receptor, is required for progression of the morphogenetic furrow in the Drosophila eye. Development 128, 1-11.
Brogiolo, W., Stocker, H., Ikeya, T., Rintelen, F., Fernandez, R., and Hafen, E. (2001). An evolutionarily conserved function of the Drosophila insulin receptor and insulin-like peptides in growth control. Current biology : CB 11, 213-221.
Brown, N.L., Sattler, C.A., Paddock, S.W., and Carroll, S.B. (1995). Hairy and emc negatively regulate morphogenetic furrow progression in the Drosophila eye. Cell 80, 879-887.
Bryant, P.J., and Simpson, P. (1984). Intrinsic and extrinsic control of growth in developing organs. Q Rev Biol 59, 387-415.
Buckingham, M., and Rigby, P.W. (2014). Gene regulatory networks and transcriptional mechanisms that control myogenesis. Developmental cell 28, 225-238.
Burke, R., and Basler, K. (1996). Dpp receptors are autonomously required for cell proliferation in the entire developing Drosophila wing. Development 122, 2261-2269.
Burtis, K.C., Thummel, C.S., Jones, C.W., Karim, F.D., and Hogness, D.S. (1990). The Drosophila 74EF early puff contains E74, a complex ecdysone-inducible gene that encodes two ets-related proteins. Cell 61, 85-99.
Caldwell, P.E., Walkiewicz, M., and Stern, M. (2005). Ras activity in the Drosophila prothoracic gland regulates body size and developmental rate via ecdysone release. Current biology : CB 15, 1785-1795.
Capdevila, J., and Guerrero, I. (1994). Targeted expression of the signaling molecule decapentaplegic induces pattern duplications and growth alterations in Drosophila wings. The EMBO journal 13, 4459-4468.
Carmona-Saez, P., Chagoyen, M., Tirado, F., Carazo, J.M., and Pascual-Montano, A. (2007). GENECODIS: a web-based tool for finding significant concurrent annotations in gene lists. Genome biology 8, R3.
Carroll, J.S., Meyer, C.A., Song, J., Li, W., Geistlinger, T.R., Eeckhoute, J., Brodsky, A.S., Keeton, E.K., Fertuck, K.C., Hall, G.F., et al. (2006). Genome-wide analysis of estrogen receptor binding sites. Nature genetics 38, 1289-1297.
Casares, F., and Mann, R.S. (1998). Control of antennal versus leg development in Drosophila. Nature 392, 723-726.
Casares, F., and Mann, R.S. (2000). A dual role for homothorax in inhibiting wing blade development and specifying proximal wing identities in Drosophila. Development 127, 1499-1508.
Cavodeassi, F., Diez Del Corral, R., Campuzano, S., and Dominguez, M. (1999). Compartments and organising boundaries in the Drosophila eye: the role of the homeodomain Iroquois proteins. Development 126, 4933-4942.
Champlin, D.T., and Truman, J.W. (1998a). Ecdysteroid control of cell proliferation during optic lobe neurogenesis in the moth Manduca sexta. Development 125, 269-277.

Champlin, D.T., and Truman, J.W. (1998b). Ecdysteroids govern two phases of eye development during metamorphosis of the moth, Manduca sexta. Development 125, 2009-2018.
Chand, A.L., Herridge, K.A., Thompson, E.W., and Clyne, C.D. (2010). The orphan nuclear receptor LRH-1 promotes breast cancer motility and invasion. Endocrine-related cancer 17, 965-975.
Chao, J.L., Tsai, Y.C., Chiu, S.J., and Sun, Y.H. (2004). Localized Notch signal acts through eyg and upd to promote global growth in Drosophila eye. Development 131, 3839-3847.
Chen, C., Jack, J., and Garofalo, R.S. (1996). The Drosophila insulin receptor is required for normal growth. Endocrinology 137, 846-856.
Chen, Q., Yang, C.Y., Tsan, J.T., Xia, Y., Ragab, A.H., Peiper, S.C., Carroll, A., and Baer, R. (1990). Coding sequences of the tal-1 gene are disrupted by chromosome translocation in human T cell leukemia. The Journal of experimental medicine 172, 1403-1408.
Chen, R., Amoui, M., Zhang, Z., and Mardon, G. (1997). Dachshund and eyes absent proteins form a complex and function synergistically to induce ectopic eye development in Drosophila. Cell 91, 893-903.
Chi, T.H., Wan, M., Lee, P.P., Akashi, K., Metzger, D., Chambon, P., Wilson, C.B., and Crabtree, G.R. (2003). Sequential roles of Brg, the ATPase subunit of BAF chromatin remodeling complexes, in thymocyte development. Immunity 19, 169-182.
Cho, K.O., and Choi, K.W. (1998). Fringe is essential for mirror symmetry and morphogenesis in the Drosophila eye. Nature 396, 272-276.
Chow, L., Levine, E.M., and Reh, T.A. (1998). The nuclear receptor transcription factor, retinoid-related orphan receptor beta, regulates retinal progenitor proliferation. Mechanisms of development 77, 149-164.
Cicatiello, L., Mutarelli, M., Grober, O.M., Paris, O., Ferraro, L., Ravo, M., Tarallo, R., Luo, S., Schroth, G.P., Seifert, M., et al. (2010). Estrogen receptor alpha controls a gene network in luminal-like breast cancer cells comprising multiple transcription factors and microRNAs. The American journal of pathology 176, 2113-2130.
Clapier, C.R., and Cairns, B.R. (2009). The biology of chromatin remodeling complexes. Annual review of biochemistry 78, 273-304.
Collins, R.T., Furukawa, T., Tanese, N., and Treisman, J.E. (1999). Osa associates with the Brahma chromatin remodeling complex and promotes the activation of some target genes. The EMBO journal 18, 7029-7040.
Colombani, J., Bianchini, L., Layalle, S., Pondeville, E., Dauphin-Villemant, C., Antoniewski, C., Carre, C., Noselli, S., and Leopold, P. (2005). Antagonistic actions of ecdysone and insulins determine final size in Drosophila. Science 310, 667-670.
Crickmore, M.A., and Mann, R.S. (2006). Hox control of organ size by regulation of morphogen production and mobility. Science 313, 63-68.
Crijns, A.P., de Graeff, P., Geerts, D., Ten Hoor, K.A., Hollema, H., van der Sluis, T., Hofstra, R.M., de Bock, G.H., de Jong, S., van der Zee, A.G., et al. (2007). MEIS and PBX homeobox proteins in ovarian cancer. Eur J Cancer 43, 2495-2505.
Curtiss, J., and Mlodzik, M. (2000). Morphogenetic furrow initiation and progression during eye development in Drosophila: the roles of decapentaplegic, hedgehog and eyes absent. Development 127, 1325-1336.

Cvekl, A., and Ashery-Padan, R. (2014). The cellular and molecular mechanisms of vertebrate lens development. Development 141, 4432-4447.
Czerny, T., Halder, G., Kloter, U., Souabni, A., Gehring, W.J., and Busslinger, M. (1999). twin of eyeless, a second Pax-6 gene of Drosophila, acts upstream of eyeless in the control of eye development. Molecular cell 3, 297-307.
Dardaei, L., Longobardi, E., and Blasi, F. (2014). Prep1 and Meis1 competition for Pbx1 binding regulates protein stability and tumorigenesis. Proceedings of the National Academy of Sciences of the United States of America 111, E896-905.
Davie, K., Jacobs, J., Atkins, M., Potier, D., Christiaens, V., Halder, G., and Aerts, S. (2015). Discovery of transcription factors and regulatory regions driving in vivo tumor development by ATAC-seq and FAIRE-seq open chromatin profiling. PLoS genetics 11, e1004994.
Day, S.J., and Lawrence, P.A. (2000). Measuring dimensions: the regulation of size and shape. Development 127, 2977-2987.
de Navas, L.F., Garaulet, D.L., and Sanchez-Herrero, E. (2006). The ultrabithorax Hox gene of Drosophila controls haltere size by regulating the Dpp pathway. Development 133, 4495-4506.
de Nooij, J.C., Letendre, M.A., and Hariharan, I.K. (1996). A cyclin-dependent kinase inhibitor, Dacapo, is necessary for timely exit from the cell cycle during Drosophila embryogenesis. Cell 87, 1237-1247.
Debril, M.B., Gelman, L., Fayard, E., Annicotte, J.S., Rocchi, S., and Auwerx, J. (2004). Transcription factors and nuclear receptors interact with the SWI/SNF complex through the BAF60c subunit. The Journal of biological chemistry 279, 16677-16686.
Delanoue, R., Slaidina, M., and Leopold, P. (2010). The steroid hormone ecdysone controls systemic growth by repressing dMyc function in Drosophila fat cells. Developmental cell 18, 1012-1021.
Delgado, I., and Torres, M. (2016). Gradients, waves and timers, an overview of limb patterning models. Semin Cell Dev Biol 49, 109-115.
DiBello, P.R., Withers, D.A., Bayer, C.A., Fristrom, J.W., and Guild, G.M. (1991). The Drosophila Broad-Complex encodes a family of related proteins containing zinc fingers. Genetics 129, 385-397.
Dickinson, M.E., Krumlauf, R., and McMahon, A.P. (1994). Evidence for a mitogenic effect of Wnt-1 in the developing mammalian central nervous system. Development 120, 1453-1471.
Dominguez, M., and de Celis, J.F. (1998). A dorsal/ventral boundary established by Notch controls growth and polarity in the Drosophila eye. Nature 396, 276-278.
Dominguez, M., Ferres-Marco, D., Gutierrez-Avino, F.J., Speicher, S.A., and Beneyto, M. (2004). Growth and specification of the eye are controlled independently by Eyegone and Eyeless in Drosophila melanogaster. Nature genetics 36, 31-39.
Dong, J., Feldmann, G., Huang, J., Wu, S., Zhang, N., Comerford, S.A., Gayyed, M.F., Anders, R.A., Maitra, A., and Pan, D. (2007). Elucidation of a universal size-control mechanism in Drosophila and mammals. Cell 130, 1120-1133.
Du, J., and Xu, R. (2012). RORalpha, a potential tumor suppressor and therapeutic target of breast cancer. International journal of molecular sciences 13, 15755-15766.
Duman-Scheel, M., Weng, L., Xin, S., and Du, W. (2002). Hedgehog regulates cell growth and proliferation by inducing Cyclin D and Cyclin E. Nature 417, 299-304.

Dupont, S., Morsut, L., Aragona, M., Enzo, E., Giulitti, S., Cordenonsi, M., Zanconato, F., Le Digabel, J., Forcato, M., Bicciato, S., et al. (2011). Role of YAP/TAZ in mechanotransduction. Nature 474, 179-183.
Eden, E., Navon, R., Steinfeld, I., Lipson, D., and Yakhini, Z. (2009). GOrilla: a tool for discovery and visualization of enriched GO terms in ranked gene lists. BMC bioinformatics 10, 48.
Ekas, L.A., Baeg, G.H., Flaherty, M.S., Ayala-Camargo, A., and Bach, E.A. (2006). JAK/STAT signaling promotes regional specification by negatively regulating wingless expression in Drosophila. Development 133, 4721-4729.
Elliott, D.A., and Brand, A.H. (2008). The GAL4 system : a versatile system for the expression of genes. Methods Mol Biol 420, 79-95.
Engler, A.J., Sen, S., Sweeney, H.L., and Discher, D.E. (2006). Matrix elasticity directs stem cell lineage specification. Cell 126, 677-689.
Ernst, J., and Kellis, M. (2010). Discovery and characterization of chromatin states for systematic annotation of the human genome. Nat Biotechnol 28, 817-825.
Eroglu, E., Burkard, T.R., Jiang, Y., Saini, N., Homem, C.C., Reichert, H., and Knoblich, J.A. (2014). SWI/SNF complex prevents lineage reversion and induces temporal patterning in neural stem cells. Cell 156, 1259-1273.
Escudero, L.M., and Freeman, M. (2007). Mechanism of G1 arrest in the Drosophila eye imaginal disc. BMC developmental biology 7, 13.
Fan, J., Liu, Y., and Jia, J. (2012). Hh-induced Smoothened conformational switch is mediated by differential phosphorylation at its C-terminal tail in a dose- and position-dependent manner. Developmental biology 366, 172-184.
Faralli, H., Martin, E., Core, N., Liu, Q.C., Filippi, P., Dilworth, F.J., Caubit, X., and Fasano, L. (2011). Teashirt-3, a novel regulator of muscle differentiation, associates with BRG1-associated factor 57 (BAF57) to inhibit myogenin gene expression. The Journal of biological chemistry 286, 23498-23510.
Farge, E. (2003). Mechanical induction of Twist in the Drosophila foregut/stomodeal primordium. Current biology : CB 13, 1365-1377.
Fernandez, B.G., Gaspar, P., Bras-Pereira, C., Jezowska, B., Rebelo, S.R., and Janody, F. (2011). Actin-Capping Protein and the Hippo pathway regulate F-actin and tissue growth in Drosophila. Development 138, 2337-2346.
Ferreira, A., and Milan, M. (2015). Dally Proteoglycan Mediates the Autonomous and Nonautonomous Effects on Tissue Growth Caused by Activation of the PI3K and TOR Pathways. PLoS biology 13, e1002239.
Filion, G.J., van Bemmel, J.G., Braunschweig, U., Talhout, W., Kind, J., Ward, L.D., Brugman, W., de Castro, I.J., Kerkhoven, R.M., Bussemaker, H.J., et al. (2010). Systematic protein location mapping reveals five principal chromatin types in Drosophila cells. Cell 143, 212-224.
Fire, A., Xu, S., Montgomery, M.K., Kostas, S.A., Driver, S.E., and Mello, C.C. (1998). Potent and specific genetic interference by double-stranded RNA in Caenorhabditis elegans. Nature 391, 806-811.
Firth, L.C., and Baker, N.E. (2005). Extracellular signals responsible for spatially regulated proliferation in the differentiating Drosophila eye. Developmental cell 8, 541-551.
Firth, L.C., and Baker, N.E. (2009). Retinal determination genes as targets and possible effectors of extracellular signals. Developmental biology 327, 366-375.

Frolov, M.V., and Dyson, N.J. (2004). Molecular mechanisms of E2F-dependent activation and pRB-mediated repression. J Cell Sci 117, 2173-2181.
Fu, W., and Baker, N.E. (2003). Deciphering synergistic and redundant roles of Hedgehog, Decapentaplegic and Delta that drive the wave of differentiation in Drosophila eye development. Development 130, 5229-5239.
Fujise, M., Takeo, S., Kamimura, K., Matsuo, T., Aigaki, T., Izumi, S., and Nakato, H. (2003). Dally regulates Dpp morphogen gradient formation in the Drosophila wing. Development 130, 1515-1522.
Gaillard, H., Fitzgerald, D.J., Smith, C.L., Peterson, C.L., Richmond, T.J., and Thoma, F. (2003). Chromatin remodeling activities act on UV-damaged nucleosomes and modulate DNA damage accessibility to photolyase. The Journal of biological chemistry 278, 17655-17663.
Gao, X., and Pan, D. (2001). TSC1 and TSC2 tumor suppressors antagonize insulin signaling in cell growth. Genes & development 15, 1383-1392.
Gao, X., Zhang, Y., Arrazola, P., Hino, O., Kobayashi, T., Yeung, R.S., Ru, B., and Pan, D. (2002). Tsc tumour suppressor proteins antagonize amino-acid-TOR signalling. Nature cell biology 4, 699-704.
Garami, A., Zwartkruis, F.J., Nobukuni, T., Joaquin, M., Roccio, M., Stocker, H., Kozma, S.C., Hafen, E., Bos, J.L., and Thomas, G. (2003). Insulin activation of Rheb, a mediator of mTOR/S6K/4E-BP signaling, is inhibited by TSC1 and 2. Molecular cell 11, 1457-1466.
Garcia-Bellido, A., and Merriam, J.R. (1969). Cell lineage of the imaginal discs in Drosophila gynandromorphs. J Exp Zool 170, 61-75.
Garelli, A., Gontijo, A.M., Miguela, V., Caparros, E., and Dominguez, M. (2012). Imaginal discs secrete insulin-like peptide 8 to mediate plasticity of growth and maturation. Science 336, 579-582.
Garelli, A., Heredia, F., Casimiro, A.P., Macedo, A., Nunes, C., Garcez, M., Dias, A.R., Volonte, Y.A., Uhlmann, T., Caparros, E., et al. (2015). Dilp8 requires the neuronal relaxin receptor Lgr3 to couple growth to developmental timing. Nat Commun 6, 8732.
Garofalo, R.S. (2002). Genetic analysis of insulin signaling in Drosophila. Trends Endocrinol Metab 13, 156-162.
Gaulton, K.J., Nammo, T., Pasquali, L., Simon, J.M., Giresi, P.G., Fogarty, M.P., Panhuis, T.M., Mieczkowski, P., Secchi, A., Bosco, D., et al. (2010). A map of open chromatin in human pancreatic islets. Nature genetics 42, 255-259.
Geerts, D., Revet, I., Jorritsma, G., Schilderink, N., and Versteeg, R. (2005). MEIS homeobox genes in neuroblastoma. Cancer Lett 228, 43-50.
Geerts, D., Schilderink, N., Jorritsma, G., and Versteeg, R. (2003). The role of the MEIS homeobox genes in neuroblastoma. Cancer Lett 197, 87-92.
Geisler, S.J., and Paro, R. (2015). Trithorax and Polycomb group-dependent regulation: a tale of opposing activities. Development 142, 2876-2887.
Geminard, C., Rulifson, E.J., and Leopold, P. (2009). Remote control of insulin secretion by fat cells in Drosophila. Cell Metab 10, 199-207.
Giot, L., Bader, J.S., Brouwer, C., Chaudhuri, A., Kuang, B., Li, Y., Hao, Y.L., Ooi, C.E., Godwin, B., Vitols, E., et al. (2003). A protein interaction map of Drosophila melanogaster. Science 302, 1727-1736.

Giresi, P.G., Kim, J., McDaniell, R.M., Iyer, V.R., and Lieb, J.D. (2007). FAIRE (Formaldehyde-Assisted Isolation of Regulatory Elements) isolates active regulatory elements from human chromatin. Genome research 17, 877-885.
Gong, F., Fahy, D., Liu, H., Wang, W., and Smerdon, M.J. (2008). Role of the mammalian SWI/SNF chromatin remodeling complex in the cellular response to UV damage. Cell Cycle 7, 1067-1074.
Gottgens, B. (2015). Regulatory network control of blood stem cells. Blood 125, 2614-2620.
Goulev, Y., Fauny, J.D., Gonzalez-Marti, B., Flagiello, D., Silber, J., and Zider, A. (2008). SCALLOPED interacts with YORKIE, the nuclear effector of the hippo tumor-suppressor pathway in Drosophila. Current biology : CB 18, 435-441.
Greenwood, S., and Struhl, G. (1999). Progression of the morphogenetic furrow in the Drosophila eye: the roles of Hedgehog, Decapentaplegic and the Raf pathway. Development 126, 5795-5808.
Gupta, S., Takebe, N., and Lorusso, P. (2010). Targeting the Hedgehog pathway in cancer. Therapeutic advances in medical oncology 2, 237-250.
Gutierrez-Avino, F.J., Ferres-Marco, D., and Dominguez, M. (2009). The position and function of the Notch-mediated eye growth organizer: the roles of JAK/STAT and four-jointed. EMBO Rep 10, 1051-1058.
Haerry, T.E., Khalsa, O., O'Connor, M.B., and Wharton, K.A. (1998). Synergistic signaling by two BMP ligands through the SAX and TKV receptors controls wing growth and patterning in Drosophila. Development 125, 3977-3987.
Halder, G., Callaerts, P., and Gehring, W.J. (1995). Induction of ectopic eyes by targeted expression of the eyeless gene in Drosophila. Science 267, 1788-1792.
Halder, G., and Johnson, R.L. (2011). Hippo signaling: growth control and beyond. Development 138, 9-22.
Hamaratoglu, F., Affolter, M., and Pyrowolakis, G. (2014). Dpp/BMP signaling in flies: from molecules to biology. Semin Cell Dev Biol 32, 128-136.
Hariharan, I.K. (2015). Organ Size Control: Lessons from Drosophila. Developmental cell 34, 255-265.
Harmansa, S., Hamaratoglu, F., Affolter, M., and Caussinus, E. (2015). Dpp spreading is required for medial but not for lateral wing disc growth. Nature 527, 317-322.
Harvey, K.F., Zhang, X., and Thomas, D.M. (2013). The Hippo pathway and human cancer. Nat Rev Cancer 13, 246-257.
Hazelett, D.J., Bourouis, M., Walldorf, U., and Treisman, J.E. (1998). decapentaplegic and wingless are regulated by eyes absent and eyegone and interact to direct the pattern of retinal differentiation in the eye disc. Development 125, 3741-3751.
Heberlein, U., Borod, E.R., and Chanut, F.A. (1998). Dorsoventral patterning in the Drosophila retina by wingless. Development 125, 567-577.
Heberlein, U., Wolff, T., and Rubin, G.M. (1993). The TGF beta homolog dpp and the segment polarity gene hedgehog are required for propagation of a morphogenetic wave in the Drosophila retina. Cell 75, 913-926.
Hepker, J., Wang, Q.T., Motzny, C.K., Holmgren, R., and Orenic, T.V. (1997). Drosophila cubitus interruptus forms a negative feedback loop with patched and regulates expression of Hedgehog target genes. Development 124, 549-558.

Herboso, L., Oliveira, M.M., Talamillo, A., Perez, C., Gonzalez, M., Martin, D., Sutherland, J.D., Shingleton, A.W., Mirth, C.K., and Barrio, R. (2015). Ecdysone promotes growth of imaginal discs through the regulation of Thor in D. melanogaster. Scientific reports 5, 12383.
Herrmann, C., Van de Sande, B., Potier, D., and Aerts, S. (2012). i-cisTarget: an integrative genomics method for the prediction of regulatory features and cis-regulatory modules. Nucleic acids research 40, e114.
Hirose, F., Yamaguchi, M., Kuroda, K., Omori, A., Hachiya, T., Ikeda, M., Nishimoto, Y., and Matsukage, A. (1996). Isolation and characterization of cDNA for DREF, a promoter-activating factor for Drosophila DNA replication-related genes. The Journal of biological chemistry 271, 3930-3937.
Ho, L., and Crabtree, G.R. (2010). Chromatin remodelling during development. Nature 463, 474-484.
Hock, H. (2012). A complex Polycomb issue: the two faces of EZH2 in cancer. Genes & development 26, 751-755.
Hsiao, P.W., Fryer, C.J., Trotter, K.W., Wang, W., and Archer, T.K. (2003). BAF60a mediates critical interactions between nuclear receptors and the BRG1 chromatin-remodeling complex for transactivation. Molecular and cellular biology 23, 6210-6220.
Huang, J., Wu, S., Barrera, J., Matthews, K., and Pan, D. (2005). The Hippo signaling pathway coordinately regulates cell proliferation and apoptosis by inactivating Yorkie, the Drosophila Homolog of YAP. Cell 122, 421-434.
Huang, S., Chen, C.S., and Ingber, D.E. (1998). Control of cyclin D1, p27(Kip1), and cell cycle progression in human capillary endothelial cells by cell shape and cytoskeletal tension. Mol Biol Cell 9, 3179-3193.
Hufnagel, L., Teleman, A.A., Rouault, H., Cohen, S.M., and Shraiman, B.I. (2007). On the mechanism of wing size determination in fly development. Proceedings of the National Academy of Sciences of the United States of America 104, 3835-3840.
Ikeya, T., Galic, M., Belawat, P., Nairz, K., and Hafen, E. (2002). Nutrient-dependent expression of insulin-like peptides from neuroendocrine cells in the CNS contributes to growth regulation in Drosophila. Current biology : CB 12, 1293-1300.
Irvine, K.D., and Harvey, K.F. (2015). Control of organ growth by patterning and hippo signaling in Drosophila. Cold Spring Harb Perspect Biol 7.
Ito, T., Yamauchi, M., Nishina, M., Yamamichi, N., Mizutani, T., Ui, M., Murakami, M., and Iba, H. (2001). Identification of SWI.SNF complex subunit BAF60a as a determinant of the transactivation potential of Fos/Jun dimers. The Journal of biological chemistry 276, 2852-2857.
Jang, A.C., Chang, Y.C., Bai, J., and Montell, D. (2009). Border-cell migration requires integration of spatial and temporal signals by the BTB protein Abrupt. Nature cell biology 11, 569-579.
Jang, C.C., Chao, J.L., Jones, N., Yao, L.C., Bessarab, D.A., Kuo, Y.M., Jun, S., Desplan, C., Beckendorf, S.K., and Sun, Y.H. (2003). Two Pax genes, eye gone and eyeless, act cooperatively in promoting Drosophila eye development. Development 130, 2939-2951.
Janody, F., Lee, J.D., Jahren, N., Hazelett, D.J., Benlali, A., Miura, G.I., Draskovic, I., and Treisman, J.E. (2004). A mosaic genetic screen reveals distinct roles for trithorax and polycomb group genes in Drosophila eye development. Genetics 166, 187-200.

Jarman, A.P., Sun, Y., Jan, L.Y., and Jan, Y.N. (1995). Role of the proneural gene, atonal, in formation of Drosophila chordotonal organs and photoreceptors. Development 121, 2019-2030.
Jemal, A., Bray, F., Center, M.M., Ferlay, J., Ward, E., and Forman, D. (2011). Global cancer statistics. CA Cancer J Clin 61, 69-90.
Jemc, J., and Rebay, I. (2007). Identification of transcriptional targets of the dual-function transcription factor/phosphatase eyes absent. Developmental biology 310, 416-429.
Jia, Y., Wang, Y., and Xie, J. (2015). The Hedgehog pathway: role in cell differentiation, polarity and proliferation. Arch Toxicol 89, 179-191.
Jung, J.W., Shim, S.Y., Lee, D.K., Kwiatkowski, W., and Choe, S. (2014). An Activin A/BMP2 chimera, AB215, blocks estrogen signaling via induction of ID proteins in breast cancer cells. BMC cancer 14, 549.
Junger, M.A., Rintelen, F., Stocker, H., Wasserman, J.D., Vegh, M., Radimerski, T., Greenberg, M.E., and Hafen, E. (2003). The Drosophila forkhead transcription factor FOXO mediates the reduction in cell number associated with reduced insulin signaling. J Biol 2, 20.
Junker, J.P., Peterson, K.A., Nishi, Y., Mao, J., McMahon, A.P., and van Oudenaarden, A. (2014). A predictive model of bifunctional transcription factor signaling during embryonic tissue patterning. Developmental cell 31, 448-460.
Jusiak, B., Karandikar, U.C., Kwak, S.J., Wang, F., Wang, H., Chen, R., and Mardon, G. (2014). Regulation of Drosophila eye development by the transcription factor Sine oculis. PloS one 9, e89695.
Katsuyama, T., Sugawara, T., Tatsumi, M., Oshima, Y., Gehring, W.J., Aigaki, T., and Kurata, S. (2005). Involvement of winged eye encoding a chromatin-associated bromo-adjacent homology domain protein in disc specification. Proceedings of the National Academy of Sciences of the United States of America 102, 15918-15923.
Kennerdell, J.R., and Carthew, R.W. (1998). Use of dsRNA-mediated genetic interference to demonstrate that frizzled and frizzled 2 act in the wingless pathway. Cell 95, 1017-1026.
Kenyon, K.L., Ranade, S.S., Curtiss, J., Mlodzik, M., and Pignoni, F. (2003). Coordinating proliferation and tissue specification to promote regional identity in the Drosophila head. Developmental cell 5, 403-414.
Kicheva, A., Pantazis, P., Bollenbach, T., Kalaidzidis, Y., Bittig, T., Julicher, F., and Gonzalez-Gaitan, M. (2007). Kinetics of morphogen gradient formation. Science 315, 521-525.
Kim, D.H., Sarbassov, D.D., Ali, S.M., King, J.E., Latek, R.R., Erdjument-Bromage, H., Tempst, P., and Sabatini, D.M. (2002). mTOR interacts with raptor to form a nutrient-sensitive complex that signals to the cell growth machinery. Cell 110, 163-175.
Kimelman, D., and Kirschner, M. (1987). Synergistic induction of mesoderm by FGF and TGF-beta and the identification of an mRNA coding for FGF in the early Xenopus embryo. Cell 51, 869-877.
King, R., Weilbaecher, K.N., McGill, G., Cooley, E., Mihm, M., and Fisher, D.E. (1999). Microphthalmia transcription factor. A sensitive and specific melanocyte marker for MelanomaDiagnosis. The American journal of pathology 155, 731-738.
Kingston, R.E., and Tamkun, J.W. (2014). Transcriptional regulation by trithorax-group proteins. Cold Spring Harb Perspect Biol 6, a019349.

Knoepfler, P.S., Calvo, K.R., Chen, H., Antonarakis, S.E., and Kamps, M.P. (1997). Meis1 and pKnox1 bind DNA cooperatively with Pbx1 utilizing an interaction surface disrupted in oncoprotein E2a-Pbx1. Proceedings of the National Academy of Sciences of the United States of America 94, 14553-14558.
Koelle, M.R., Talbot, W.S., Segraves, W.A., Bender, M.T., Cherbas, P., and Hogness, D.S. (1991). The Drosophila EcR gene encodes an ecdysone receptor, a new member of the steroid receptor superfamily. Cell 67, 59-77.
Koller, K., Pichler, M., Koch, K., Zandl, M., Stiegelbauer, V., Leuschner, I., Hoefler, G., and Guertl, B. (2014). Nephroblastomas show low expression of microR-204 and high expression of its target, the oncogenic transcription factor MEIS1. Pediatr Dev Pathol 17, 169-175.
Koppens, M., and van Lohuizen, M. (2016). Context-dependent actions of Polycomb repressors in cancer. Oncogene 35, 1341-1352.
Kosan, C., and Godmann, M. (2016). Genetic and Epigenetic Mechanisms That Maintain Hematopoietic Stem Cell Function. Stem Cells Int 2016, 5178965.
Koyama, T., Mendes, C.C., and Mirth, C.K. (2013). Mechanisms regulating nutrition-dependent developmental plasticity through organ-specific effects in insects. Front Physiol 4, 263.
Kramer, H.B., Lai, C.F., Patel, H., Periyasamy, M., Lin, M.L., Feller, S.M., Fuller-Pace, F.V., Meek, D.W., Ali, S., and Buluwela, L. (2016). LRH-1 drives colon cancer cell growth by repressing the expression of the CDKN1A gene in a p53-dependent manner. Nucleic acids research 44, 582-594.
Kumar, J.P. (2010). Retinal determination the beginning of eye development. Curr Top Dev Biol 93, 1-28.
Kwon, C.S., and Wagner, D. (2007). Unwinding chromatin for development and growth: a few genes at a time. Trends in genetics : TIG 23, 403-412.
Kwon, Y.S., Garcia-Bassets, I., Hutt, K.R., Cheng, C.S., Jin, M., Liu, D., Benner, C., Wang, D., Ye, Z., Bibikova, M., et al. (2007). Sensitive ChIP-DSL technology reveals an extensive estrogen receptor alpha-binding program on human gene promoters. Proceedings of the National Academy of Sciences of the United States of America 104, 4852-4857.
Lai, Z.C., Wei, X., Shimizu, T., Ramos, E., Rohrbaugh, M., Nikolaidis, N., Ho, L.L., and Li, Y. (2005). Control of cell proliferation and apoptosis by mob as tumor suppressor, mats. Cell 120, 675-685.
Lam, G.T., Jiang, C., and Thummel, C.S. (1997). Coordination of larval and prepupal gene expression by the DHR3 orphan receptor during Drosophila metamorphosis. Development 124, 1757-1769.
Lane, M.E., Sauer, K., Wallace, K., Jan, Y.N., Lehner, C.F., and Vaessin, H. (1996). Dacapo, a cyclin-dependent kinase inhibitor, stops cell proliferation during Drosophila development. Cell 87, 1225-1235.
Langmead, B., and Salzberg, S.L. (2012). Fast gapped-read alignment with Bowtie 2. Nature methods 9, 357-359.
Lazarus, K.A., Brown, K.A., Young, M.J., Zhao, Z., Coulson, R.S., Chand, A.L., and Clyne, C.D. (2014). Conditional overexpression of liver receptor homolog-1 in female mouse mammary epithelium results in altered mammary morphogenesis via the induction of TGF-beta. Endocrinology 155, 1606-1617.

Lecuit, T., Brook, W.J., Ng, M., Calleja, M., Sun, H., and Cohen, S.M. (1996). Two distinct mechanisms for long-range patterning by Decapentaplegic in the Drosophila wing. Nature 381, 387-393.
Lecuit, T., and Cohen, S.M. (1998). Dpp receptor levels contribute to shaping the Dpp morphogen gradient in the Drosophila wing imaginal disc. Development 125, 4901-4907.
Lee, J.D., and Treisman, J.E. (2001). The role of Wingless signaling in establishing the anteroposterior and dorsoventral axes of the eye disc. Development 128, 1519-1529.
Legoff, L., Rouault, H., and Lecuit, T. (2013). A global pattern of mechanical stress polarizes cell divisions and cell shape in the growing Drosophila wing disc. Development 140, 4051-4059.
Lewis, E.B. (1978). A gene complex controlling segmentation in Drosophila. Nature 276, 565-570.
Lickert, H., Takeuchi, J.K., Von Both, I., Walls, J.R., McAuliffe, F., Adamson, S.L., Henkelman, R.M., Wrana, J.L., Rossant, J., and Bruneau, B.G. (2004). Baf60c is essential for function of BAF chromatin remodelling complexes in heart development. Nature 432, 107-112.
Ligoxygakis, P., Yu, S.Y., Delidakis, C., and Baker, N.E. (1998). A subset of notch functions during Drosophila eye development require Su(H) and the E(spl) gene complex. Development 125, 2893-2900.
Lin, X., Buff, E.M., Perrimon, N., and Michelson, A.M. (1999). Heparan sulfate proteoglycans are essential for FGF receptor signaling during Drosophila embryonic development. Development 126, 3715-3723.
Locker, M., Agathocleous, M., Amato, M.A., Parain, K., Harris, W.A., and Perron, M. (2006). Hedgehog signaling and the retina: insights into the mechanisms controlling the proliferative properties of neural precursors. Genes & development 20, 3036-3048.
Lopes, C.S., and Casares, F. (2010). hth maintains the pool of eye progenitors and its downregulation by Dpp and Hh couples retinal fate acquisition with cell cycle exit. Developmental biology 339, 78-88.
Lopes, C.S., and Casares, F. (2015). Eye selector logic for a coordinated cell cycle exit. PLoS genetics 11, e1004981.
Lowe, N., Rees, J.S., Roote, J., Ryder, E., Armean, I.M., Johnson, G., Drummond, E., Spriggs, H., Drummond, J., Magbanua, J.P., et al. (2014). Analysis of the expression patterns, subcellular localisations and interaction partners of Drosophila proteins using a pigP protein trap library. Development 141, 3994-4005.
Luchetti, G., Sircar, R., Kong, J.H., Nachtergaele, S., Sagner, A., Byrne, E.F., Covey, D.F., Siebold, C., and Rohatgi, R. (2016). Cholesterol activates the G-protein coupled receptor Smoothened to promote morphogenetic signaling. Elife 5.
Lyne, R., Smith, R., Rutherford, K., Wakeling, M., Varley, A., Guillier, F., Janssens, H., Ji, W., McLaren, P., North, P., et al. (2007). FlyMine: an integrated database for Drosophila and Anopheles genomics. Genome biology 8, R129.
Ma, C., Zhou, Y., Beachy, P.A., and Moses, K. (1993). The segment polarity gene hedgehog is required for progression of the morphogenetic furrow in the developing Drosophila eye. Cell 75, 927-938.
Mangelsdorf, D.J., Thummel, C., Beato, M., Herrlich, P., Schutz, G., Umesono, K., Blumberg, B., Kastner, P., Mark, M., Chambon, P., et al. (1995). The nuclear receptor superfamily: the second decade. Cell 83, 835-839.

Mao, Y., Tournier, A.L., Hoppe, A., Kester, L., Thompson, B.J., and Tapon, N. (2013). Differential proliferation rates generate patterns of mechanical tension that orient tissue growth. The EMBO journal 32, 2790-2803.
Marinho, J., Martins, T., Neto, M., Casares, F., and Pereira, P.S. (2013). The nucleolar protein Viriato/Nol12 is required for the growth and differentiation progression activities of the Dpp pathway during Drosophila eye development. Developmental biology 377, 154-165.
Mascarenhas, J.B., Young, K.P., Littlejohn, E.L., Yoo, B.K., Salgia, R., and Lang, D. (2009). PAX6 is expressed in pancreatic cancer and actively participates in cancer progression through activation of the MET tyrosine kinase receptor gene. The Journal of biological chemistry 284, 27524-27532.
Massague, J. (2008). TGFbeta in Cancer. Cell 134, 215-230.
Masucci, J.D., and Hoffmann, F.M. (1993). Identification of two regions from the Drosophila decapentaplegic gene required for embryonic midgut development and larval viability. Developmental biology 159, 276-287.
Masucci, J.D., Miltenberger, R.J., and Hoffmann, F.M. (1990). Pattern-specific expression of the Drosophila decapentaplegic gene in imaginal disks is regulated by 3' cis-regulatory elements. Genes & development 4, 2011-2023.
McBeath, R., Pirone, D.M., Nelson, C.M., Bhadriraju, K., and Chen, C.S. (2004). Cell shape, cytoskeletal tension, and RhoA regulate stem cell lineage commitment. Developmental cell 6, 483-495.
McKay, D.J., and Lieb, J.D. (2013). A common set of DNA regulatory elements shapes Drosophila appendages. Developmental cell 27, 306-318.
McKillip, E., and Klueg, K. (2006) DGRC Vector Standard Operating Procedure 1.0: Processing Clones for Whatman FTA Discs.
Metcalf, D. (1963). The Autonomous Behaviour of Normal Thymus Grafts. Aust J Exp Biol Med Sci 41, SUPPL437-447.
Mirth, C., Truman, J.W., and Riddiford, L.M. (2005). The role of the prothoracic gland in determining critical weight for metamorphosis in Drosophila melanogaster. Current biology : CB 15, 1796-1807.
Mirth, C.K., Truman, J.W., and Riddiford, L.M. (2009). The ecdysone receptor controls the post-critical weight switch to nutrition-independent differentiation in Drosophila wing imaginal discs. Development 136, 2345-2353.
Misra, J.R., and Irvine, K.D. (2016). Vamana Couples Fat Signaling to the Hippo Pathway. Developmental cell 39, 254-266.
Mohrmann, L., Langenberg, K., Krijgsveld, J., Kal, A.J., Heck, A.J., and Verrijzer, C.P. (2004). Differential targeting of two distinct SWI/SNF-related Drosophila chromatin-remodeling complexes. Molecular and cellular biology 24, 3077-3088.
Mohrmann, L., and Verrijzer, C.P. (2005). Composition and functional specificity of SWI2/SNF2 class chromatin remodeling complexes. Biochimica et biophysica acta 1681, 59-73.
Moller, A., Avila, F.W., Erickson, J.W., and Jackle, H. (2005). Drosophila BAP60 is an essential component of the Brahma complex, required for gene activation and repression. J Mol Biol 352, 329-337.
Mortazavi, A., Williams, B.A., McCue, K., Schaeffer, L., and Wold, B. (2008). Mapping and quantifying mammalian transcriptomes by RNA-Seq. Nature methods 5, 621-628.

Moses, K., Ellis, M.C., and Rubin, G.M. (1989). The glass gene encodes a zinc-finger protein required by Drosophila photoreceptor cells. Nature 340, 531-536.
Nakae, J., Kido, Y., and Accili, D. (2001). Distinct and overlapping functions of insulin and IGF-I receptors. Endocr Rev 22, 818-835.
Nakano, Y., Guerrero, I., Hidalgo, A., Taylor, A., Whittle, J.R., and Ingham, P.W. (1989). A protein with several possible membrane-spanning domains encoded by the Drosophila segment polarity gene patched. Nature 341, 508-513.
Nakato, H., Futch, T.A., and Selleck, S.B. (1995). The division abnormally delayed (dally) gene: a putative integral membrane proteoglycan required for cell division patterning during postembryonic development of the nervous system in Drosophila. Development 121, 3687-3702.
Nellen, D., Burke, R., Struhl, G., and Basler, K. (1996). Direct and long-range action of a DPP morphogen gradient. Cell 85, 357-368.
Nestler, E.J., and Hyman, S.E. (2002) Neuropsychopharmacology: The Fifth Generation of Progress, Chapter 17: Regulation of gene expression. Philadelphia, Pennsylvania: Lippincott, Williams, & Wilkins.
Neto, M., Aguilar-Hidalgo, D., and Casares, F. (2016). Increased avidity for Dpp/BMP2 maintains the proliferation of progenitors-like cells in the Drosophila eye. Developmental biology 418, 98-107.
Neto-Silva, R.M., de Beco, S., and Johnston, L.A. (2010). Evidence for a growth-stabilizing regulatory feedback mechanism between Myc and Yorkie, the Drosophila homolog of Yap. Developmental cell 19, 507-520.
Neumann, C.J., and Cohen, S.M. (1996). Distinct mitogenic and cell fate specification functions of wingless in different regions of the wing. Development 122, 1781-1789.
Nienhaus, U., Aegerter-Wilmsen, T., and Aegerter, C.M. (2009). Determination of mechanical stress distribution in Drosophila wing discs using photoelasticity. Mechanisms of development 126, 942-949.
Nijhout, H.F., Riddiford, L.M., Mirth, C., Shingleton, A.W., Suzuki, Y., and Callier, V. (2014). The developmental control of size in insects. Wiley Interdiscip Rev Dev Biol 3, 113-134.
Nogales-Cadenas, R., Carmona-Saez, P., Vazquez, M., Vicente, C., Yang, X., Tirado, F., Carazo, J.M., and Pascual-Montano, A. (2009). GeneCodis: interpreting gene lists through enrichment analysis and integration of diverse biological information. Nucleic acids research 37, W317-322.
Nolo, R., Morrison, C.M., Tao, C., Zhang, X., and Halder, G. (2006). The bantam microRNA is a target of the hippo tumor-suppressor pathway. Current biology : CB 16, 1895-1904.
Nusslein-Volhard, C., and Wieschaus, E. (1980). Mutations affecting segment number and polarity in Drosophila. Nature 287, 795-801.
O'Kane, C.J., and Gehring, W.J. (1987). Detection in situ of genomic regulatory elements in Drosophila. Proceedings of the National Academy of Sciences of the United States of America 84, 9123-9127.
Obier, N., and Bonifer, C. (2016). Chromatin programming by developmentally regulated transcription factors: lessons from the study of haematopoietic stem cell specification and differentiation. FEBS Lett.

Oh, H., and Irvine, K.D. (2008). In vivo regulation of Yorkie phosphorylation and localization. Development 135, 1081-1088.
Oh, H., and Irvine, K.D. (2011). Cooperative regulation of growth by Yorkie and Mad through bantam. Developmental cell 20, 109-122.
Oh, H., Slattery, M., Ma, L., Crofts, A., White, K.P., Mann, R.S., and Irvine, K.D. (2013). Genome-wide association of Yorkie with chromatin and chromatin-remodeling complexes. Cell reports 3, 309-318.
Okumura, K., Saito, M., Isogai, E., Aoto, Y., Hachiya, T., Sakakibara, Y., Katsuragi, Y., Hirose, S., Kominami, R., Goitsuka, R., et al. (2014). Meis1 regulates epidermal stem cells and is required for skin tumorigenesis. PloS one 9, e102111.
Orlovsky, K., Kalinkovich, A., Rozovskaia, T., Shezen, E., Itkin, T., Alder, H., Ozer, H.G., Carramusa, L., Avigdor, A., Volinia, S., et al. (2011). Down-regulation of homeobox genes MEIS1 and HOXA in MLL-rearranged acute leukemia impairs engraftment and reduces proliferation. Proceedings of the National Academy of Sciences of the United States of America 108, 7956-7961.
Ostrin, E.J., Li, Y., Hoffman, K., Liu, J., Wang, K., Zhang, L., Mardon, G., and Chen, R. (2006). Genome-wide identification of direct targets of the Drosophila retinal determination protein Eyeless. Genome research 16, 466-476.
Padgett, R.W., St Johnston, R.D., and Gelbart, W.M. (1987). A transcript from a Drosophila pattern gene predicts a protein homologous to the transforming growth factor-beta family. Nature 325, 81-84.
Pai, C.Y., Kuo, T.S., Jaw, T.J., Kurant, E., Chen, C.T., Bessarab, D.A., Salzberg, A., and Sun, Y.H. (1998). The Homothorax homeoprotein activates the nuclear localization of another homeoprotein, extradenticle, and suppresses eye development in Drosophila. Genes & development 12, 435-446.
Pan, D. (2007). Hippo signaling in organ size control. Genes & development 21, 886-897.
Pan, Y., Heemskerk, I., Ibar, C., Shraiman, B.I., and Irvine, K.D. (2016). Differential growth triggers mechanical feedback that elevates Hippo signaling. Proceedings of the National Academy of Sciences of the United States of America.
Papayannopoulos, V., Tomlinson, A., Panin, V.M., Rauskolb, C., and Irvine, K.D. (1998). Dorsal-ventral signaling in the Drosophila eye. Science 281, 2031-2034.
Pavlidis, P., and Noble, W.S. (2001). Analysis of strain and regional variation in gene expression in mouse brain. Genome biology 2, RESEARCH0042.
Peng, H.W., Slattery, M., and Mann, R.S. (2009). Transcription factor choice in the Hippo signaling pathway: homothorax and yorkie regulation of the microRNA bantam in the progenitor domain of the Drosophila eye imaginal disc. Genes & development 23, 2307-2319.
Peter, I.S., and Davidson, E.H. (2011). A gene regulatory network controlling the embryonic specification of endoderm. Nature 474, 635-639.
Pfaffl, M.W., Horgan, G.W., and Dempfle, L. (2002). Relative expression software tool (REST) for group-wise comparison and statistical analysis of relative expression results in real-time PCR. Nucleic acids research 30, e36.
Phelps, C.B., and Brand, A.H. (1998). Ectopic gene expression in Drosophila using GAL4 system. Methods 14, 367-379.

Pichaud, F., and Casares, F. (2000). homothorax and iroquois-C genes are required for the establishment of territories within the developing eye disc. Mechanisms of development 96, 15-25.
Pignoni, F., Hu, B., Zavitz, K.H., Xiao, J., Garrity, P.A., and Zipursky, S.L. (1997). The eye-specification proteins So and Eya form a complex and regulate multiple steps in Drosophila eye development. Cell 91, 881-891.
Potier, D., Atak, Z.K., Sanchez, M.N., Herrmann, C., and Aerts, S. (2012). Using cisTargetX to predict transcriptional targets and networks in Drosophila. Methods Mol Biol 786, 291-314.
Potier, D., Davie, K., Hulselmans, G., Naval Sanchez, M., Haagen, L., Huynh-Thu, V.A., Koldere, D., Celik, A., Geurts, P., Christiaens, V., et al. (2014). Mapping gene regulatory networks in Drosophila eye development by large-scale transcriptome perturbations and motif inference. Cell reports 9, 2290-2303.
Quiring, R., Walldorf, U., Kloter, U., and Gehring, W.J. (1994). Homology of the eyeless gene of Drosophila to the Small eye gene in mice and Aniridia in humans. Science 265, 785-789.
Ready, D.F., Hanson, T.E., and Benzer, S. (1976). Development of the Drosophila retina, a neurocrystalline lattice. Developmental biology 53, 217-240.
Reddy, B.V., and Irvine, K.D. (2011). Regulation of Drosophila glial cell proliferation by Merlin-Hippo signaling. Development 138, 5201-5212.
Reddy, B.V., Rauskolb, C., and Irvine, K.D. (2010). Influence of fat-hippo and notch signaling on the proliferation and differentiation of Drosophila optic neuroepithelia. Development 137, 2397-2408.
Reisman, D., Glaros, S., and Thompson, E.A. (2009). The SWI/SNF complex and cancer. Oncogene 28, 1653-1668.
Reiter, L.T., Potocki, L., Chien, S., Gribskov, M., and Bier, E. (2001). A systematic analysis of human disease-associated gene sequences in Drosophila melanogaster. Genome research 11, 1114-1125.
Ren, F., Zhang, L., and Jiang, J. (2010). Hippo signaling regulates Yorkie nuclear localization and activity through 14-3-3 dependent and independent mechanisms. Developmental biology 337, 303-312.
Restrepo, S., Zartman, J.J., and Basler, K. (2014). Coordination of patterning and growth by the morphogen DPP. Current biology : CB 24, R245-255.
Revet, I., Huizenga, G., Chan, A., Koster, J., Volckmann, R., van Sluis, P., Ora, I., Versteeg, R., and Geerts, D. (2008). The MSX1 homeobox transcription factor is a downstream target of PHOX2B and activates the Delta-Notch pathway in neuroblastoma. Experimental cell research 314, 707-719.
Rewitz, K.F., Yamanaka, N., Gilbert, L.I., and O'Connor, M.B. (2009). The insect neuropeptide PTTH activates receptor tyrosine kinase torso to initiate metamorphosis. Science 326, 1403-1405.
Reynolds-Kenneally, J., and Mlodzik, M. (2005). Notch signaling controls proliferation through cell-autonomous and non-autonomous mechanisms in the Drosophila eye. Developmental biology 285, 38-48.
Riddiford, L.M. (1993). Hormone receptors and the regulation of insect metamorphosis. Receptor 3, 203-209.

Rieckhof, G.E., Casares, F., Ryoo, H.D., Abu-Shaar, M., and Mann, R.S. (1997). Nuclear translocation of extradenticle requires homothorax, which encodes an extradenticle-related homeodomain protein. Cell 91, 171-183.
Rogers, E.M., Brennan, C.A., Mortimer, N.T., Cook, S., Morris, A.R., and Moses, K. (2005). Pointed regulates an eye-specific transcriptional enhancer in the Drosophila hedgehog gene, which is required for the movement of the morphogenetic furrow. Development 132, 4833-4843.
Salzer, C.L., and Kumar, J.P. (2010). Identification of retinal transformation hot spots in developing Drosophila epithelia. PloS one 5, e8510.
Sansores-Garcia, L., Bossuyt, W., Wada, K., Yonemura, S., Tao, C., Sasaki, H., and Halder, G. (2011). Modulating F-actin organization induces organ growth by affecting the Hippo pathway. The EMBO journal 30, 2325-2335.
Sarbassov, D.D., Guertin, D.A., Ali, S.M., and Sabatini, D.M. (2005). Phosphorylation and regulation of Akt/PKB by the rictor-mTOR complex. Science 307, 1098-1101.
Schoonjans, K., Dubuquoy, L., Mebis, J., Fayard, E., Wendling, O., Haby, C., Geboes, K., and Auwerx, J. (2005). Liver receptor homolog 1 contributes to intestinal tumor formation through effects on cell cycle and inflammation. Proceedings of the National Academy of Sciences of the United States of America 102, 2058-2062.
Schubiger, M., and Truman, J.W. (2000). The RXR ortholog USP suppresses early metamorphic processes in Drosophila in the absence of ecdysteroids. Development 127, 1151-1159.
Schuettengruber, B., Chourrout, D., Vervoort, M., Leblanc, B., and Cavalli, G. (2007). Genome regulation by polycomb and trithorax proteins. Cell 128, 735-745.
Segraves, W.A., and Hogness, D.S. (1990). The E75 ecdysone-inducible gene responsible for the 75B early puff in Drosophila encodes two new members of the steroid receptor superfamily. Genes & development 4, 204-219.
Shain, A.H., and Pollack, J.R. (2013). The spectrum of SWI/SNF mutations, ubiquitous in human cancers. PloS one 8, e55119.
Shraiman, B.I. (2005). Mechanical feedback as a possible regulator of tissue growth. Proceedings of the National Academy of Sciences of the United States of America 102, 3318-3323.
Singh, A., Kango-Singh, M., and Sun, Y.H. (2002). Eye suppression, a novel function of teashirt, requires Wingless signaling. Development 129, 4271-4280.
Slaidina, M., Delanoue, R., Gronke, S., Partridge, L., and Leopold, P. (2009). A Drosophila insulin-like peptide promotes growth during nonfeeding states. Developmental cell 17, 874-884.
Slattery, M., Voutev, R., Ma, L., Negre, N., White, K.P., and Mann, R.S. (2013). Divergent transcriptional regulatory logic at the intersection of tissue growth and developmental patterning. PLoS genetics 9, e1003753.
Slifer, E.H. (1942) A mutant stock of Drosophila with extra sex-combs. Journal of experimental zoology 90, 31-40.
Somogyi, K., and Rorth, P. (2004). Evidence for tension-based regulation of Drosophila MAL and SRF during invasive cell migration. Developmental cell 7, 85-93.
Song, Z., Guan, B., Bergman, A., Nicholson, D.W., Thornberry, N.A., Peterson, E.P., and Steller, H. (2000). Biochemical and genetic interactions between Drosophila caspases and the proapoptotic genes rpr, hid, and grim. Molecular and cellular biology 20, 2907-2914.

Spencer, F.A., Hoffmann, F.M., and Gelbart, W.M. (1982). Decapentaplegic: a gene complex affecting morphogenesis in Drosophila melanogaster. Cell 28, 451-461.
Staehling-Hampton, K., Jackson, P.D., Clark, M.J., Brand, A.H., and Hoffmann, F.M. (1994). Specificity of bone morphogenetic protein-related factors: cell fate and gene expression changes in Drosophila embryos induced by decapentaplegic but not 60A. Cell growth & differentiation : the molecular biology journal of the American Association for Cancer Research 5, 585-593.
Staley, B.K., and Irvine, K.D. (2010). Warts and Yorkie mediate intestinal regeneration by influencing stem cell proliferation. Current biology : CB 20, 1580-1587.
Stathopoulos, A., and Iber, D. (2013). Studies of morphogens: keep calm and carry on. Development 140, 4119-4124.
Struhl, G., and Basler, K. (1993). Organizing activity of wingless protein in Drosophila. Cell 72, 527-540.
Subramanian, A., Tamayo, P., Mootha, V.K., Mukherjee, S., Ebert, B.L., Gillette, M.A., Paulovich, A., Pomeroy, S.L., Golub, T.R., Lander, E.S., et al. (2005). Gene set enrichment analysis: a knowledge-based approach for interpreting genome-wide expression profiles. Proceedings of the National Academy of Sciences of the United States of America 102, 15545-15550.
Talbot, W.S., Swyryd, E.A., and Hogness, D.S. (1993). Drosophila tissues with different metamorphic responses to ecdysone express different ecdysone receptor isoforms. Cell 73, 1323-1337.
Tanaka-Matakatsu, M., and Du, W. (2008). Direct control of the proneural gene atonal by retinal determination factors during Drosophila eye development. Developmental biology 313, 787-801.
Tang, C.Y., and Sun, Y.H. (2002). Use of mini-white as a reporter gene to screen for GAL4 insertions with spatially restricted expression pattern in the developing eye in drosophila. Genesis 34, 39-45.
Tani, M., Shindo-Okada, N., Hashimoto, Y., Shiroishi, T., Takenoshita, S., Nagamachi, Y., and Yokota, J. (1997). Isolation of a novel Sry-related gene that is expressed in high-metastatic K-1735 murine melanoma cells. Genomics 39, 30-37.
Tanimoto, H., Itoh, S., ten Dijke, P., and Tabata, T. (2000). Hedgehog creates a gradient of DPP activity in Drosophila wing imaginal discs. Molecular cell 5, 59-71.
Tapon, N., Harvey, K.F., Bell, D.W., Wahrer, D.C., Schiripo, T.A., Haber, D., and Hariharan, I.K. (2002). salvador Promotes both cell cycle exit and apoptosis in Drosophila and is mutated in human cancer cell lines. Cell 110, 467-478.
Thiruchelvam, P.T., Lai, C.F., Hua, H., Thomas, R.S., Hurtado, A., Hudson, W., Bayly, A.R., Kyle, F.J., Periyasamy, M., Photiou, A., et al. (2011). The liver receptor homolog-1 regulates estrogen receptor expression in breast cancer cells. Breast cancer research and treatment 127, 385-396.
Thomas, B.J., Gunning, D.A., Cho, J., and Zipursky, L. (1994). Cell cycle progression in the developing Drosophila eye: roughex encodes a novel protein required for the establishment of G1. Cell 77, 1003-1014.
Thomas, B.J., Zavitz, K.H., Dong, X., Lane, M.E., Weigmann, K., Finley, R.L., Jr., Brent, R., Lehner, C.F., and Zipursky, S.L. (1997). roughex down-regulates G2 cyclins in G1. Genes & development 11, 1289-1298.

Thomas, H.E., Stunnenberg, H.G., and Stewart, A.F. (1993). Heterodimerization of the Drosophila ecdysone receptor with retinoid X receptor and ultraspiracle. Nature 362, 471-475.
Thompson, B.J., and Cohen, S.M. (2006). The Hippo pathway regulates the bantam microRNA to control cell proliferation and apoptosis in Drosophila. Cell 126, 767-774.
Thummel, C.S. (2001). Molecular mechanisms of developmental timing in C. elegans and Drosophila. Developmental cell 1, 453-465.
Thummel, C.S., Burtis, K.C., and Hogness, D.S. (1990). Spatial and temporal patterns of E74 transcription during Drosophila development. Cell 61, 101-111.
Tomoeda, M., Yuki, M., Kubo, C., Yoshizawa, H., Kitamura, M., Nagata, S., Nishizawa, Y., and Tomita, Y. (2011). Role of Meis1 in mitochondrial gene transcription of pancreatic cancer cells. Biochem Biophys Res Commun 410, 798-802.
Towers, M., Mahood, R., Yin, Y., and Tickle, C. (2008). Integration of growth and specification in chick wing digit-patterning. Nature 452, 882-886.
Trapnell, C., Pachter, L., and Salzberg, S.L. (2009). TopHat: discovering splice junctions with RNA-Seq. Bioinformatics 25, 1105-1111.
Treisman, J.E., Luk, A., Rubin, G.M., and Heberlein, U. (1997). eyelid antagonizes wingless signaling during Drosophila development and has homology to the Bright family of DNA-binding proteins. Genes & development 11, 1949-1962.
Tsai, Y.C., and Sun, Y.H. (2004). Long-range effect of upd, a ligand for Jak/STAT pathway, on cell cycle in Drosophila eye development. Genesis 39, 141-153.
Tsuneizumi, K., Nakayama, T., Kamoshida, Y., Kornberg, T.B., Christian, J.L., and Tabata, T. (1997). Daughters against dpp modulates dpp organizing activity in Drosophila wing development. Nature 389, 627-631.
Turkel, N., Sahota, V.K., Bolden, J.E., Goulding, K.R., Doggett, K., Willoughby, L.F., Blanco, E., Martin-Blanco, E., Corominas, M., Ellul, J., et al. (2013). The BTB-zinc finger transcription factor abrupt acts as an epithelial oncogene in Drosophila melanogaster through maintaining a progenitor-like cell state. PLoS genetics 9, e1003627.
Twitty, V.C., and Schwind, J.L. (1931). The growth of eyes and limbs transplanted heteroplastically between two species of Amblystoma. Journal of Experimental Zoology 59, 61-86.
Usary, J., Llaca, V., Karaca, G., Presswala, S., Karaca, M., He, X., Langerod, A., Karesen, R., Oh, D.S., Dressler, L.G., et al. (2004). Mutation of GATA3 in human breast tumors. Oncogene 23, 7669-7678.
van der Lugt, N.M., Domen, J., Linders, K., van Roon, M., Robanus-Maandag, E., te Riele, H., van der Valk, M., Deschamps, J., Sofroniew, M., van Lohuizen, M., and Berns, A. (1994). Posterior transformation, neurological abnormalities, and severe hematopoietic defects in mice with a targeted deletion of the bmi-1 proto-oncogene. Genes & Development 8, 757-769.
Venkatesan, K., McManus, H.R., Mello, C.C., Smith, T.F., and Hansen, U. (2003). Functional conservation between members of an ancient duplicated transcription factor family, LSF/Grainyhead. Nucleic acids research 31, 4304-4316.
Vrailas, A.D., and Moses, K. (2006). Smoothened, thickveins and the genetic control of cell cycle and cell fate in the developing Drosophila eye. Mechanisms of development 123, 151-165.

Walkiewicz, M.A., and Stern, M. (2009). Increased insulin/insulin growth factor signaling advances the onset of metamorphosis in Drosophila. PloS one 4, e5072.
Wang, G.G., Pasillas, M.P., and Kamps, M.P. (2006). Persistent transactivation by meis1 replaces hox function in myeloid leukemogenesis models: evidence for co-occupancy of meis1-pbx and hox-pbx complexes on promoters of leukemia-associated genes. Molecular and cellular biology 26, 3902-3916.
Wang, Y., Dakubo, G.D., Thurig, S., Mazerolle, C.J., and Wallace, V.A. (2005). Retinal ganglion cell-derived sonic hedgehog locally controls proliferation and the timing of RGC development in the embryonic mouse retina. Development 132, 5103-5113.
Wartlick, O., Julicher, F., and Gonzalez-Gaitan, M. (2014). Growth control by a moving morphogen gradient during Drosophila eye development. Development 141, 1884-1893.
Wartlick, O., Mumcu, P., Kicheva, A., Bittig, T., Seum, C., Julicher, F., and Gonzalez-Gaitan, M. (2011) Dynamics of Dpp signaling and proliferation control. Science 331, 1154–1159.
Wei, X., Shimizu, T., and Lai, Z.C. (2007). Mob as tumor suppressor is activated by Hippo kinase for growth inhibition in Drosophila. The EMBO journal 26, 1772-1781.
Weirauch, M.T., Yang, A., Albu, M., Cote, A.G., Montenegro-Montero, A., Drewe, P., Najafabadi, H.S., Lambert, S.A., Mann, I., Cook, K., et al. (2014). Determination and inference of eukaryotic transcription factor sequence specificity. Cell 158, 1431-1443.
Welboren, W.J., van Driel, M.A., Janssen-Megens, E.M., van Heeringen, S.J., Sweep, F.C., Span, P.N., and Stunnenberg, H.G. (2009). ChIP-Seq of ERalpha and RNA polymerase II defines genes differentially responding to ligands. The EMBO journal 28, 1418-1428.
Wiersdorff, V., Lecuit, T., Cohen, S.M., and Mlodzik, M. (1996). Mad acts downstream of Dpp receptors, revealing a differential requirement for dpp signaling in initiation and propagation of morphogenesis in the Drosophila eye. Development 122, 2153-2162.
White, K., Ma, L., and Slattery, M. (2008) http://www.ncbi.nlm.nih.gov/geo/query/acc.cgi?acc=GSE50338.
Wong, P., Iwasaki, M., Somervaille, T.C., So, C.W., and Cleary, M.L. (2007). Meis1 is an essential and rate-limiting regulator of MLL leukemia stem cell potential. Genes & development 21, 2762-2774.
Woodard, C.T., Baehrecke, E.H., and Thummel, C.S. (1994). A molecular mechanism for the stage specificity of the Drosophila prepupal genetic response to ecdysone. Cell 79, 607-615.
Wu, S., Huang, J., Dong, J., and Pan, D. (2003). hippo encodes a Ste-20 family protein kinase that restricts cell proliferation and promotes apoptosis in conjunction with salvador and warts. Cell 114, 445-456.
Wu, S., Liu, Y., Zheng, Y., Dong, J., and Pan, D. (2008). The TEAD/TEF family protein Scalloped mediates transcriptional output of the Hippo growth-regulatory pathway. Developmental cell 14, 388-398.
Xin, S., Weng, L., Xu, J., and Du, W. (2002). The role of RBF in developmentally regulated cell proliferation in the eye disc and in Cyclin D/Cdk4 induced cellular growth. Development 129, 1345-1356.
Xiong, G., and Xu, R. (2014). RORalpha binds to E2F1 to inhibit cell proliferation and regulate mammary gland branching morphogenesis. Molecular and cellular biology 34, 3066-3075.

Yagi, R., Mayer, F., and Basler, K. (2010). Refined LexA transactivators and their use in combination with the Drosophila Gal4 system. Proceedings of the National Academy of Sciences of the United States of America 107, 16166-16171.
Yan, D., and Lin, X. (2009). Shaping morphogen gradients by proteoglycans. Cold Spring Harb Perspect Biol 1, a002493.
Yang, C.H., Simon, M.A., and McNeill, H. (1999). mirror controls planar polarity and equator formation through repression of fringe expression and through control of cell affinities. Development 126, 5857-5866.
Yang, M., Nelson, D., Funakoshi, Y., and Padgett, R.W. (2004). Genome-wide microarray analysis of TGFbeta signaling in the Drosophila brain. BMC developmental biology 4, 14.
Yao, J.G., Weasner, B.M., Wang, L.H., Jang, C.C., Weasner, B., Tang, C.Y., Salzer, C.L., Chen, C.H., Hay, B., Sun, Y.H., et al. (2008). Differential requirements for the Pax6(5a) genes eyegone and twin of eyegone during eye development in Drosophila. Developmental biology 315, 535-551.
Yao, T.P., Forman, B.M., Jiang, Z., Cherbas, L., Chen, J.D., McKeown, M., Cherbas, P., and Evans, R.M. (1993). Functional ecdysone receptor is the product of EcR and Ultraspiracle genes. Nature 366, 476-479.
Yao, T.P., Segraves, W.A., Oro, A.E., McKeown, M., and Evans, R.M. (1992). Drosophila ultraspiracle modulates ecdysone receptor function via heterodimer formation. Cell 71, 63-72.
Yenush, L., Fernandez, R., Myers, M.G., Jr., Grammer, T.C., Sun, X.J., Blenis, J., Pierce, J.H., Schlessinger, J., and White, M.F. (1996). The Drosophila insulin receptor activates multiple signaling pathways but requires insulin receptor substrate proteins for DNA synthesis. Molecular and cellular biology 16, 2509-2517.
Zaret, K.S., and Mango, S.E. (2016). Pioneer transcription factors, chromatin dynamics, and cell fate control. Curr Opin Genet Dev 37, 76-81.
Zecca, M., Basler, K., and Struhl, G. (1995). Sequential organizing activities of engrailed, hedgehog and decapentaplegic in the Drosophila wing. Development 121, 2265-2278.
Zeisig, B.B., Milne, T., Garcia-Cuellar, M.P., Schreiner, S., Martin, M.E., Fuchs, U., Borkhardt, A., Chanda, S.K., Walker, J., Soden, R., et al. (2004). Hoxa9 and Meis1 are key targets for MLL-ENL-mediated cellular immortalization. Molecular and cellular biology 24, 617-628.
Zeng, X., Lin, X., and Hou, S.X. (2013). The Osa-containing SWI/SNF chromatin-remodeling complex regulates stem cell commitment in the adult Drosophila intestine. Development 140, 3532-3540.
Zhang, L., Ren, F., Zhang, Q., Chen, Y., Wang, B., and Jiang, J. (2008). The TEAD/TEF family of transcription factor Scalloped mediates Hippo signaling in organ size control. Developmental cell 14, 377-387.
Zhang, Y., Chen, X., Qiao, M., Zhang, B.Q., Wang, N., Zhang, Z., Liao, Z., Zeng, L., Deng, Y., Deng, F., et al. (2014). Bone morphogenetic protein 2 inhibits the proliferation and growth of human colorectal cancer cells. Oncology reports 32, 1013-1020.
Zhao, B., Wei, X., Li, W., Udan, R.S., Yang, Q., Kim, J., Xie, J., Ikenoue, T., Yu, J., Li, L., et al. (2007). Inactivation of YAP oncoprotein by the Hippo pathway is involved in cell contact inhibition and tissue growth control. Genes & development 21, 2747-2761.
Zhao, Y., Tong, C., and Jiang, J. (2007). Hedgehog regulates smoothened activity by inducing a conformational switch. Nature 450, 252-258.

Zhu, J., Nakamura, E., Nguyen, M.T., Bao, X., Akiyama, H., and Mackem, S. (2008). Uncoupling Sonic hedgehog control of pattern and expansion of the developing limb bud. Developmental cell 14, 624-632.
Zhu, L.J., Christensen, R.G., Kazemian, M., Hull, C.J., Enuameh, M.S., Basciotta, M.D., Brasefield, J.A., Zhu, C., Asriyan, Y., Lapointe, D.S., et al. (2011). FlyFactorSurvey: a database of Drosophila transcription factor binding specificities determined using the bacterial one-hybrid system. Nucleic acids research 39, D111-117.
Zhu, Y., Li, D., Wang, Y., Pei, C., Liu, S., Zhang, L., Yuan, Z., and Zhang, P. (2015). Brahma regulates the Hippo pathway activity through forming complex with Yki-Sd and regulating the transcription of Crumbs. Cell Signal 27, 606-613.

7

ANNEXES

Annex A

Additional Methods for Results Part I

GEO accession numbers

GSE65252 contains two series: RNA-seq (GSE65250) and FAIRE-seq (GSE65251) data.

RNA-seq and FAIRE-seq reads preprocessing

Reads containing residuals of adapters sequences were discarded (FastX clipper version 0.013 with option -M15). Quality control assessment on the reads was performed using the software FastQC (version 0.9), checking for PHRED quality >20 and different primer contaminations. Reads passing the filtering were mapped against D.melanogaster FlyBase genome release 5 with TOPHAT v2.0 (default parameters) (Trapnell et al. 2009).

RNA-seq differential expression analysis

To compute gene expression levels, we performed HTSeq (option str=no) (Anders and Huber 2010). Only uniquely mapped reads falling in exons based on the species-specific FlyBase annotation D.melanogaster 5.45 were considered. Differential expression analysis between HTH+TSH (two replicates) and wt (one replicate) was performed using the Bioconductor package DESeq version 1.10.1 (R version 2.15). For contrasts with no replicates available, such as HTH vs wt and TSH vs wt, we utilized the parameters method='blind', shareMode='fit-only' to estimate dispersions across samples. Genes presenting low expression across samples, namely, less than 1RPKM in more than 3 samples were not considered for differential expression analysis.

FAIRE-seq analysis

Pre-processed reads were mapped against D. melanogaster reference genome release 5 using Bowtie2 (Langmead and Salzberg 2012). Open chromatin levels were computed as the number of reads mapping within Drosophila pre-defined regions (Herrmann et al. 2012) using HTSeq (Anders and Huber 2010), parameter (str=no). The set of pre-computed D. melanogaster regulatory regions are defined by a thorough genome-cut which considers sequence conservation, exon skipping and insulator class I binding (Herrmann et al. 2012).

FAIRE-seq differential expression

Regions with less than 10RPKM in three samples were excluded for differential open chromatin analysis. Differential open-chromatin was performed as described in the RNA-seq differential expression analysis section. The main difference is that instead of genes we use as features regulatory regions ids. The contrast performed defined differential open regions between HTH+TSH (two replicates) and wild-type (two replicates).

Association between genes and open-chromatin regions

Peaks were assigned to a gene if they were falling 5-kb upstream of its TSS or either limited by the nearest upstream gene, in its intronic regions or in 5-kb downstream of a gene limited by the closest downstream gene.

Association between open-chromatin and HTH binding

ChIP for HTH, Sd, Yki transcription factors in late third instar (wandering) larvae has been performed by (Slattery et al. 2013). ChIP locations were translated to regulatory region ids if they were presenting an overlap fraction of 40% (overlapSelect f=0.4). To assess whether differential open regions between

HTH+TSH and wt were associated with HTH binding we compared the log2 fold change of FAIRE regions in bound and not bound HTH regions. Wilcoxon singed-ranked test was performed to assess its statistically significance.

Co-expression using Pavlidis Template Matching

Pavlidis Template Matching (Pavlidis and Noble, 2001) was used to find genes showing a similar or opposite expression profile of EcR (by starting from EcR expression template, p-value<0.01).

Gene Ontology term enrichment

Gene ontology enrichment for different gene sets was computed using the tool FlyMine (Lyne et al. 2007), whereas ranked lists of genes were inputted in GOrilla (Eden et al. 2009).

Motif enrichment discovery

Motif discovery was performed with the tools i-cistarget (Herrmann et al. 2012) and its Cytoscape version, iRegulon (PMID: 25058159). In brief it searches for overrepresented motifs in a set of co-expressed genes and across evolution. The following parameters were used: motif collection version 2 (6385 position weight matrices) and region mapping equal to 5Kb upstream and full transcript. i-cistarget is a hybrid method that allows finding both known and new motifs. The new motifs are also represented as position weight matrices and are a collection of thousands of "candidate" motifs found by other studies for which the binding factor is yet unknown. This collection includes highly conserved words, but also enriched words discovered in chromatin binding data from ENCODE and modENCODE. In addition, i-cistarget allows finding motifs from orthologous factors, including yeast, mouse, and human, thereby greatly expanding the number of possible TFs. Finally, the number of Drosophila transcription factors

without a possible motif is very limited, thanks to recent high-throughput approaches (Zhu et al., 2011), and the porting of binding motifs from other species (Weirauch et al., 2014).

Gene Set Enrichment Analysis

We used the tool Gene Set Enrichment Analysis (GSEA) (Subramanian et al. 2005) to assess if open-chromatin regions are enriched in either up or down-regulated genes at the gene expression level (hth+tsh versus control). Therefore, we inputted two sets of genes with significantly up or down open-chromatin regions and a ranked list of genes based on the –log p value from the differential expression analysis.

mRNA expression and DNA copy number analysis in human cancer datasets

Affymetrix datasets of 103 different studies on human cancer types were retrieved from the public Gene Expression Omnibus (GEO) dataset on the National Center for Biotechnology Information (NCBI) website (Barrett et al., 2009). We selected studies using the Affymetrix Gene Chip Human Genome U133 Plus 2.0 array plafform (Affymetrix, Santa Clara, CA) since this was the most common platform in the database. Also, probes for the TSHZ1-3 genes are not present on earlier versions of the Affymetrix platform. Annotations and clinical data for the datasets analyzed are available through their GEO ID's (Table C.3) from http://www.ncbi.nlm.nih.gov/geo/query/. CEL data were downloaded, and analyzed as described (Revet et al., 2008). Briefly, gene transcript levels were determined from data image files using GeneChip operating software (MAS5.0 and GCOS1.0, from Affymetrix). Samples were scaled setting the average intensity of the middle 96 % of all probe-set signals to a fixed value of 100 for every sample in the dataset, to allow transcript level comparison between micro-arrays and between studies. The TranscriptView genomic analysis and visualization tool (http://bioinfo.amc.uva.nl/human-genetics/transcriptview/) was used to select

probe-sets. These had to show unique mapping in an anti-sense position within a 3' exon and/or the 3' UTR of the gene. When multiple correct probe-sets were available for a gene, the probe-set with the highest average expression and amount of present calls for that dataset was considered as the best probe-set. These were: 204069_at (MEIS1), 210174_at (NR5A2), 226682_at (RORA), 242385_at (RORB), 223283_s_at (TSHZ1), 235815_at (TSHZ2), 223392_s_at (TSHZ3), and 224894_at (YAP1). When results of the best probe-set conflicted with other probe-sets for that gene, the data are not presented. Analyses on the GEO datasets Analyses were performed using R2; a genomics analysis and visualization platform developed in the Department of Oncogenomics at the Academic Medical Center, Amsterdam, The Netherlands (http://r2.amc.nl).

Statistical analysis of mRNA expression and DNA copy number in human cancer

Correlations between MEIS1 and other gene mRNA expression in R2 were calculated using a Pearson test on 2log-transformed expression values (with the significance of a correlation determined by t = R/sqrt((1-r^2)/(n-2)), where R is the correlation value and n is the number of samples, and distribution measure is approximately as t with n-2 degrees of freedom). The Statistical Package for the Social Sciences software package for Windows (Version 13.0) was used for all statistical analyses. All numerical results are expressed as the mean value ± S.E.M., and $P < 0.05$ was considered significant in all tests. For all tests on Oncomine (http://www.oncomine.org), the website standard settings were used, and values are shown as 2log-median centered, with statistically significant differences determined by t-testing.

Annex B

Additional Methods for Results Part II

Quantification of spatial profiles and calculation of effective parameters

Spatial profiles of pMad are assumed to follow Dpp dynamics, thus they can be fitted from the solution of a reaction-diffusion equation (see below for details) that leads to an exponential function in the form:

$$C(x) = C_0 e^{-\frac{x}{\lambda}},$$

with C_0 the concentration of C at position $x = 0$, which is a function of the kinetic parameters in the form:

$$C_0 = \frac{v}{\sqrt{Dk}},$$

and λ the decay length of the concentration profile, defined as:

$$\lambda = \sqrt{\frac{D}{k}}.$$

With the expressions for C_0 and λ we can compare ratios of two profiles α and β such that

$$\frac{k^\alpha}{k^\beta} = \frac{C_0^\beta \lambda^\beta}{C_0^\alpha \lambda^\alpha},$$

and

$$\frac{D^\alpha}{D^\beta} = \frac{C_0^\beta \lambda^\alpha}{C_0^\alpha \lambda^\beta}.$$

Real fit is done using function NonLinearModelFit in software Mathematica. Experimental error is included as data weight in the fit process.

To fit pMad profiles, we have placed position $x = 0$ at the anterior boundary of the morphogenetic furrow. This position is estimated from comparison between *dpp3.0Z* and pMad profiles (Figure A.1). We then fitted the concentration profile in

the anterior compartment. For convention, we use negative sign to positions to the left side of $x = 0$, thus the fit function must read $C(x) = C_0 e^{\frac{x}{\lambda}}$, with negative x.

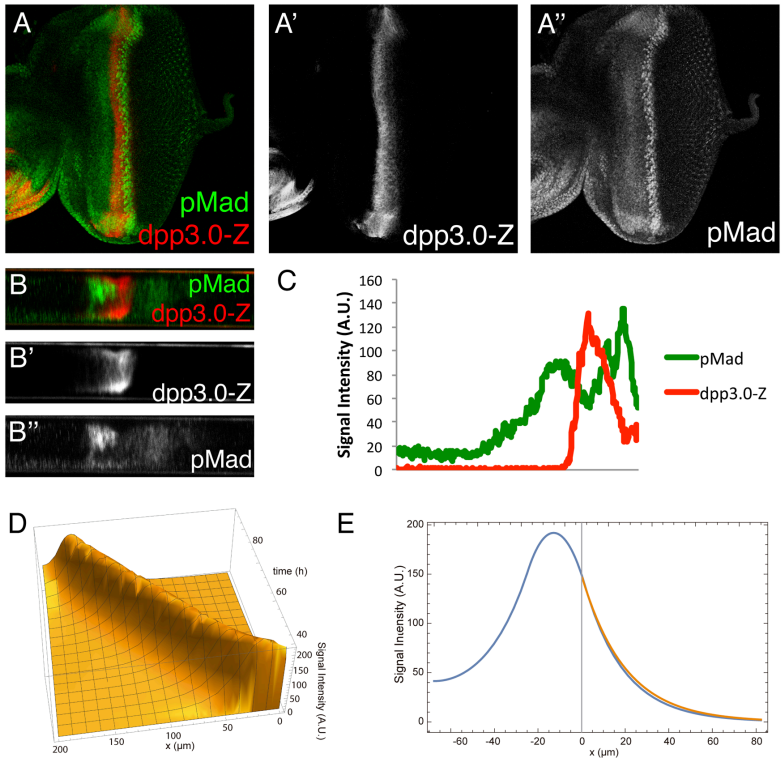

Figure A.1. Comparison of Dpp profile shapes with moving and non-moving source. *dpp3.0-lacZ* third instar discs (A-A") and a corresponding vertical cross-section (B-B'') stained with anti-pSmad3 and anti-β-galactosidase. (C) Signal intensity histogram of pSmad3 (green) and dpp3.0-lacZ (red). Signal intensity, expressed in arbitrary units, is measured from the MF. (D) Simulation of equation 2 (in annex B) for a Dpp moving source. (E) Comparison of Dpp profile shape, at a specific time point, when considering a moving source (as in D, in blue) and a assuming a quasi-steady-state regime for Dpp dynamics and a point source (equation 3 in annex B, in orange). The shape of the Dpp profile in a quasi-steady-state regime is quantitatively very similar to the moving source case, thus justifying its use for fitting purposes. Parameters: D=0.1 um^2/s, k=0.000252/s, v=3.1 m/s.

We observed that some of the profiles showed a peak of signaling in a position anterior to the furrow, due to a peak of proliferation (Wartlick et al., 2014). This proliferation peak modifies pMad profiles shapes. For fitting purposes, as a direct readout of Dpp should peak at the furrow (position $x = 0$ in the case of fitting just anterior compartment), we assumed pMad concentration is depleted right anterior to the furrow with respect to the Dpp profile, thus we eliminated from the fits this depletion zone (marked in grey in Figures R2.12 and R2.13).

Derivation of fit equation for pMad spatial profiles

In the eye disc, Dpp is secreted from a moving stripe of cells in the dorsoventral direction called the morphogenetic furrow. The furrow sweeps from the posterior to the anterior edge of the disc at approximately constant speed υ (Wartlick et al., 2014). Dpp spreads effectively to the anterior-posterior direction forming a concentration graded pattern. Describing such pattern is not trivial due to tissue growth and furrow movement.

An equation describing Dpp patterning in the eye disc reads:

$$D_t C(x,t) = \nabla D \nabla C(x,t) - (k + g(x,y,t))C + \upsilon_c \theta\,(\upsilon t + w - x, x - \upsilon t)\,, \qquad (1)$$

with D and k effective kinetic parameters, diffusion coefficient and degradation rate, respectively. C refers to Dpp concentration, θ is the Heaviside theta function, w is the source width and g is the growth function. As commented above, Dpp effectively spreads in one dimension, however, growth anisotropy may affect patterning. For this reason, we introduce growth $g = gx + gy$ as a two spatial dimension function. This function can also be expressed in one dimension dependent on an anisotropy parameter $\varepsilon = gy/gx$ (experimentally measured in (Wartlick et al., 2014)), thus $g = g_x(1 + \varepsilon)$. D_t is the convected derivative, defined as $D_t = \partial_t + u \cdot \nabla$, where u is the velocity field, such that $\nabla u = g$.

Typically, equation (1) can be simplified by taking certain limits, such as constant D and k, smaller g than k and negligible convection. These limits have been taken to describe Dpp dynamics in the wing disc (Wartlick et al., 2014). In the eye disc, dynamics of Dpp have not been quantified so far but growth. Average growth rate in the eye disc is $g = 1.6 \cdot 10^{-5}\ s^{-1}$. If we asume similar Dpp dynamics to the wing disc's, with constant D and k, this growth rate is one order of magnitude smaller than the reported effective degradation rate $k = 2.5 \cdot 10^{-4}\ s^{-1}$ (Kicheva et al, 2007), thus supporting the small growth limit. The application of these limits to equation (1) leads to the following equation:

$$\partial_t C = D\,\partial^2_x C - k\,C + \upsilon_c \theta\,(\upsilon t + w - x, x - \upsilon t)\,. \qquad (2)$$

The reported furrow velocity υ = 3.1 μm/s may not be negligible against the

relaxation time of Dpp (in 45 minutes, assuming similar dynamics as in the wing disc, the furrow moves 2.3 μm, in an anterior compartment that varies size between approximately 100 μm and 60μm). We performed a control study of the spatial profile of *C* from equation (2) to determine whether such profile can be effectively considered in a quasi-steady-state dynamical regime. This means that Dpp pattern relaxes faster than the furrow movement perturbs its shape.

Though equation (2) can be analytically solved for time and space, its solution is too complex to learn from it. Thus, we decided to numerically solve equation (2) for kinetic parameters taken from Dpp effective dynamics in the wing disc (Kicheva et al, 2007), see Figure A.1D. We applied reflecting boundary conditions at the borders of the disc to numerically solve equation (2), and compare its solution with a simplified version, equation (3), solved for the same parameters in free space (production rate ν in equation (3) is adjusted to fit C_0 in the simulation of equation (2)), see Figure A.1E.

$$\partial_t C = D\, \partial^2_x C - k\, C + \nu\, \delta\,(x)\,. \qquad (3)$$

In equation (3), furrow velocity is considered sufficiently small so that dynamics of *C* can be studied in a quasi-steady-state regime, and furrow width is assumed to be punctual.

From the comparison between solutions for equations (2) and (3), we observe that both spatial profiles are quantitatively similar such that the measure error in data is larger than their difference, see Figure A.1E. Thus we choose solution for equation (3) in steady-state as model equation to fit experimental data. As the assumptions taken for equation (3) allow us to consider *C* profile in quasi-steady-state, the solution to equation (3) leads to the fit equation:

$$C(x) = C_0 e^{-\frac{x}{\lambda}}\,, \qquad (4)$$

with C_0 the concentration of *C* at position $x = 0$, which is a function of the kinetic parameters in the form:

$$C_0 = \frac{\nu}{\sqrt{D\,k}} \qquad (5)$$

and λ the characteristic length scale (decay length) of the concentration profile, defined as:

$$\lambda = \sqrt{\frac{D}{k}}. \tag{6}$$

Quantification of results from real fits

With the expressions for C_0 and λ, equations (5) and (6), we can compare ratios of two profiles α and β such that

$$\frac{k^{\alpha}}{k^{\beta}} = \frac{C_0^{\beta}\lambda^{\beta}}{C_0^{\alpha}\lambda^{\alpha}}, \tag{7}$$

and

$$\frac{D^{\alpha}}{D^{\beta}} = \frac{C_0^{\beta}\lambda^{\alpha}}{C_0^{\alpha}\lambda^{\beta}}. \tag{8}$$

Table A.1 shows ratios of pMad signal intensity at position x=0 (C_0), characteristic length scale of the gradient (λ), effective degradation (k) and effective diffusion coefficient (D), between experiment genotype (α) and its respective control (β).

Table A.1. Ratios of pMad signal intensity at position x=0 (C_0), characteristic length scale of the gradient (λ), effective degradation (k) and effective diffusion coefficient (D), between experiment genotype (α) and its respective control (β). For α = (Hth+Tsh, Hth+Tsh+SflRNAi, SflRNAi) → β = GFP.

	Hth+Tsh	Hth+Tsh+SflRNAi	SflRNAi
C_0^{α}/C_0^{β}	1.02 ± 0.02	1.15 ± 0.03	1.10 ± 0.02
$\lambda^{\alpha}/\lambda^{\beta}$	1.32 ± 0.09	0.75 ± 0.07	0.44 ± 0.03
k^{α}/k^{β}	0.74 ± 0.06	1.17 ± 0.11	2.05 ± 0.19
D^{α}/D^{β}	1.30 ± 0.10	0.65 ± 0.06	0.40 ± 0.04

Annex C

Additional Methods for Results Part III

Sample preparation for RNA-sequencing

Eye-antennal discs from either *tip-tioA4-GAL4; UAS-GFP (tio>GFP)* or *tip-tioA4-GAL4; UAS-GFP*:hth *(tio>GFP:hth)* third instar larvae (L3) were used to obtain GFP positive cells characterizing the progenitor and precursor/early differentiation states. To maximize GAL4-driven expression, larvae were grown at 25°C for 48h and then transferred at 29°C. 50-60 eye-antennal discs were dissected. GFP-expressing cells were FAC-sorted. Cells with a minimum of 95% of purity were selected. After sorting, about 3000 GFP positive cells were used to synthesize the cDNA directly from the cells, following the protocol described in the "SOLID System Library Preparation" for a whole transcriptome of a single-cell, the main advantage of which is the possibility to get enough material to characterize a whole transcriptome when the amount of tissue or cells is limiting. Double-strand cDNAs were run in a 2% agarose gel in order to select fragments between 500–3000-bp, to then be used as the DNA template for the Illumina library construction. The quality of this resulting double-strand cDNAs was assessed using the Nanodrop ND-100 7500 spectrophotometer (Nanodrop).

Expression profiling and analysis of differential expression

cDNA samples were sequenced using a Illumina Genome Analyser IIx (Baylor College, Houston, TX, USA) used a single-end chemistry and 75pb reads. The quality of the RNA-seq data was evaluated using the FastQC program and after, reads were mapped against the *Drosophila melanogaster* genome (dm3, BDGP5 release 5). The alignment of the reads against the reference genome was done using Bowtie. Mapped read counts for each gene were normalized for RNA length and for the total read number in the lane according to reads per kilobase of exon model per million mapped reads (RPKM), which facilitates comparison of

transcript levels between samples (Mortazavi et al., 2008). Fold change was calculated as the log2 (*tio>GPP/tio> GFP:hth*).

Funtional annotation (GO analysis)

GO analysis was performed using the GeneCoDis2.0 web server (Carmona-Saez et al., 2007; Nogales-Cadenas et al., 2009) using default settings. Analysis was done all GO categories “Biological Process,” “Molecular Function,” and “Cellular Component”. One of the advantages of this program is that find the relationships among annotations based on co-occurrence patterns that can extend the understanding of the biological events associated to a given experimental system (http://genecodis.dacya.ucm.es/).

Real-Time qPCR validation

cDNA from the same GFP positives cells that RNA-seq experiments was used to perform a technical validation by qPCR. A total of 19 genes with different relative abundances in the RNA-seq experiment were selected. Actin was used as a housekeeping gene to normalize the PCR reactions. Prior to the analysis of gene expression, the efficiency of PCR reactions was calculated for all the target genes and several control genes. cDNA from both experimental conditions were pooled, and a dilution series made (1:2, 1:10 , and 1:100) then each gene was amplified in triplicate. Efficiencies were calculated as indicated by (Pfaffl et al., 2002).

Primers were designed using Primer3 (http://frodo.wi.mit.edu/) setting a Tm of 60-62°C, an amplicon size between 100 to 190 bp and a GC content of 50-80%. Details of primer sequences and amplicon sizes are shown in the table below.

Table A.2. qPRC primers and amplicon sizes.

Name	Forward Sequence(5'-3')	Reverse Sequence (5'-3')	Amplicon size
ACT5C-M	CTGTTCCAGCCCTCGTTCTT	ACAGCACGGTGTTGGCATAC	118
Ama	AACCAACTCTCCGGATTCGT	GACCCGGATCAACCTCTTGT	104
CG10200	CGTCTTCACCTACGCCTCAC	CATCAAAGGACACACCACCA	113
CG12237	AACGATCGTGTGGTCGAAGT	CTCGAACCAGGAGCAGTCAC	112
CG32207	CGACGGTTATCAGGACAAGG	CATTCTGCAGTCAGCAGTGG	111
CG32212	CTGGCGTACACTGGTCCTCT	GTTGTTCCTGGCGATACTGG	114
CG4210	TCTTCTTGGAGGTTGCATCG	ACGGCACCAAGACTTTCGTA	109
CG42500	AGCATTGACTGGGTGTCCTC	CTCTGTGTGCCTTCCTCCTC	101
CG4468	GGAACAAGCACGGTAAAGGA	TCATCCTTCTCGTCCACCTT	118
CG4914	AGCGCCAGGATCTATTTGTG	AACGGGAACTTCAACCTCCT	107
CG6040	TGTCGATCTCCAGCAAACTG	CTGTTGATCTTGCGGACTGA	103
CG6610	GTTCCCGCATCCACATTATC	ACTCCGTTACGTCGTCCAAG	102
CG7016	TTTGCAGTCTCCTCGTCCTC	TGGCATTGATCAGTCCATTG	109
CG8498	GCTTGTACAAACAGGCCACTG	CGGTATTGCTCATTCCCTTG	117
egr	ACTCCATTCCTGCAGTGCTT	GATCCTCTCGTTTCGTTCCA	105
hth-1	GTCTGTTCGTCGGAATCGTT	CTTGCACCATCAGTGAGTCG	112
mRpS16	CCAATCGGCCTTTTTATCAC	CCACCAGTCGTTCGTTGTAA	120
Obp99a	CGTGGAGAACATCCACCAAC	ATTGGATCCCTGCTCGTTCT	106
scrt	CCTCCAGTGAAAGGAAGTGC	GGCTTGTCGTCCAAGGAATA	100
TektinC	GTGGACGAAACGAAGGACAC	TCAACTCGTCCACCAGGAAT	100
Bap60	CACTGCGAGCCAACAGGAGATC	GGATTGCCAGCTACATCGGTCATC	189

PCR reactions were performed in a total volume of 20 µL using a Power SYBR Green PCR Master Mix (Applied Biosystems), 10ng of cDNA template and 0.25 µM of each primers. Triplicate reactions were amplified using an “ABI PRISM 7000 Sequence Detection system” thermocycler (Applied Biosynthesis). Cycle parameters were 95°C for 10 min and then 40 cycles at 95°C for 15 sec and 60°C for 1 min. Each run was completed with a melting curve analysis to confirm the specificity of amplification and lack of primer dimmers. Results were analyzed using REST-MCS software (Pfaffl et al., 2002), where our reference or control condition was tio>GFP. This program use a mathematical model based on randomization test, which avoid any assumption about the data.

Annex D

Supplementary Figures

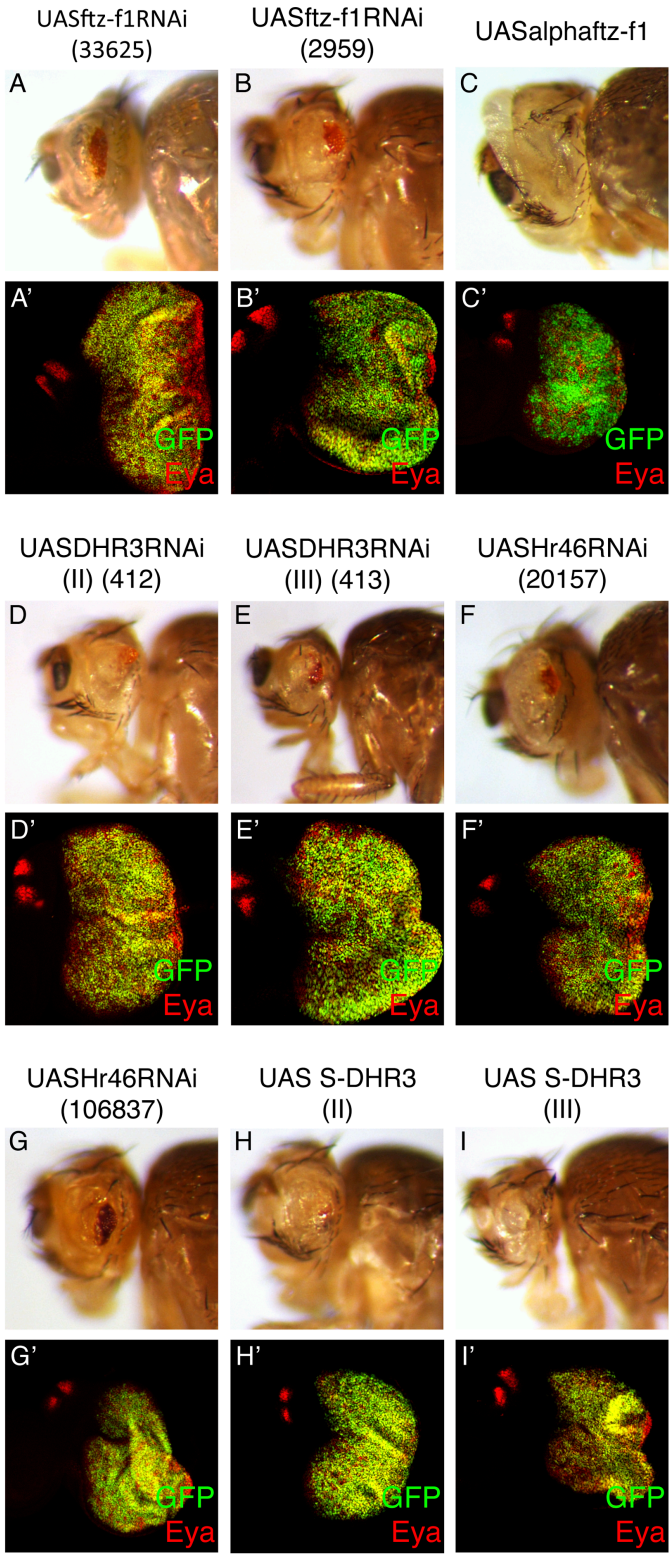

Figure A.2. Functional interaction of hth+tsh with *Hr46* and *ftz-f1.* Adult (upper panels) and eye disc (lower panels) phenotypes of *optix>hth+tsh+X,* with X being the UAS constructs indicated. Representative cases are shown.

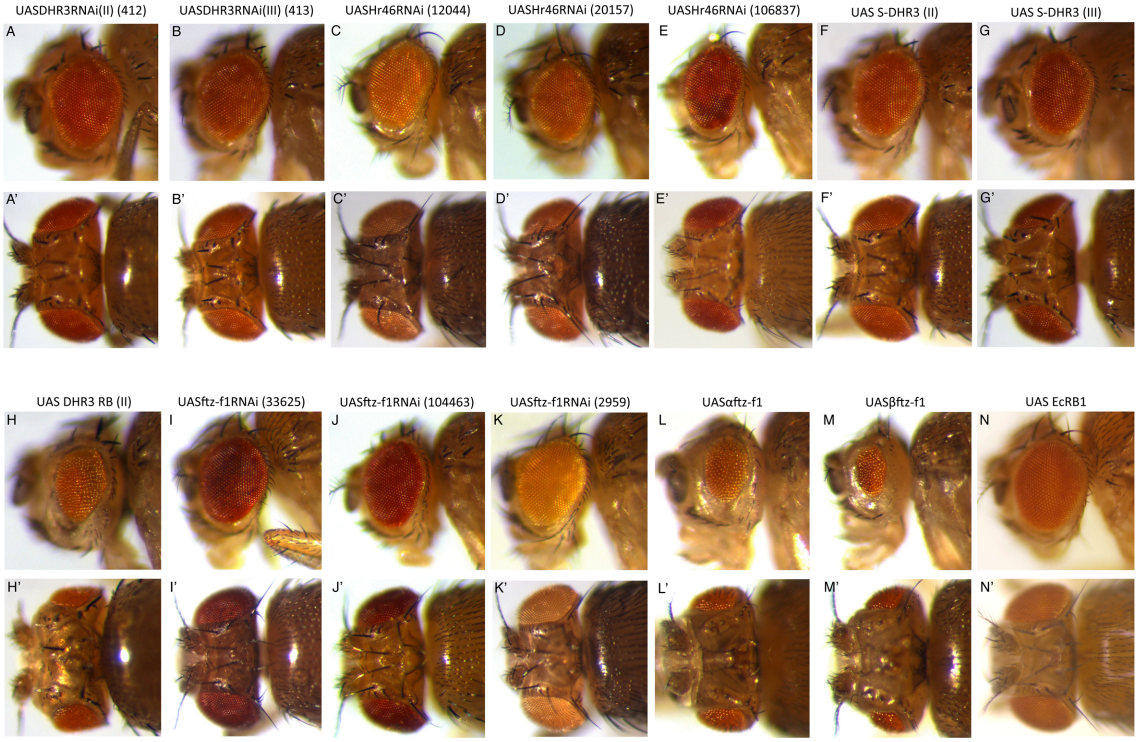

Figure A.3. Adult phenotypes produce by the overexpression or RNAi-mediated attenuation of *Hr46/DHR3, ftz-f1* and *EcR.* Lateral and dorsal views of adult heads expressing different UAS lines using the optix2.3-GAL4 line: *DHR3RNAi* #412(A,A'), *DHR3RNAi* #413 (B,B'), *Hr46RNAi* #12044 (C,C'), *Hr46RNAi* #20157 (D,D'), *Hr46RNAi* #106837 (E,E'), *S-DHR3*(II) (F,F'), *S-DHR3*(III) (G,G'), *DHR3 RB* (H,H'), *ftz-f1RNAi* #33625 (I,I'), *ftz-f1RNAi* #104463 (J,J'), *ftz-f1RNAi* #2959 (K,K'), *αftz-f1* (L,L'), *βftz-f1* (M,M'), EcRB1 (N,N').

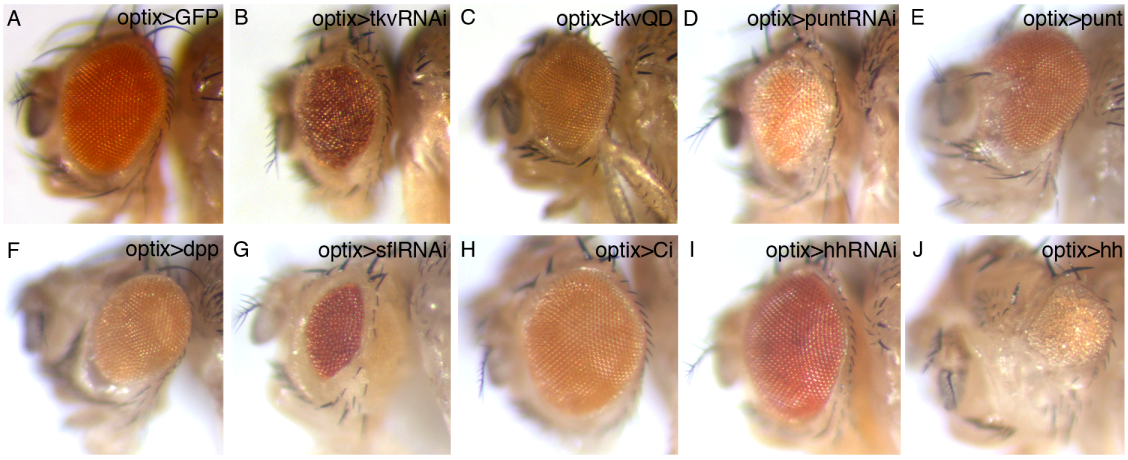

Figure A.4. Adult phenotypes produce by the overexpression or RNAi-mediated attenuation of *tkv, punt, dpp, sfl, ci* and *hh.* Lateral views of adult heads expressing different UAS lines using the optix2.3-GAL4 line: *GFP*(A), *tkvRNAi* (B), *tkvQD* (C), *puntRNAi* (D), *punt* (E), *dpp* (F), *sflRNAi* (G), *Ci* (H), *hhRNAi* (I) and *hh* (J).

Annex E

Publication

Developmental Biology 418 (2016) 98–107

Contents lists available at ScienceDirect

Developmental Biology

journal homepage: www.elsevier.com/locate/developmentalbiology

Increased avidity for Dpp/BMP2 maintains the proliferation of progenitors-like cells in the *Drosophila* eye

Marta Neto [a,b], Daniel Aguilar-Hidalgo [c], Fernando Casares [a,*]

[a] CABD (Andalusian Centre for Developmental Biology), CSIC-UPO-JA, Campus Universidad Pablo de Olavide, 41013 Seville, Spain
[b] IBMC/Instituto de Investigação e Inovação em Saúde (i3S), Universidade do Porto, Rua Alfredo Allen, 208, 4200-135 Porto, Portugal
[c] Department of Biological Physics, Max Planck Institute for the Physics of Complex Systems, 01187 Dresden, Germany

ARTICLE INFO

Article history:
Received 21 July 2016
Received in revised form
26 July 2016
Accepted 4 August 2016
Available online 5 August 2016

Keywords:
Drosophila eye
Progenitors
Growth
Dpp/BMP2
Homothorax
Proteoglycans

ABSTRACT

During organ development, the progenitor state is transient, and depends on specific combinations of transcription factors and extracellular signals. Not surprisingly, abnormal maintenance of progenitor transcription factors may lead to tissue overgrowth, and the concurrence of signals from the local environment is often critical to trigger this overgrowth. Therefore, identifying specific combinations of transcription factors/signals promoting -or opposing- proliferation in progenitors is essential to understand normal development and disease. We have investigated this issue using the *Drosophila* eye as model. Transcription factors *hth* and *tsh* are transiently expressed in eye progenitors causing the expansion of the progenitor pool. However, if their co-expression is maintained experimentally, cell proliferation continues and differentiation is halted. Here we show that Hth+Tsh-induced tissue overgrowth requires the BMP2 Dpp and the abnormal hyperactivation of its pathway. Rather than using autocrine Dpp expression, Hth+Tsh cells increase their avidity for Dpp, produced locally, by upregulating extracellular matrix components. During normal development, Dpp represses *hth* and *tsh* ensuring that the progenitor state is transient. However, cells in which Hth+Tsh expression is forcibly maintained use Dpp to enhance their proliferation.

1. Introduction

Normal organ growth depends on the balance between proliferation and differentiation of progenitor cells. Proliferation is controlled by intrinsic determinants (mostly transcription factors and epigenetic regulators) and extrinsic signals, acting locally or at longer range. In overproliferative diseases, specific aberrant combinations of intrinsic factors and signals result in deregulated growth and organ failure. Therefore it is essential to define these specific combinations of intrinsic and extrinsic factors to understand both normal development and overproliferative diseases. The development of the fly eye has been used to understand the mechanisms that control progenitor proliferation. In this system, the pax6-expressing progenitors are maintained undifferentiated and proliferative as long as they express a combination of two transcription factors: *homothorax (hth),* a TALE-class homeodomain homologue to the MEIS1 proto-oncogene, and *teashirt (tsh)* a Zn-finger-type transcription factor also with homologues in mammals, the TSHZ gene family (Bessa et al., 2002). Importantly, when Hth+Tsh are forcibly maintained, progenitors remain proliferative and their differentiation into retinal cell types is blocked (Bessa et al., 2002; Lopes and Casares, 2010; Peng et al., 2009). Further studies showed that this proliferative effect was mediated, at least partly, through Hth and Tsh directly interacting with Yki, the YAP/TAZ homologue in the fly and transcriptional coactivator downstream of the Warts/Hippo (Wrts/Hpo) tumor-suppressor pathway (Huang et al., 2005; Peng et al., 2009). In eye progenitors, Hth and Tsh would serve as transcriptional partners of Yki, with Hth providing a DNA-binding domain to the Hth:Tsh:Yki complex. The Wrts/Hpo pathway is a major controller of organ growth in flies and vertebrates and its malfunction has been also implicated in cancer in mammals (Dong et al., 2007). Wrts/Hpo may be in charge of translating information on tissue tension through a system that integrates planar epithelial polarity and cytoskeletal organization (Fernandez et al., 2011; Rauskolb et al., 2014; Sansores-Garcia et al., 2011). In addition to this global control, growth regulation is linked to organ patterning by secreted signaling molecules. In the eye primordium, these signaling molecules (and their pathways) include wingless-Int (Wnt), Decapentaplegic (Dpp)/BMP2, Hedgehog (Hh) and JAK/STAT (reviewed in Amore and Casares (2010)). However, neither the Wnt, JAK/STAT nor the

* Corresponding author.
E-mail address: fcasfer@upo.es (F. Casares).

http://dx.doi.org/10.1016/j.ydbio.2016.08.004
0012-1606/

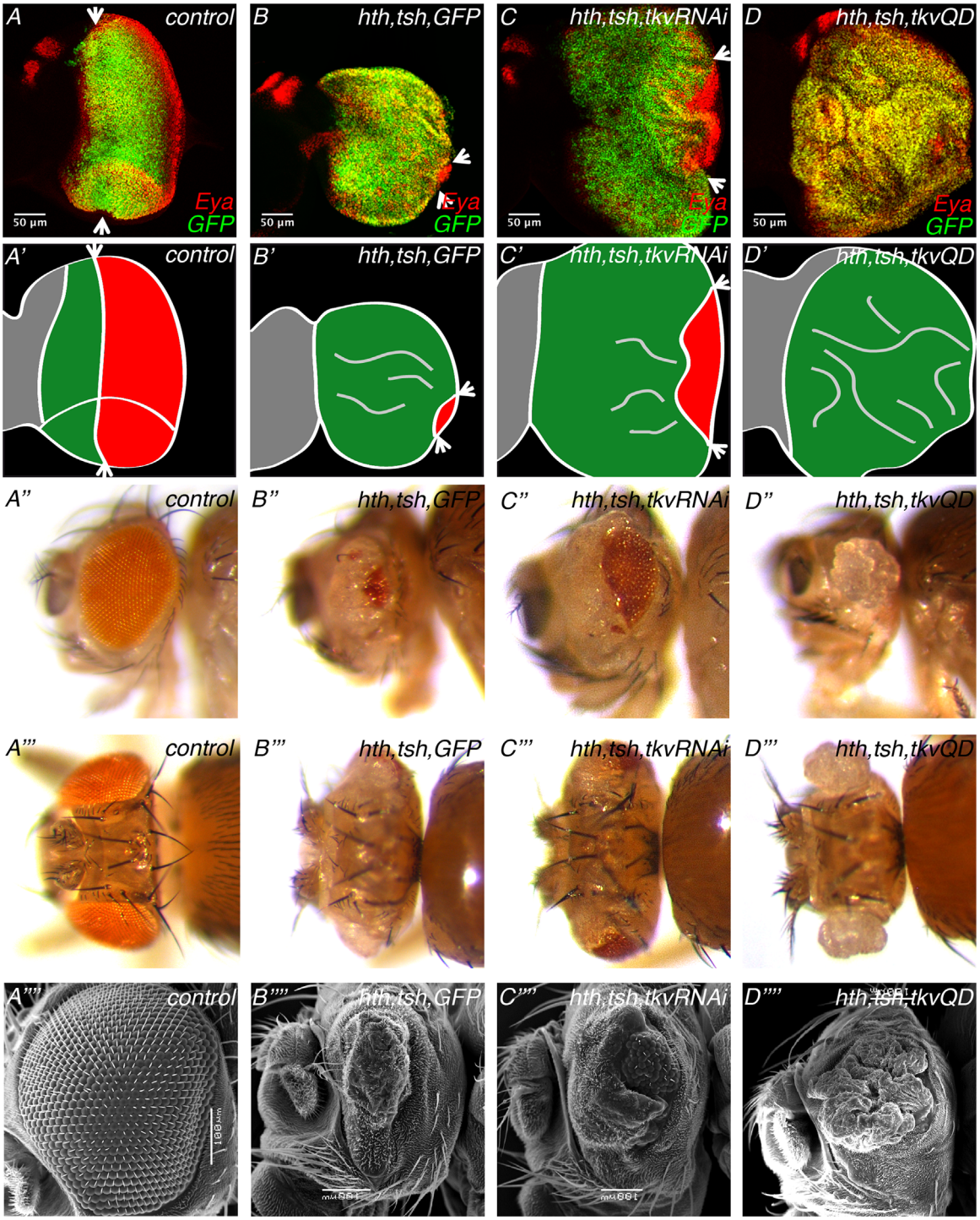

Fig. 1. Altered expression of Tkv levels, either through RNAi or overexpression, in an Hth+Tsh background results in clear functional genetic interactions. Control late third instar (L3) eye disc (A) or eye discs expressing *Hth+Tsh+GFP* (B), *Hth+Tsh+tkvRNAi* (C) or *Hth+Tsh+tkvQD* (D) in undifferentiated cells using the optix2.3-GAL4 line. All discs are stained with anti-Eya (red); GFP in (A) comes from an UAS-GFP line, in (B) from UAS-GFP + UAS-131-GFPhth lines and in (C,D) from UAS-131-GFPhth line. Discs are oriented with anterior to the left and dorsal up (this orientation will be maintained throughout). Morphogenetic furrow is marked with arrows. (A'–D') Schematic representation of the discs above –antenna in grey, progenitor cells in green and differentiated cells in red. Lateral (A"–D") and dorsal views (A"'–D"') of adult heads of the same genotypes as above. Horizontal bars represent the percentages of flies with different phenotypes: flies with normal eyes (represented in green), flies with a medium eye (represented in blue), flies with a small number of organized ommatidias (represented in orange) and flies with a total loss of retina (represented in red). (A""–D"") SEM images of lateral views of adult heads of the above genotypes. In imaginal discs, Hth+Tsh overexpression resulted in the maintenance of progenitors and in the almost complete disappearance of the morphogenetic furrow, which marks the wavefront of retinal differentiation. Adult flies showed small patches of differentiated retina surrounded by an indistinct cuticle. Reducing the levels of Tkv by RNAi in an Hth+Tsh background resulted in a partial rescue of the morphogenetic furrow movement that led to a partly rescued eye. The expression of an activated version of Tkv (TkvQD) together with Hth+Tsh gave rise to highly folded discs with no morphogenetic furrow and overgrowths of indistinct cuticle in the adult. Scale bars: 50 μm.

Notch pathway (another non-autonomous but locally acting signaling pathway) seemed to contribute to Hth+Tsh function (Peng et al., 2009). A potential role for Dpp has not been tested. The Dpp pathway has been shown to act antagonistically to *hth* and *tsh*, by repressing *hth* at long range and contributing to a shorter range repression of *tsh* as well (Bessa et al., 2002; Firth and Baker, 2009; Lopes and Casares, 2010). By doing so, Dpp signaling switches the progenitor cell state into the precursor state (also known as preproneural, (Greenwood and Struhl, 1999) thus allowing the initiation of retinal differentiation. The repressive action on *hth* and *tsh*, together with its potential antiproliferative role in the eye, makes Dpp, in principle, an unlikely candidate to synergize with Hth+Tsh. However, Dpp is necessary for the proliferation of other discs, such as the wing (reviewed in Restrepo et al. (2014)), and in the eye activation of the Dpp pathway can increase the proliferation of eye progenitors (Firth and Baker, 2009). In addition, while during normal development Dpp would ensure that high Dpp-signaling would be mutually exclusive with Hth+Tsh expression in progenitors, forcing Hth+Tsh maintenance might expose Hth+Tsh-expressing cells to high Dpp levels, which they would not encounter otherwise. Here we have tested specifically the effects that manipulating the Dpp/BMP2 pathway has on the maintenance of Hth+Tsh-driven progenitor state, as a model of progenitor-induced tissue overgrowth.

2. Results

2.1. Proliferation induced by combined expression of hth+tsh requires Dpp signaling

Drosophila eye progenitors co-express the transcription factors *hth* and *tsh* (Bessa et al., 2002). The forced maintenance of these progenitor transcription factors causes the overproliferation of the eye primordium (called "eye disc") and blocks differentiation, and as a consequence the final adult eye is reduced (Bessa et al., 2002; Peng et al., 2009). To investigate the functional requirements of extrinsic signaling pathways in promoting this overgrowth, we used a genotype in which *hth* and *tsh* expression was driven to the undifferentiated population of the eye disc using the *optix2/3-GAL4* driver ("optix-GAL4"; (Ostrin et al., 2006) and Fig. 1A; see Section 4). In *optix > hth+tsh* discs retinal differentiation was halted and accumulated hth+tsh-expressing cells, causing folds of the epithelium (Fig. 1B). This tissue overgrowth is the consequence of increased cell proliferation, as the mitotic index increased significantly by about 25% in *optix > hth+tsh* compared to control discs (Fig. S1). In *optix > hth+tsh* adults, the eye was dramatically reduced and sometimes absent, and replaced by sacs of undifferentiated cuticle (Fig. 1B"-B"" and Fig. S2).

During the development of the eye, the fast proliferation of progenitors has been attributed to Hth and Tsh acting jointly as transcriptional cofactors of Yki in a cell-autonomous manner (Peng et al., 2009). Indeed, Yki overexpression alone also results in eye primordium overgrowths (Huang et al., 2005). However, the phenotypic outcome of Hth+Tsh and Yki-overexpressing eyes was different (Fig. S2). This different phenotype indicated that, although the Hippo pathway contributed to the phenotype induced by Hth+Tsh, it could not fully explain it, and pointed to the existence of additional inputs. To test the possibility that Dpp synergizes with Hth+Tsh in driving tissue overgrowth, we altered the expression levels of components of the Dpp pathway in the Hth+Tsh-overexpressing background (Fig. 1 and Fig. S3). All genotypes contained an equal number of UAS-transgenes, to rule out that phenotypic differences could be due to different GAL4/UAS ratios. To evaluate the functional interactions, we analyzed changes in the size and extent of differentiation of late third eye discs, as well as the size and morphology of the eye disc derivatives in adult flies. In general, manipulations that increased Dpp-signaling activity exacerbated the phenotype, while genotypes that weakened the pathway partly suppressed the Hth+Tsh phenotypes in discs and adult heads (Fig. 1 and Fig. S3). The strongest interaction was observed with the type I Dpp receptor, *thick veins (tkv)*: RNAi-mediated silencing of *tkv* (*optix > hth+tsh+tkvRNAi)* caused a partial rescue of the differentiated area in the eye primordium (observed as Eya-expressing assembled ommatidia) and of the adult eye size (Fig. 1C). The opposite effect was observed when a constitutively active form of *tkv,* TkvQD, was coexpressed together with *hth* and *tsh*: *optix > hth+tsh+tkvQD* eye discs were more overgrown and folded than *optix > hth+tsh* discs, with fewer or no ommatidia, and the adults developed large sacs of undifferentiated cuticle without retinal tissue (Fig. 1D). The expression of *tkvQD* (*optix > tkvQD*) or *tkvRNAi* (*optix > tkvRNAi*) caused a small kink on the anterior eye or a mild eye reduction, respectively (Fig. S3), indicating that the interaction between hth+tsh and *tkv* was non-additive.

2.2. Hth+tsh-expressing cells increase the levels of Dpp signaling in a position-dependent manner

We next analyzed the activity status of the Dpp pathway in Hth+Tsh cells by using phosphorylated-Mad (pMad), the active form of the nuclear transducer of the pathway, as a readout (reviewed by Affolter and Basler (2007)). Of the three genotypes tested (*optix > hth, optix > tsh* and *optix > hth+tsh),* only coexpression of Hth and Tsh (*optix > hth+tsh)* resulted in an increased pMad signal, affecting both its amplitude and range (Fig. S4). We note that in *optix > hth+tsh* discs, in which differentiation does not progress, the increased pMad signal is seen close to the margin, which is the normal site of production of *dpp before* differentiation onset. In order to determine whether the Dpp signaling increase is cell autonomous within the Hth+Tsh cells, and to more clearly analyze the spatial dependence of signal activation, we induced randomly located Hth+Tsh-expressing clones to examine their effects on pMad levels, this time in both wing and eye primordia. While cell clones expressing either Hth or Tsh alone did not show activation of the pathway (Fig. 2A, B), some Hth+Tsh clones showed a strong, cell autonomous increase in pMad signal. This effect was strongly position-dependent: only clones located near an endogenous source of Dpp (the AP boundary in the wing and the posterior margin and the morphogenetic furrow in the eye) exhibited high pMad, while pMad levels within the clones decreased as the clones were located farther away from these sources (Fig. 2C, D and Fig. S5). These results suggested that the activation of the Dpp signaling pathway in Hth+Tsh cells was induced by Dpp produced at its normal sites of production within the primordia, rather than by a Hth+Tsh-induced Dpp. To test this point specifically, we analyzed the expression of a *dpp* transcriptional reporter (*dpp-LacZ,* containing the "dpp-disc" enhancer (Masucci and Hoffmann, 1993) in Hth+Tsh clones in which pMad levels were increased. In these clones, *dpp-Z* was not activated (Fig. S5), ruling out the autocrine production of Dpp as a cause for Dpp-pathway activation.

2.3. Hth+tsh cells accumulate Dpp

The fact that hth+tsh cells do not activate *dpp* transcription, together with the requirement of the Dpp receptor *tkv* to promote the growth of these cells, led us to address directly the possibility that Hth+Tsh cells were using Dpp produced from local sources. To do so, we combined two binary gene expression systems: Gal4/UAS (Brand and Perrimon, 1993) and lexA/lexO (Yagi et al., 2010). A GFP-tagged form of Dpp (lexO-eGFP::Dpp) was driven using a *dpp-*

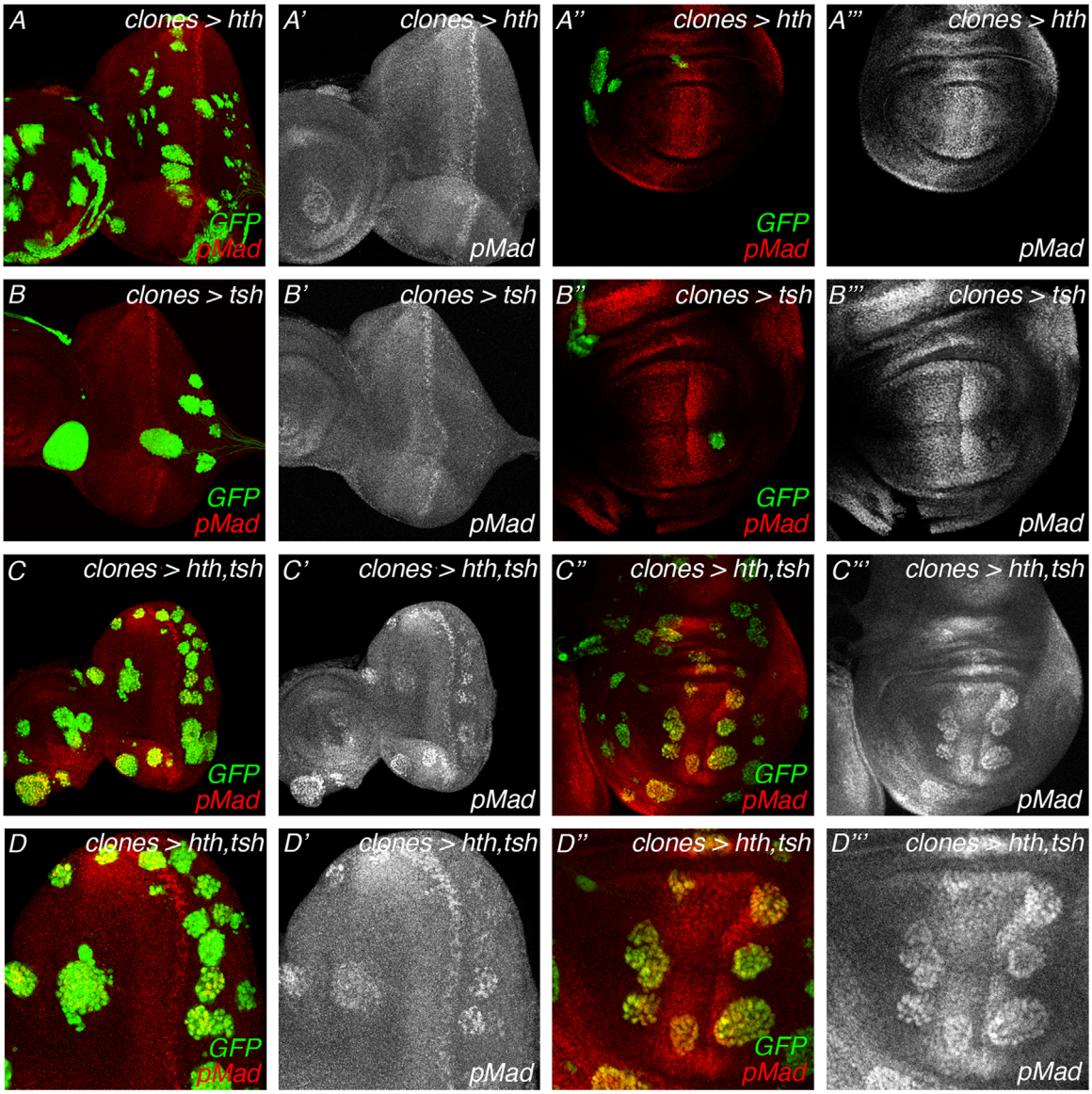

Fig. 2. Forced maintenance of Hth+Tsh in clones results in a cell-autonomous accumulation of pMad. Hth- (A-A'''), Tsh- (B-B''') or Hth+Tsh-expressing (C-D''') clones, marked by GFP, were induced in the eye and wing imaginal discs at 48–72 h after egg laying. Anti-pSmad3 was used to detect endogenous pMad. Clones expressing Hth or Tsh alone did not show changes in the levels of pMad when compared to the wild-type neighboring cells. Hth+Tsh clones showed a spatial dependent accumulation of pMad in a cell-autonomous manner. pMad levels ranged from high in clones nearby sources of Dpp (AP boundary in the wing disc and posterior margin, and morphogenetic furrow in the eye disc) to background in clones located far away from these sources.

lexA transgene. This driver was chosen for two reasons: first, it drove eGFP::Dpp in endogenous *dpp*-expression domains (i.e. in a stripe along the AP boundary in the wing primordium and around the posterior margin of the developing eye); and second, because the *dpp* enhancer ("dpp-disc" (Masucci et al., 1990; Muller and Basler, 2000)) used to drive lexA is not activated by Hth+Tsh (as shown in Fig. S5), effectively making the Dpp-producing system independent of Hth+Tsh. In this context, HA-tagged Hth+Tsh clones were randomly induced throughout the primordia. Indeed, Hth+Tsh-expressing clones retained high levels of eGFP::Dpp that were produced at *dpp*-expressing endogenous sites (Fig. 3). We propose that maintenance of Hth+Tsh expression makes cells capture distantly produced Dpp that would then lead to the strong cell-autonomous pathway activation we observe. We noted that the levels of eGFP::Dpp in Hth+Tsh cells were high, suggesting an increased avidity for the Dpp ligand in these cells. Accumulation of eGFP::Dpp was detected even in clones that lie in regions where the surrounding eGFP::Dpp signal is low (Fig. 3C'''). A similar phenomenon has been observed in clones expressing a membrane-tethered nanobody that traps eGFP (Harmansa et al., 2015).

2.4. Enhanced Dpp signaling and tissue growth is associated to increased levels of the proteoglycan components dally and Dlp and require normal proteoglycan biosynthesis

The Dpp receptor Tkv is known to limit Dpp mobility, likely sequestering it and elevated *tkv* levels enhance Dpp signaling (Haerry et al., 1998; Lecuit and Cohen, 1998; Tanimoto et al., 2000). Therefore, one way to explain the increased avidity for Dpp would be if Hth+Tsh cells upregulated *tkv* expression. To test if this was the case, we analyzed the expression of the *tkv* trascriptional reporter *tkv-Z* in Hth+Tsh-expressing clones in the eye primordium, but found that *tkv-Z* was often repressed in these clones (Fig. S6). This repression can be explained by the fact that *tkv* is itself a negative target of the Dpp pathway (Lecuit and Cohen, 1998; Tanimoto et al., 2000). Another way in which Hth+Tsh cells could

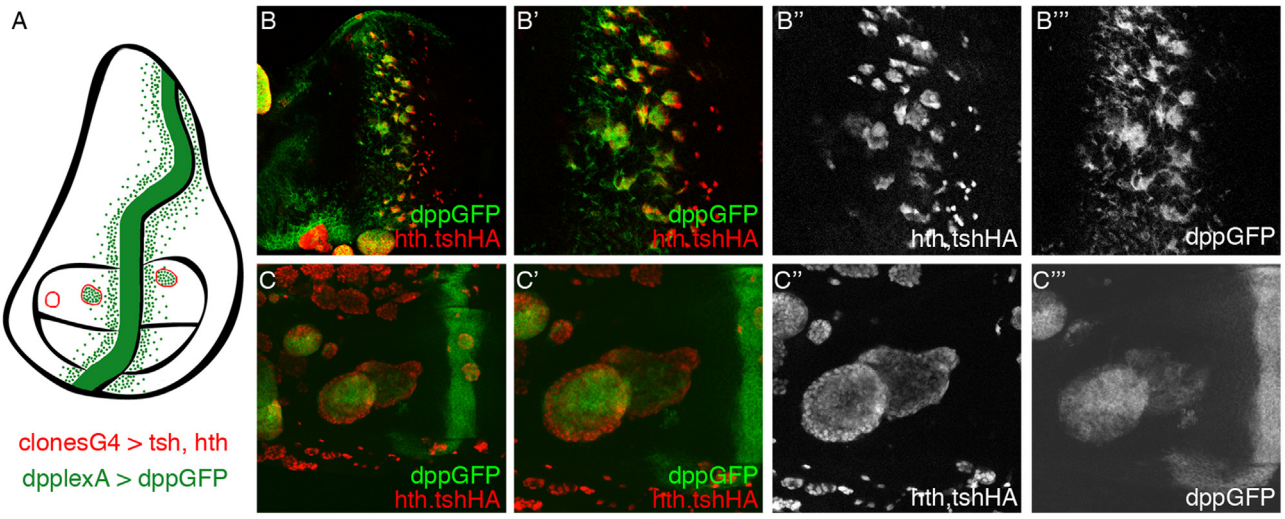

Fig. 3. Hth+Tsh cells located near an endogenous source of Dpp are able to accumulate the morphogen. (A) Schematic representation of a Hth+Tsh wing imaginal disc using a combination of two binary gene expression systems. Green represents eGFP::Dpp produced at the endogenous *dpp*-expressing stripe along the AP boundary under the control of the lexA/lexO system. Hth+Tsh clones are represented in red, induced by the Gal4/UAS system. (B–C''') Hth+Tsh-expressing clones, marked by anti-HA, were induced in the eye and wing imaginal discs at 72–96 h after egg laying using the Gal4/UAS system; simultaneously in the same discs eGFP::Dpp was expressed using the *dpp-lexA* driver through the lexA/lexO system. Hth+Tsh-expressing clones located near the Dpp source accumulated GFP-tagged Dpp.

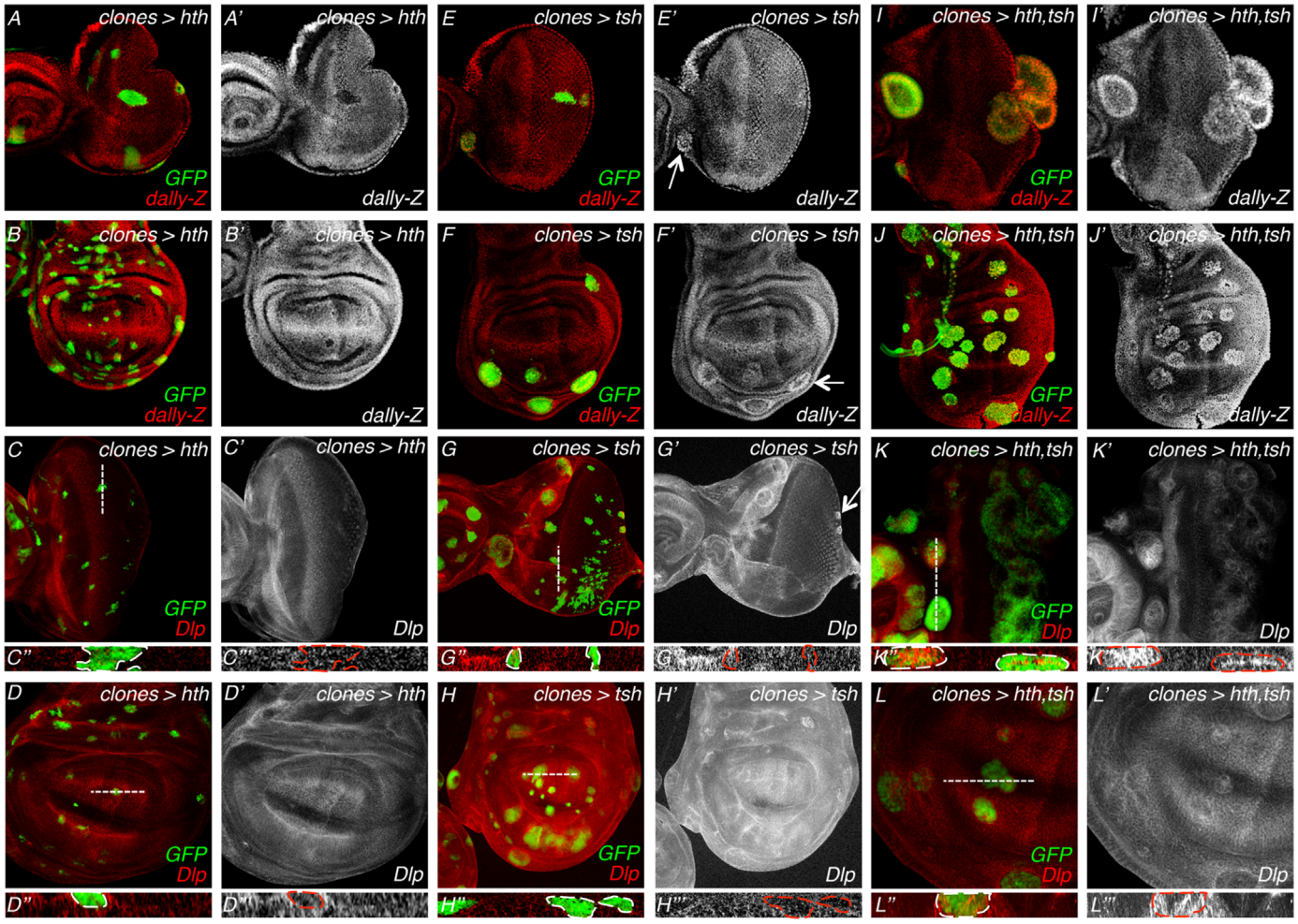

Fig. 4. Hth+Tsh activate *dally* transcription and Dlp levels. Hth- (A-D'''), Tsh- (E-H''') or Hth+Tsh-expressing (I-L''') clones, marked by GFP, induced in the eye and wing imaginal discs at 48–72 h after egg laying. Clones induced in a *dally*-lacZ background were stained with anti-β-galactosidase to monitor *dally* transcription (A-B', E-F', I-J'). The other discs (C-D''', G-H''', K-L''') were stained with anti-Dlp. The dashed lines approximately mark the optical cross-sections shown in (D'', D''', H'', H''', L'', L'''). Hth-expressing clones showed a decrease *dally-Z* levels and no significant changes in Dlp levels. Clones expressing Tsh did not show detectable differences in *dally* or Dlp, unless they were in a domain that expresses *hth* endogenously, in which case they showed higher levels of both glypicans (arrow). Hth+Tsh-expressing clones showed increased levels of *dally* transcription and Dlp protein.

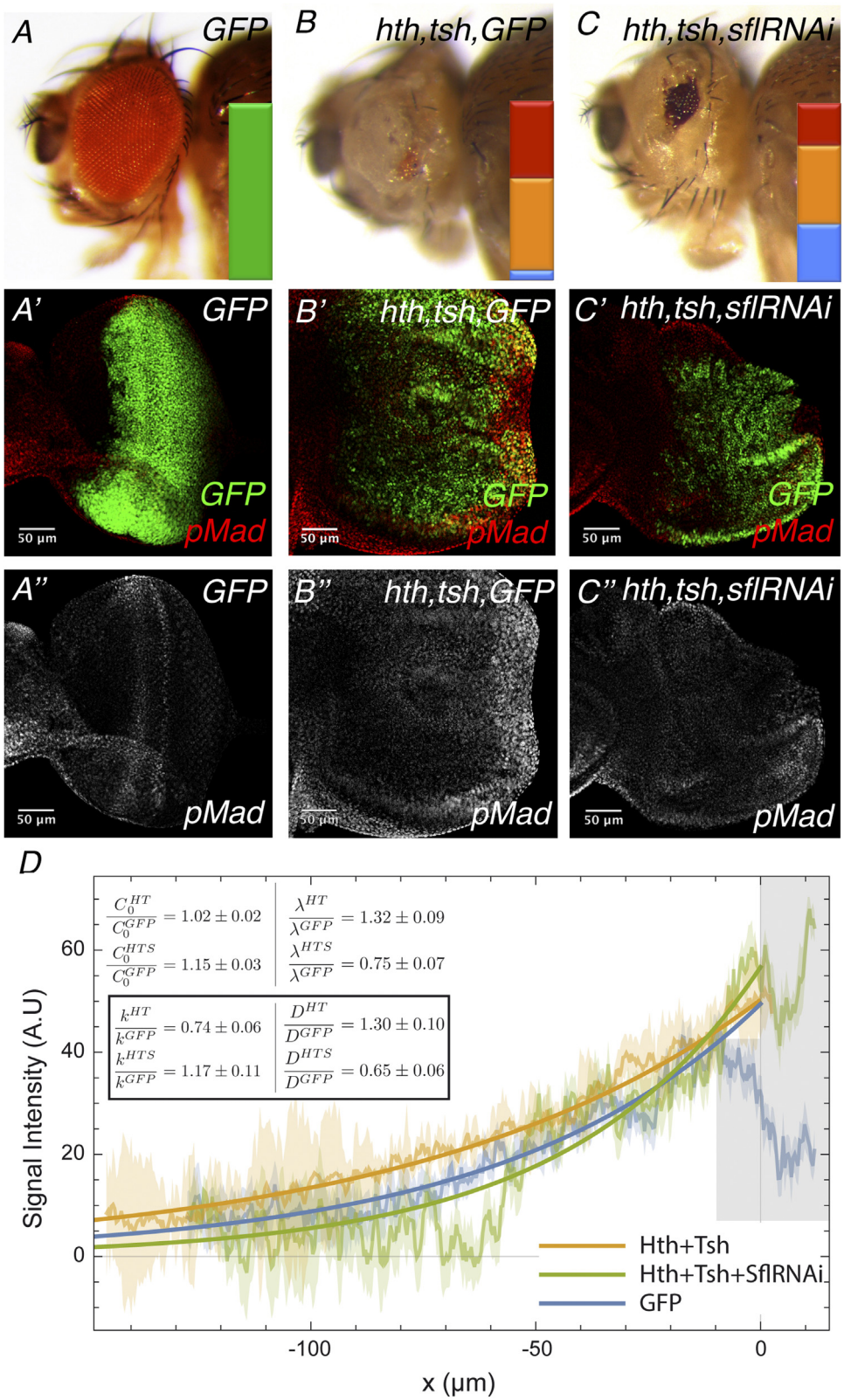

Fig. 5. Reduction of *sulfateless (sfl)* levels through RNAi in an Hth+Tsh background results in a partial rescue of the Hth+Tsh-phenotype. Lateral view of adult heads from control (A), Hth+Tsh+GFP (B), Hth+Tsh+sflRNAi (C) expressed in undifferentiated cells using the optix2.3-GAL4 line. Horizontal bars represent the percentages of flies with different phenotypes: flies with normal eyes (represented in green), flies with a medium eye (represented in blue), flies with a small number of organized ommatidias (represented in orange) and flies with a total loss of retina (represented in red). (A'-C') Late third instar eye discs of the above genotypes stained with anti-pSmad3. (D) Signal intensity histograms of pMad of control (blue), hth+tsh-expressing (green) and hth+tsh+sflRNAi-expressing (red) discs. Signal intensity, expressed in arbitrary units, is measured ahead of the MF in control, and from the posterior margin in hth+tsh- and hth+tsh+sflRNAi-expressing discs ($n \geq 5$ for each genotype). The standard error to the mean is represented with a lighter shaded area. Fit to mean in solid lines. Data in a shaded grey area was excluded from fits. Ratios of signal intensity at position $x=0$ (C_0), characteristic length scale of the gradient (λ), effective degradation (k) and effective diffusion coefficient (D) are shown inlay. Reducing the levels of *sfl* by RNAi in an hth+tsh background resulted in a partial rescue of the phenotype and in slightly reduced pMad signal. Scale bars: 50 µm.

concentrate Dpp would be by increasing the expression of heparin-sulphate proteoglycans, extracellular matrix components known to act as key regulators of the distribution and activity of ligands such as Hh, Dpp or Wg (reviewed in (Yan and Lin, 2009). To test this possibility, we analyzed the expression of the two glypicans *dally* and *dlp* in Hth+Tsh-expressing cells, using a *dally-Z* transcriptional reporter and an anti-Dlp antibody. Clones expressing Hth alone resulted in a cell autonomous downregulation of *dally* transcription, while the Dlp levels did not seem to be affected (Fig. 4A–D). Tsh-expressing clones that fell within an endogenous Hth-expressing domain showed upregulation of *dally* transcription and Dlp levels, but all other clones did not (Fig. 4E–H). However, Hth+Tsh clones showed high levels of *dally* transcription and Dlp membrane accumulation (Fig. 4I–L). To evaluate whether this increase in glypican levels was responsible for the hth+tsh-induced phenotype –including the enhanced Dpp signaling- we decreased the expression levels of *sulfateless (sfl)*, one of the enzymes involved in the biosynthesis of proteoglycans, in the hth+tsh-expressing background (Ferreira and Milan, 2015; Lin et al., 1999). The RNAi-mediated silencing of *sfl* resulted in a partial rescue of the adult eye size (Fig. 5A–C), even though silencing *slf* alone caused a small eye reduction (nor shown). To understand the effects of these manipulations on the formation of the Dpp signaling gradient, we quantified the pMad profiles and fitted them to an exponentially decaying gradient. With this approximation we can gain information regarding two key Dpp properties: *k,* the Dpp effective degradation rate (which is an inverse measure of its stability), and *D,* its effective diffusion coefficient (Wartlick et al., 2011) and Supplementary material; Fig. 5D). The pMad profile in *optix > hth+tsh* discs, when compared to controls (*optix > GFP*), indicated a relative increase in Dpp stability ($k_{HT}/k_{GFP}=0.74$) and diffusion ($D_{HT}/D_{GFP}=1.30$). The additional RNAi-mediated attenuation of *sfl* (*optix > hth+tsh+slfRNAi*) partly rescued the normal pMad profile, indicating an almost normal Dpp stability ($k_{HTS}/k_{GFP}=1.17$) and a further decrease in Dpp diffusion ($D_{HTS}/D_{GFP}=0.65$) (Fig. 5D). Indeed the sole attenuation of *slf* function in *ey > slf* resulted in a clear reduction of both stability and diffusion of Dpp (Fig. S7). These results indicate that the extracellular matrix proteoglycans are indeed necessary for the tissue overgrowth and differentiation blockade induced by hth+tsh, and point to the elevation in *dally* and *Dlp* levels as likely responsible for the increased retention of Dpp and intracellular signaling in hth+tsh cells.

3. Discussion

Abnormal maintenance of transcription factors that promote an undifferentiated, proliferative state is often an initiating event in tumors. However, abnormal growth is dependent on specific non-autonomous signals provided by the microenvironment. In this paper, we have used an experimental system that results in continuous growth to identify these signals and the mechanism of action. In this system, the GAL4-driven maintenance during eye development of *hth* and *tsh,* two transcription factors normally transiently co-expressed in eye progenitors, cause cells to increase their avidity for Dpp. This, in turn, leads to a hyper-activation of the pathway, which is necessary to maintain the proliferative/undifferentiated phenotype. We show that the increased avidity for Dpp is mediated, at least partly, through increased expression of the proteoglycans components encoded by *dally* and *dlp,* functionally modified by *slf.*

Progenitor cells, forced to maintain Hth and Tsh (hth+tsh progenitor-like cells) trap Dpp produced at local sources, which then causes an increased in intracellular signaling. The mechanism responsible of this trapping seems to be the increase of extracellular matrix (ECM) components. First, we find a cell-autonomous increase in *dally* transcription and Dlp membrane levels, the two glypican moieties of heparane sulphate proteoglycans. Second, the RNAi-mediated attenuation of *sfl* function, a gene encoding an enzyme required for the biosynthesis of these proteoglycans, is required for the overgrowth/eye-suppression phenotype induced by hth+tsh maintenance. A third line of support comes from examination of the effects of hth+tsh or hth+tsh+slfRNAi on the pMad profiles (Fig. 5). Considering that the Dpp production remains unaltered, hth+tsh tissue shows an increase in both pMad signal amplitude and range, which is consistent with the increase in proteoglycans simultaneously augmenting Dpp diffusion and stability (Akiyama et al., 2008; Belenkaya et al., 2004; Ferreira and Milan, 2015; Fujise et al., 2003). On the contrary, reducing proteoglycan biosynthesis in hth+tsh+slfRNAi cells results in the retraction of the pMad signaling range back towards control values, which again is expected if Dpp's diffusion depends on proteoglycans.

By forcing the expression of hth and tsh in eye precursors, these cells are exposed to signaling levels higher than they would normally encounter. This is because during normal eye development Dpp, produced at the furrow, represses first *hth* and then, closer to the furrow, also *tsh,* so that the cells approaching the furrow and receiving the highest Dpp levels no longer co-express *hth* and *tsh* (Bessa et al., 2002; Firth and Baker, 2009; Lopes and Casares, 2010). The loss of *hth* marks the transition between proliferation/undifferentiation and cell quiescence/commitment (Bras-Pereira et al., 2015; Lopes and Casares, 2010). This transition coincides with a transient proliferative wave (the so-called "first mitotic wave") that precedes entry into G1 (Escudero and Freeman, 2007; Lopes and Casares, 2010). This transition zone corresponds to a region where low, but not null, levels of Hth and pMad signals overlap (Fig. S8). If the interaction between hth+tsh and the Dpp pathway we have described here were to hold also in the zone of hth/Dpp signal overlap during normal eye development (remember that *hth* -positive cells co-express normally *tsh* too), one prediction would be that the mitotic wave would be lost if either *hth* or *dpp*-signaling were removed. Indeed this has been shown to be the case: RNAi-mediated attenuation of *hth* (Lopes and Casares, 2010) or abrogation of Dpp signaling (Wartlick et al., 2014) result in the loss of the first mitotic wave. However, we do not think that the mechanisms driving Dpp-mediated proliferation of *optix > hth+tsh* cells are necessarily the same as those operating normally in hth+tsh-expressing progenitors during eye development, because of the following experiment. We generated discs expressing in their dorsal domain an RNAi targeting Hth's partner, the Pbx gene *extradenticle (exd)* (*iro-GAL4; UAS-exdRNAi, "D > exdRNAi").* In the absence of Exd, Hth is degraded (Rieckhof et al., 1997). Therefore, a depletion of Exd causes an effective loss of Hth. Knowing that in *optix > hth+tsh* the stability and diffusion of Dpp were increased, the prediction would be that the loss of *hth* (in *exd*-depleted cells) should cause a *decrease* in both the stability and diffusion of Dpp. However, when we compared quantitatively the dorsal ("exd-") with the ventral ("exd+") pMad profiles of *D > exdRNAi* discs we found that both the stability and diffusion of Dpp *increased* by the *loss of hth* (Fig. S9). This result suggests that during normal eye development *hth* (perhaps together with *tsh*) influences Dpp signaling, but the mechanisms we have described as triggered by forced hth+tsh expression are likely different.

The upregulation of *dally* and *dlp* by hth+tsh is likely the consequence of the transcriptional activity of Hth+Tsh in partnership with the YAP/TAZ homologue, Yki, as previous work showed that loss of the protocadherin genes *fat* (*ft*) and *dachsous* (*ds),* which causes the activation of Yki, results in an upregulation of *dally* and *dlp* in the wing primordium (Baena-Lopez et al., 2008). In fact, Slattery and co-workers found, in imaginal tissues, binding

of Yki and Hth to nearby sites on the *dlp* locus (Slattery et al., 2013), suggesting that some of this regulation might be direct. All these data make Yki a necessary component of the molecular machinery responsible for the increased avidity of hth+tsh cells for Dpp. However, in the eye primordium, the overexpression of Yki induces a different phenotype than hth+tsh (Fig. S2). More importantly, in the eye primordium, *yki+* clones do not cause the autonomous upregulation of pMad signal (Fig. S10) that hth+tsh clones do (Fig. 2). Therefore, a specific stoichiometry among Hth, Tsh and Yki is likely necessary to induce the Dpp signaling-dependent properties of hth+tsh cells, at least in the developing eye. Alternatively, Hth and Tsh may activate Yki-independent targets that would be required for the full expression of the phenotype. Recently, Oh and Irvine described that Yki and the Dpp pathway synergize in stimulating tissue overgrowth, both in eye and wing primordia, through the physical association between Yki and Mad (Oh et al., 2013). Our results suggest that hth+tsh progenitor-like cells establish a positive feedback, in which the growth promoting activity of the Hth:Tsh:Yki complex would be enhanced by increasing levels of pMad activated by Dpp. This feedback would be region-specific, as it depends on sources of Dpp that are localized within the eye primordium. Further work is needed to investigate the molecular mechanisms behind this feedback. Finally, it has been shown recently that tissue growth promoted by the PI3K/PTEN and TSC/TOR nutrient-sensing pathways also requires Dally which, in turn, increases the avidity of the growing tissue for Dpp (Ferreira and Milan, 2015). Therefore, increasing the avidity for Dpp by augmenting proteoglycan levels may be a common strategy of tissues to sustain their growth.

4. Materials and methods

4.1. Fly strains and genetic manipulations

All crosses were set up and raised at 25 °C under standard conditions. The UAS/GAL4 system (Brand and Perrimon, 1993) and the lexA/lexO system (Yagi et al., 2010) were used for targeted misexpression. The fly stocks used were: *optix2.3-GAL4* (from R. Chen, Baylor College of Medicine); *ey-GAL4* (Halder et al., 1995); *iro-GAL4* (Mazzoni et al., 2008); *UAS-yki* (Staley and Irvine, 2010); *UAS-GFP* (Bessa and Casares, 2005); *UAS-131-GFPhth* (Casares and Mann, 2000); *UAS-Flag-HA-tsh and UAS-Flag-HA-hth* (synthesized by C. M. Luque, formerly at the Casares laboratory, currently at Universidad Autónoma, Madrid, Spain); *yw,* hs-*FLP*^{122}; *act > y+ >* Gal4 (Struhl and Basler, 1993) with a recombined UAS-*GFP* transgene; *yw*, *hs*-FLP^{122}, *act > hs*CD2 > Gal4 (Basler and Struhl, 1994); *dpp-lacZ* (Masucci et al., 1990); *UAS-exdRNAi (VDRC #7802); UAS-sflRNAi* (Trip #34601); *tkv-lacZ* (Tanimoto et al., 2000) and *hth-YFP* (CPTI-001356; Flannotator). *dpp-LHG86Fb* and *lexO-eGFP::Dpp* (Yagi et al., 2010) were a kind gift of K. Basler. The lines used to alter the levels of *dpp*-pathway components *were: UAS-TkvRNAi* (VDRC #3059); *UAS-TkvQD* (Nellen et al., 1996); *UAS-puntRNAi* (VDRC #37279); *UAS-Punt* (Nellen et al., 1996); *UAS-Dad.T* (Tsuneizumi et al., 1997) and *UAS-Dpp.S* (Staehling-Hampton et al., 1994).

In order to obtain *optix > hth+tsh* flies we used two strategies: either we crossed the optix2.3-GAL4 driver to *UAS-Flag-HA-tsh; UAS-131-GFPhth* flies or used a stable *optix2.3-GAL4,UAS-Flag-HA-tsh;UAS-131-GFPhth/SM6TM6B* stock. We observed that the phenotypes in eye discs, adult eyes and pMad profiles were stronger in individuals from the cross.

The *dpp*-pathway lines were crossed to the *optix2.3-GAL4,UAS-Flag-HA-tsh;UAS-131-GFPhth/SM6TM6B* stock. Flies were observed under a LEICA MZ 9.5 stereomicroscope and pictures of adult heads from each genotype were taken with a LEICA DFC320 digital camera.

Random ectopic expression clones were generated using the flip-out method (Struhl and Basler, 1993). *yw, hs-FLP*^{122}*; act > y+ > Gal4;; UAS-GFP/TM6B* females were crossed to *UAS-yki, UAS-Flag-HA-tsh*, *UAS-131-GFPhth* or *UAS-Flag-HA-tsh;UAS-131-GFPhth* males and transferred to 25 °C. Clones were positively marked with GFP.

For the combination of Gal4/UAS and lexA/lexO systems, *yw*, *hs*-FLP^{122}, *act > hsCD2 > Gal4*;*UAS-Flag-HA-hth*;*lexO-eGFP::Dpp* females were crossed to *UAS-Flag-HA-tsh;dpp-LHG86Fb* males. Flip-out clones were induced by heat shock (10 min at 35,5 °C) between 72 h and 96 h AEL and then maintained at 25 °C. Clones were stained with anti-HA and anti-GFP.

4.2. Immunostaining

Eye-antennal and wing imaginal discs from wandering third instar larvae were dissected and fixed according to standard protocols. Primary antibodies used were: mouse anti-Eya 10H6 at 1:100 (DSHB); rabbit anti-phosphoSmad3 1880-1 at 1:100 (Epitomics), used here to detect *Drosophila* phosphorylated-Mad (pMad) because of its crossreactivity; mouse anti-ßGal at 1:1000 (Sigma); rabbit anti-ßGal at 1:1000 (Cappel); rat anti-HA at 1:500 (Roche); mouse anti-GFP at 1:1000 (Molecular Probes); mouse anti-Dlp 13G8 at 1:5 (DSHB); mouse anti-Armadillo N27A1 at 1:100 (DSHB); mouse anti-CycB F2F4 at 1:100 (DSHB); rabbit *anti*-phospho-histone H3 (PH3) at 1:1000 (Sigma); mouse anti-Exd B11M at 1:5 (DSHB); Alexa-Fluor conjugated secondary antibodies were from Molecular Probes. Images were obtained with a Leica SP2 confocal system and processed with Adobe Photoshop.

4.3. Scanning electron microscopy (SEM)

Adult females were transferred to 75% ethanol for 24 h at room temperature. Flies were dehydrated through an ethanol series (80%, 90%, 95% and twice 100%; 12–24 h each step). Flies were then air-dried and mounted onto SEM stubs covered with carbon tape and sputter-coated with gold (Edwards Six Sputter). Images were obtained using a JEOL 6460LV scanning electron microscope.

4.4. pMad expression profiles

optix > GFP, optix > 131-GFPhth, optix > Flag-HA-tsh and *optix > 131-GFPhth+Flag-HA-tsh* L3 eye imaginal discs were stained simultaneously with anti-Arm and anti-pSmad3. *optix > GFP, optix,131-GFPhth+Flag-HA-tsh/TM6B and optix > 131-GFPhth+Flag-HA-tsh+UASsflRNAi* L3 eye imaginal discs were stained simultaneously with anti-pSmad3. Confocal imaging was done on the same day after the laser intensity had stabilized. The expression profiles were obtained using ImageJ. Signal intensity for anti-pSmad3 was measured in at least five independent discs. Measurements were taken ahead of the morphogenetic furrow, when present, or starting at the posterior margin of the disc when absent. The mean profile of each set of profiles and the standard error of the mean were represented in arbitrary units using Microsoft Excel.

4.5. Adult eye phenotype scores

Adult flies from *optix > GFP*, *optix > 131-GFPhth+Flag-HA-tsh+UAS-GFP*, *optix > 131-GFPhth+Flag-HA-tsh+UAS-tkvRNAi*, *optix > 131-GFPhth+Flag-HA-tsh+UAS-tkvQD* and *optix > 131-GFPhth+Flag-HA-tsh+UASsflRNAi* were collected and several representative pictures of adult eyes (n=36–68) were obtained. Each phenotype was scored in a semi-quantitative manner by grouping the phenotype scores in phenotypic classes. These classes were

defined as: flies with normal eyes (represented in green), flies with an mild reduction (represented in blue), flies with a severe eye reduction, comprising a small number of organized ommatidia (represented in orange), and flies with a total loss of retina (represented in red). Proportion of flies belonging to each class were represented.

4.6. Quantification of PH3$^+$ cells

Third instar eye imaginal discs from optix > GFP and optix > 131-GFPhth+Flag-HA-tsh were stained with anti-PH3 and anti-CycB. The anterior area of the eye disc was defined by creating a surface and the PH3$^+$ cells first were automatically identified and then manually curated. Finally, the number of PH3$^+$ cells that fall within the created surface were detected. This analysis was made using the IMARIS x64 7.7.2 software. The ratios between the PH3$^+$ cells and the anterior area (n=10 for optix > GFP and n=14 for optix > 131-GFPhth+Flag-HA-tsh ("optix > hth+tsh") were calculated and represented as dots (control) and squares (experiment); the means were represented as horizontal bars. The graphical output was generated using GraphPad Prism 6.0. Statistical significance was determined using an ANOVA test.

4.7. Quantification of spatial profiles and calculation of effective parameters

Spatial profiles of pMad are assumed to follow Dpp dynamics, thus they can be fitted from the solution of a reaction-diffusion equation (see Sup. Mat. For details) that leads to an exponential function in the form:

$$C(x) = C_0 e^{-\frac{x}{\lambda}},$$

with C_0 the concentration of C at position $x = 0$, which is a function of the kinetic parameters in the form:

$$C_0 = \frac{v}{\sqrt{Dk}},$$

and λ the decay length of the concentration profile, defined as:

$$\lambda = \sqrt{\frac{D}{k}}.$$

With the expressions for C_0 and λ we can compare ratios of two profiles α and β such that

$$\frac{k^\alpha}{k^\beta} = \frac{C_0^\beta \lambda^\beta}{C_0^\alpha \lambda^\alpha},$$

and

$$\frac{D^\alpha}{D^\beta} = \frac{C_0^\beta \lambda^\alpha}{C_0^\alpha \lambda^\beta}.$$

Real fit is done using function NonLinearModelFit in software Mathematica. Experimental error is included as data weight in the fit process.

To fit pMad profiles, we have placed position $x = 0$ at the anterior boundary of the morphogenetic furrow. This position is estimated from comparison between *dpp3.0Z* and pMad profiles (Fig. S11A–C). We then fitted the concentration profile in the anterior compartment. For convention, we use negative sign to positions to the left side of $x = 0$, thus the fit function must read $C(x) = C_0 e^{\frac{x}{\lambda}}$, with negative x.

We observed that some of the profiles showed a peak of signaling in a position anterior to the furrow, due to a peak of proliferation (Wartlick et al., 2014). This proliferation peak modifies pMad profiles shapes. For fitting purposes, as a direct readout of Dpp should peak at the furrow (position $x = 0$ in the case of fitting just anterior compartment), we assumed pMad concentration is depleted right anterior to the furrow with respect to the Dpp profile, thus we eliminated from the fits this depletion zone (marked in grey in Fig. 5, S7 and S9).

Competing interests

The authors declare they have no competing interests.

Author contributions

FC conceived the study; MN and FC designed the experiments; MN carried out most of the experiments with some carried out by FC; DAH carried out mathematical analysis of quantitative data; MN and FC wrote the manuscript.

Funding

Grants BFU2012-34324 and BFU2015-66040 (Spanish Ministry for Economy and Competitiveness (MINECO) co-funded by FEDER) to FC, and grants BFU2014-55738-REDT and BFU2014-57703-REDC, in which FC is participant. MN was a FCT, Portugal PhD fellow (SFRH/BD/69222/2010).

Summary statement

In Drosophila, combined expression of the eye progenitor transcription factors homothorax, the Meis1 homologue, and *teashirt* sustains the proliferation of progenitor-like cells by increasing their avidity for BMP produced by the local microenvironment.

Acknowledgements

We thank K. Basler and the Bloomington and VDRC stock centers for fly stocks, and the Developmental Studies Hybridoma Bank, University of Iowa, for antibodies, C.S. Lopes for critical reading of the manuscript, A. Iannini for technical assistance and the CABD Advanced Light Microscopy facility and the CITIUS (U. of Sevilla) SEM facility for imaging support.

Appendix A. Supplementary material

Supplementary data associated with this article can be found in the online version at http://dx.doi.org/10.1016/j.ydbio.2016.08.004.

References

Affolter, M., Basler, K., 2007. The Decapentaplegic morphogen gradient: from

pattern formation to growth regulation. Nat. Rev. Genet. 8, 663–674.
Akiyama, T., Kamimura, K., Firkus, C., Takeo, S., Shimmi, O., Nakato, H., 2008. Dally regulates Dpp morphogen gradient formation by stabilizing Dpp on the cell surface. Dev. Biol. 313, 408–419.
Amore, G., Casares, F., 2010. Size matters: the contribution of cell proliferation to the progression of the specification Drosophila eye gene regulatory network. Dev. Biol. 344, 569–577.
Baena-Lopez, L.A., Rodríguez, I., Baonza, A., 2008. The tumor suppressor genes dachsous and fat modulate different signalling pathways by regulating dally and dally-like. Proc. Natl. Acad. Sci. USA 105, 9645–9650.
Basler, K., Struhl, G., 1994. Compartment boundaries and the control of Drosophila limb pattern by hedgehog protein. Nature 368, 208–214.
Belenkaya, T.Y., Han, C., Yan, D., Opoka, R.J., Khodoun, M., Liu, H., Lin, X., 2004. Drosophila Dpp morphogen movement is independent of dynamin-mediated endocytosis but regulated by the glypican members of heparan sulfate proteoglycans. Cell 119, 231–244.
Bessa, J., Casares, F., 2005. Restricted teashirt expression confers eye-specific responsiveness to Dpp and Wg signals during eye specification in Drosophila. Development 132, 5011–5020.
Bessa, J., Gebelein, B., Pichaud, F., Casares, F., Mann, R.S., 2002. Combinatorial control of Drosophila eye development by eyeless, homothorax, and teashirt. Genes Dev. 16, 2415–2427.
Brand, A.H., Perrimon, N., 1993. Targeted gene expression as a means of altering cell fates and generating dominant phenotypes. Development 118, 401–415.
Bras-Pereira, C., Casares, F., Janody, F., 2015. The retinal determination gene Dachshund restricts cell proliferation by limiting the activity of the Homothorax-Yorkie complex. Development 142, 1470–1479.
Casares, F., Mann, R.S., 2000. A dual role for homothorax in inhibiting wing blade development and specifying proximal wing identities in Drosophila. Development 127, 1499–1508.
Dong, J., Feldmann, G., Huang, J., Wu, S., Zhang, N., Comerford, S.A., Gayyed, M.F., Anders, R.A., Maitra, A., Pan, D., 2007. Elucidation of a universal size-control mechanism in Drosophila and mammals. Cell 130, 1120–1133.
Escudero, L.M., Freeman, M., 2007. Mechanism of G1 arrest in the Drosophila eye imaginal disc. BMC Dev. Biol. 7, 13.
Fernandez, B.G., Gaspar, P., Bras-Pereira, C., Jezowska, B., Rebelo, S.R., Janody, F., 2011. Actin-Capping Protein and the Hippo pathway regulate F-actin and tissue growth in Drosophila. Development 138, 2337–2346.
Ferreira, A., Milan, M., 2015. Dally proteoglycan mediates the autonomous and nonautonomous effects on tissue growth caused by activation of the PI3K and TOR pathways. PLoS Biol. 13, e1002239.
Firth, L.C., Baker, N.E., 2009. Retinal determination genes as targets and possible effectors of extracellular signals. Dev. Biol. 327, 366–375.
Fujise, M., Takeo, S., Kamimura, K., Matsuo, T., Aigaki, T., Izumi, S., Nakato, H., 2003. Dally regulates Dpp morphogen gradient formation in the Drosophila wing. Development 130, 1515–1522.
Greenwood, S., Struhl, G., 1999. Progression of the morphogenetic furrow in the Drosophila eye: the roles of Hedgehog, Decapentaplegic and the Raf pathway. Development 126, 5795–5808.
Haerry, T.E., Khalsa, O., O'Connor, M.B., Wharton, K.A., 1998. Synergistic signaling by two BMP ligands through the SAX and TKV receptors controls wing growth and patterning in Drosophila. Development 125, 3977–3987.
Halder, G., Callaerts, P., Gehring, W.J., 1995. Induction of ectopic eyes by targeted expression of the eyeless gene in Drosophila. Science 267, 1788–1792.
Harmansa, S., Hamaratoglu, F., Affolter, M., Caussinus, E., 2015. Dpp spreading is required for medial but not for lateral wing disc growth. Nature.
Huang, J., Wu, S., Barrera, J., Matthews, K., Pan, D., 2005. The Hippo signaling pathway coordinately regulates cell proliferation and apoptosis by inactivating Yorkie, the Drosophila Homolog of YAP. Cell 122, 421–434.
Lecuit, T., Cohen, S.M., 1998. Dpp receptor levels contribute to shaping the Dpp morphogen gradient in the Drosophila wing imaginal disc. Development 125, 4901–4907.
Lin, X., Buff, E.M., Perrimon, N., Michelson, A.M., 1999. Heparan sulfate proteoglycans are essential for FGF receptor signaling during Drosophila embryonic development. Development 126, 3715–3723.
Lopes, C.S., Casares, F., 2010. hth maintains the pool of eye progenitors and its downregulation by Dpp and Hh couples retinal fate acquisition with cell cycle exit. Dev. Biol. 339, 78–88.
Masucci, J.D., Hoffmann, F.M., 1993. Identification of two regions from the Drosophila decapentaplegic gene required for embryonic midgut development and larval viability. Dev. Biol. 159, 276–287.
Masucci, J.D., Miltenberger, R.J., Hoffmann, F.M., 1990. Pattern-specific expression of the Drosophila decapentaplegic gene in imaginal disks is regulated by 3' cis-regulatory elements. Genes Dev. 4, 2011–2023.
Mazzoni, E.O., Celik, A., Wernet, M.F., Vasiliauskas, D., Johnston, R.J., Cook, T.A., Pichaud, F., Desplan, C., 2008. Iroquois complex genes induce co-expression of rhodopsins in Drosophila. PLoS Biol. 6, e97.
Muller, B., Basler, K., 2000. The repressor and activator forms of Cubitus interruptus control Hedgehog target genes through common generic gli-binding sites. Development 127, 2999–3007.
Nellen, D., Burke, R., Struhl, G., Basler, K., 1996. Direct and long-range action of a DPP morphogen gradient. Cell 85, 357–368.
Oh, H., Slattery, M., Ma, L., Crofts, A., White, K.P., Mann, R.S., Irvine, K.D., 2013. Genome-Wide Association of Yorkie with Chromatin and Chromatin-remodeling complexes. Cell Rep. 3, 309–318.
Ostrin, E.J., Li, Y., Hoffman, K., Liu, J., Wang, K., Zhang, L., Mardon, G., Chen, R., 2006. Genome-wide identification of direct targets of the Drosophila retinal determination protein Eyeless. Genome Res. 16, 466–476.
Peng, H.W., Slattery, M., Mann, R.S., 2009. Transcription factor choice in the Hippo signaling pathway: homothorax and yorkie regulation of the microRNA bantam in the progenitor domain of the Drosophila eye imaginal disc. Genes Dev. 23, 2307–2319.
Rauskolb, C., Sun, S., Sun, G., Pan, Y., Irvine, K.D., 2014. Cytoskeletal tension inhibits Hippo signaling through an Ajuba-Warts complex. Cell 158, 143–156.
Restrepo, S., Zartman, J.J., Basler, K., 2014. Coordination of patterning and growth by the morphogen DPP. Curr. Biol. 24, R245–R255.
Rieckhof, G.E., Casares, F., Ryoo, H.D., Abu-Shaar, M., Mann, R.S., 1997. Nuclear translocation of extradenticle requires homothorax, which encodes an extradenticle-related homeodomain protein. Cell 91, 171–183.
Sansores-Garcia, L., Bossuyt, W., Wada, K., Yonemura, S., Tao, C., Sasaki, H., Halder, G., 2011. Modulating F-actin organization induces organ growth by affecting the Hippo pathway. EMBO J. 30, 2325–2335.
Slattery, M., Voutev, R., Ma, L., Negre, N., White, K.P., Mann, R.S., 2013. Divergent transcriptional regulatory logic at the intersection of tissue growth and developmental patterning. PLoS Genet. 9, e1003753.
Staehling-Hampton, K., Jackson, P.D., Clark, M.J., Brand, A.H., Hoffmann, F.M., 1994. Specificity of bone morphogenetic protein-related factors: cell fate and gene expression changes in Drosophila embryos induced by decapentaplegic but not 60A. Cell Growth Differ. 5, 585–593.
Staley, B.K., Irvine, K.D., 2010. Warts and Yorkie mediate intestinal regeneration by influencing stem cell proliferation. Curr. Biol. 20, 1580–1587.
Struhl, G., Basler, K., 1993. Organizing activity of wingless protein in Drosophila. Cell 72, 527–540.
Tanimoto, H., Itoh, S., ten Dijke, P., Tabata, T., 2000. Hedgehog creates a gradient of DPP activity in Drosophila wing imaginal discs. Mol. Cell 5, 59–71.
Tsuneizumi, K., Nakayama, T., Kamoshida, Y., Kornberg, T.B., Christian, J.L., Tabata, T., 1997. Daughters against dpp modulates dpp organizing activity in Drosophila wing development. Nature 389, 627–631.
Wartlick, O., Julicher, F., Gonzalez-Gaitan, M., 2014. Growth control by a moving morphogen gradient during Drosophila eye development. Development 141, 1884–1893.
Wartlick, O., Mumcu, P., Kicheva, A., Bittig, T., Seum, C., Julicher, F., Gonzalez-Gaitan, M., 2011. Dynamics of Dpp signaling and proliferation control. Science 331, 1154–1159.
Yagi, R., Mayer, F., Basler, K., 2010. Refined LexA transactivators and their use in combination with the Drosophila Gal4 system. Proc. Natl. Acad. Sci. USA 107, 16166–16171.
Yan, D., Lin, X., 2009. Shaping Morphogen Gradients by proteoglycans. Cold Spring Harb. Perspect. Biol. 1, a002493.